Immobilisation of Bio-molecules on Magnetisable Solid Supports for Applications in Bio-catalysis and Bio-sensors

By

Ben Joseph Hodgson

A thesis submitted in partial fulfilment for the requirements for the degree of Doctor of Philosophy in Chemistry at the University of Central Lancashire, in collaboration with Q-Bioanalytic GmbH, Bremerhaven, Germany

January 2014

DECLARATION

No part of this dissertation/thesis has been submitted in support of an application for any degree or qualification of the University of Central Lancashire or any other University or Institute of learning.

Ben Joseph Hodgson

January 2014

ABSTRACT

A series of core and core-shell nanoparticles with superparamagnetic properties were synthesised and surface functionalised using three different amino-silanes by a chemical conjugation method. The functionalised nanoparticles were characterised and further modified by chemical conjugation with two different classes of bio-molecules; (i) enzymes and (ii) single stranded DNA primers. The resultant nanoparticles (nano-bio conjugates) were used for applications in (i) enzyme catalysis and (ii) bio-separation / bio-sensing.

Magnetite and amorphous silica-coated core-shell nanoparticles were synthesised on both small (5 g) and large (20 g) scales and were characterised using transmission electron microscopy (TEM), X-ray diffraction (XRD), Brunauer-Emmett-Teller (BET) surface area measurement and vibrating sample magnetometry (VSM). Silica-coated core-shell nanoparticles were functionalised by silanisation with three different aminosilanes [3-aminopropyl tri-ethoxysilane (APTS), 3-aminopropyl di-ethoxymethylsilane (APDS) and 3-aminopropyl mono-ethoxydimethylsilane (APMS)] and two different methods: water (classical method) or a Tri-phasic Reverse Emulsion (TPRE) using toluene and a surfactant (Triton X-100). It was observed that the materials prepared using the TPRE method produced higher surface amine density values on average.

The first application involved bio-catalysis where lipases [*Pseudomonas Fluorescens* lipase (PFL) and *Candida Rugosa* lipase (CRL)] were chemically conjugated (covalently linked) *via* glutaraldehyde-modification onto the amino-functionalised nanoparticles for applications such as: (i) hydrolysis of *p*-nitrophenyl palmitate to produce palmitic acid and *p*-nitrophenol (model reaction), (ii) transesterification of ethyl butyrate with *n*-butanol to produce butyl butyrate and (iii) partial and selective hydrolysis of *cis*-3,5-diacetoxy-1-cyclopentene to produce pharmaceutically important and expensive chiral intermediate molecules. Various reaction parameters such as (a) water concentration in a bi-phasic solvent mixture and (b) temperature were investigated to determine the optimum conditions. All reactions were carried out using free lipases and the physically adsorbed lipases in order to compare the performance with chemically conjugated nano-biomaterials.

It was observed from the bio-catalytic reaction (i) that the conversion values given by lipase-immobilised materials were comparable to those given by free lipases with the added advantage of being re-usable for further catalytic cycles. PFL-immobilised nanoparticles were shown to be more effective catalysts than CRL-immobilised materials. In the bio-

catalytic reaction (ii), Lipase-immobilised materials were shown to exhibit reasonable conversion values (maximum 53%) along with easy separability by one-step magnetic separation from the reaction mixture and re-usability. Finally, in the bio-catalytic reaction (iii), lipase-immobilised materials were shown to give lower total conversion values compared to free enzymes, but a higher proportion of desired products [(1S,4R)-*cis*-4-acetoxy-2-cyclopenten-1-ol and (1R,4S)-*cis*-4-acetoxy-2-cyclopenten-1-ol]. PFL (both free and immobilised) materials were shown to give higher conversion and enantioselectivity towards the desired (1S,4R)-enantiomer (93-100% *ee)* than CRL materials (30-40% *ee*).

The second application involved bio-separation and bio-sensing where 5′-NH_2-modified oligonucleotide sequences specific to either *Listeria Monocytogenes* (LM) or *Escherichia Coli* (EC) were immobilised onto the surface of glutaraldehyde modified nanoparticles to assess the specific capture and enhance the sensitivity of detection of pathogenic bacterial DNAs from food samples. Firstly, the oligonucleotide-grafted nanoparticles were used in a hybrid capture assay (model assay) at UCLan using specific single stranded DNA primers of our interest followed by the application in real food samples at Q-Bioanalytic GmbH, Germany. Capture of the complementary sequences was reasonably high (48-70% for LM-specific materials and 48-55% for EC-specific materials) when calculated as a molar ratio of conjugated oligonucleotides to complementary oligonucleotides captured. Specific capture was determined to be 33-52% for LM-specific oligonucleotide-grafted nano-materials and 59-60% for EC-specific oligonucleotide-grafted nano-materials. Dehybridisation of captured sequences was shown to be efficient for all oligonucleotide-grafted materials (72-97% for LM-specific materials and 86-87% for EC-specific materials), indicating that the materials were ready for real applications using food matrices at Q-Bioanalytic GmbH, Germany.

Nucleic acid DNA was extracted from a real food sample inoculated with either LM or EC and the extracted DNA was used for specific capture using the oligonucleotide-grafted materials tested at UCLan. Dehybridised oligonucleotides were amplified and analysed using quantitative real-time PCR (qPCR). The results showed that using a one-step hybrid capture assay, LM-specific oligonucleotide-grafted materials were successful at detecting LM from an undiluted solution of LM only and from a 1:1 mixture of LM and EC. Using a two-step assay where the forward and reverse oligonucleotide-grafted materials were applied for capture separately, only EC-specific materials were successful for the detection of EC from an undiluted solution, and also from a 1:1 mixture of LM and EC.

MOTIVATION FOR THE PROJECT

The motivation for this project was to overcome the current problems associated with the applications in industrial bio-catalysis using enzymes and easy separation / rapid detection of microbial contamination in food / water samples. Transesterification of large molecular weight fatty acid esters to low molecular weight alkyl esters is important for the production of bio-diesels and flavouring agents. Similarly, partial and selective hydrolysis of *cis*-3,5-diacetoxy-1-cyclopentene is a powerful reaction to produce pharmaceutically important and expensive chiral intermediate molecules. The above reactions were carried out either by free enzymes or by enzymes supported on a solid matrix as the recovery of expensive enzymes and recycling of enzymes supported on solid matrices are challenging steps for industry. In this context, recent development of nano-materials / nano-technology at UCLan motivated the investigation of such important bio-catalytic reactions using core-shell superparamagnetic nanoparticles as supports for enzymes due to their simple one-step recovery by an external magnetic field with maximum efficiency in re-cycling the enzymes.

Similarly, microbial contamination in food / water samples can have devastating effects upon human health. Several reports have come to the public domain related to food poisoning due to the contamination by pathogenic bacteria such as *Listeria Monocytogenes* (LM). *Salmonella,* etc. Hence, the separation of such microbes from food samples and their rapid detection is a key issue for health industries. In this context, past activity at UCLan in collaboration with Q-Bioanalytic GmbH, Germany using nanoparticle-based sensors created an opportunity for investigating the use of superparamagnetic nanoparticles for such purposes. Similarly, the presence of bacteria is the main indication of water contamination in the developing world. A survey conducted by the World Health Organization (WHO) showed that 80% of total reported diseases are due to contaminated drinking water. Hence, the separation of water-borne microbes such as *Escherichia Coli* (EC) and their rapid detection was key for the investigation of EC primer attached superparamagnetic nanoparticles in the context of an on-going project between UCLan, Fudan University, China and Feedwater Ltd. UK.

ACKNOWLEDGEMENTS

I would like to extend a special thank you to Dr Tapas Sen for the opportunity to work with him on this project. I am extremely grateful for all of the help, guidance and continued support he has provided throughout my PhD project at UCLan.

I would like to thank Dr Boris Oberheitmann, CEO of Q-Bioanalytic GmbH, Germany, for financial support and providing me with the opportunity to visit the company on many occasions and test my samples there. I would also like to thank the Royal Society of Chemistry (RSC) Small Grants Scheme for partial financial support.

I am indebted to the following people for their help with analysis of my samples and general advice: Dr Jennifer Readman (UCLan, UK) for all of her help with XRD, Dr Tim Mercer (UCLan, UK) for his help with VSM, Dr Runjie Mao (UCLan, UK) for his help with BET surface area, Jens-Oliver Axe (Q-Bioanalytic GmbH, Germany) for his help with qPCR, my colleague Maneea Eizadi Sharifabad for her help with TEM and all of the technicians and staff from the analytical unit at UCLan.

I would to thank my parents, family and friends for their continued support and encouragement.

Finally, I would like to give special thanks to Rachel for her continued love and support during my work.

ABBREVIATIONS AND UNITS

Abbreviations

A	adenine
APDS	3-aminopropyl di-ethoxymethylsilane
APhTS	(4-aminophenyl)-trimethoxysilane
APMS	3-aminopropyl mono-ethoxydimethylsilane
APTS	3-aminopropyl tri-ethoxysilane
ATP	adenosine triphosphate
BET	Brunauer-Emmett-Teller surface area analysis
BSA	Bovine serum albumin
C	cytosine
C18T MS	*n*-octadecyltrimethoxysilane
CA	chronoamperometry
CAL-B	*Candida Antarctica* Lipase-B
CLEA	cross-linked enzyme aggregates
CLEC	cross-linked enzyme crystals
CRL	*Candida Rugosa* lipase
CTAB	cetyltrimethylammonium bromide
CTAC	cetyltrimethylammonium chloride
CV	cyclic voltammetry
D_C	critical diameter
DNA	deoxyribonucleic acid
dNTP	deoxyribonucleotide triphosphate
dUTP	deoxyuridine triphosphate
EC	*Escherichia Coli*
EDTA	ethylenediaminetetraacetic acid
EIS	electrochemical impedance spectroscopy
ELISA	enzyme-linked immunosorbent assay
FID	flame ionisation detector
G	guanine
GC	gas chromatography
GC-MS	gas chromatography – mass spectrometry
Glu	glutamic acid
Gly	glycine
HBV	hepatitis B virus
His	histidine
HIV	human immunodeficiency virus
HPBEt	(R,S)-2-hydroxy-4-phenylbutyric acid ethyl ester
IAC	internal amplification control
ICP-MS	inductively coupled plasma – mass spectrometry
IMS	immunomagnetic separation
LM	*Listeria Monocytogenes*
LDH	L-lactate dehydrogenase
Lys	lysine
MCM-41	hexagonal array mesoporous silica molecular sieve
MNP	magnetic nanoparticle
4-NBA	4-nitrobenzaldehyde
PBS	phosphate buffered saline
PCR	polymerase chain reaction
PEG	polyethylene glycol
PFL	*Pseudomonas Fluorescens* lipase
PGA	phosphoglyceric acid
PNP	*p*-nitrophenol
PNPB	*p*-nitrophenyl butyrate
PNPP	*p*-nitrophenyl palmitate
PPL	Porcine Pancreatic Lipase
PSL	*Pseudomonas* sp. Lipase
PVA	polyvinyl alcohol
qPCR	quantitative real-time polymerase chain reaction
RNA	Ribonucleic acid
R_T	retention time
RT-PCR	reverse transcriptase polymerase chain reaction

Abbreviations continued

RuBisCO	ribulose-1,5-biphosphate carboxylase oxygenase
SBA-15	hexagonal array mesoporous silica molecular sieve
S.E.M.	standard error of the mean
Ser	serine
SPIONs	superparamagnetic iron oxide nanoparticles
SSC	Buffer consisting of sodium chloride, sodium citrate and water
T	thymine
TEN	buffer consisting of Tris-HCl, EDTA, sodium chloride and water
TEOS	tetraethyl orthosilicate
TMAOH	tetramethylammonium hydroxide
TLL	*Thermomyces lanuginosus* lipase
TPRE	tri-phasic reverse emulsion
UNG	Uracil-N-glycosylase
VSM	vibrating sample magnetometry

Units

Å	ångström or angstrom = 1×10^{-10} m
°C	degree Celsius
CFU	colony forming units
emu	electromagnetic units
fg	femtogram (1×10^{-15} g)
g	gram
h	hour
K	degree Kelvin
kOe	kilooersted (1×10^{3} Oe)
km	kilometre (1×10^{3} m)
kV	kilovolt (1×10^{3} V)
m	metre
M	molarity (moles per litre)
mg	milligram (1×10^{-3} g)
mins	minutes
mL	millilitre (1×10^{-3} L)
mm	millimetre (1×10^{-3} m)
mmol	millimoles (1×10^{-3} moles)
µg	microgram (1×10^{-6} g)
µL	microlitre (1×10^{-6} L)
µm	micrometre (1×10^{-6} m)
µmol	micromoles (1×10^{-6} moles)
nm	nanometre (1×10^{-9} m)
nmol	nanomoles (1×10^{-9} moles)
rpm	revolutions per minute
v/v	volume per volume
w/v	weight per volume

TABLE OF CONTENTS

CHAPTER 1

INTRODUCTION TO NANOPARTICLES AND NANOTECHNOLOGY

1.1 Aims and Objectives of the Project

The aims of the project were as follows:

1. Synthesise a range of superparamagnetic magnetite nanoparticles and coat with silica to produce amorphous core-shell silica-magnetite nanoparticles.
2. Use both classical (water method) and novel (TPRE method) techniques to functionalise the surface of the nanoparticles using a range of aminosilanes (APTS, APDS, APMS).
3. Fully characterise the materials made in this project both physically and chemically, using DNA binding and elution assays, transmission electron microscopy (TEM), UV-Visible colorimetric assay of amine density, Brunauer-Emmett-Teller surface area analysis (BET), vibrating sample magnetometry (VSM) and X-ray diffraction (XRD), where relevant.
4. Covalently immobilise lipases (CRL and PFL) onto the aminosilane-functionalised nanoparticle surface (*via* the glutaraldehyde coupling method) to produce bio-catalytically active materials.
5. Employ the lipase-immobilised nanoparticles for a model catalysis reaction (hydrolysis of PNPP), and use the best materials for useful bio-catalytic applications including the transesterification of ethyl butyrate and the synthesis of pharmaceutically important chiral compounds *via* selective hydrolysis.
6. Covalently immobilise specific single-stranded oligonucleotides onto the aminosilane-functionalised nanoparticle surface (*via* glutaraldehyde) to produce materials with uses in bio-separation and bio-sensor applications.
7. Employ the oligonucleotide-grafted nanoparticles for a model hybrid capture assay (monitoring the hybridisation and dehybridisation efficiency of complementary oligonucleotide sequences using UV-Visible spectroscopy), followed by the specific capture and detection of *Listeria Monocytogenes* (LM) from food samples in collaboration with Q-Bioanalytic GmbH, Bremerhaven, Germany, using real-time PCR (qPCR).
8. Employ the oligonucleotide-grafted nanoparticles for a model hybrid capture assay (monitoring the hybridisation and dehybridisation efficiency of complementary oligonucleotide sequences using UV-Visible spectroscopy), followed by the specific capture and detection of *Escherichia Coli* (EC) from wastewater samples in collaboration with Fudan University, Shanghai, China.

1.2 Introduction to Nanoparticles and Nanotechnology

The prefix 'nano-' means a billionth, or 1×10^{-9}. Thus, a nanometre (nm) is defined as 1×10^{-9} m. Nanotechnology and nanochemistry deal with structures in the size range of around 1-100 nm. Although the field of nanotechnology is quite new, nanostructures exist in abundance in nature, for example in the very hard shell of the abalone mollusc,[1] upon geckos' feet to enable them to walk on vertical or even upside-down surfaces,[2] in butterfly wings producing bright colours[3] and in mineralised collagen fibrils; the building blocks of bone.[4] Deoxyribonucleic acid (DNA) and proteins are also nanometre-scale materials. Some of the earliest reported incidents of humans utilising nanotechnology were in the 4th-century A.D., when Roman glassmakers produced glasses, containing nanosized metals like gold and silver, which could change colour when light was passed through them. Another early use was making brightly coloured stained-glass windows in churches and cathedrals; metal nanoparticles were present in the glass. Photography (developed in the eighteenth/nineteenth century) is dependent on the production of light-sensitive silver nanoparticles from decomposing silver halides present in the film.

The material properties of solids are dependent on the size range in which they are measured. Properties observed on traditional size scales (mm – km) have been seen to change when measured in the micrometre-nanometre scale (μm – nm), including mechanical, ferroelectric and ferromagnetic properties.[5] Thus, controlling the properties of the nanoscale such as particle size, morphology and magnetism enables control of the desired properties of the bulk material. Commonly used materials for nanoparticles include metal oxides such as magnetite, polymers such as polystyrene, group IV elements like Si or Ge and semiconducting materials such as TiO_2 and CdS. The preparation of iron, platinum, cadmium, palladium, silver, copper, nickel and gold metal nanoparticles has also been reported.[6] They are typically made *via* the 'top-down' or 'bottom-up' methods. Top-down methods (such as ball-milling) involve miniaturising current methods to produce nanostructures, whereas 'bottom-up' processes (such as molecular self-assembly) involve the construction of nanostructures from smaller subunits, as far down as individual atoms.

An excellent review on the history of nanoparticles was written by Kreuter in 2007.[7] From this review, it can be seen that research into nanoparticles and nanotechnology really took off in the mid-to-late 1970's with scientists such as Birrenbach, Speiser and Kreuter all working together; employing various methods to synthesise nanoparticles for applications in drug

delivery[8-13] and later, nucleic acid, DNA fragments and gene delivery,[14] cancer therapy[15-20] and AIDS treatment.[21,22] Since these early developments, research into nanoparticles and their uses has increased significantly in the areas of bio-catalysis, bio-separations, bio-medicines and bio-sensors.[23] As with many newer areas in science, long-term safety and bio-compatibility of many nanoparticles have not yet been fully explored, prompting concerns and slight hesitation for society as a whole to fully accept nanotechnology, as outlined in the review by Albrecht *et al* in 2006.[24] Despite this hesitation, nanotechnology has been hailed as revolutionary, with the ability to impact on many areas including the economy, technology industries, military fields, medicine fields, sustainable technology development and the petrochemical industries.[24]

1.3 Introduction to Magnetism and Magnetite Nanoparticles

Magnetic materials have a magnetic field created by the motions of their electrons. A unified magnetic field can be produced in materials when the magnetic moments of the electrons align with each other. This field has a direction of flow and will attempt to align with an externally applied magnetic field. Alignment of magnetic moments in different types of magnetic materials can be observed in Figure 1.1, below.

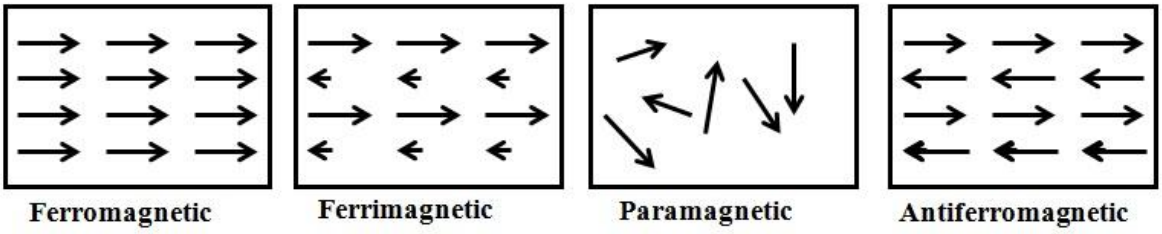

Figure 1.1: Alignment of magnetic moments (without the presence of an external magnetic field) in ferromagnetic, ferrimagnetic, paramagnetic and antiferromagnetic materials.[1] Diamagnetic materials are omitted as they have no magnetic moment. Superparamagnetic materials contain a single magnetic domain, which aligns with an externally applied magnetic field.

A more in-depth explanation of the types of magnetism will be discussed herein. The six types of magnetism are:

- **Ferromagnetism** – All magnetic moments contribute positively to the net magnetisation of the material. All magnetic moments are aligned; the materials possess a permanent magnetic field and can exhibit spontaneous magnetisation. They are the most

common type of known ‘magnetic material’. Examples of ferromagnetic materials are cobalt, iron, nickel and hematite, α-Fe_2O_3.

- **Ferrimagnetism** – Similar to ferromagnetism, but some of the magnetic moments are anti-aligned, subtracting from the net magnetisation of the material. They also exhibit spontaneous magnetisation and have a permanent magnetic field. Bulk magnetite (Fe_3O_4) is an example of a ferromagnetic material.
- **Paramagnetism** – Have close to zero net magnetic moment, but become slightly attracted to externally applied magnetic fields. They have randomly oriented magnetic moments and retain no magnetisation following the removal of the external magnetic field[25]. Most chemical elements are paramagnetic.
- **Diamagnetism** – Materials create an opposite magnetic field to one which is externally applied and are repelled by them (have no magnetic moment, retain no magnetisation following removal of the external magnetic field). Examples of diamagnetic materials are quartz, calcite, sodium chloride and water.
- **Antiferromagnetism** – Magnetic moments align in regular, opposite fashion (no overall bulk spontaneous magnetisation (when an external magnetic field is applied, a small amount of ferromagnetic behaviour is observed). Below 250 K, hematite is antiferromagnetic, becoming weakly ferromagnetic between 250-948 K and paramagnetic above 948 K.[26]
- **Superparamagnetism** – Occurs in ferri- or ferromagnetic nanoparticles. Superparamagnetism occurs in nanoparticles; due to their size they are composed of just a single magnetic domain, so the entire nanoparticle aligns with the applied field. Magnetic moments can flip direction at random, depending on temperature. The time it takes is called the Néel relaxation time. Without the presence of an external magnetic field, the Néel relaxation time is much shorter than the time used to measure the magnetisation and the net magnetisation is observed as zero – this phenomenon is called superparamagnetism. The materials can be magnetised *via* an external field, much more strongly than regular paramagnetic materials.[25] They retain no magnetisation when the external magnetic field is removed. Magnetite nanoparticles are an example of a superparamagnetic material, having different magnetic properties to bulk magnetite.[27]

It is crucial to explain why superparamagnetic materials, particularly magnetite nanoparticles, are of such interest. An advantage to using magnetic particles in general is that they can easily be separated from the reaction mixture by the application of an external magnetic field. This makes magnetic supports more attractive from both green chemistry and economical

standpoints because of increased recovery, re-usability and lifetime that can be obtained from bio-molecules immobilised on superparamagnetic nanoparticles. Their superparamagnetic properties allow them to remain relatively dispersed in suspension without being magnetically attracted to each other and aggregating.

The first reported use of magnetic separation was reported in 1973 by Robinson *et al*,[28] who used silica-coated iron oxide to immobilise α-chymotrypsin and β-galactosidase for applications in bio-reactors. Since this first reported use, magnetic separation has become an increasingly popular tool for separations involving bio-molecules.[29] Following this, potential applications of magnetic nanoparticles have been explored for over four decades. The following paragraph will detail the methods of synthesising magnetite (Fe_3O_4) nanoparticles, as they are the materials I have used and are of most relevance to this project.

1.4 Synthesis of Magnetite

Magnetite, Fe_3O_4, has an inverse-spinel structure. The unit cell consists of thirty-two oxygen atoms forming a face-centred-cubic (fcc) closed-packing structure, with iron cations located at octahedral and tetrahedral sites.[30,31] The unit cell edge length is 0.839 nm. The crystal structure can be written as $Fe^{2+}Fe^{3+}{}_2O_4$ where the Fe^{2+} ions and half of the Fe^{3+} ions occupy octahedral sites and the second half of the Fe^{3+} ions occupy the tetrahedral sites; i.e. $[Fe^{3+}]_{Th}[Fe^{3+}Fe^{2+}]_{Oh}O_4$, where Th represents tetrahedral sites and Oh represents octahedral sites. The characteristic black colour of magnetite arises from inter-valence charge transfer between octahedral Fe^{2+} and Fe^{3+} ions within the crystal structure.[31,32] The structure is shown in Figure 1.2, reproduced from reference 33.

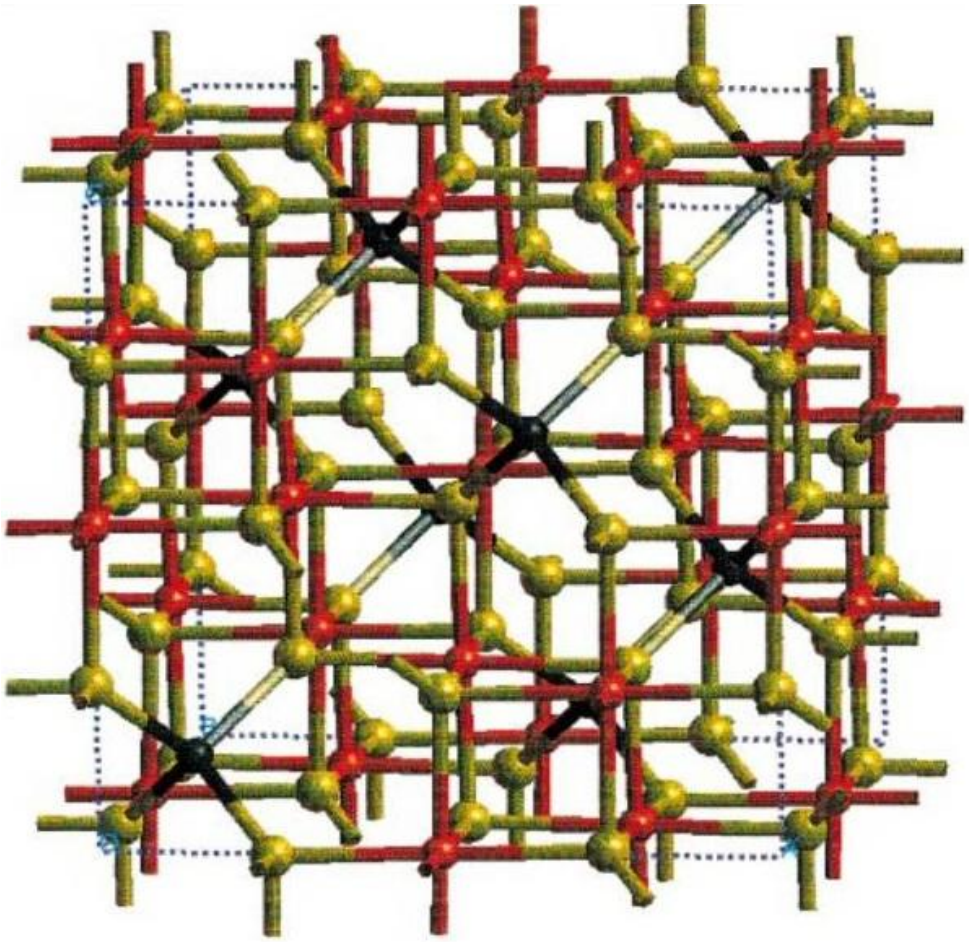

Figure 1.2: The crystal structure of magnetite, Fe_3O_4, reproduced from reference 33. The black spheres represent tetrahedral Fe^{3+} ions, red spheres represent octahedral Fe^{2+} or Fe^{3+} ions and the yellow spheres correspond to oxygen anions.

Sugimoto and Matijević first reported the synthesis of uniform, spherical magnetite particles (30 – 1100 nm diameter) using ferrous hydroxide gels in 1980.[34] An example of this is the synthesis of magnetite nanoparticles *via* the oxidative hydrolysis of iron sulphate in alkaline media.[29,34] Since then, many methods of synthesising magnetite have been developed with the aim of controlling particle size, morphology, stability and dispersity. These factors have been found to be dependent on the reaction temperature, pH, ionic strength of the media, ferrous/ferric (Fe^{2+}/Fe^{3+}) chloride ratio and the type of salts used.[35]

One simple, convenient method of magnetite synthesis is *via* co-precipitation of aqueous Fe^{2+}/Fe^{3+} salt solutions by adding base under inert atmosphere at various temperatures.[29,36-38] Materials made using this method tend to be quite poly-dispersed, possibly due to uncontrolled growth following nucleation and controlling the growth is crucial in the production of mono-dispersed nanoparticles. This can be done by using stabilising agents such as polyvinyl alcohol (PVA) .[39] Recently, studies have shown oleic acid to be the most

effective candidate for stabilising magnetite nanoparticles and is widely used for passivation of magnetite nanoparticle surfaces, producing mono-dispersed and highly uniform nanoparticles.[40]

Another method of synthesis commonly employed is thermal decomposition of organometallic compounds (such as iron choline citrate,[41] iron carbonate[42] and iron carboxylate[43]) with surfactants in organic media.[35,44]

An alternative method that allows control of the nanoparticle morphology and size is the microemulsion method (water-in-oil), which uses water droplets as nano-reactors in the oil phase, with surfactants (used to produce micellisation of the water droplets and dispersion of the nanoparticles).[45-47] Iron precursors are precipitated into the water phase within the micelles and not the organic/oil phase, as they are unreactive in the oil phase. Particle size is dictated by control of the water droplet size.[44]

In 2005, Wang *et al*[48] reported the hydrothermal synthesis of noble metal, magnetic, dielectric, semiconducting and rare-earth fluorescence nanocrystals using a three phase liquid-solid-solution (LSS) system. The reaction involved reduction of metal ions by ethanol at the interfaces between the solid (metal linoleate), liquid (ethanol-linoleic acid) and solution (water-ethanol) phases. The microwave hydrothermal synthesis of magnetite has also been reported.[49] This method produced nanoparticles of various sizes and shapes with extensive potential applications.

Other methods of nanoparticle synthesis include:

- Sonochemical[50]
- Biomimetic[51-53]
- Sol-gel[54]
- Electrochemical deposition[55]
- Physical methods such as aerosols,[56] ball milling[57] and gas phase deposition.[58]

Table 1.1 summarises the most commonly used methods of nanoparticle synthesis outlined earlier in this section (modified from Lu *et al*'s review entitled: Magnetic Nanoparticles: Synthesis, Protection, Functionalisation, and Application[35]).

For protection against oxidation, erosion by acidic/basic species and for increased stability in suspension, nanoparticles are typically either coated by an inorganic component (typically silica,[59] carbon[60] or precious metals[61,62]) to produce a core-shell structure, or coated with an organic shell (surfactants or polymers).[63,64] Oxidation of the magnetite core can affect the magnetic ability of the nanoparticles. The nanoparticles can also be dispersed or embedded into a polymer, silica or carbon matrix to form a composite structure. However, the nanoparticles are then fixed in the composite matrix and are not freely dispersible in reaction media. In the context of this project, silica coatings will be considered and explored.

Table 1.1: Summary of the four most common methods of nanoparticle synthesis outlined in this section.

Synthetic Method	**Synthetic Conditions**	**Typical Solvent**	**Particle Size Distribution**	**Shape Control**
Co-precipitation[29,36-40]	Simple, ambient conditions. 20-90ºC, reaction time of minutes. High yield, able to scale-up.	Water	Relatively narrow	Not good
Thermal Decomposition[41-43]	Complicated, inert atmosphere. 100-320ºC, reaction time of hours-days. High yield, able to scale-up.	Organic compound	Very narrow	Very good
Microemulsion[45-47]	Complicated, ambient conditions. 20-50ºC, reaction time of hours. Relatively low-yielding.	Organic compound	Relatively narrow	Good
Hydrothermal Synthesis[48,49]	Simple, high pressure. 220ºC, reaction time of hours-days. Moderate yield.	Water-ethanol	Very narrow	Very good

1.5 Silica Coating on Magnetite Nanoparticles

Coating magnetic nanoparticles with a silica shell protects the magnetite core from oxidation, erosion and unwanted interactions with species that are later linked to the silica surface such as bio-molecules. Silica coatings make the nanoparticles stable under aqueous conditions at low-neutral pH, bio-compatible, allow simple surface modification, shell thickness control and easy control of inter-particle interactions.[35] The main methods for silica coating are the Stöber method[65] and sol-gel methods.[36] The Stöber method (also a sol-gel method) is the base-catalysed synthesis of silica particles from alkoxysilanes. In this way, the polycondensation/polymerisation of silicic acid to form siloxane (Si-O-Si) bonds generates a silica sol (colloidal suspension) which polymerises into a colloidal silica gel when intra-molecular water is eliminated from the system.[66] These processes rely on the use of silicon alkoxides (such as TEOS) as the silica source; the silica coating is precipitated onto the magnetic nanoparticles in a basic ethanol/water mixture in the presence of ammonia.[67,68] Ethanol acts as a co-solvent in the reaction, with ammonia acting as morphological catalyst.[69]

Silica coatings can be either amorphous or mesoporous. Amorphous silica coatings, which are non-porous and non-crystalline, first reported by Philipse *et al* in 1994[36] *via* the sol-gel method, allow the nanoparticles' surface to retain a negative charge above silica's isoelectric point (~pH 2). Amorphous coatings are produced if no templating systems are present in the coating process. This provides applications in bio-separations by using electrostatic interactions to bind bio-molecules. In addition to this, the silica possesses silanol functional groups (Si-OH) which can be used to covalently bond to organosilanes in order to further functionalise the surface. Another method of amorphous silica-coating is *via* the deposition of silicic acid, which was reported on the large scale by Bruce *et al* in 2004.[29] Reverse microemulsion methods have been used to produce a coating as thin as 1 nm.[70]

In order to increase surface area, various routes have been taken to prepare magnetite nanoparticles with microporous (zeolites) and mesoporous silica shells. The first reported synthesis of mesoporous magnetite nanocomposites particles was reported by Wu *et al* in 2004.[71] They used CTAC micelles as molecular templates. In 2005, Zhao *et al* produced uniform magnetic nanocomposites spheres with a mesoporous silica shell.[72] They employed simultaneous sol-gel polymerisation of a silica source (TEOS) and a surfactant (*n*-octadecyltrimethoxysilane (C18TMS)) onto hematite (Fe_2O_3), followed by removal of the organic group. This method produced uniform mesoporous core-shell superparamagnetic

nanoparticles (~270 nm diameter) with high surface area and pore volume, which can be used for drug delivery applications. The template-assisted preparation of mesoporous silica-magnetite nanocomposites has been reported.[73] This was performed by adding a silica source (TEOS), a surfactant (CTAB) and a base (NaOH) to magnetite in water at room temperature, followed by slow titration to pH 7 with HCl. In 2009, Deng *et al*[74] combined sol-gel synthesis and vapour-phase transport to produce magnetic zeolites microspheres for the immobilisation of trypsin.

1.5.1 Applications of Silica-coated Magnetite Nanoparticles

A popular application of both colloidal silica and silica-coated nanoparticles is in the quick and efficient purification on DNA and RNA from biological samples.[66,75,76] At physiological pH values, silica is weakly acidic (as its isoelectric point is pH ~2), giving it a weakly negative surface charge[77] ($Si\text{-}O^-$ as opposed to Si-OH). In the presence of high concentrations of chaotropic salts (salts which disrupt and denature the structure of nucleic acids and destabilise hydrogen bonds), cations are able to form a stable layer around the negatively charged silica surface, effectively giving it a positive charge. DNA is actually quite stable in the presence of chaotropic salts and retains its negative charge in aqueous solution.[66] The phosphate groups present in the DNA 'backbone' are strongly acidic and are deprotonated in aqueous media at physiological pH values, having an overall negatively charged surface. As a result of this, DNA can bind effectively *via* the 'cation bridge' to the now positively-charged silica surface. The DNA out-competes other molecules to bind to the silica surface and they are left in solution. The newly formed DNA-silica complex is washed in either a salt solution or an ethanol/water mixture to remove impurities, which aren't as tightly bound as the DNA.[78] The purified DNA can then be eluted from the silica using a buffer containing low salt concentrations, or water. The mechanism is shown in Figure 1.3.

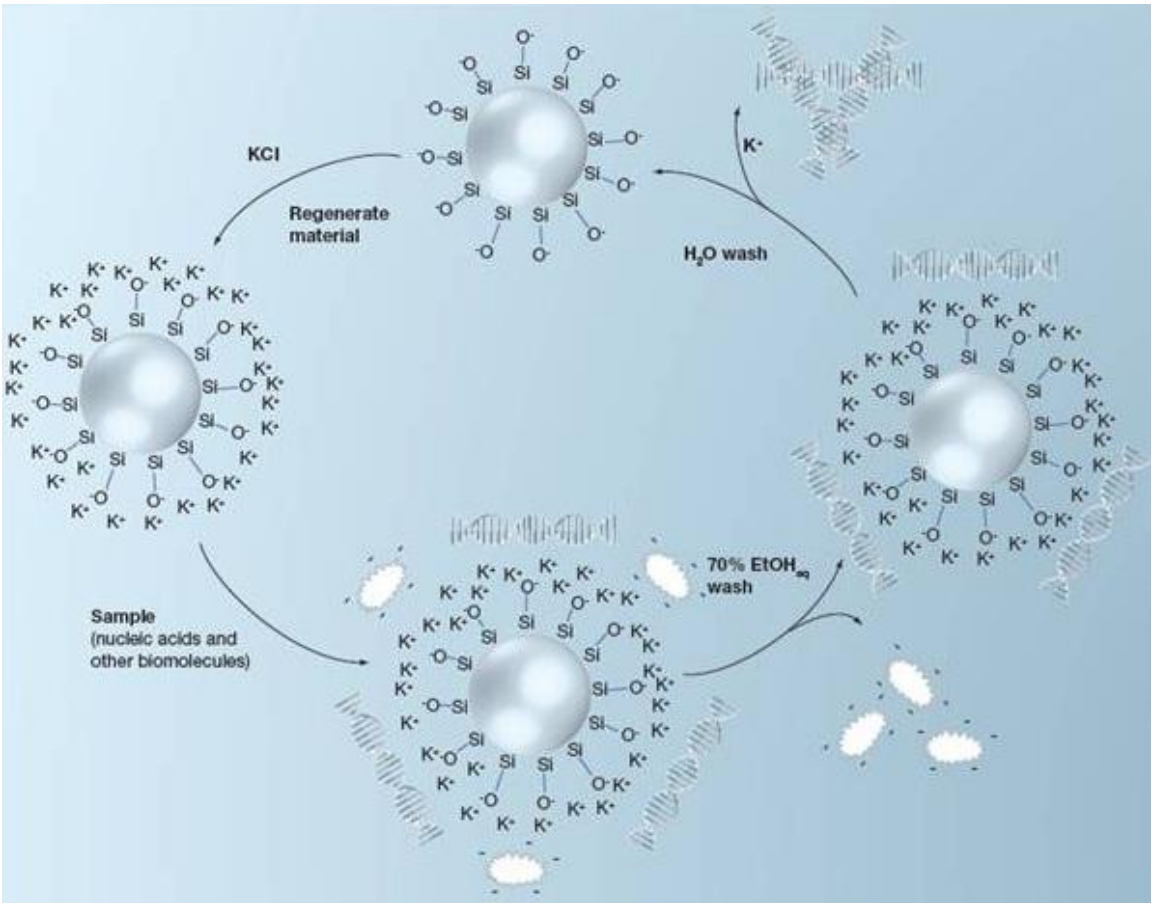

Figure 1.3: Purification of DNA using silica-coated nanoparticles under chaotropic salt conditions.[66] (Reproduced with the kind permission of Dr Tapas Sen).

In 2007, Deng *et al*[79] reported the synthesis of superparamagnetic high-magnetisation microspheres with an iron oxide core coated in amorphous silica which was then surrounded by a mesoporous SiO_2 shell for the removal of microcystins, which are very toxic heptapeptides, occurring in eutrophic waters. The microspheres were found to be effective absorbents for fast, convenient and efficient removal of microcystins with excellent recyclability and activity over at least 8 cycles.[79] For further applications in bio-catalysis, bio-separations and bio-sensors, the silica-coated surface can then be functionalised with surface-activating species (such as organosilanes) *via* the silanol functionality. Bio-molecules can then be immobilised/coupled/adsorbed on the surface of the silica-coated magnetic nanoparticles. The functional groups are not entrapped or sterically hindered close to the surface and instead they are able to interact with substrate species in the vicinity around the external surface. Surface functionalisation of nanoparticles is discussed in the next section.

1.6 Introduction to Surface Functionalisation of Core-Shell Nanoparticles

Manipulating the surface chemistry of any materials can lead to improvements in the way they interact with other materials. In the context of this work, organosilanes (particularly aminosilanes) are the most useful compounds for the surface functionalisation of silica-coated magnetic nanoparticles. They are useful as they can conjugate a wide selection of bio-molecules (such as enzymes, proteins and oligonucleotides) to surfaces which have amine or carboxyl groups present.[66] They are also readily available and easy to use.

Organosilanes are bi-functional reagents, identified by the chemical formula $X\text{-}(CH_2)_n\text{-}SiR_n(OR')_{3-n}$. X represents the headgroup, $(CH_2)_n$ is a flexible alkyl chain spacer group and the $Si(OR')_n$ groups are anchor groups which attach to the silanol hydroxyl groups on the silica surface following hydrolysis of the alkoxy (OR′) group. Aminosilanes are simply organosilanes possessing an amino group as the X functionality. They are commercially available and are commonly employed in the silanisation of surfaces by organic phase, aqueous phase or chemical vapour deposition processes.[80] Three commonly used aminosilanes for surface functionalisation [(3-aminopropyl)-triethoxysilane (APTS), (3-aminopropyl)-diethoxymethylsilane (APDS) and (3-aminopropyl)-monoethoxydimethylsilane (APMS)] are shown in Figure 1.4.

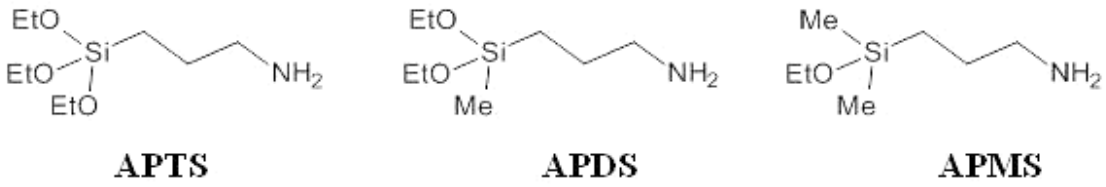

Figure 1.4: APTS = (3-aminopropyl)-triethoxysilane, APDS = (3-aminopropyl)-diethoxymethylsilane, APMS = (3-aminopropyl)-monoethoxydimethylsilane.

The headgroup can also be altered to be a vinyl, mercaptan, epoxy or halogen functionality. An example of this is a publication by Huang and Hu[81], who reported that surface modification of Si-MNP's with γ-mercaptopropyltrimethoxysilane can lead to fast, selective and efficient solid phase extraction of trace amounts of heavy metals in environmental/biological samples, prior to their determination by ICP-MS.[81] This is essential with respect to water purification as heavy metals are severely toxic to living organisms and can bio-accumulate in the food chain, so their removal from water and concentration measurement is of great importance.[82,83]

As aminosilanes are most commonly used, their mechanism of action will be described in further detail. The process of surface functionalisation with aminosilanes depends on two simultaneous reactions; (i) the hydrolysis of the *n* silane alkoxy groups ($Si(OR')_n$) to the corresponding reactive silanol species and (ii) the condensation of the resultant silanol species with the free hydroxyl groups on the silica surface to form stable Si-O-Si bonds. An example of this reaction scheme using APTS is shown in Scheme 1.1 below.

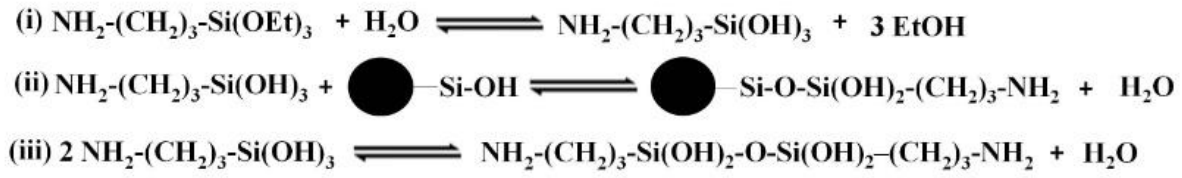

Scheme 1.1: Schematic representation of the (i) hydrolysis (ii) subsequent condensation onto silanol-functionalised surface and (iii) auto catalysed hydrolysis and polymerisation of APTS in water.

The third reaction (iii) represents the hydrolysis and spontaneous oligomerisation / polymerisation of APTS that occurs in water. This is auto-catalysed, due to the basic nature of the amino group and is a competing process with the condensation onto the silica-coated surface of the nanoparticles. As a result of this, APTS oligomerisation / polymerisation and condensation in water is largely uncontrolled and surfaces functionalised by APTS have a tendency to be multi-layered and disordered.[84] This process is much slower in organic solvents. The amino groups (either those of the free aminosilane or already bound aminosilanes) or silanol headgroups can also hydrogen bond to silanol groups on the nanoparticle surface during condensation, decreasing the effective amine density.[66] APTS possesses three alkoxy groups which can anchor to the silanol groups on the nanoparticle surface. Due to having three of these groups, APTS is believed to be more susceptible to intermolecular cross-linking reactions than both APDS and APMS, which have two and one alkoxy groups respectively.[85] The alkoxysilane groups in these two compounds are replaced by unreactive methyl groups, thus less intermolecular cross-linking between aminosilanes is achieved. In this way, the aminosilanes can bond to the surface of the nanoparticles in a more orderly fashion. Figure 1.5 represents what an ideal aminosilane-functionalised silica-coated nanoparticle surface should look like.

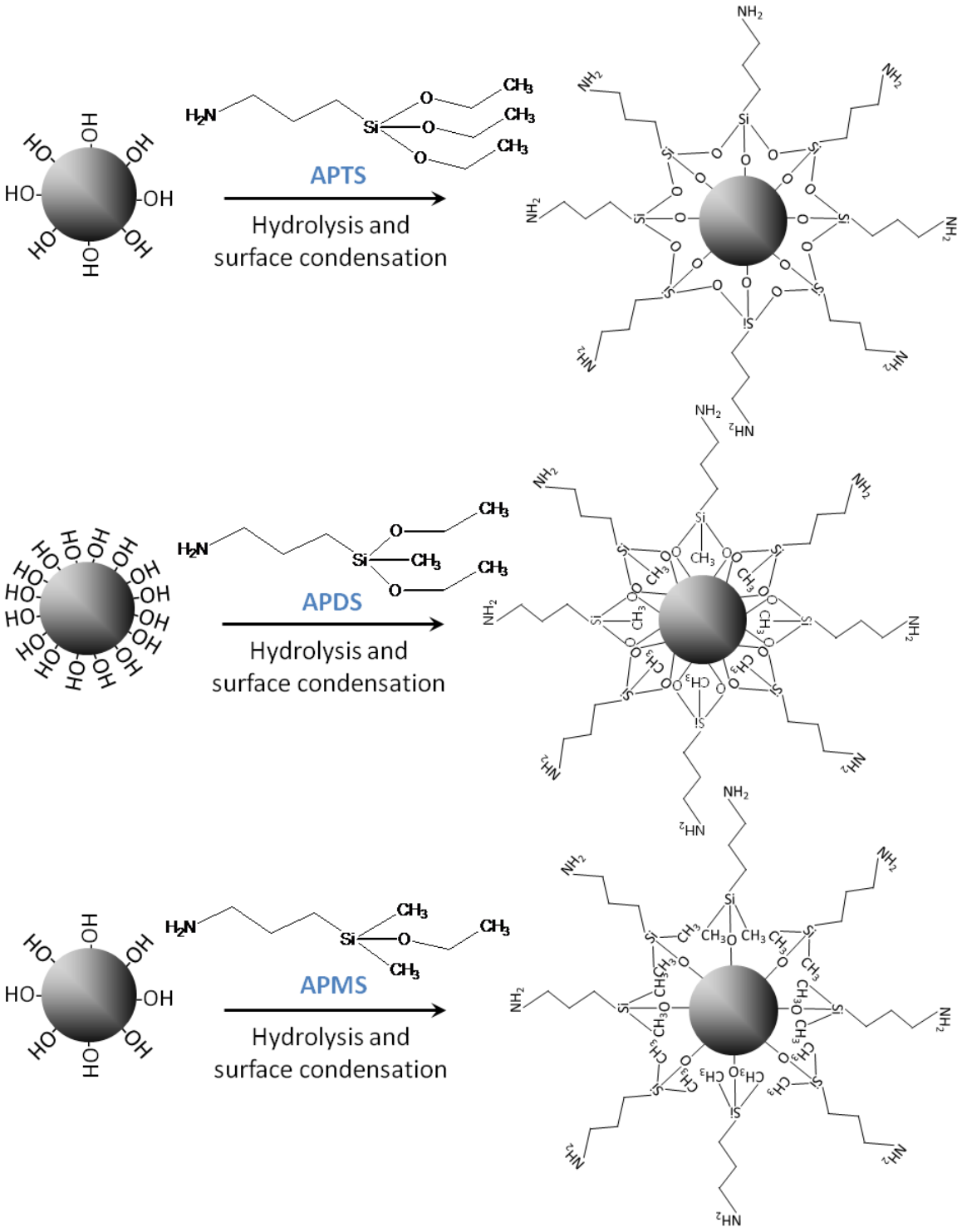

Figure 1.5: The 'ideal' orientation of aminosilanes on the surface of silica-coated nanoparticles. (Reproduced with the kind permission of Dr Tapas Sen).

As flat surfaces have only two dimensions, the surface functionalisation can be more controlled (often by ready elimination of water from the surface using a drying step) than in the three-dimensional nanoparticles. In the suspension phase, as well as oligomerisation / polymerisation of aminosilanes and hydrogen bonding to the surface, other interactions such

as nanoparticle aggregation can cause unforeseen problems and reductions in total surface amine density. Another competing process to condensation of the aminosilanes to the silica-surface of the nanoparticles is the multilayer formation of aminosilanes which results in the sequestration of amino groups away from the surface, hence making them unavailable for bio-molecule binding (shown below in Figure 1.6). Again these issues are prevalent in aqueous systems. A monolayer is the ideal scenario (shown above in Figure 1.5), in which case all of the aminosilane groups would not be cross-linked, hydrogen bonded or sequestered and all of the amino groups would be available to bind to bio-molecules.

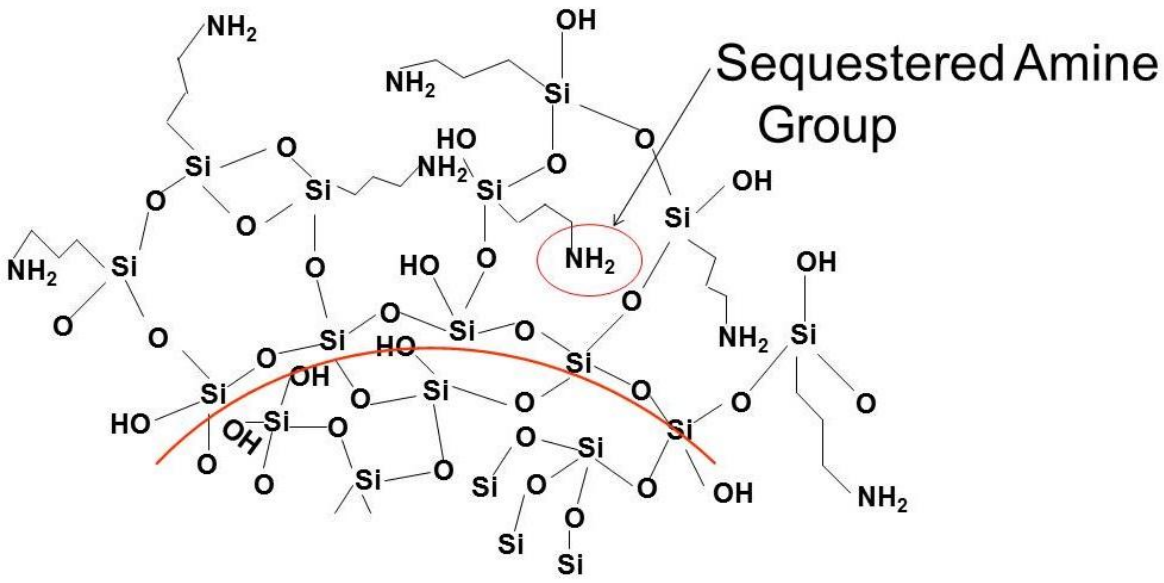

Figure 1.6: Demonstrating the sequestration of amino groups in a disordered multilayer aminosilane arrangement.[86,87] The red line represents a spherical nanoparticle surface.

In 1996, Moon *et al*[88] reported the comparison of four different aminosilanes (APTS, APDS, APMS and (4-aminophenyl)-trimethoxysilane (APhTS)) for producing uniform aminosilane thin layers on the flat surfaces of fused silica and oxidised silicon wafers. They measured the relative surface density of amine groups by ellipsometry and *via* a coupling reaction with 4-nitrobenzaldehyde (4-NBA) to form imine-bonded species which could be confirmed by UV-Visible spectroscopy. Following the coupling, the 4-NBA species could be removed by hydrolysis, which was also confirmed by UV-Visible spectroscopy. This assay was further developed by van de Waterbeemd[86] *et al* in 2010. In regard to nanoparticles in suspension, ellipsometry cannot be used so along with the detection of reversible coupling and hydrolysis of UV-Visible active reagents such as 4-NBA, chemical and elemental combustion analysis

methods can be used to provide information about the surface amine density and availability[86] (see Figure 1.7 below).

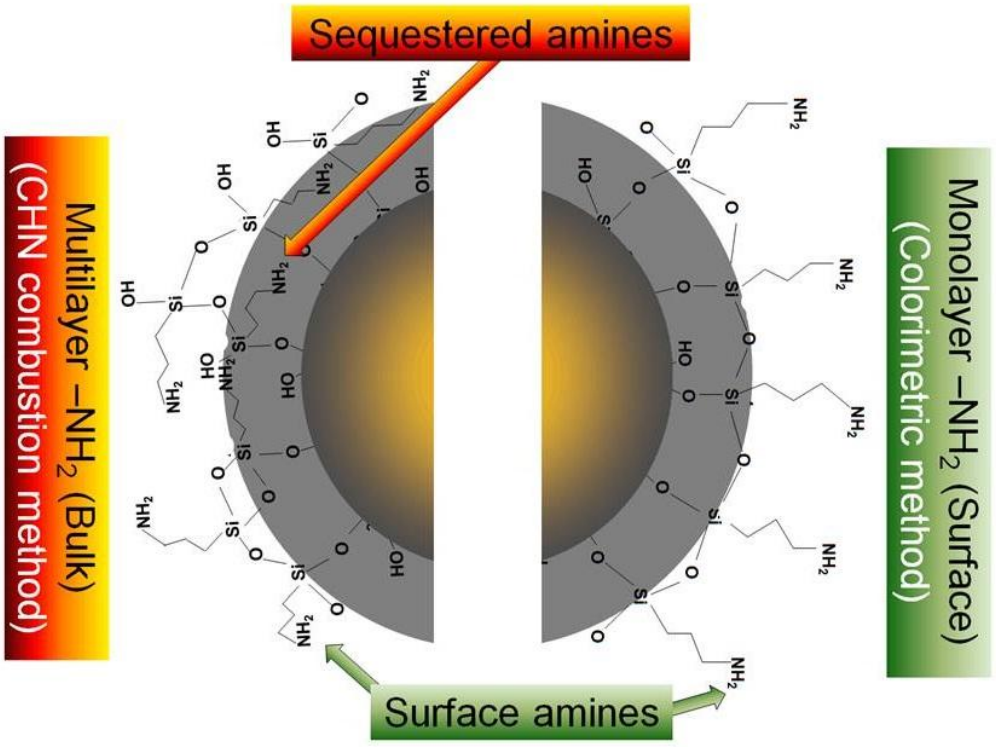

Figure 1.7: Total amine density, including sequestered amines, on the left side; identified by chemical and elemental combustion. The right side shows the surface amines which can be identified using the 4-NBA colorimetric assay. Comparison of the results obtained from both methods are used to calculate surface amine density and total amine density. (Reproduced with the kind permission of Dr Tapas Sen).

It was the combination of these two methods of analysis that allowed the improved understanding of surface and sequestered amino groups on the mono- and multi-layered aminosilane functionalised surface of nanoparticles.

Sen and Bruce recently reported the novel strategy of surface activation of nanoparticulates in suspension using a tri-phasic reverse emulsion (TPRE).[87,89] The TPRE system consisted of solid silica-coated magnetite nanoparticles (solid phase), surrounded by a surface water phase dispersed within an organic solvent phase (toluene), in the presence of a bio-compatible, non-ionic surfactant (Triton X-100). APTS was used as aminosilane and was found to be soluble, but did not hydrolyse or self-condense in toluene. It can only perform these reactions in the presence of water. By having just a small amount of adsorbed water on the nanoparticle surface, APTS could react in a much more controlled fashion, producing an ordered uniform layer on the surface. Dispersion of the nanoparticles in the TPRE avoids their aggregation

and spontaneous and uncontrolled polymerisation of APTS in water is eliminated. Amino-functionalised nanoparticles prepared by this method exhibited a higher surface to total amine density (>80%) than those prepared using bulk water phase surface functionalisation (20%). The materials were used for successful DNA grafting and capture in magnetic bio-separations.

As bio-molecules frequently possess surface amine groups, to allow for easier conjugation of bio-molecules to amino-functionalised surfaces, it is important for coupling reagents to be used to allow the coupling of two species.

1.6.1 Coupling Reagents for Bio-molecule Conjugation

The crosslinking of enzymes to supports typically happens *via* the amino groups of enzyme residues on the enzyme/protein surface. Coupling reagents such as glutaraldehyde and glyoxyl groups are used to change aminosilane-functionalised surfaces to an aldehyde functionality, to allow the covalent cross-linking to other amino-groups. Carbodiimide reagents can be used to couple surface carboxyl groups with amino groups, producing stable secondary amines/amides.[90,91] They do this by activating carboxyl groups in water, allowing them to react with amine groups. Highly reactive groups used to immobilise proteins *via* aldehyde surface modification, such as glutaraldehyde and cyanogen bromide, can bind the enzyme to the support in mild conditions (physiological pH, ambient temperature). This suggests immobilisation involves exposed residues that are reactive at these pH values such as terminal amino groups. Due to their high reactivity, these reagents become unstable at alkaline pH values. As a result, proteins are mainly immobilised with these reagents by a single point covalent attachment *via* the terminal amino group at neutral pH. The attachment is formed due to formation of an imine bond, or Schiff base (R-CH=N-R′).

Glutaraldehyde is the most popular and widely used reagent for surface activation and subsequent bio-molecule immobilisation. It is a linear, 5-carbon di-aldehyde (CHO-$(CH_2)_3$-CHO) homo bi-functional coupling reagent which also converts surface amine groups to aldehydes.[92] It permits cross-linking of the bio-molecule (primarily with terminal amine groups[66]) to the support *via* a single, strong imine bond. Glutaraldehyde can be used at slightly acidic and neutral pH values, making it useful and convenient. Examples of glutaraldehyde being used as a coupling/crosslinking reagent for immobilising enzymes are numerous.[93-98] Scheme 1.2 shows the cross-linking process using glutaraldehyde to cross-link

enzymes onto hierarchically ordered porous magnetic nanocomposites reported by Sen *et al.*[99,100] The efficient coupling of bio-molecules for various applications can then take place. The first of these bio-molecules to be discussed will be enzymes.

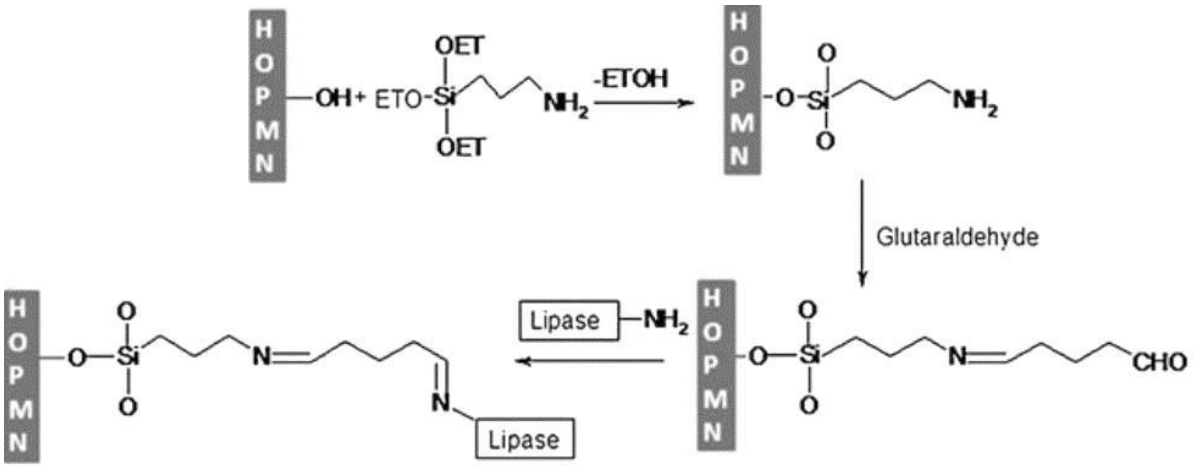

Scheme 1.2: The cross-linking process using glutaraldehyde to cross-link enzymes onto hierarchically ordered porous magnetic nanocomposites[99,100].

In contrast to the reagents which work optimally in neutral pH and ambient conditions is glyoxal, a two-carbon di-aldehyde (CHO-CHO), which has also been used to activate support surfaces for the immobilisation of various bio-molecules; primarily enzymes.[101-103] Immobilisation only proceeds in alkaline conditions and slight changes in pH and temperature lead to big reductions in immobilisation rate. The support must be highly activated before immobilisation and immobilisation is *via* multiple points, as the amino-glyoxyl bond is very weak. Compounds with a single amino group do not undergo a significant amount of immobilisation to glyoxyl supports. At alkaline pH values, lysine (Lys) residues become more reactive. As Lys residues possess two amine groups, glyoxyl groups can immobilise proteins *via* these points, so they are immobilised in the areas which have the highest density of Lys residues on the surface (shown below in Figure 1.8). This can be advantageous as immobilisation may be directed towards the area of the enzyme/protein where multipoint covalent bonding is most likely and hence, stabilisation can be achieved.[104] Conformation and biological activity is preserved as the Lys residues are typically on the outer surface of the enzyme structure, away from the active site and thus are not as affected by steric hindrances.

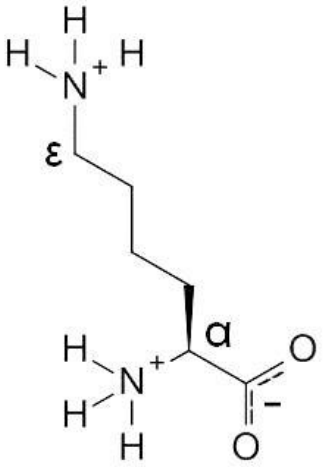

Figure 1.8: Lysine residue containing the ε- and α-amino groups.

Imine bonds are quite sensitive to hydrolysis, so stability can be improved by selective reduction with sodium cyanoborohydride ($NaBH_3CN$), forming a stable secondary amine[66]. As glutaraldehyde possesses the ability to work at acidic-neutral pH values, ambient conditions and its commercial availability and ease of use, it is the coupling reagent that I have chosen to utilise for the purposes of this study for the immobilisation of both enzymes and oligonucleotides. The following section introduces the concepts of enzymes; and their applications as bio-catalysts.

1.7 Introduction to Enzymes and Bio-catalysis

Enzymes are natural proteins which catalyse chemical reactions. Their molecular weight can vary from several thousand to several million, but they can catalyse reactions on molecules as small as nitrogen and carbon dioxide.[105] They catalyse chemical reactions by lowering transition-state energies and energetic intermediates by increasing the ground-state energy. The initial phase of an enzyme-catalysed reaction is the formation of an enzyme-substrate (E·S) complex *via* binding of the substrate to the catalytic active site (this E·S complex is also known as the *Michaelis* complex).[105] The active site is made up of around a dozen amino acid residues, of which only two or three are directly involved in the substrate binding and catalysis of the reaction. It is thought that the rest of the enzyme structure is needed to maintain the structural integrity of the active site for optimal substrate binding and catalysis. In addition to accelerating the rate of chemical reactions, enzymes are also selective and have high specificity. The transition state is extremely short-lived and high-energy. It is bound around 10^{12} times more tightly than the substrate or products and once bound, the enzyme

catalyses the conversion of substrates to products, forming an enzyme-product (E·P) complex, *via* various mechanisms including approximation, desolvation; as well as covalent, electrostatic and general acid/base catalysis.[105] This is another tightly-bound, high-energy, short-lived transition-state complex. Following formation of the E·P complex, the interactions present in stabilising the transition-state complexes are no longer present and the now poorly bound products are expelled from the active site. This can also be due to repulsive interactions between the products and active site residues, triggered by changes in electronic distribution due to bond breakage/formation, leading to opening of the active site and product expulsion.[106]

The basic kinetics and mechanism of an enzyme-catalysed reaction is shown in Scheme 1.3.

$$E + S \underset{k_{-1}}{\overset{k_1}{\rightleftharpoons}} E{\cdot}S \overset{k_2}{\rightleftharpoons} E{\cdot}P \longrightarrow E + P$$

Scheme 1.3: General mechanism for enzyme-catalysed reactions. E represents the enzyme and S represents the substrate. k_1 denotes the rate constant of formation of the E·S complex, k_2 denotes the rate constant of formation of the E·P complex and k_{-1} denotes the rate constant of breakdown of the E·S complex.[105]

The stability of the E·S complex is related to substrate's affinity towards the enzyme and is measured by its K_S value. This is called the dissociation constant of the complex, calculated by the equation in Scheme 1.4 below:

$$K_S = \frac{k_{-1}}{k_1}$$

Scheme 1.4: Definition of the dissociation constant, K_S, of an enzyme-substrate complex.[105]

If the rate of E·P complex formation is much greater than the rate of dissociation of the E·S complex, then k_2 can be called k_{cat} (catalytic rate constant) and K_s becomes K_m (Michaelis-Menten constant). The catalytic rate constant, k_{cat} represents the 'turnover number': the maximum number of substrate molecules converted to product molecules per active site per unit time (typically around 10^3 s^{-1}, ~1000 molecules per second are converted to product from substrate).[105]

Enzymes have several important functions in nature. In humans and animals, protein kinases and phosphatases are involved in cell regulation and signalling[107] and myosin enables muscle contraction *via* the hydrolysis of ATP.[108] In digestion, carbohydrases and amylases break down carbohydrates and starch (*via* hydrolysis of starch chains into smaller molecules which

can be absorbed in the intestines), proteases break down proteins into small peptides and amino acids (*via* hydrolysis of peptide bonds in polypeptide chains that link amino acids) and lipases break down lipids (*via* hydrolysis of triglycerides to free fatty acids and glycerol). In viruses, integrases are produced to allow the genetic material of the virus to be integrated into the infected cell's DNA.[109] Neuraminidase allows the viral release of the influenza virus from cells.[110] Herbivores produce cellulase in their ruminating chambers to allow the breakdown of cellulose in plants and grasses to β-glucose. In the second stage of photosynthesis in plants (The Calvin Cycle), ribulose-1,5-biphosphate carboxylase oxygenase (RuBisCO) catalyses the fixation of atmospheric carbon dioxide (carboxylation) to RuBP, causing its breakdown to phosphoglyceric acid (PGA), which is then converted to phosphoglyceraldehyde and is further broken down into energy-rich sugars, fatty acids and amino acids.[111] RuBisCO is thought to be the most abundant protein on Earth.

1.7.1 General Applications of Enzymes

Enzymes are widely used in the chemical industry for homogeneous catalysis as a result of their high chemo-, regio- and enantioselectivity. Within the pharmaceutical industry, increased demand for new, more potent drugs and medicines has opened the door for the exploration of novel methods of efficient stereoselective synthesis and since the mid-to-late 1990's,[112] bio-catalysis using enzymes has been seen to be the answer. In a review by Roberts,[113] a vast range of useful enzyme-catalysed reactions are explored, such as hydrolysis,[93,114,115] esterifications,[116-118] oxidations,[119-121] carbon-carbon bond formations[122,123] and bio-transformations.[124,125] Roberts also remarked that due to the wide variety of enzymes that are readily available and the reactions being relatively easy to scale-up, the use of enzymes in bio-catalysis is "one of the most powerful techniques for the preparation of optically active compounds using asymmetric catalysts." It is also important to mention that as well as being efficient and selective bio-catalysts, enzymes typically require mild reaction conditions and produce much less waste and harmful by-products than other catalysts, making them a more attractive option for chemical synthesis. The most widely used group of enzymes for such applications are lipases, which are discussed in the following section.

1.7.2 Lipases: Structure, Function and Activation

Lipases, also known as triacylglycerol hydrolases (E.C. 3.1.1.3), are one of the most popular classes of enzymes used for bio-transformations and are ubiquitous; found in most living

organisms.[126,127] In nature, they are used to digest, transport and process fats, oils, triglycerides and other lipids,[128] and function by catalysing the hydrolytic cleavage of triglycerides into fatty acids and glycerol at water-lipid interfaces. In the weight loss industry, lipase-inhibitors such as Orlistat® are used to inhibit gastric and pancreatic lipases in the gastrointestinal tract to decrease dietary fat adsorption.[129] Under micro-aqueous conditions, lipases have the unique ability to carry out esterification, alcoholysis and acidolysis reactions on various esters at the water-lipid interface.[130] Table 1.2 below illustrates the reactions that lipases catalyse.

Table 1.2: Basic mechanisms of various lipase-catalysed reactions. Reactions (ii)-(v) are classified as transesterification reactions.

Reaction Type		**Scheme**
(i)	**Hydrolysis**	$R_1COOR_2 + H_2O \longleftrightarrow R_1COOH + R_2OH$
(ii)	**Esterification**	$R_1COOH + R_2OH \longleftrightarrow R_1COOR_2 + H_2O$
(iii)	**Interesterification**	$R_1COOR_2 + R_3COOR_4 \longleftrightarrow R_1COOR_4 + R_3COOR_2$
(iv)	**Alcoholysis**	$R_1COOR_2 + R_3OH \longleftrightarrow R_1COOR_3 + R_2OH$
(v)	**Acidolysis**	$R_1COOR_2 + R_3COOH \longleftrightarrow R_3COOR_2 + R_1COOH$

Lipases are serine hydrolases belonging to the α/β-hydrolase fold superfamily,[131] possessing a core structure of a central, mostly parallel β-pleated sheet (consisting of 8 β-strands) flanked on each side by α-helices[131](only the second β-strand is anti-parallel). They hydrolyse ester bonds using a catalytic triad comprising of a nucleophillic residue (serine), an acidic residue (aspartate/glutamate) and histidine in the active site. The structure of the α/β-hydrolase fold is shown below in Figure 1.9.[132]

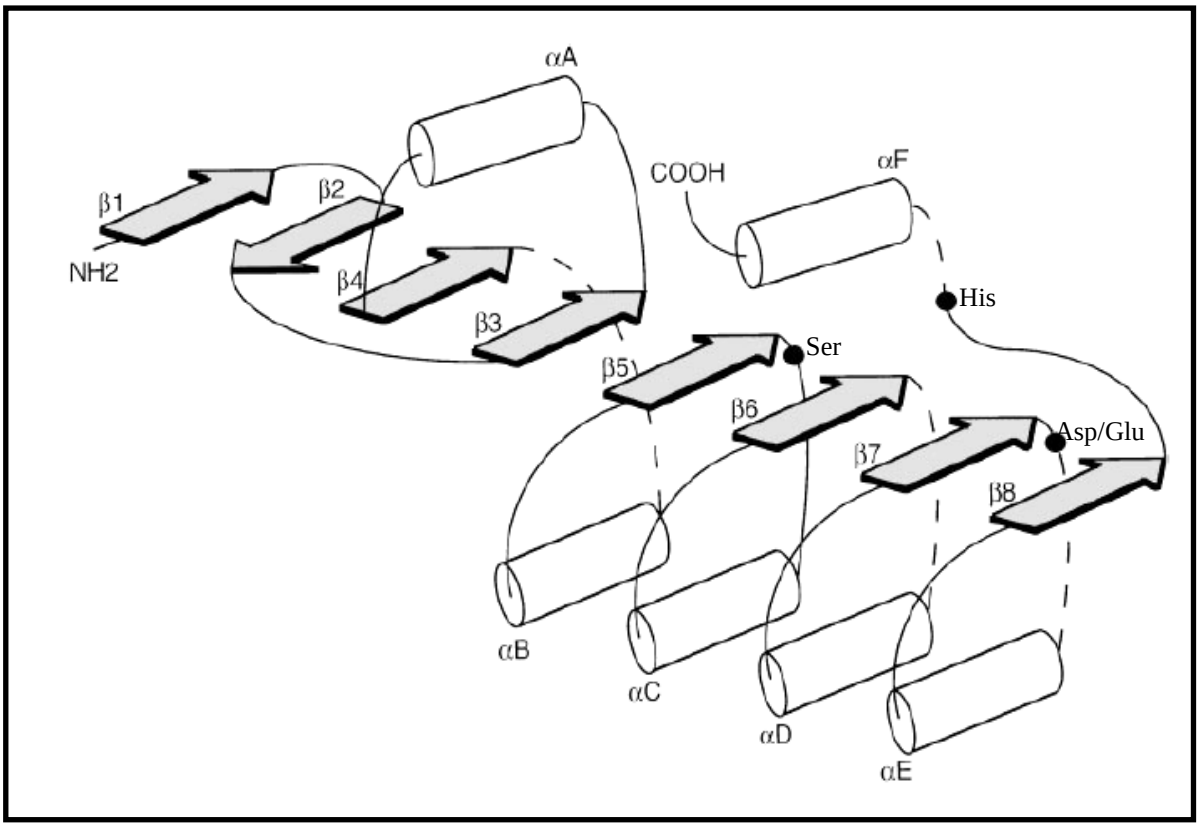

Figure 1.9: The structure of the α/β-hydrolase fold. α-helices are shown by cylinders; β-sheets are shown by arrows. Reproduced from Ollis *et al* (1992).[131,132]

The serine residue is located in a highly conserved Gly-X-Ser-X-Gly pentapeptide sequence (X = unspecified amino acid residue), forming a sharp turn between the β5-strand and the αC-helix. As close contact exists between the residues in the highly conserved sequence, one or often both of these residues in these positions are small glycine groups. It is this β-strand-nucleophile-α-helix arrangement which is termed the 'nucleophile elbow'.[126,133,134] The tightness of this arrangement forces the nucleophillic residue (serine) to adopt "energetically unfavourable mainchain torsion angles",[135] imposing a steric hindrance on residues in the immediate vicinity. The nucleophile elbow's geometry also aids the formation of the 'oxyanion hole', formed by two backbone nitrogen atoms around the active site which helps to stabilise the negatively charged transition state species formed during hydrolysis. In a mechanism known as the charge relay system, the nucleophillic serine residue is activated by hydrogen bonding to the histidine and aspartate/glutamate residues.[136, 137] The mechanism for the charge relay system is shown in Figure 1.10.

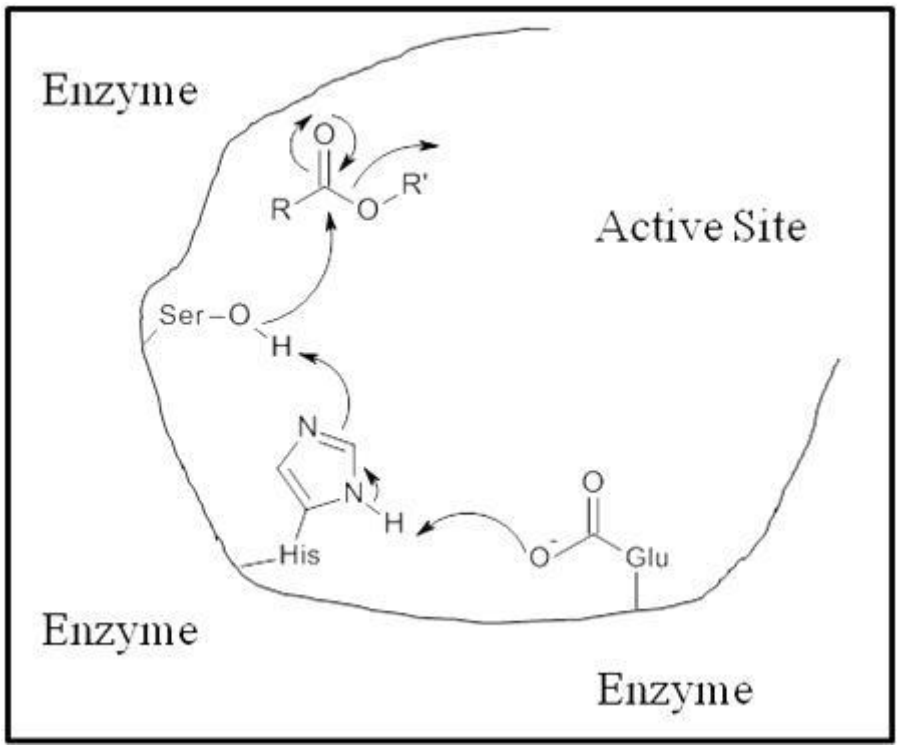

Figure 1.10: Active Site Charge Relay System with Serine activation (adapted from reference 136).

A structural feature found in many lipases is that of a 'lid' composed of either one or two amphiphillic α-helices that cover the active site, blocking substrate access in its closed conformation. The side of the lid facing towards the active site is hydrophobic and the side facing away is hydrophilic, stabilised by protein surface interactions.[136] In the closed conformation, the hydrophilic surface is exposed to water solvation and the hydrophobic surface facing the active site is hidden by the lid.[137] Interfacial activation is caused by reorientation of the α-helix lid by increasing the hydrophobicity of the surface in the immediate area surrounding the active site, exposing a large hydrophobic area which can interact with the hydrophobic interface and the catalytic triad becomes accessible to the hydrophobic substrate (see Figure 1.11). In 2009, Reis *et al* published a review which addresses the reactions involving lipases which take place at interfaces, interfacial engineering and properties, limitations and their bio-catalytic applications.[138]

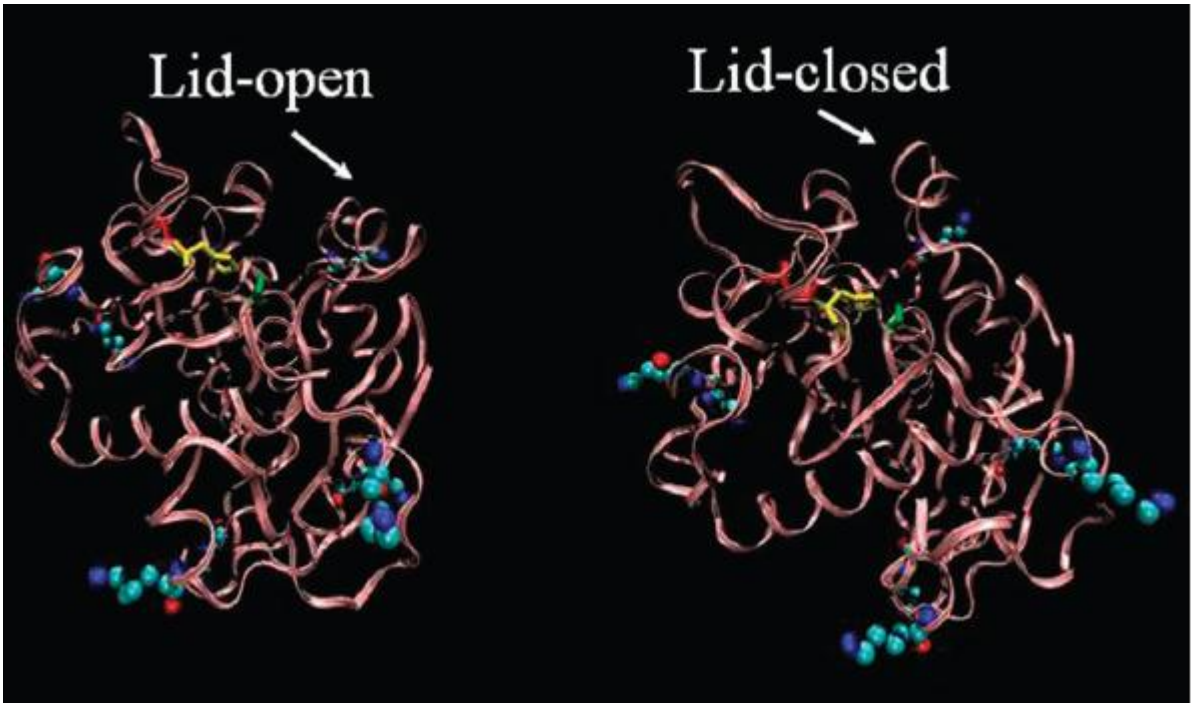

Figure 1.11: Computer simulations of the open-active and closed-inactive structures of *Thermomyces lanuginosus* lipase (TLL). The left side of the diagram depicts the open-active conformation and demonstrates how the lid position changes to expose the catalytic triad of the active site (Ser = green, His = yellow, Asp = red). The right side illustrates the closed-inactive conformation. Surface Lys residues are visualised using a space-filling modality, indicating the positions most likely to be involved in covalent binding to functionalised supports. Adapted from Hanefield *et al*'s review on Understanding Enzyme Immobilisation.[137]

Lipases require no cofactors to function, are commercially available and are easy to handle. They are typically prepared for commercial use by cultivation of microorganisms or by extraction from plant/animal tissue.[139] Microbial lipases are easier to manipulate *via* genetic engineering (or directed evolution[130]) and can be grown year-round on relatively inexpensive media. Their production is convenient, safer and they are more stable than their plant- and animal-derived equivalents, making them more desirable.[140] Bacterial strains are generally favoured over yeasts as enzyme sources, offering higher activity, being thermostable and having neutral or alkaline pH optima. Microbial cells also have short generation times, simple nutritional needs, easy screening for desired characteristics and can be genetically or environmentally manipulated to increase their yield and enzyme activity.[140,141]

1.7.3 Bio-catalytic Applications of Lipases

Lipases are widely used catalysts for the hydrolysis of oils/fats and the synthesis of esters. There have been many reviews published on their bio-chemical properties,[130,142] industrial

applications[140] and overall applications as bio-catalaysts.[132,136,139,143-145] The following section will serve to outline a few of the bio-catalytic applications that utilise lipases.

In the pharmaceutical industry, lipases are commonly used as chiral catalysts in the synthesis of fine chemicals and pharmaceutical compounds. An example of this is in the synthesis of enantiopure secondary alcohols, which are used as intermediates in the synthesis of many drug molecules, such as Dorzolamide, an antiglaucoma drug.[128] They also exhibit high enantioselectivity by successfully recognising enantiomeric molecules/enantiotopic groups on prostereogenic molecules,[146] which is useful as they can be used to kinetically resolve racemic chiral compounds with a theoretical yield of 50%. In the case of prochiral compounds, they can achieve asymmetrisation with a reasonable yield.[146] It has been found that enantioselectivity of lipases can be improved *via* crosslinking,[147] crystallisation,[148] organic solvent pre-treatment[149,150] and lipid coating,[151] amongst other methods.[152] Consequently, due to their high enantioselectivity, lipases are seen as important bio-catalysts for enantiopure building blocks in the production of commercially available organic compounds.

Two particularly important lipases, with respect to this project, are *Candida Rugosa* Lipase (CRL) and *Pseudomonas Fluorescens* Lipase (PFL). *Candida Rugosa* is a non-sporogenic, unicellular, non-pathogenic yeast that synthesises and secretes a mixture of at least five iso-enzymes. Each of the secreted iso-enzymes possesses a single 543-amino acid polypeptide chain and a molecular weight of around 60 kDa.[153,154] It's active site has been extensively studied and characterised and it's catalytic triad consists of the Ser-209, Glu-341 and His-449 residues.[155] CRL claims more applications than any other bio-catalysts and there have been many publications concerned with its molecular biology and structure,[154] catalytic mechanism,[156] interfacial activation,[155] and bio-catalytic applications (see Table 1.3 and following section).

Pseudomonas Fluorescens is a rod-shaped, Gram-negative bacterium that produces *Pseudomonas Fluorescens* Lipase (PFL). *Pseudomonas* lipases are classed in three groups depending on amino acid homology and biological properties.[142,157] PFL belongs to the sub-family I.2 of *Pseudomonas* lipases,[158] and contains a 475-amino acid polypeptide chain. Fernández-Lorente *et al* have reported that PFL has a molecular weight of 33 kDa at low enzyme concentrations, but has a tendency to aggregate into more stable, more

enantioselective, but less catalytically active bi-molecular structures of around 66 kDa molecular weight.[159] The reduction in activity of the bi-molecular structure is thought to be due to the aggregation occurring between the hydrophobic regions surrounding the active centres of the two uni-molecular structures in their open form, suggesting that interfacial activation competes with formation of the bi-molecular structure. Though the structure of its active site is much less studied than that of CRL, as PFL is also an α/β-hydrolase, the catalytic triad is still confirmed to contain the characteristic Ser-His-Asp/Glu residues. Literature on PFL is less abundant than that on CRL and although there are publications on the structures of other Pseudomonas lipases,[160] currently the exact 3-dimensional structure of PFL is not known.[161] However, there have been publications regarding its growth and isolation,[162,163] purification and characterisation,[164-166] physiochemical properties[167] and bio-catalytic applications (see Table 1.3 and the following section).

A review by Gandhi in 1997[144] addressed the many hundreds of catalytic applications that lipases have in industry. Some of the applications of free CRL and free PFL have been picked out and are described in Table 1.3 below.

Table 1.3: A selection of the catalytic applications of CRL and PFL outlined in Gandhi's review[144].

Lipase	Application	Reference
CRL	Hydrolysis of fish oil to concentrate polyunsaturated fatty acids	168
	Enantioselective esterification of racemic ibuprofen	169
	Hydrolysis of milk fat (butter oil)	170
	Kinetic study of the hydrolysis of triacetin	171
	Esterification of sugars in the enzymatic synthesis of carbohydrate esters of fatty acids	172
	Transesterification of vinyl acrylate to produce acrylic esters	173
	Enzymatic hydrolysis of olive oil to produce glycerol and fatty acids	174
PFL	Hydrolysis of racemic methyl-branched octanoic acid thioesters to determine stereoselective mechanism of action	175
	Regioselective deprotection of 3′,5′-O-acylated pyrimidine nucleosides	176
	Synthesis of low molecular weight esters in non-aqueous systems (CRL also used in this study)	177
	Intramolecular esterification (direct lactonisation synthesis of cyclopentadecanolide from 15-hydroxypentadecanoic acid)	178
	Regioselective acylation of 2′ deoxypyrimidine nucleosides with an acid anhydride in dry apolar solvents	179
	Preparation of a chiral building block based on 1,3-*syn*-diol and its application to the synthesis of a hunger modulator	180

A further search of the literature reveals that CRL has been used extensively as a bio-catalyst for more applications including:

- Esterification of methyl branched carboxylic acids for the resolution of citronellic acid.[181]
- Hydrolysis of racemic methyl esters (such as naproxen) in supercritical CO_2.[182]

- Preparation of L-amino acyl esters of various carbohydrates.[183]
- Enhancement of enantioselectivity for the chiral resolution of carboxylic acids in organic solvents.[184]
- Stereoselective esterifications of relatively short chain primary alcohols[185] and hundreds of similar applications to the ones listed.

In addition to the applications reviewed by Gandhi,[144] PFL has been commonly used in other applications such as the enantioselective hydrolysis of a selection of 3-(2-nitrophenoxy) butanoates,[186] exhibiting enantiomeric excesses greater than 99.9%. The use of PFL has been reported in the enzymatic resolution of various fluorinated arylethyl chloroacetamides *via* alcoholysis of the chloroacetamide group (using *n*-amyl alcohol in diisopropyl ether), with high enantioselectivity[187] (E = 25 to >100). This is an important application as the trifluoromethyl group is commonly used in organic chemistry due it's substantial electron-withdrawing ability and small size combining to stabilise small rings and change the reactivity and regioselectivity of substituted compounds.[187] Intensity and fastness of dyes increases in the presence of a $-CF_3$ group and optically active α-trifluoromethlyated amines are useful building blocks in the synthesis of pharmaceuticals, so increased yield, resolution and rate of reaction inferred by PFL is extremely beneficial to this reaction. Another application of PFL has been in the kinetic resolution of phenothiazine-based ethanol derivatives, which are pharmaceutically important and are known for their important biological activity.[188,189] Other applications of PFL include (but are not limited to):

- Preparation of optically active 4,4,4-trifluoro-3-(indole-3-) butyric acid, which is a novel plant growth regulator.[190]
- Selective enrichment of C_{18}-C_{20} acyl-chain polyunsaturated fatty acids from sardine oil.[191]
- Irreversible and highly enantioselective acylation of 2-halo-1-arylethanols in organic solvents.[192]
- Interesterification of butter fat.[193]
- Enantioselective transesterification of 2-methyl-1,3-propanediol derivatives in organic solvent.[194]

CRL and PFL have both been employed to catalyse transesterification synthesis reactions of citronellyl esters, which are used as a flavouring agents,[195,196] giving fruity and floral aromas.

The transesterification synthesis of citronellyl acetate, catalysed by CRL, PFL and many other enzymes was reported by Xiong *et al*[196] and is shown in Scheme 1.5 below.

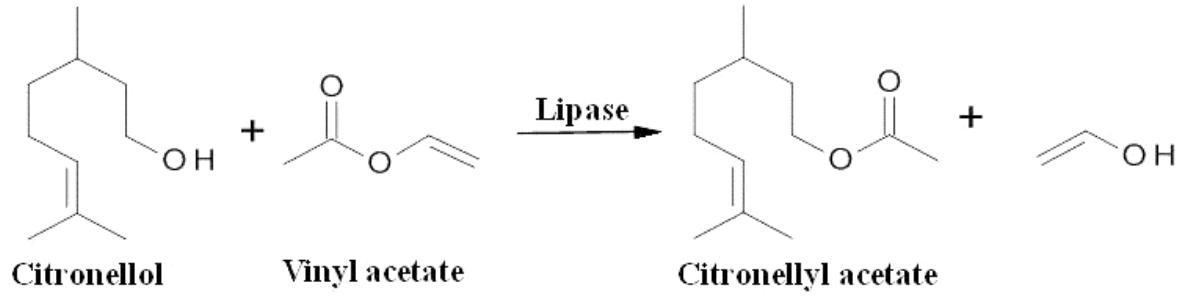

Scheme 1.5: The transesterification synthesis of citronellyl acetate from citronellol and vinyl acetate. PFL obtained yields of up to 99.4% conversion, whereas CRL only achieved up to 20.4%.

Another area of developing interest is in the lipase-catalysed production of biodiesel. Biodiesel consists of fatty acid methyl esters which are typically derived from the transesterification of triglycerides with methanol. In 1999, Ma and Hanna published 'Biodiesel production: A review' which summarised the most common methods of synthesis and addressed the emerging use of lipases as bio-catalysts for the application.[197] In 2001, Fukuda *et al* published an article covering biodiesel production by transesterification of oils,[198] though this was only one of many. This area is attractive to industry as both the fatty acid products and glycerol by-products are easy to recover and have commercial applications.[199,200] Kaieda *et al* have reported that methyl esters synthesised *via* methanolysis of plant oil are potentially important as biodiesel fuels.[201] They used both CRL and PFL (and also *Pseudomonas cepacia* lipase) to catalyse the methanolysis of soybean oil in aqueous conditions, remarking that all lipases exhibited particularly high catalytic ability for the application. A general and basic schematic representation of the enzyme-catalysed production of biodiesel is shown below in Scheme 1.6.

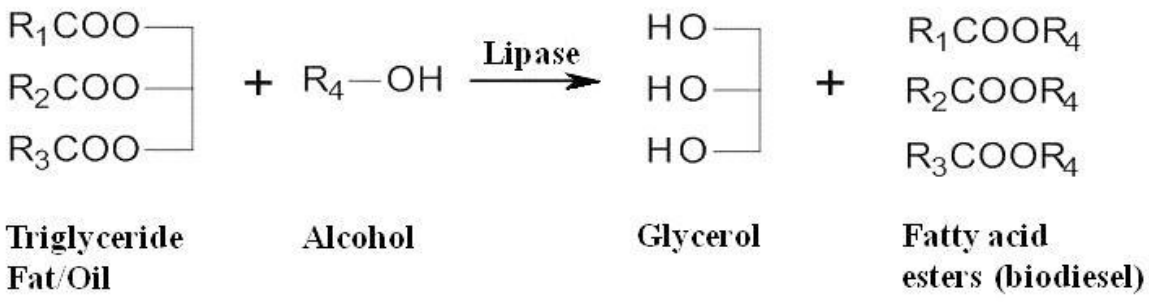

Scheme 1.6: Lipase-catalysed transesterification of fats and oils with alcohol to produce biodiesel and glycerol.

In 2007, Al-Zuhair published an article on the 'Production of biodiesel: possibilities and challenges' which addressed the use of immobilised enzymes to overcome limitations regarding enzyme cost, re-usability, recoverability and reductions in activity.[202] In 2008, Fjerbaek *et al* reviewed the state of biodiesel production using enzyme-catalysed transesterification.[203] It can be seen that the use of lipases to catalyse the production of biodiesel is an area that has gained considerable interest in recent years. This could be due to optimisation of the process using immobilised enzymes for the many advantages they offer. The use of supported enzymes for various applications will be discussed in the following section.

As has been explored and discussed, enzymes in their free forms can be used to catalyse a vast range of chemically and pharmaceutically important reactions and can be used under mild conditions while still producing tremendous chemo-, regio- and enantioselectivity. However, the use of free enzymes to catalyse these reactions presents a problem: the enzyme cannot be recycled or re-used once it is introduced to the system. Also, enzymes are fairly expensive so being able to re-use them is cost effective and would make the system more commercially viable. Another problem is that most organic compounds that are of commercial interest are often insoluble/partially soluble in water, which requires a lot of energy to remove.[204] A way around this is to use organic solvents, which leads to high substrate solubility, higher reaction rates and increased ease of recovery of the enzyme from the system. However, a disadvantage of using lipases in organic solvents is that catalytic activity can decrease dramatically compared to aqueous systems,[205,206] due to diffusional limitations, enzyme destabilisation and changes in protein flexibility.[204,207,208] As has been previously explained, it has been reported that employing micro-aqueous conditions permits interfacial activation and 'lid-opening' of the lipase's active site, which can overcome this problem and greatly increase catalytic activity. An effective and convenient solution to these problems and limitations is to immobilise the enzymes onto a solid support, which creates a heterogeneous system. The supported enzyme can be introduced into the reaction mixture, the reaction can be carried out and then the enzyme-immobilised solid support can be recovered, washed and re-used for further reactions. Magnetic nanoparticles are particularly useful for these applications as they can be easily removed from the reaction mixtures by magnetic immobilisation.

1.8 Immobilisation of Enzymes

This section of the introduction will serve to outline the most commonly used support materials for enzyme immobilisation, typical enzyme immobilisation strategies and their optimisation, as well as some bio-catalytic applications of immobilised enzymes and their advantages over free enzymes.

Mateo *et al*[209] explained that in terms of multipoint-covalent binding of the enzyme to the support in order to rigidify and stabilise the enzyme structure, certain characteristics must be considered when deciding on a suitable support.[209] These include:

- The support should have high internal surface areas so that there can be no geometrical or steric hindrance to the enzyme.
- The support surface should provide a high density of reactive groups so an intense multipoint covalent attachment can be achieved.
- The reactive groups should provide minimal steric hindrance during the reaction as the attachment requires contact between groups bound to rigid structures.
- The reactive support surface moieties should interact and react with groups introduced to the enzyme surface and they should also be stable enough to permit lengthy enzyme-support reaction times.
- Finally, it should not be difficult to get a final inert surface in the support following immobilisation without affecting the bound enzyme.[209]

Support materials that have been found to fulfil many of the criteria are agarose beads,[103,210-213] zeolites,[214-216] amorphous and porous silica supports,[217,218] epoxy resins[219-221] and magnetic nanoparticles.[222] Immobilisation of enzymes on agarose beads activated using glyoxyl groups only proceeds at alkaline pH and catalytic activity is reported to be pH dependent. Enzymes that have been immobilised in this way include alcalase and carboxypeptidase A for the hydrolysis of proteins,[212,213] esterase[103] and many others.[210,223] Zeolites are widely used for a range of bio-catalytic applications, ranging between immobilising trypsin for peptide synthesis,[216] cutinases for alcoholysis reactions[215] and lipases on hydrophilic and hydrophobic zeolites for hydrolysis and esterification reactions.[214] Silica supports can undergo surface modification with aminosilanes to permit the formation of siloxane bonds to amine residues on the enzyme. An example of this method being used is

in the immobilisation of apricot pectinesterase on porous glass following aminosilane surface modification, which is then used in the food processing industry.[218] Sepabeads are macroporous epoxy-resins and are an example of a divinylbenzene copolymer.[224] They are a common example of a widely used epoxy support. They are shown to remain very stable when obtaining Lipase B from *Candida Antarctica* in the presence of hydrogen peroxide[220] as well as finding application in hydrolysis of lactose in dairy products *via* immobilisation of thermophilic β-galactosidase on its surface.[221] Dyal *et al* were one of the first groups to report the use of enzymes immobilised on magnetic nanoparticles and used CRL immobilised on γ-Fe_2O_3 to catalyse the ester cleavage of *p*-nitrophenol butyrate (PNPB), reporting the long-term stability and economic viability of immobilised enzymes for bio-catalysis.[222]

1.8.1 Porous Supports

A prevalent method of enzyme stabilisation is by immobilisation on porous silica supports of various pore diameters (Å to μm scale). Immobilisation within the porous structure of a solid can permit the enzyme to fully disperse and utilise the intended surface area. This means they are protected from interactions with external surfaces and molecules, as well as molecules from the enzymatic sample which prevents aggregation, autolysis or proteolysis from the sample and will be homogenously dispersed throughout the pores.[209] The enzyme will also be protected from external hydrophobic surfaces such as gas bubbles which may inactivate the enzyme.[225]

In the process of immobilisation, the surface of the support should be functionalised *via* one of the methods outlined previously (in the case of this project; amino-silanisation). Following this, the surface-functionalised material can be activated (using coupling reagents) to enable the efficient conjugation of bio-molecules to the surface.

1.8.2 Enzyme Immobilisation Strategies and Optimisation

Enzymes have been immobilised in many ways, the main methods include adsorption (non-covalent), binding (covalent), self-immobilisation, entrapment and encapsulation.[226] An important point to consider is choosing the correct support to optimise catalytic activity and stability of the enzyme when it is immobilised. Entrapments generally use either an organic polymer network or sol-gel matrix and are often performed *in situ*.[227] The entrapped enzymes are then protected from the effects of gas bubbles, mechanical damage and hydrophobic solvents, but entrapped enzymes can suffer from mass transfer limitations and lower enzyme loadings[228] than other immobilisation methods.[229] Encapsulation is similar to entrapment as

the enzyme is protected from many external factors but has limited use in bio-catalysis of large substrates due to mass transfer limitations again.[228,229] Self-immobilisation is commonly carried out in the case of carrier-free immobilisation, made possible using a bi-functional cross-linking molecule, such as glutaraldehyde, to bind enzymes to each other without needing a support.[229] Examples include cross-linked enzyme crystals (CLEC's)[230] and cross-linked enzyme aggregates (CLEA's).[231,232] Figure 1.12 below is reproduced from a review article by Brady and Jordan on "Advances in Enzyme Immobilisation", showing the main strategies involved.[229] Figure 1.12 presents the main enzyme immobilisation strategies that are commonly employed.

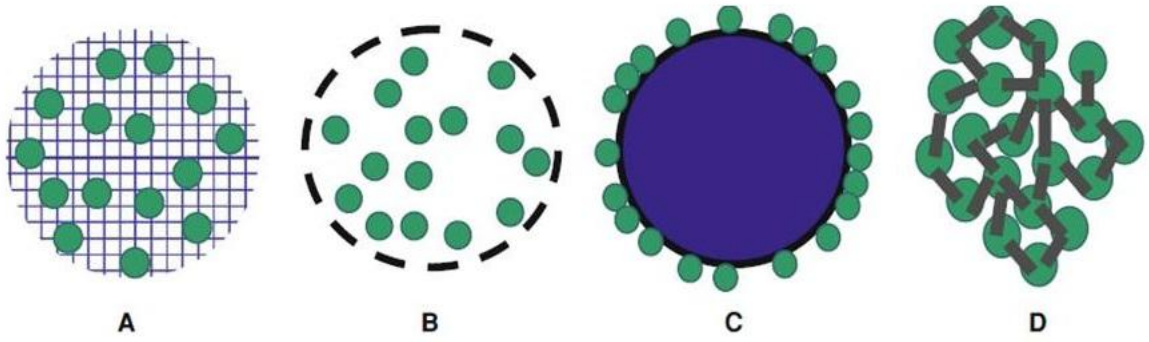

Figure 1.12: The main enzyme immobilisation strategies: a) entrapment b) encapsulation c) solid support by surface conjugation d) self-immobilisation. Enzymes are represented by the green dots in the figure, reproduced from Brady and Jordaan.[229]

An example of various immobilisation methods being used in the same reaction is reported with PFL. Immobilisation *via* adsorption, cross-linked enzyme adsorption and sol-gel encapsulation was reported for the kinetic resolution of several 3-aryl-3-hydroxypropanoates.[233] Immobilisation was shown to increase stability, activity and re-usability. The bi-molecular form[159] exhibited increased thermal stability and activity in catalysing the transesterification of olive oil with benzyl alcohol. PFL was also immobilised on glyoxyl supports at alkaline pH for the hydrolysis of (R,S)-2-hydroxy-4-phenylbutyric acid ethyl ester (HPBEt) in both its mono- and bi-molecular forms.[234]

1.9 Supported Enzymes as Bio-catalysts

Advantages of immobilisation such as separability and re-usability are important and allow greater control over the reaction process. It is also well documented that enzyme activity increases when immobilised on solid supports and enzymes become more robust when

supported in solid matrix.[204] The main focus of this section of the introduction is to explore the wide range of solid supports that have been used, various methods of immobilisation and the important bio-catalytic applications that these immobilised enzymes (primarily lipases) are employed in.

When covalently immobilised *via* just a single point to the solid support, immobilised enzymes can retain rigidity similar to free soluble enzymes and are much less susceptible to aggregation, proteolysis and interaction with other surfaces.[235] However, it is well documented that enzymes attached to the support at many points become more rigid[236] and stabilised against distorting agents, as the relative positions of groups involved in immobilisation remain unchanged during any conformational change.[237] This means they can be used in any medium, as opposed to adsorbed enzymes, which can only be used in organic solvents/hydrophobic reactants due to problems associated with leaching into the solution.[137] It is also thought that immobilisation leads to the enzyme being dispersed over a large surface area, enhancing mass transfer and preventing aggregation.[238] Figure 1.13 presents the effect of multipoint immobilisation on enzyme stability.

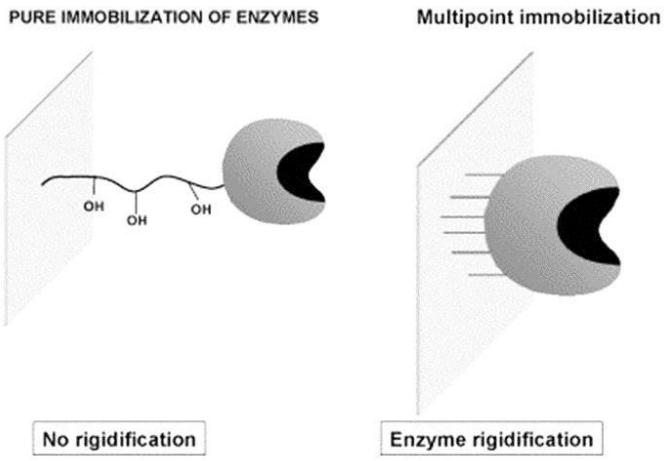

Figure 1.13: The effect of multipoint immobilisation on enzyme stability. Reproduced from Mateo *et al*.[209]

1.9.1 Bio-catalytic Applications of Supported Enzymes

An emerging area of particular importance is the production of fatty acid esters, better known as biodiesel (production with free lipases is addressed earlier in Section 1.7.3). CRL immobilised on chitosan (a linear polysaccharide) was used to catalyse (and optimise) the preparation of biodiesel from rapeseed soapstock using methanol.[239] This method led to methyl conversion of 63.6% and methyl ester (biodiesel) contents of over 95% following

molecular distillation. Various lipases (CRL, PFL and others) immobilised on porous kaolinite were used for the transesterification synthesis of biodiesel using *n*-butanol.[240] PFL was observed to have the highest activity and was selected as catalyst for the production of propyl- and butyl-oleate esters from triolein. Immobilised PFL exhibited increased activity, stability and re-usability over free PFL. Various immobilised and free lipases were compared for the enzymatic alcoholysis of sunflower oil with methanol to produce biodiesel.[241] PFL immobilised on polypropylene (EP 100) was found to have the second highest activity after 24h, giving 72.4% conversion of triolein to fatty acid ester products (*Rhizomucor miehei* immobilised on an ion-exchange resin gave 96.3% conversion in 24 h). Alkali lipase from *Penicillium expansum* immobilised on functionalised ceramic foams have been utilised for the hydrolysis of olive oil.[242] As can be seen from the many reactions outlined for the production of biodiesel, enzyme-catalysed synthesis is both widely used and efficient.

Another reaction class of interest is kinetic resolution of racemic mixtures. The resolution of (R,S)-2-octanol with SBA-15 (a hexagonal array mesoporous silica molecular sieve), *Pseudomonas* sp. Lipase (PSL) and vinyl acetate to produce (R)-2-octanol and (R)-2-octanol acetate has been reported.[243] 2-octanol, or capryl alcohol, is commonly used as a raw material to make caproic acid, which is used as a flavour intermediate, or 2-octanol itself can be refined to produce plasticisers.[244] The reaction is summarised in Scheme 1.7 below.

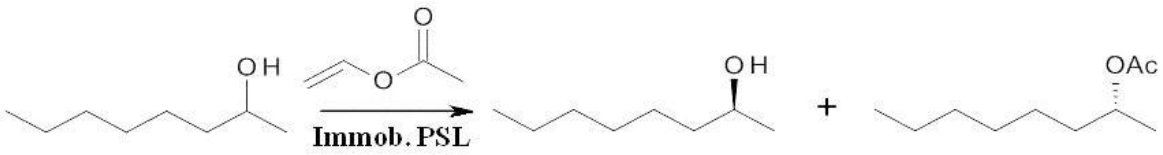

Scheme 1.7: Lipase-catalysed resolution of (R,S)-2-octanol with vinyl acetate.

Full resolution of racemic 1-phenylethanol to (R)-1-phenylethanol and (R)-1-phenylethyl acetate using immobilised *Candida Antarctica* lipase B on a modified silica meso-cellular foam has been reported.[245] This is important because chiral alcohols can be used in enantioselective organic synthesis. α-Chymotrypsin immobilised on MCM-41 has been utilised by Fadnavis *et al*[246] in the chiral resolution of (±)-*trans*-4-methoxy-3-phenylglycidic acid methyl ester, shown in Scheme 1.8.

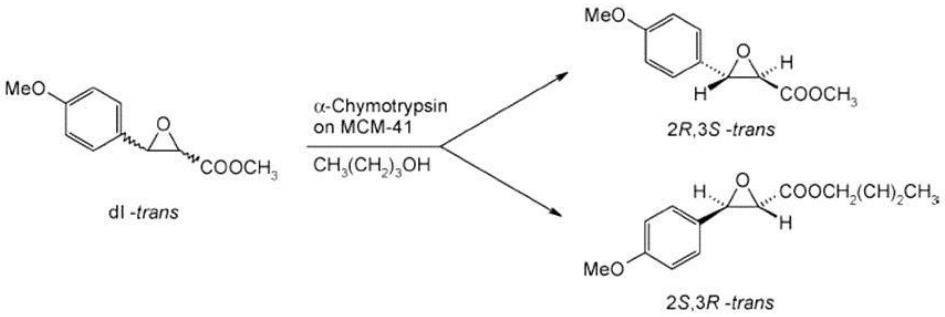

Scheme 1.8: Kinetic resolution of (±)-*trans*-4-methoxy-3-phenylglycidic acid methyl ester glycidate with α-Chymotrypsin immobilised on MCM-41. Reproduced from Fadnavis *et al*.[246]

The resolutions of racemic mixtures explained above have all been catalysed by lipases which have been immobilised on silica supports. Other supported lipases used for resolving racemic mixtures include:

- Novozym® 435 (*Candida Antarctica* Lipase-B (CAL-B) immobilised on acrylic resin).[115,247]
- Magnetic nanoparticles.[248-250]
- Celite,[251] epoxy resins[252] and many others.[223]

However, the most widely used support material for enzyme immobilisation is silica. In addition to the methods outlined above which are used to produce biodiesels, in 2011 mesoporous silica prepared *via* the sol-gel method was used to immobilise cellobiase enzyme which was then used in the enzymatic hydrolysis of biomass, generating ethanol for biofuels.[253] In the same year, lipase-immobilised mesoporous silica were used in the methanolysis of soybean oil to biodiesel.[254] These are just a small fraction of the uses of porous silica as a support.

1.9.2 Silica Supports

Applications of various enzymes immobilised on silica are copious and porous silica has found the most applications as a support material. It has been widely used for a long time to immobilise various enzymes to carry out a huge range of applications. In 1982, glucoamylase was immobilised on various porous silicas' (macroporous silica gels, silochromes and porous glasses) for starch hydrolysis.[255] In 1984, the kinetics of the hydrolysis of starch, amylase and maltose were investigated using glucoamylase immobilised on alkylamine derivatives of Ti(IV)-activated porous silica.[256]

More recently, it has been exhibited that enzymes can be immobilised on porous silica (pore size ~2 nm) nanotubes with higher catalyst loadings than other mesoporous silica materials.[257] In 2000, porous silica beads with immobilised Porcine Pancreatic Lipase (PPL) were used in the enzymatic ring-opening polymerisation of cyclic phosphates.[258] CRL immobilised on amorphous silica nanoparticles has been used to synthesise ethyl isovalerate, a flavouring agent commonly found in fruits.[259]

In an excellent article by Hartmann and Jung, the significant reactions carried using immobilised enzymes on mesoporous silica are reviewed;[260] the three most common being: resolutions of racemic mixtures, hydrolysis reactions and selective oxidations.

1.10 Bio-catalytic Applications of Supported Enzymes on Magnetic Nanoparticles

The area which is of most relevance to this project is the use of silica-coated superparamagnetic iron oxide (magnetite, Fe_3O_4) nanoparticles (SPIONs) as solid supports for lipase immobilisation. An excellent review of SPIONs and their development, surface modification and applications in chemotherapy can be found in reference 44. Previous work in the field has shown that magnetic nanoparticles (MNP's) coated in amorphous silica[217] have been used in the isolation of bio-molecules, such as genomic[76] and plasmid[261] DNA, extraction of nucleic acids from soil,[262] drug delivery[263] and extraction of phenolic compounds from environmental water.[264] MNP's coated with mesoporous silica[99,265] have been found to be useful in controlled drug delivery,[266,267] hyperthermia,[268] removal of mercury from- and desulfurisation of -industrial effluent,[269] fluorescence, magnetic resonance imaging[270] and isolation of plasmid and genomic DNA similar to MNP's coated with amorphous silica.

Certain properties of nanoparticles that make them attractive for use in drug delivery - such as high surface area, ability to cross cellular and tissue barriers and resistance to bio-degradation - have been found to increase their cytotoxic potential relative to the bulk material.[271] Whereas the iron oxide core alone has been associated with causing inflammatory responses[274] and inducing oxidative stress – leading to apoptosis (programmed cell death),[272-274] silica-coated magnetite nanoparticles are bio-compatible.[275,276] It is important to assess how the drug and shell materials interact with each other to avoid bursting which could lead to the formation and release of toxic chemicals in the body.[44]

It has also been found that mesoporous, macroporous and meso-cellular silica foams with immobilised enzymes on the surface lack ordering in the pore structure when they were studied for bio-catalysis.[94] In a method to overcome this, Sen *et al* have reported the template assisted fabrication of hierarchically ordered porous magnetic nanocomposites and their potential as supports for bio-catalysis.[100] In their study, they investigated the catalytic activity of CRL immobilised on hierarchically ordered porous magnetic nanocomposites to convert *p*-nitrophenyl palmitate (PNPP) to palmitic acid and *p*-nitrophenol *via* ester hydrolysis. The immobilised enzymes were found to exhibit catalytic conversion values of roughly 100 times less than that of pure lipase in homogeneous conditions, but retained most of their catalytic activity and stability after many cycles, which is impossible using free enzymes in solution as they are unrecoverable. This reaction is useful as palmitic acid is a well-known substrate for lipase-activity;[277] was formerly used in napalm synthesis;[278] its derivatives have been investigated for use in anti-psychotic drugs;[279] and it is one of the major components of palm oil found in foods, or used to produce biodiesel.[280] The reaction is shown below in Scheme 1.9.

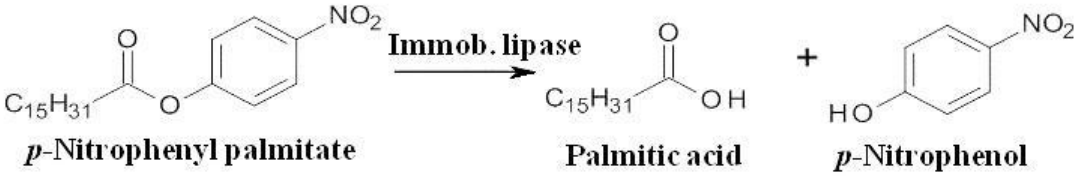

Scheme 1.9: Immobilised lipase-catalysed hydrolysis of PNPP.

The catalysis of *p*-nitrophenyl butyrate (PNPB) is much less documented but has been done before, using free enzymes,[281] and recently a study comparing enzyme-immobilisation methods on the bio-catalytic hydrolysis of PNPB has been carried out.[282] The study concluded that lipases immobilised on solid supports (zeolites in this case) exhibited higher specific activity than cross-linked enzyme aggregates (CLEA's) and supplied a "heterogeneous catalyst with promising catalytic properties".[282] Using the materials produced in this project for the catalysis of PNPP hydrolysis, comparisons can be made with previous studies.

Magnetic silica nanoclusters (clusters of silica-coated magnetic nanoparticles of roughly 500 nm) have been used and benefited from increased chemical stability and decreased aggregation.[283,284] It has recently been reported that L-lactate dehydrogenase (LDH),

covalently immobilised on silica-coated magnetic nanoclusters, could be suitable for catalysing the chiral synthesis of pharmaceutical compounds.[285] Netto *et al*[286] have reported that *Candida Antarctica* lipase (CAL) immobilised on superparamagnetic silica-coated nanoparticles can be used to catalyse enantioselective transesterification reactions, such as the enantioselective acetylation (and hence kinetic resolution) of alcohols derived from (R,S)-1-phenylethanol using vinyl acetate as acyl donor.[286] This group also tested catalytic activity by examining the hydrolysis of PNPP. This study is useful to our project as it shows the viability of enantioselectively-acylating secondary alcohols using enzymes immobilised on superparamagnetic silica-magnetite nanoparticles.

One reaction that will be performed during the bio-catalysis phase is the use of a selection of lipase enzymes (CRL and PFL), immobilised on silica-coated SPION's for the bio-catalytic partial and selective hydrolysis of *cis*-3,5-diacetoxy-1-cyclopentene (**3** in Scheme 1.10, shown below) to obtain enantiomerically pure (1S,4R)-*cis*-4-acetoxy-2-cyclopenten-1-ol and its (1R,4S) enantiomer (**2a** and **2b** respectively).

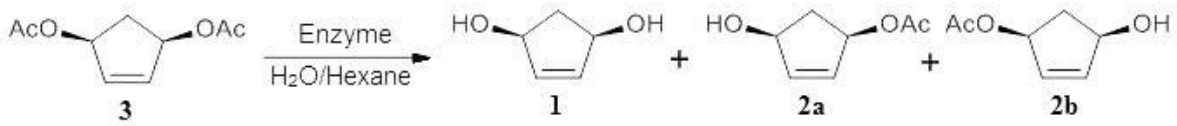

Scheme 1.10: Enzyme-catalysed hydrolytic synthesis of (1S,4R)-*cis*-4-acetoxy-2-cyclopenten-1-ol (2a) and its enantiomer (2b).

Although this reaction has been reported previously, catalysed by lipase from *Mucor* sp.,[287] pancreatin[288] and immobilised *Mucor miehei* lipase (Chirazyme®),[289] to the best of my knowledge, this reaction has not been carried out using immobilised lipases on magnetic nanoparticles. The products are high cost synthetic chiral intermediates which are starting materials for the synthesis of carbocyclic nucleoside analogs[290] (useful immunosuppressants) and particularly eicosanoid compounds:[291] (bio-active lipids derived from 20-carbon unsaturated fatty acids[292] which act as signalling molecules involved in the regulation of bodily systems including inflammation, immunity and as messengers in the central nervous system[293-295]) specifically prostaglandins, prostacyclins and thromboxanes.[289,296-298] Figure 1.14 presents the structure of Prostaglandin E_1, pharmaceutically known as the drug alprostadil, which is a vasodilator used to treat erectile dysfunction.[299,300]

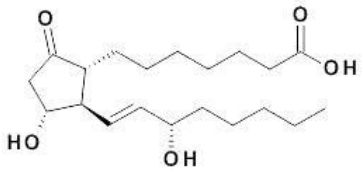

Prostaglandin E_1

Figure 1.14: The structure of Prostaglandin E_1.

Considering the high demand for these chiral intermediates, development of economically viable enzymatic technology to catalyse their large-scale synthesis is a key synthetic objective and one which is currently relevant.

Another common reaction catalysed by lipase-immobilised magnetic nanoparticles is the transesterification (alcoholysis) of short chain alkyl esters. The alcoholysis of ethyl butyrate with *n*-butanol has been previously reported using CRL immobilised on surfactant-, fatty acid- and polymer-coated magnetite nanoparticles[301] along with immobilised *Mucor miehei* (Lipozyme®)[302] and free rape-seedling lipase[303] (among many others). The mechanism of the reaction is shown in Figure 1.15.

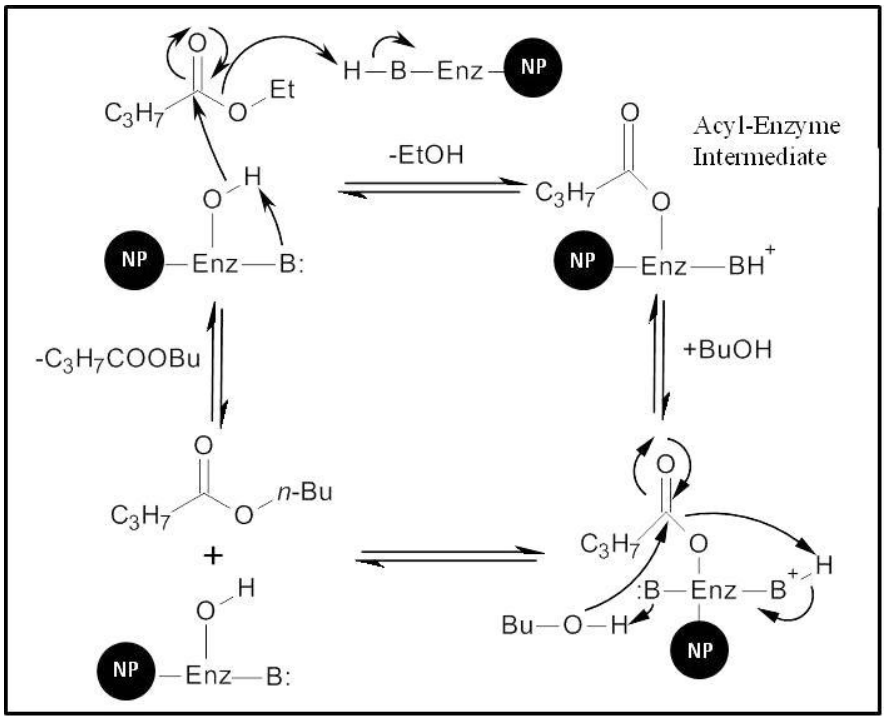

Figure 1.15: The mechanism of lipase-catalysed transesterification (alcoholysis) of ethyl butyrate with *n*-butanol. NP denotes surface-functionalised, silica-coated magnetic nanoparticles, Enz denotes enzyme, B denotes basic group and Bu denotes butyl group.

1.10.1 Bio-catalysis with Supported Enzymes: Summary

A wide range of enzymes (particularly lipases) immobilised on various support materials have been utilised successfully as bio-catalysts. Table 1.4 provides a comprehensive listing of the main types of bio-catalytic reactions outlined in Section 1.9, along with the types of support used.

Table 1.4: A summary of the main types of supports and enzymes used.

Support type	Enzyme(s)	Studied Reaction(s) and Reaction Class(es)	Ref.
Silica	Lipases, dehydrogenases, peroxidases and oxidases.	Various including oxidation, hydrolysis, esterification and kinetic resolution.	260
Agarose beads	Carboxypeptidase A, Alcalase, Esterases, Lipases.	Protein hydrolysis, Esterification.	103,210-213
Zeolites	Trypsins, Cutinases, Lipases.	Peptide synthesis, alcoholysis, hydrolysis, esterification.	214-216
Porous glasses	Apricot pectinesterase.	Hydrolysis of methoxyl groups of methylated galacturonic residues in pectin molecules.	218
Epoxy resins	Lipases, B-galactosidase, cytosine deaminase, 5-fluorocytosine.	Hydrolysis of dairy products, cancer chemotherapy.	219-221

Table 1.4: Continued

Support type	Enzyme(s)	Studied Reaction(s) and Reaction Class(es)	Ref.
Magnetic NPs	CRL	Hydrolysis of *p*-nitrophenyl esters, esterification synthesis of ethyl isovalerate, transesterification of ethyl butyrate.	222,259,301
Silica-coated magnetic NPs	Lipases, Dehydrogenases, Various others.	Enantioselective esterification, hydrolysis, isolation of bio-molecules, extraction of nucleic acids, controlled drug delivery, water purification, fluorescence and magnetic resonance.	44,73,81, 217, 261-263,269,270 279,283, 284,286,304

1.11 Introduction to Bio-separations and Bio-sensors Using Magnetic Nanoparticles

1.11.1 Bio-separations

Bio-separation involves the selective separation and purification of target bio-molecules from a mixture of biological components. Typical methods used in bio-separations are:[305]

- Physical and mechanical methods such as various adsorption,[306] filtration,[307] centrifugation[308] and magnetic separation techniques.[309,310]
- Chemical and thermal methods such as reverse osmosis,[311] ion-exchange,[312] chromatography[313] and electrophoresis[314] techniques.

Magnetic nanoparticles and functionalised magnetic nanoparticles have been widely used in bio-separations for numerous applications, outlined below:

- Protein recovery and separation from protein mixtures.[315,316]
- Immunomagnetic cell isolation and separation.[317,318]
- Immunomagnetic assays, i.e. a chemiluminescence enzyme immunoassay for sensitive and rapid detection of immunoglobulin G,[319] a fluoroimmunoassay for the

detection and removal of *E.Coli*[320] and an enzyme-linked immunosorbent assay (ELISA) for detection of *Staphylococcus* spp. bacteria in milk.[321]

1.11.2 Bio-sensors

Bio-sensors are biological analytical devices that combine a biological recognition element with a physicochemical detector (such as a transducer).[322] They can be classified according to the detection methods used and some examples using magnetic nanoparticles are explained in detail below.

Optical bio-sensors: are powerful tools for detection and analysis that have many applications in the bio-medical, pharmaceutical and military industries.[323] Detection is typically either fluorescence-based (binding of fluorescence-tagged target or receptor molecules resulting in a measurable increase in fluorescence) or label-free (by measuring changes in optical properties such as refractive index and optical absorption).

Optical bio-sensor systems incorporating magnetic nanoparticles have been used for the detection of: drugs in human blood serum/plasma and saliva,[324] antigens related to Alzheimer's disease,[325] myocardial infarction diagnosis[326] and others,[327] food-borne pathogens,[328] DNA, RNA and protein molecules.[329-331] In 2010, Smith *et al* reported the impact of using magnetic extraction using antibody-conjugated MNP's labelled with fluorescent proteins for both target pre-concentration and integration into immunoassays leading to enhanced signal generation.[332]

Electrochemical bio-sensors: are widely used as they can directly convert a biological "event" to an electric signal, i.e. by measuring current (amperometric), charge accumulation (potentiometric) or changes in conductive properties between electrodes in a medium (conductometric).[322] They typically employ screen-printed electrodes as both the solid-phase for the immunoassay and the electrochemical transducers. Specific enzyme-labelled antibodies/antigens are directly immobilised onto the electrode surface and produce electroactive products upon binding with their target which can be detected at the electrode surface[333]. However, this can lead to problems such as shielding of the surface by the bound antibody-antigen complex.

The use of bio-ligand-functionalised magnetic nanoparticles as the solid phase for the reaction leaves the electrode surface free and the product can diffuse onto the bare electrode surface without steric hindrances. Typical detection methods are cyclic voltammetry (CV),

chronoamperometry (CA), electrochemical impedance spectroscopy (EIS), potentiometry and others.[322] Examples of magnetic nanoparticles being used for electrochemical bio-sensor applications are outlined in Table 1.5 below.

Table 1.5: Examples of electrochemical bio-sensors and their applications.

Bio-sensor System	**Species Detected and Application**	**Ref.**
Screen-printed carbon electrodes (SPCEs) coated with ferricyanide magnetite, yeast YADH and NAD^+ cofactor.	Ethanol from fermentation and distillation processes.	334
Glucose oxidase layered on drop-coated ferricyanide magnetite on SPCEs.	Sensitive detection of glucose as a clinical indicator of diabetes and in the food industry.	335
Laccase immobilised on core-shell silica-magnetite nanoparticles, attached to a carbon paste electrode.	Detection of hydroquinone in compost (due to being hazardous and degradation-resistant in the environment).	336
Tyrosinase immobilised on magnetic $MgFe_2O_4$ nanoparticles, attached to a carbon paste electrode.	Detection of phenol, a contaminant in ground and surface water.	337
Glutathione oxidase immobilised on chitosan-functionalised gold-coated magnetite nanoparticles, attached to a modified Pt electrode.	Detection of glutathione, a human health bio-marker overexpressed in tumour tissues and altered levels in plasma are implicated in diagnosis of Alzheimer's, Parkinson's, diabetes and HIV.	338
PEGylated arginine functionalised magnetite nanoparticles, coated on a glassy carbon electrode.	Detection of dopamine, a neurotransmitter that plays an important role in the function of the central nervous, renal and hormonal systems. Low or abnormal metabolisms of dopamine are associated with Parkinson's, schizophrenia, epilepsy and others.	339

The second aim of this project is to develop both bio-separation and bio-sensor systems for the detection of pathogenic *Listeria Monocytogenes* (LM) in real food samples and *Escherichia Coli* (EC) in both food and wastewater. In terms of bio-separation, LM- or EC-specific oligonucleotides or antibodies will be covalently attached to functionalised magnetic nanoparticles for the specific capture of LM or EC from a mixture of bacteria and nucleic acids. In the case of oligonucleotide capture, the LM or EC bacteria captured on the nanoparticles will be removed by dehybridisation and amplified and quantified using real-time quantitative PCR. Hence, it is important to discuss why both LM and EC are of such interest.

1.11.2.1 *Listeria Monocytogenes* (LM)

Listeria Monocytogenes (LM) is a Gram-positive, rod-shaped facultative anaerobic bacterium and is widespread, with the ability to multiply at low temperatures (refrigeration temperatures) and within a wide pH range (4.39-9.40).[340,341] It can contaminate foods such as cheeses, raw milk, ice cream, raw and cooked poultry and fish, raw vegetables and raw sausages[342] - causing listeriosis; a severely infectious disease known to cause meningitis, septicaemia and spontaneous abortion, as well as fatality in around 30% of all cases.[343,344] Therefore, it is important to find suitable materials and processes in order to detect low levels of LM in food samples in conjunction with the European quality of safety directly related to human health.

1.11.2.2 *Escherichia Coli* (EC)

Escherichia Coli (EC) is a Gram-negative, rod-shaped facultative anaerobic bacterium commonly found in the intestinal tract of animals.[345] Most strains of EC are harmless, but some serotypes are inherently pathogenic, leading to infections including urinary tract infection [uropathogenic (UPEC)],[346] meningitis in newborns [newborn-meningitis-causing (NMEC)][346] and enteric/diarrheal diseases [enterotoxigenic (ETEC), enteroinvasive (EIEC), enterohemorrhagic (EHEC), enteropathogenic (EPEC) and enteroaggregative (EAEC)].[347,348] EC is serotyped according to its somatic (O), flagellar (H) and capsular (K) surface antigen profiles. Enterohemorrhagic EC (EHEC) can be identified as pathogenic and dangerous as it produces the major virulence factor, the Shiga toxin, which is cytotoxic.[349] These strains are also known as Shiga toxin-producing *Escherichia Coli* (STEC) strains and well-known outbreaks of contamination have been found to be caused by strains including *Escherichia Coli* O104:H4 (enteroaggregative – causing persistent diarrhea[350]) and O157:H7

(enterohemorrhagic – causing bloody diarrhea[350]), both found in undercooked ground beef, raw milk, cheese, vegetables and water, amongst other things.[346-349,351-353] These are the specific strains that this project will attempt to selectively isolate and detect from real samples.

1.11.2.3 Typical Bacteria Detection Methods

Typical methods of detection involve placing the bacteria sample in an enrichment broth with or without selective agents for around 48 hours. After 24 and 48 hours, the enriched cultures are streaked onto Agar plates, which contain selective isolation media to only permit the growth of a specific species. The plates are incubated at 30-35ºC for 24-48 hours, depending on the media present. The bacteria is then often isolated for analysis and identification[341,354]. Following enrichment and culturing, the sample can then be analysed using a range of detection methods. There are three main methods of bacteria/microbe capture and detection used in industry today.[355] They are:

1. **Molecular whole-cell and surface recognition methods**: This method involves binding to molecular structures on the surface or interior structures of the target microorganisms (bacteria, viruses, genetic materials). This is typically carried out with immunoassay techniques, bacteriophages and specific probes (for example ELISA assays and immunomagnetic separations).

2. **Enzyme/substrate methods**: Based on existing widely-used chromogenic or fluorogenic substrate methods, or done by developing new enzyme-substrate methods. This method is done by the capture of fluorophore- (or chromophore-) tagged growth substrates by the enzyme. This is followed by the substrate growth and subsequent enzymatic cleavage of the fluorophore, causing an increase in fluorescence which can be detected. Examples include agarose gel electrophoresis and Southern blotting.

3. **Nucleic acid detection methods**: These methods capture target specific microorganism nucleic acid sequences, which are then amplified for detection. Common methods of amplification include: Polymerase chain reaction (PCR), reverse transcriptase PCR (RT-PCR), quantitative PCR (qPCR), nucleic acid based amplification and microarrays.

The primary method chosen for detection of both LM and EC (following bio-separation) in this project is PCR, as it is possible to target specific nucleic acid sequences for amplification and detection. It also has the advantage over typical microbiological detection methods as it is more sensitive, requiring the culture to be enriched for a shorter time. It can provide rapid, accurate results and is a very widely used, efficient method commonly used for bacteria detection. For specific LM detection, the virulence protein listeriolysin O, encoded by the gene *hlyA*, is commonly the target of the primers in the PCR reaction,[309,356,357] although others can be targeted.[358] For specific EC detection, targets include: β-galactosidase, encoded by the gene *lamB*;[359] β-D-glucoronidase, encoded by the gene *uid*;[360] and the chromosonal gene, *eae*.[361] Initially separating the target species from a mixture can make detection much quicker, efficient and more sensitive. For this reason, bio-separations with magnetic nanoparticles for the specific detection of LM or EC will be discussed first.

1.11.3 Immobilisation of Bio-molecules for the Detection of Specific Target Bacteria

In PCR, *Taq* polymerase (a recombinant thermostable DNA polymerase used to catalyse DNA synthesis) can suffer from inhibition in the presence of some components of food, enrichment media, or particularly large amounts of DNA. As a pre-PCR step, immunological techniques such as the enzyme-linked immunosorbent assay (ELISA) can be used alone to detect and isolate specific bacterial cells or antigens within samples. However, as they require a detection limit of 10^5-10^7 colony-forming units per millilitre of reaction medium (CFU/mL), they still require lengthy enrichment and plating steps.[362] Therefore, the use of immunological methods combined with separation techniques is useful as a method of isolating specific bacteria from enrichment broths and samples before PCR. Immunomagnetic separation (IMS) is a commonly used technique that combines both methods; permitting specific capture of bacteria/antigens from an enrichment broth, while concentrating the target cells and removing PCR-amplification inhibiting species.[341,363] Immunomagnetic separation (IMS) requires specific receptor molecules (typically antibodies) immobilised on magnetic solid supports which bind to target molecules (antigens) within the sample.[362,364]

1.11.3.1 Using Immobilised Antibodies

Methods involving covalently immobilised antibodies on magnetic nanoparticles have been previously reported by many groups[341,365-368] and when combined with PCR or qPCR, offer increased sensitivity of detection over techniques such as classical microbiological enrichment and culture plating, gel electrophoresis and Southern blotting. These methods are

the basis of immunomagnetic procedures.[369] In 1993, Fluit *et al* first reported the use of magnetic nanoparticles coated with LM-specific monoclonal antibodies for the detection of LM in cheese.[362] Since this first reported use of immunomagnetic separation, many groups have used this method.

For detection of *Listeria*, IMS has been popular due to the commercial availability of anti-*Listeria* immunomagnetic beads, such as anti-*Listeria* Dynabeads® (Dynal Biotech ASA).[341,363] However, these beads capture all *Listeria* species and are not specific for LM only. Yang *et al* reported that carboxyl-modified magnetic nanoparticles with covalently immobilised rabbit anti-LM antibodies were used for the IMS and detection of LM in artificially contaminated milk.[341] Their findings confirmed that immobilised rabbit anti-LM antibodies on functionalised magnetic nanoparticles afforded higher capture efficiency and specificity for the target LM antigen. Reasons for these results could be that the magnetic nanoparticles are much smaller (70-100 nm) than the commercial Dynabeads® (which are ~2.8 μm diameter), having a higher surface-to-volume ratio and efficient diffusion properties, facilitating the rapid binding kinetics to target cells within the milk.[341]

For specific EC detection, IMS methods involving magnetic nanoparticles have been used with classical microbiological plating[370,370] as well as in combination with techniques such as chemiluminescence,[371] electrochemiluminescence,[372] ELISA,[373] flow cytometry[374] and others.[375-377] A good example of IMS combined with another technique is reported by Yu and Bruno,[372] who combined immunomagnetic separation (with antibody-coated magnetic beads) with electrochemiluminescent detection to target EC O157:H7 and *Salmonella typhimurium* in both food and environmental water samples. Various IMS assays have also been developed for the detection of *Salmonella*[310,364,378,379] and others.[380-383]

1.11.3.2 Using Immobilised Oligonucleotides

Nucleic acid bio-separation relies on the hybrid capture of a target oligonucleotide sequence using a specific complementary oligonucleotide sequence covalently-immobilised on functionalised magnetic nanoparticles. The immobilised captured target sequence can then be washed to remove impurities from the system before being dehybridised and used for amplification and detection using techniques such as qPCR. It is a modification of typical IMS techniques and is much less common. By selectively isolating target DNA from a complex sample mixture, time-consuming cultural enrichment steps can be avoided and shorter specific nucleic acid enrichment periods can be implemented. Total detection time is

decreased and PCR sensitivity can be increased due to removal of inhibiting species and non-target DNA.

Initial techniques used biotinylated capture probes to capture target DNA from samples, followed by immobilisation upon Streptavidin- or avidin-coated magnetic supports, which were then actually used in the PCR reaction itself.[384-388] One of the first reported applications of this technique was in 1994, when Heerman *et al* used hepatitis B virus (HBV) DNA as a template nucleic acid for hybrid capture, immobilisation and subsequent PCR amplification and detection.[384] The first step was to chemically denature HBV proteins, the second step was to hybridise biotinylated oligonucleotides to the HBV-DNA in the liquid-phase and then the final step was to immobilise them onto Streptavidin-coated magnetic nanoparticles. The samples were then analysed using PCR. Since this first reported use, the same method has been used for capture and detection of chronic enteric pathogens,[385] mycobacterial DNA (for the diagnosis of tuberculosis),[386] poliovirus,[387] hepatitis C virus,[388,389] and others.[390]

More recently, methods that utilise capture oligonucleotides covalently-immobilised on functionalised magnetic nanoparticles have started to gain popularity, particularly for the detection of LM.[344,391] In 2006, Amagliani *et al* developed a rapid and sensitive method for detecting LM in milk samples using a LM-specific, covalently immobilised (*via* imine bond) oligonucleotide (capture probe) on functionalised core-shell silica-magnetite nanoparticles.[344] The oligonucleotide sequence was selected from a highly conserved region of the listeriolysin O gene (*hlyA*) and was located outside the desired specific PCR site to avoid cross-contamination. The captured sequence was then dehybridised and qPCR was used for amplification and detection. Scheme 1.11 provides a schematic representation of the oligonucleotide capture and dehybridisation sequence.

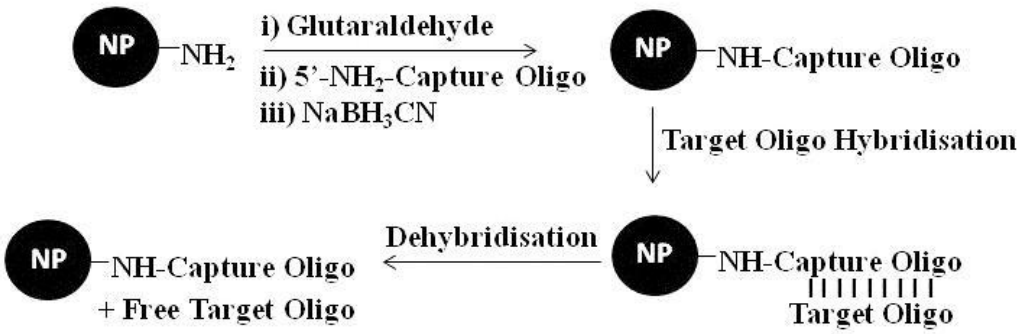

Scheme 1.11: Schematic representation of target sequence capture by an immobilised capture oligonucleotide.

In 2010, the same group developed a multiplex magnetic hybrid capture assay for simultaneous detection of *Salmonella* spp. and LM DNA from seafood.[392] They utilised a 1:1 mixture of immobilised *Salmonella* spp. and LM capture probes on functionalised silica-magnetite nanoparticles for simultaneous and selective isolation of the target DNA sequences from samples contaminated with both species. Following isolation of the target species, a triplex real-time PCR (qPCR) was carried out in the presence of an Internal Amplification Control (IAC) to simultaneously amplify, detect and quantify the amount of the target species in each sample.

In 2012, Zhu *et al* developed a novel nanomagnetic primer based electrochemiluminescence-PCR strategy for genome detection and analysis. The process relies on two *in situ* processes: 1) PCR on the magnetic nanoparticle surface and 2) Magnetic nanoparticle loading onto a magnetic electrochemiluminescence readout platform.[391] This method was used to rapidly and selectively detect LM at limits of 500 fg/μL in 1 hour, a limit comparable to that of qPCR.

Examples of similar methods that use capture oligonucleotides covalently-immobilised onto functionalised nanoparticles in the detection of EC are less common than LM, but include:

- Detection of EC from stool samples using primer-immobilised magnetic nanoparticles to detect enterotoxigenic EC (ETEC) using PCR.[393]
- Detection of EC O157:H7 using oligonucleotide-functionalised gold nanoparticles in combination with piezoelectric bio-sensing.[394]
- Detection of EC using gold nanoparticles and a thiolated capture oligonucleotide (from EC) immobilised into a 3-dimensional mercaptosilane-based sol-gel polymeric network, formed onto a screen printed gold electrode surface for electrochemical detection.[395]

Further examples of target species that have been detected using oligonucleotide-grafted nanoparticles include genetically-modified organisms,[396] *Alexandrium* species that cause harmful algal blooms in the Mediterranean Sea[397] and rotavirus (an enteric diarrhoea causing pathogen).[398] It is interesting to note that most of the methods which used PCR as a detection method, have used the hybridised capture and target sequences immobilised on the magnetic nanoparticles directly in the PCR, without prior dehybridisation of the target sequence from the support. This is in contrast to using dehybridised single-stranded DNA, which can avoid

slight steric hindrances of DNA and primer target recognition on the nanoparticle surface in the PCR reaction. Many new processes are using PCR combined with other detection techniques such as electrochemiluminescence to afford quicker and more sensitive results.[391,398]

As has been mentioned previously in this section, following the selective isolation of the target species from a sample, the purified or captured materials can then be amplified and detected by a variety of methods, leading to accurate quantification of the target species. With regards to this project, the most important of these detection methods is the polymerase chain reaction (PCR), which will be discussed in detail in the upcoming section.

1.11.4 Polymerase Chain Reaction (PCR)

Initially developed in 1983 by Mullis[399] (later earning him the 1993 Nobel Prize in Chemistry), PCR is an *in vitro* method used for the amplification of DNA. PCR uses two oligonucleotides (short lengths of single-stranded DNA, also known as primers) complementary to opposite strands of the target DNA, to specifically amplify the regions between them in order to direct the target-specific synthesis of new DNA copies (amplicons). The primers provide the initiation site for DNA synthesis, catalysed by a thermostable DNA polymerase (such as the recombinant thermostable DNA polymerase from the *Thermus Aquaticus* microorganism - *Taq* polymerase).

The new DNA which is synthesised by *Taq* polymerase is then used itself for further replication, hence giving rise to a chain reaction in which the target DNA sequence becomes exponentially amplified. PCR relies on a three-step thermal cycling method to synthesise new DNA sequences from an original DNA template sequence:

1. **Denaturation/melting**: The original DNA is heated in order to separate the two strands in its double helix. This step is typically around 95ºC, time can vary from 30 seconds to 10 minutes.
2. **Hybridisation/annealing**: Specific oligonucleotide sequences (primers) to each strand of the DNA are added in vast excess to the original DNA[400] (due to the huge amount of copies to be made) and are then hybridised (annealed) to the separated single-strands at around 40-65ºC for a short time (usually less than 1 minute). The temperatures used can vary, but are usually just under the melting point (T_m) of the primer-DNA complex. If the primer and DNA sequences are complementary, then

stable bonds will form between them and the *Taq* polymerase then begins to attach additional complementary nucleotides at these sites.

3. **Extension/elongation**: The temperature is increased to 70-75ºC (typically 72^{o}C) as this is close to the optimum working temperature of *Taq* polymerase, which works by adding complementary nucleotides to the developing DNA strands, forming a new double stranded DNA molecule. Also, non-complementary bonds between the primer and DNA sequence are broken in this step.

These steps 1-3 are then repeated with the newly formed DNA amplicons for 20-45 cycles. The process is shown below in Figure 1.16.

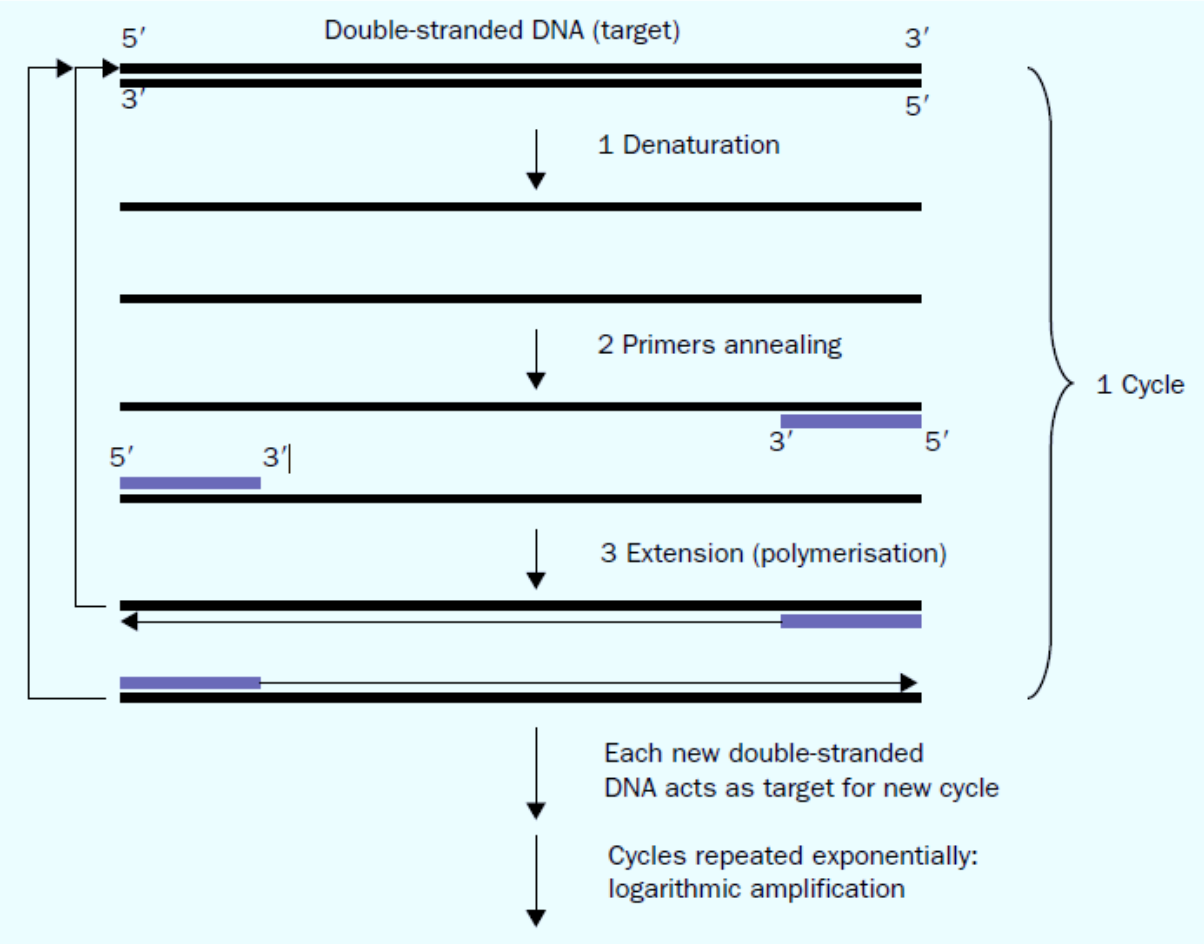

Figure 1.16: Schematic representation of the PCR process. Step 1 is denaturation at around 95ºC to separate double-stranded DNA to single-stranded DNA. Step 2 is the annealing of primers to their complementary target sequences on the single-stranded DNA at around 60ºC. Step 3 is the extension phase using *Taq* polymerase to generate a new sequence of double-stranded DNA. At the end of the first cycle, the newly formed double-stranded DNA sequences are used as templates for subsequent cycles. Figure reproduced and adapted from reference 401, which had mixed up the 3′ and 5′ ends of the primer bound to the upper strand of the denatured double-stranded DNA.

Following the first cycle, two new DNA amplicons (identical to the target) are formed, but without a clearly defined 3′ end. They do, however, possess the precisely defined 5′ end and as the number of cycles increases, newly formed amplicons with more defined lengths are used as DNA templates and new DNA amplicons synthesised from these have clearly defined lengths limited at either end by the 5′ group of the two primers (can be seen in Figure 1.16). For example, in the second cycle, a discrete double-stranded product is formed which is exactly the length between the primer ends on the original DNA template. Each of these strands are complementary to the primers and are used as templates in subsequent cycles to produce new double-stranded DNA amplicons with a precisely defined length. After 20 cycles, around 1 million molecules are cloned from a single segment of the original double-stranded DNA. In the absence of any inhibiting species in the reaction mixture, the amount of DNA copies will approximately double with every cycle.

1.11.4.1 PCR Optimisation

In order to work most effectively, PCR requires optimisation of the following:

- Template DNA sequence
- Specific primers
- Thermostable DNA polymerase (such as *Taq* polymerase)
- Deoxyribonucleotide triphosphate (dNTP) mixture
- $MgCl_2$
- Specific PCR buffer (with K^+ ions, usually from KCl)

The template DNA should be purified and only a small amount is required (0.1-1 µg for genomic DNA).[400] Larger amounts can often contribute to the increased yield of non-specific PCR products. Primers are used in great excess to the template DNA (typically around 10^7 times) and should have similar melting temperatures (within 5ºC of each other).[400,402] They should not be self-complementary or complementary to other oligonucleotides in the reaction mixture to prevent secondary structures from forming, such as primer-dimers and hairpins, which lead to decreased availability, efficiency and ability to bind to the target sequence.[403] Formation of these undesirable secondary DNA structures competes with synthesis of the target DNA and can drastically affect product yields.

Primers should also be short in length (18-30 nucleotides) and GC content should be 40-60%[400,404]. Melting temperature can be modified by changing the GC content, as guanine (G)

and cyanine (C) share three hydrogen bonds, making the interaction between them more stable than that between thymine (T) and guanine (G), which share just two hydrogen bonds. Increasing the temperature can decrease non-specific primer annealing. Melting temperature (T_m) can be simply estimated from Scheme 1.12 below:[404]

$$\mathbf{T_m} = 2(A+T) + 4(G+C)$$

Scheme 1.12: Estimate of melting temperature (T_m) based on nucleotide composition.

$MgCl_2$ acts as a co-factor to *Taq* polymerase and also forms stabilising complexes with the original DNA templates, primers and dNTP's[405] (K^+ also helps to stabilise the *Taq* polymerase). Its concentration must be optimised (usually 1-3 mM) as too much will increase the yield of non-specific products and too little will decrease the yield of specific PCR products. The concentration of the *Taq* polymerase must be optimised as too much can lead to the production of non-specific products, which is again undesirable.[406] The buffer acts to help the mixture retain constant pH and salt concentrations, so that the DNA polymerase can retain maximum activity throughout the reaction.

1.11.4.2 *Taq* Polymerase: Mechanism of Action

Primers, like DNA, have a 5′ and 3′ end and the *Taq* polymerase uses the original single strands of DNA to add complementary deoxyribonucleotide triphosphates (dNTPs: better known as nucleotide bases A, C, G and T) from the reaction mixture to the 3′ end of the primer to synthesise a section of double-stranded DNA specific to the region of interest. The 5′ end of the primer remains unchanged as, like in most DNA replication processes, *Taq* polymerase only synthesises new DNA in the 5′ → 3′ direction (*via* the 3′-OH group on the nucleotide at the end of the oligonucleotide sequence).[407] It also possesses only 5′→ 3′ exonuclease activity- meaning that it cleaves 5′ terminal oligonucleotides of double-stranded DNA and releases mono- and oligonucleotides.[408] Without 3′ → 5′ exonuclease activity, *Taq* polymerase lacks proofreading activity (the ability to reverse its direction of synthesis to remove an incorrect base pair and replace it with the correct one) and can have a high error rate, up to 1 in 10,000 nucleotide mutations per cycle.[409-411]

dNTP's are added by the *Taq* polymerase to the 3′-OH end of the primer (forming a phospodiester bond), resulting in the loss of a pyrophosphate group each time a new dNTP is added to the extending chain.[412,413] The active site of *Taq* polymerase features two metal ions which facilitate the binding of dNTPs to the primer strand.[414] The first metal ion is the

nucleotide-binding ion and coordinates the α-, β- and γ-phosphate oxygens of the incoming dNTP. The second is the catalytic ion which coordinates the α-phosphate of the dNTP and the 3′-oxygen of the primer strand. The coordination of the catalytic metal ion to the 3′-oxygen on the primer is what facilitates the chemical reaction, which is nucleophillic attack of the 3′-OH on the dNTP.[414] The nucleotide-binding metal ion also assists the leaving of pyrophosphate from the active site. The two metal ions are commonly Mg^{2+}.[415] Figure 1.17 below demonstrates the two metal ion catalytic mechanism.

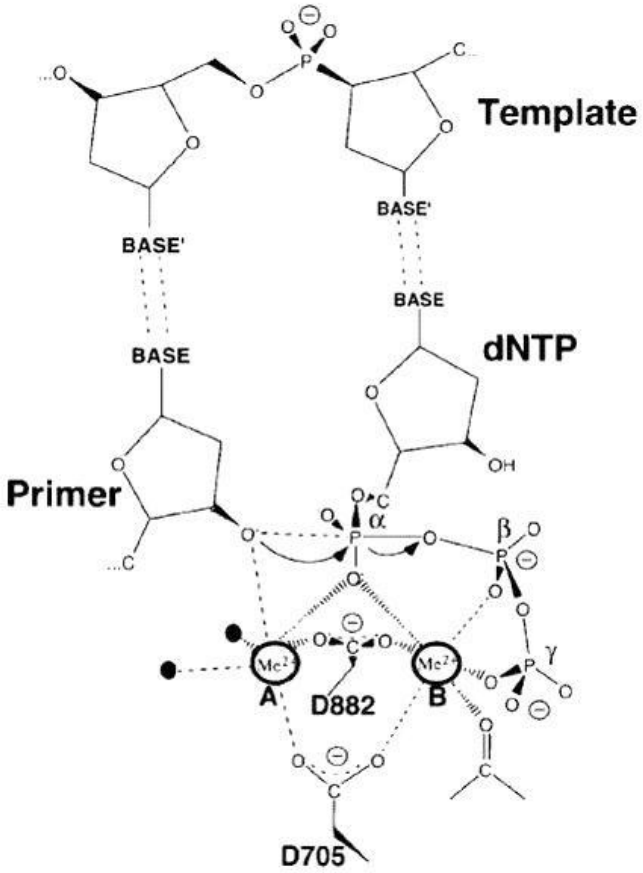

Figure 1.17: The two-metal ion mechanism of DNA polymerase. The two conserved aspartate residues D705 and D882 have the *E.Coli* DNA polymerase I numbers. *Taq* polymerase is homologous to *E.Coli* DNA Polymerase I,[416] but in *Taq* polymerase, the aspartate residues are numbered differently (Asp-610 and Asp-785).[416] Metal ion A can be seen to activate the 3′-OH group of the primer for nucleophillic attack on the α-phosphate on the dNTP. Metal ion B stabilises the negative charge on the leaving oxygen and chelates the β- and γ-phosphates. The figure is reproduced from reference 413.

1.11.4.3 Post-PCR Processing

In the initial phases of a PCR, amplification is exponential and the number of amplicons will double with every cycle (assuming 100% efficiency). As reagents are consumed and

depleted, the PCR slows down and eventually plateaus. Traditionally, it is at this plateau phase when traditional PCR can begin to detect the products. The amplified DNA products from the PCR can then be analysed using techniques such as:

- **Gel electrophoresis (DNA electrophoresis):** DNA molecules are placed into a gel matrix and an electric field is applied, moving the anionic DNA molecules through the gel matrix. Smaller molecules migrate further than large molecules as they can move more easily throughout the pores within the gel matrix. This process is known as sieving. The DNA molecules are typically stained with ethidium bromide (or SYBR® Green I – an asymmetric fluorescent cyanine dye used for nucleic acid staining) which fluoresces under UV light upon intercalation with DNA, making them visible when UV light is applied. Common stabilising media used as gels today are agarose and polyacrylamide.[417,418] "Ladders" are solutions of DNA molecules with varying known length added into the gel matrix and are used to help approximate the size of the DNA molecule of interest.
- **Southern Blotting**: Single- or double-stranded DNA molecules undergo gel electrophoresis, followed by transfer to a nylon membrane. Double stranded DNA is often denatured to produce single-stranded, blotted DNA, which is then heated or illuminated under UV light. Solutions that contain single-stranded labelled hybridisation probes that are complementary to the target sequences are then added under various conditions (i.e. changing temperature and salt concentration) and the hybridised DNA-probe complex will remain attached to the nylon membrane throughout multiple washing steps. The probes are often radio- or fluorophore-labelled, allowing the detection of the target sequence by measuring fluorescence, for example. This method is up to 100 times more sensitive than gel electrophoresis alone, allowing the differentiation between specific and non-specific PCR products.[419]
- Colorimetric assays, dot-spot analysis, oligomer-restriction and many others.[419]

Techniques such as gel electrophoresis and Southern blotting are relatively slow, non-automated, require post-PCR processing, have low sensitivity and precision and rely on discrimination of products by size or charge only. They provide qualitative analysis of PCR products. Also, as these techniques analyse the amount of DNA following both the exponential linear phase of amplification and the plateau phase, it is more difficult to determine the original amount of template DNA. However, a technique known as real-time

quantitative PCR (qPCR) allows the measurement and quantification of PCR products as they accumulate. This permits quantitative analysis of the DNA amplicons at all phases of the PCR amplification. This allows for more accurate determination of DNA concentration.[420,421]

Real-time PCR uses changes in fluorescence to quantify and detect the amount of DNA amplicons that have been synthesised in the PCR. Intercalating fluorescent dyes such as SYBR® Green I fluoresce when bound to double-stranded DNA, hence fluorescence will increase as the number of DNA amplicons increases. This can be detected by the PCR instrument which can also quantify the amount of fluorescence emitted. However, this method can lack specificity as all DNA in the reaction causes fluorescence of the dye, not just the specific required amplicon.[422] Another method of monitoring the qPCR is with fluorescent probes, which are complementary to the target DNA sequence. These probes are labelled at one end with a fluorescent reporter (donor) molecule on one end and a quencher (acceptor) at the other. In their normal, unbound state, fluorescence of the probe is low as the quencher is able to act upon the fluorescent reporter. During PCR, the probe binds to the target sequence of interest and is cleaved from this site by the $5' \rightarrow 3'$ exonuclease activity of *Taq* polymerase during the elongation step.[408] At this point, the reporter and quencher molecules become separated and fluorescence increases. As more copies of the DNA amplicon are made, more of the fluorescent probe molecules bind to the target DNA sequence and are cleaved by the *Taq* polymerase, resulting in an increase in fluorescence.[421] A reference dye may also be used to normalise the signal within the instrument and correct for any well-to-well changes.[421] Examples of fluorescent probes are *Taq*Man® probes and molecular beacons.[420,422] The mechanism of action of a *Taq*man® probe is shown below in Figure 1.18.

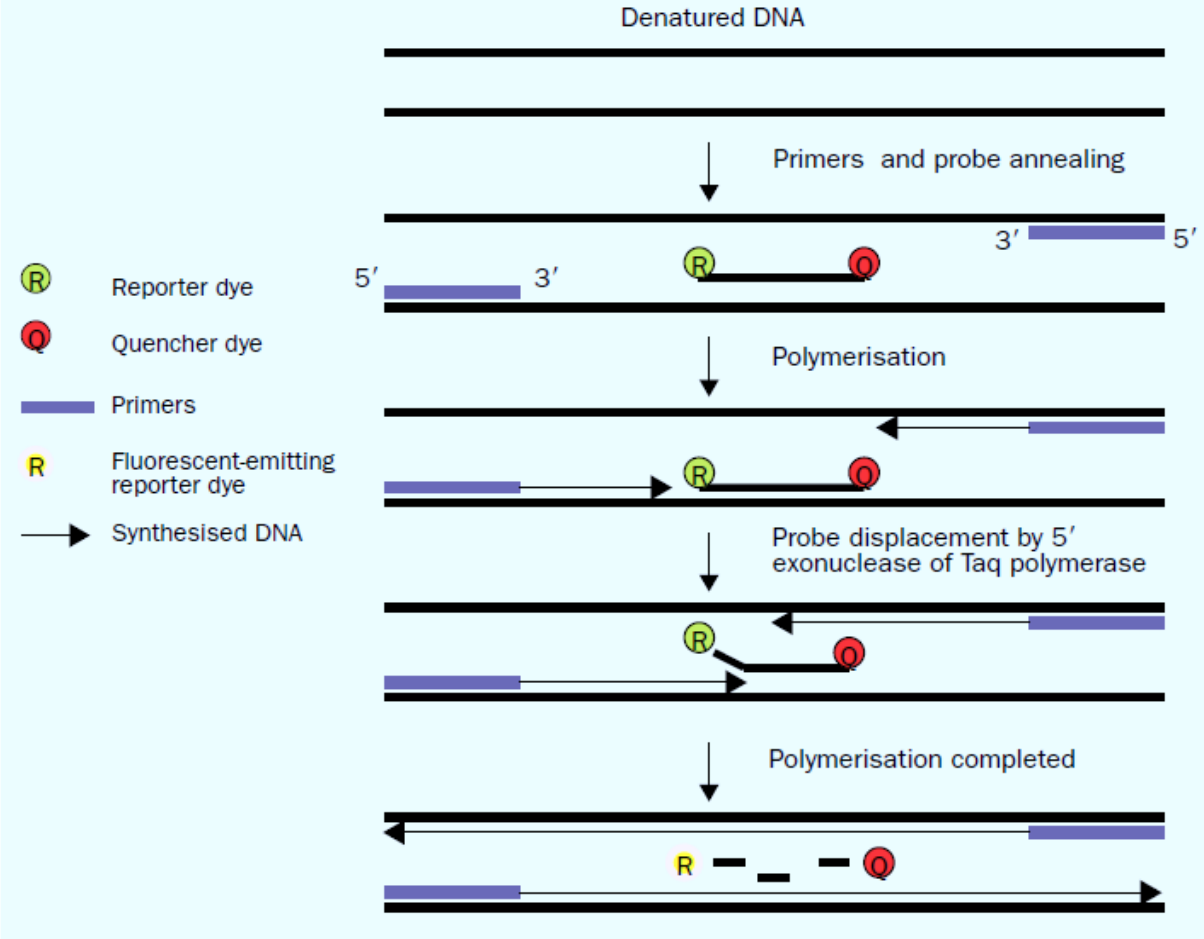

Figure 1.18: The mechanism of action of a *Taq*man® probe in real-time PCR. The probe sequence is homologous to a region with the target sequence. When the probe is intact, the reporter emission is quenched by the quencher molecule. During extension, the probe is cleaved *via* the 5′ exonuclease activity of the *Taq* polymerase, releasing the reporter and quencher resulting in an increase in fluorescence, which can be detected and quantified in real-time. As amplification continues, the strength of fluorescence will be proportional to the amount of PCR product made. Figure reproduced from reference 413.

1.12 Summary

With the current drive for 'greener' chemistry, magnetic nanoparticles functionalised with bio-molecules can potentially provide the answer, in the fields of bio-catalysis, bio-medicine, bio-separation and bio-sensors. Further strategies for immobilisation will emerge due to a current emphasis on research into alternative support materials. In terms of enzymes, even though extremely effective and applicable, methods that reduce activity such as cross-linking could lose focus in the search for methods which can increase catalytic activity while keeping the current advantages that enzymes possess.[423] It is envisaged that strategies to enable enzymes to be functional in more harsh conditions such as high/low temperature, pH and pressure and various organic solvents will be researched heavily to make them applicable in all fields. In the bio-medical industry, bio-functionalised magnetic nanoparticles are finding increasing application in areas such as cancer diagnosis, chemotherapy, hyperthermia, magnetic resonance imaging (MRI) and many more. In the areas of bio-separations and bio-sensors, it seems that a combination of effective separation and detection methods could be used together in order to provide more rapid and sensitive results. It is the aim of this project to immobilise various useful bio-molecules onto silica-coated SPIONs in order to produce efficient materials for applications in bio-catalysis, bio-medicine, bio-separation and bio-sensing with commercial viability.

CHAPTER 2

MATERIALS AND METHODS

2.1 Chemicals and Bio-molecules

All reagents employed in this study were available commercially, of highest purity grade and used as purchased unless otherwise stated.

Specialist reagents were obtained as follows: 3-aminopropyl tri-ethoxysilane (APTS) was obtained from Sigma-Aldrich, UK; 3-aminopropyl di-ethoxymethylsilane (APDS) and 3-aminopropyl mono-ethoxydimethylsilane (APMS) were both obtained from ABCR Specialty Chemicals, Germany. Lipases [*Candida Rugosa* (CRL) and *Pseudomonas Fluorescens*(PFL)], bovine serum albumen (BSA), Bradford reagent, salmon sperm DNA, glutaraldehyde solution (Grade I, 25% in H_2O), 4-nitrobenzaldehyde (4-NBA), *p*-nitrophenyl palmitate (PNPP), *p*-nitrophenol (PNP), sodium cyanoborohydride and chiral reagents [*cis*-3,5-dihydroxycyclopentene, *cis*-3,5-diacetoxy-1-cyclopentene, (1S,4R)-*cis*-4-acetoxy-2-cyclopenten-1-ol and (1R,4S)-*cis*-4-acetoxy-2-cyclopenten-1-ol] were all purchased from Sigma-Aldrich, UK. Ethanol (Absolute, 200 proof, Molecular Biology grade) was purchased from Fisher Scientific, UK. Oligonucleotide sequences specific to *Listeria Monocytogenes* (LM), shown in Table 2.1, were purchased from TIB-MOLBIOL, Germany.

Table 2.1: Single-stranded oligonucleotides specific to *Listeria Monocytogenes* (LM), used in the project.

Name	Oligonucleotide Sequence	Concentration of Stock Solution (nmol/mL)
C6-T1NH2 1.0 OD	5′-NH_2-dc_6- GGTGGCAAACGGTATTTGGCAT	4.10
C6-T1NH2	5′-NH_2-dc_6- GGTGGCAAACGGTATTTGGCAT	41.1
C12-T1NH2	5′-NH_2-dc_{12}- GGTGGCAAACGGTATTTGGCAT	41.1
C6-T2NH2 1.0 OD	5′-NH_2-dc_6- CACATTTGTCACTGCATCTCCGTG	4.30
C6-T2NH2	5′-NH_2-dc_6- CACATTTGTCACTGCATCTCCGTG	43.1
C12-T2NH2	5′-NH_2-dc_{12}- CACATTTGTCACTGCATCTCCGTG	43.1
T1-Comp Seq.	5′-ATGCCAAATACCGTTTGCCACC	44.3
T2-Comp Seq.	5′-CACGGAGATGCAGTGACAAATGTG	35.8
6F-T1-Comp Seq. 1.0 OD	5′-6FAM- ATGCCAAATACCGTTTGCCACC	4.40
6F- T1-Comp Seq.	5′-6FAM- ATGCCAAATACCGTTTGCCACC	44.4
6F-T2-Comp Seq. 1.0 OD	5′-6FAM- CACGGAGATGCAGTGACAAATGTG	3.60
6F-T2-Comp Seq.	5′-6FAM- CACGGAGATGCAGTGACAAATGTG	35.9

Oligonucleotide sequences specific to *Escherichia Coli* (EC), shown in Table 2.2, were also purchased from TIB-MOLBIOL, Germany.

Table 2.2: Single-stranded oligonucleotides specific to *Escherichia Coli* (EC), used in the project.

Name	Oligonucleotide Sequence	Concentration of Stock Solution (nmol/mL)
EC_541_FOR	5′-NH_2-dc_6-GGTCATATCTCTAACGCCATCC	45.7
EC_637_REV	5′-NH_2-dc_6-TGGCGTCGTGCATTAGTT	54.9
Comp FOR	5′-GGATGGCGTTAGAGATATGACC	40.0
Comp REV	5′-AACTAATGCACGACGCCA	49.6

2.2 Solutions and Buffers

All solutions were made up using E-pure deionised water supplied from a Thermo Scientific Barnstead Nanopure Water Deionisation System unless otherwise stated. All stock solutions and buffers were typically made up as shown in Table 2.3.

Table 2.3: Description, use and storage information of solutions and buffers used in the project.

Solution	Description	Use	Storage
Coupling solution	1 litre of solution was prepared containing 0.8% w/v acetic acid (glacial) in methanol	UV-Visible colorimetric assays and storage of NH_2 modified nanoparticles	1 litre capped clear glass bottle at 25ºC
Hydrolysis solution	1:1 mixture of methanol and water containing 0.15% acetic acid (glacial)	UV-Visible colorimetric assays	1 litre capped clear glass bottle at 25ºC
4-NBA solution (700 µg/ml)	7 mg of 4-NBA was dissolved in 10 ml coupling solution	UV-Visible colorimetric assays	Centrifuge tubes at 4ºC in the dark (used on the day of production)
Glutaraldehyde solution (5% w/v)	10 ml stock solution was typically prepared containing 1.886 ml glutaraldehyde and 8.114 ml 20×SSC buffer	Conversion of surface amine groups to aldehydes	Centrifuge tubes at -18ºC

Table 2.3: Continued.

Solution	Description	Use	Storage
$NaBH_3CN$ solution (0.03% w/v)	Stock solution was made by dissolving 3 mg $NaBH_3CN$ in 10 ml 1×SSC buffer	Reduction of C-N bond in oligonucleotide grafting	Centrifuge tubes at 4ºC
BSA solution (0.05% w/v)	Stock solution was made by dissolving 5 mg BSA in 10 ml 13×SSC buffer	Blocking solution used in hybridisation reactions	Centrifuge tubes at 4ºC
Salmon sperm DNA solution (1 mg/ml)	DNA (10 mg) was dissolved and sheared repeatedly with a syringe in sterile distilled water (10 ml), giving suspension density of 1 mg/mL	Salmon sperm DNA binding and elution assays	Centrifuge tubes at -18ºC
TEN buffer	Stock solution was made by mixing Tris-HCl (100 mM), EDTA (50 mM), NaCl (500 mM) and 100 ml distilled water	Salmon sperm DNA binding and elution assays	Capped clear glass bottle at 4ºC
20% PEG/4 M NaCl solution	Stock solution was made by dissolving 40 g polyethylene glycol (Mr 8000) in 200 ml NaCl (4 M)	Salmon sperm DNA binding and elution assays	Capped clear glass bottle at 4ºC
20×SSC stock buffer	Stock solution was made by dissolving 175.3 g NaCl and 88.2 g sodium citrate in 1 L water. The pH was adjusted to 7.4	Conversion of surface amine groups to aldehydes. Grafting and hybrid capture of oligonucleotides	Capped clear glass bottle at 25ºC
1×SSC and 13×SSC buffer solutions	20×SSC stock buffer solution was diluted respectively to produce 1× and 13×SSC buffers	Conversion of surface amine groups to aldehydes. Grafting and hybrid capture of oligonucleotides	Capped clear glass bottle at 25ºC
Reagent A	Gum Arabic (0.0667g), sodium deoxycholate (0.267g), Tris-HCl (12 mL, 250 mM) was added to 48 mL deionised water	Hydrolysis of PNPP reaction solvent in 1:1 mixture with isopropanol	Capped clear glass bottle at 25ºC
PBS Buffer	1×PBS tablet (136 mM NaCl, 3 mM KCl, 10 mM Na_2HPO_4, 2 mM KH_2PO_4) dissolved in 200mL water	Washing and storage of lipase- materials.	Capped clear glass bottle at 25ºC

2.3 Synthesis of Magnetite Nanoparticles, Fe_3O_4

2.3.1 Co-precipitation of Iron Chloride Solutions in Alkaline Media

Magnetite was prepared by the co-precipitation of ferrous and ferric chloride solutions in alkaline media and was carried out as follows.[424] Iron(III) chloride hexahydrate (10.8120 g, 0.04mol) was dissolved in 40 mL distilled, deionised water in a 1 litre round-bottomed flask equipped with a magnetic stirrer. To this, iron(II) chloride tetrahydrate (3.9762 g, 0.02 mol) dissolved in 10 mL HCl (2 M) was added whilst stirring. The brown/orange solution was stirred at room temperature whilst 500 mL of ammonium hydroxide solution (0.7 M) was added slowly, turning the solution black. The reaction was allowed to proceed with stirring at room temperature for a further 30 minutes. Following this, the reaction mixture was transferred to a 1 litre conical flask and the black precipitate was washed to neutral pH with distilled, deionised water *via* magnetic sedimentation and decantation using a slab magnet. The product, named **R1MA,** was observed to be dark red-brown in colour, having a slow response to the slab magnet. The supernatant was observed to be brown. The co-precipitation reaction is represented by the following Scheme 2.1:[425]

$$Fe^{2+} + 2\ OH^- \longrightarrow Fe(OH)_2$$

$$Fe^{3+} + 3\ OH^- \longrightarrow Fe(OH)_3$$

$$Fe^{2+} + 2\ Fe^{3+} + 8\ OH^- \longrightarrow Fe_3O_4 + 4\ H_2O$$

Scheme 2.1: The co-precipitation of iron(II) and iron(III) chloride.

Due to the weak magnetic response, this material was not used for further silica-coating, or for any bio-catalytic, bio-separation or bio-sensor applications.

2.3.2 Oxidative Hydrolysis of Iron Sulphate

This method involved the oxidative hydrolysis of iron(II) sulphate heptahydrate as the iron source under nitrogen at 90ºC.[29,424] Iron(II) sulphate heptahydrate (23.60 g, 0.085 mol) was dissolved in 220 mL degassed, deionised, distilled water in a 500 mL round-bottomed three-necked flask equipped with a magnetic stirrer, nitrogen inlet, condenser and thermometer. The solution was heated to 90ºC whilst stirring under nitrogen. To the solution, potassium nitrate (5.39 g, 0.053 mol) and potassium hydroxide (12.60 g, 0.225 mol) were added to the green solution whilst stirring. The resulting jet-black mixture was kept at 90ºC, with stirring under nitrogen for a further 4 hours. Subsequently, the mixture was allowed to cool for one

hour and was transferred to a 1 litre conical flask. The black precipitate was washed to neutral pH with distilled, deionised water *via* magnetic sedimentation and decantation using a slab magnet. The product, named **R2MC,** was observed to be black and had a strong affinity for the slab magnet. The supernatant was clear during storage.

Large-scale magnetite was prepared using a scaled-up version of the method used to prepare **R2MC**, similar to that reported by Bruce *et al*.[29] This method again involved the oxidative hydrolysis of iron(II) sulphate heptahydrate as the iron source under nitrogen at 90ºC[29]. Iron(II) sulphate heptahydrate (354.20 g, 1.27 mol) was dissolved in 3 litres degassed, deionised, distilled water in a 5 litre round-bottomed three-necked flask equipped with a magnetic stirrer, nitrogen inlet, condenser and thermometer. The solution was heated to 90ºC whilst stirring under nitrogen. Separately, potassium nitrate (80.90 g, 1.25 mol) was dissolved into 1 litre of degassed, distilled, deionised water in a 2 litre conical flask and potassium hydroxide (188.60 g, 3.36 mol) was added to the dissolved potassium nitrate solution whilst stirring. This mixture was heated to 65ºC and degassed with nitrogen for a further 5 minutes, before it was added to the iron sulphate solution dissolved previously. The resulting jet-black mixture was kept at 90ºC, with stirring under nitrogen for a further 4 hours. Subsequently, the mixture was allowed to cool for one hour and was transferred to a 5 litre conical flask. The black precipitate was washed to neutral pH with distilled, deionised water *via* magnetic sedimentation and decantation using a slab magnet. The method regularly yielded ~20 g of product. The product, **QBLSBM**, was observed to be black and had a strong affinity for the slab magnet. The supernatant was clear during storage.

The oxidative hydrolysis reaction is represented by Scheme 2.2:[34]

$$FeSO_4 + 2OH^- \longrightarrow Fe(OH)_2$$

$$3Fe(OH)_2 + NO_3^- \longrightarrow Fe_3O_4 + NO_2^- + 3H_2O$$

$$3Fe(OH)_2 + 2NO_2^- \longrightarrow Fe_3O_4 + 2NO + 2H_2O + 2OH^-$$

$$15Fe(OH)_2 + 2NO \longrightarrow 5Fe_3O_4 + 2NH_3 + 12H_2O$$

Scheme 2.2: The oxidative hydrolysis of iron(II) sulphate heptahydrate.

2.4 Silica-Coating of Magnetite Nanoparticles

2.4.1 Small-scale Amorphous Coating

Silica-coated magnetite nanoparticles were prepared *via* the small scale deposition of silica onto magnetite nanoparticles **R2MC** (see Section 2.3.2), from silicic acid solution at pH 10.[29] Aqueous sodium silicate solution, 20.75 g (13.80 mL, 27% SiO_2) was dissolved in water to a total volume of 500 mL with distilled, deionised water. A column containing 110 g of Amberlite IR-120 ion-exchange resin was regenerated with 1 litre each of the following: Hot water (70ºC), 3 M HCl and cold water. Sodium silicate solution was passed down the column, allowing the first 50 mL to pass uncollected. The subsequent 450 mL of the eluate (now in the form of silicic acid) was taken and it's pH was immediately raised to pH 12 with aqueous TMAOH (25%) to prevent homogeneous silica nucleation.[426] In addition to this, 5 g of magnetite suspension (R2MC) was mixed with 225 mL fresh distilled, deionised water and titrated to pH 12 with aqueous TMAOH (25%). With continued stirring, the silicic acid eluate (at pH 12) was added to the magnetite suspension. The mixture was then slowly titrated to pH 10.0 using 0.5 M HCl over approximately 1 hour. The mixture at pH 10.0 was stirred for another 2 hours at room temperature before transferring to a 2 litre conical flask. The silica-magnetite nanoparticles were washed once with 1 litre of TMAOH solution at pH 10.0 and then many times with 1 litre distilled, deionised water (*via* magnetic sedimentation) until the supernatant reached neutral pH. Four consecutive depositions (as described by the method above) were carried out for each material. Between each deposition, the silica-magnetite was washed with water until the supernatant reached neutral pH. An aliquot of suspension (20-50 mL) was retained for analysis following each deposition. The product, **CR2MC**, was observed to be black and had a strong affinity for the slab magnet. The supernatant was clear during storage.

2.4.2 Large-scale Amorphous Coating

Silica-coated magnetite nanoparticles were prepared *via* the large scale deposition of silica onto magnetite nanoparticle sample **QBLSBM** (see Section 2.3.2), from silicic acid solution at pH 10.[29] Aqueous sodium silicate solution, 83.0 g (55.2 mL, 27% SiO_2) was dissolved in water to a total volume of 2 litres with distilled, deionised water. A column containing 110 g of Amberlite IR-120 ion-exchange resin was regenerated with 1 litre each of the following: Hot water (70ºC), 3 M HCl and cold water. Sodium silicate solution was passed down the column, allowing the first 100 mL to pass uncollected. The subsequent 1800 mL of the eluate

(now in the form of silicic acid) was taken and its pH was immediately raised to pH 12 with aqueous TMAOH (25%) to prevent homogeneous silica nucleation. In addition to this, 20 g of magnetite suspension (**QBLSBM**, see Section 2.3.2) was mixed with 900 mL fresh distilled, deionised water and titrated to pH 12 with aqueous TMAOH (25%). With continued stirring, the silicic acid eluate (at pH 12) was added to the magnetite suspension. The mixture was then slowly titrated to pH 10.0 using 0.5 M HCl over approximately 1 hour. The mixture at pH 10.0 was stirred for another 2 hours at room temperature before transferring to a 5 litre conical flask. The silica-magnetite nanoparticles were washed once with 2 litres of TMAOH solution at pH 10.0 and then many times with 2 litres distilled, deionised water (*via* magnetic sedimentation) until the supernatant reached neutral pH. Four consecutive depositions (as described by the method above) were carried out for each material. Between each deposition, the silica-magnetite was washed with water until the supernatant reached neutral pH. An aliquot of suspension (20-50 mL) was retained for analysis following each deposition. The product, **QBLSSM**, was observed to be black and had a strong affinity for the slab magnet. The supernatant was clear during storage. The silicic acid deposition process used for coating the magnetite nanoparticles is represented by Figure 2.1.

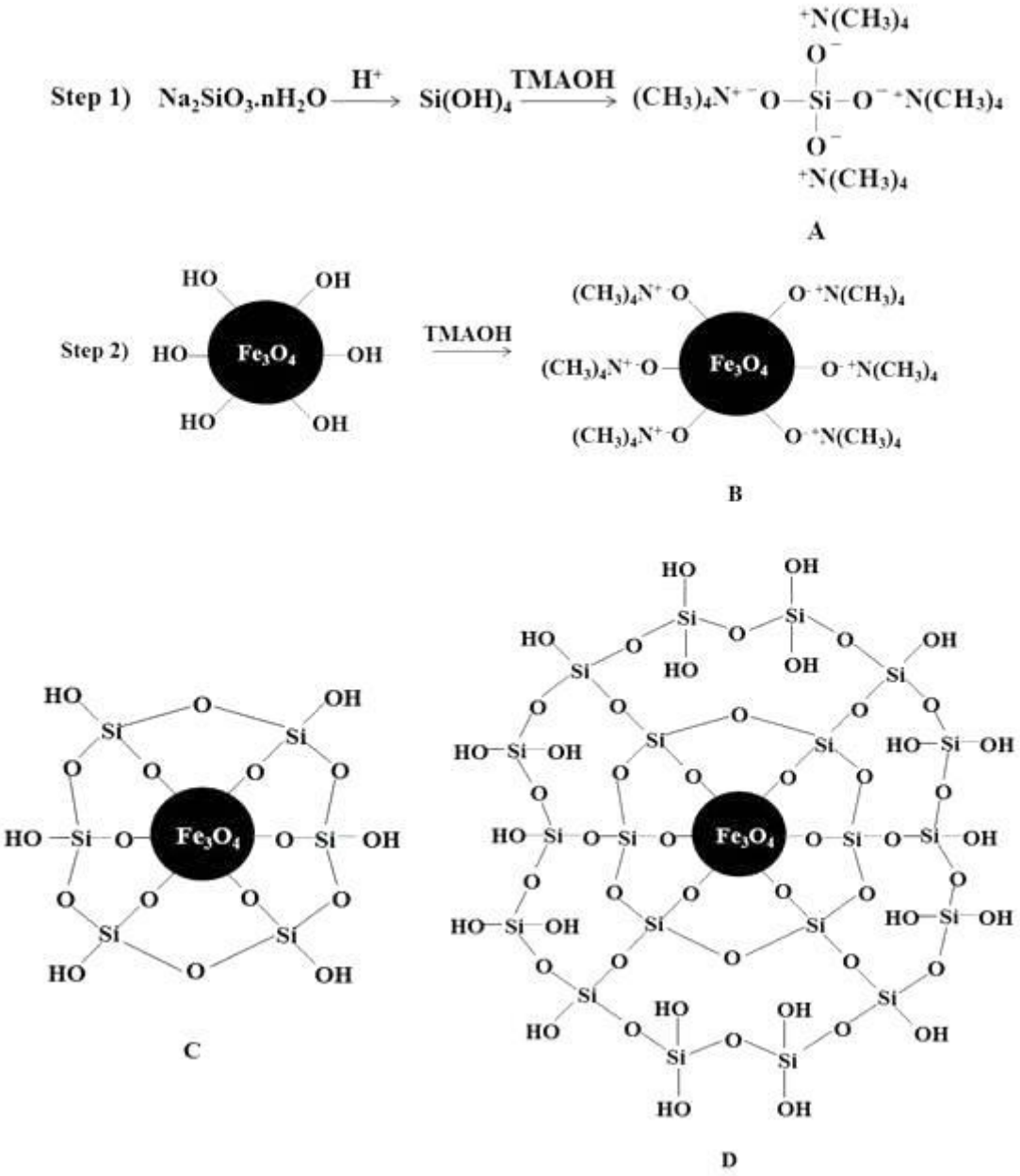

Figure 2.1: Representing the mechanism of the silica-coating process using the silicic acid deposition method. Step 1 involves the acidification of sodium silicate using an ion-exchange resin (Amberlite IR-120), followed by raising the pH to 12 using TMAOH to avoid nucleation of the silicic acid, forming A. Step 2 raises the pH of magnetite nanoparticles (forming B) in solution to around 12 so that when they are mixed with the silicic acid solution, the deposition and polycondensation of the silica can be controlled. When the magnetite nanoparticles and the silicic acid solutions are mixed at pH 12 and the pH is slowly adjusted to 10, the controlled and orderly deposition of silica onto the magnetite surface (*via* the Fe-O^- groups) takes place, forming product C. As the materials are allowed to mix further, polycondensation and polymerisation of silica takes place on the surface *via* the Si-OH groups, as shown by the formation of product D, producing a silica core-shell around the magnetite nanoparticles. Products are not drawn to scale and the figure is a schematic structural representation.

2.5 Surface Functionalisation of Silica-Magnetite Nanoparticles

2.5.1 'Classical' Silanisation of Silica and Silica-Magnetite Nanoparticles (Water Method)

Surface modification (silanisation) of silica-magnetite nanoparticles using various aminosilanes was performed as follows, using a modified method from that developed by Bruce *et al*.[80] Silica-magnetite nanoparticles (150 mg) were added to a freshly prepared solution of 30 mL of aminosilane in water (APTS, APDS or APMS, 2% w/v) in a 50 mL screw-capped centrifuge tube. The mixture was allowed to react at 50ºC for 20 hours in an incubator with end-over-end rotation at 40 rpm. Silanised silica-magnetite nanoparticles were washed with 3×10 mL coupling solution (0.8% v/v glacial acetic acid in methanol) and re-suspended in 10 mL of the solution at 5ºC. The products **TWQB, DWQB** and **MWQB** were all prepared from QBLSSM using APTS, APDS and APMS as the aminosilane sources, respectively. Surface amine densities were determined by colorimetric assay using 4-NBA.[88,427] It was observed in a detailed study by De Waterbeemd[428] that surface amine density suffered substantial decreases after prolonged storage and as a result, fresh batches of surface-functionalised nanoparticles were produced every month.

2.5.2 Tri-phasic Reverse Emulsion (TPRE) Silanisation of Silica and Silica-Magnetite Nanoparticles (TPRE method)[87,89]

Surface modification (silanisation) of silica-magnetite nanoparticles using various aminosilanes was performed as follows, using a modified method from Sen and Bruce.[89] Silica-magnetite nanoparticles (150 mg) were collected in a 50 mL screw-capped centrifuge tube *via* magnetic separation and to these, 30 mL of toluene and 5 g Triton X-100 were added. The mixture was shaken to form a tri-phasic reverse emulsion (TPRE). To this, the appropriate aminosilane (APTS, APDS or APMS, 2% w/v) was added to the emulsion and the mixture was allowed to react at 50ºC for 20 hours in an incubator with end-over-end rotation at 40 rpm. Functionalised silica-magnetite nanoparticles were washed with 3×10 mL coupling solution (0.8% v/v glacial acetic acid in methanol) and re-suspended in 10 mL of the solution at 5ºC. The products **TTQB, DTQB** and **MTQB** were all prepared QBLSSM using APTS, APDS and APMS as the aminosilane sources, respectively. Surface amine densities were determined by colorimetric assay using 4-NBA.[88,427] See Figure 1.5 in Section 1.6 for a representation of the ideal surface functionalised materials. It was observed in a detailed study by De Waterbeemd[428] that surface amine density suffered substantial decreases after

prolonged storage and as a result, fresh batches of surface-functionalised nanoparticles were produced every month.

2.6 Covalent Immobilisation of Lipase on the Functionalised Silica-Magnetite Nanoparticle Surface for Bio-catalytic Applications

2.6.1 Conversion of Surface Amine Groups to Aldehyde Groups Using Glutaraldehyde[80]

SSC buffer (20×) was prepared by dissolving sodium chloride (175.3 g) and sodium citrate (88.2 g) in 1 litre distilled, deionised water (final pH 7.4). SSC buffer (1×) was prepared by diluting 50 mL 20×SSC buffer to 1 litre with distilled, deionised water. Glutaraldehyde solutions were prepared immediately prior to their use. Aminosilane-modified silica-magnetite nanoparticles (50 mg) were washed 3 times with 10 mL 1×SSC buffer and the supernatant removed. Subsequently, 4 mL of a 5% w/v glutaraldehyde solution (in 20×SSC buffer) was added and the suspension was incubated for 3 hours at 18ºC with end-over-end rotation (40 rpm). After 3 hours, the nanoparticles were collected magnetically and the supernatant was removed. The nanoparticles were washed 3 times with 5 mL 1×SSC buffer to remove excess glutaraldehyde and then washed 3 times with 5 mL of PBS buffer (pH 7.2) before immobilisation of lipase.

2.6.2 Immobilisation of Enzymes

50 mg of non-functionalised (leading to physical adsorption) or glutaraldehyde-modified (covalent immobilisation) nanoparticles were magnetically collected and the supernatant removed. To these nanoparticles, 4 mL of lipase solution (CRL or PFL, 1 mg/mL in PBS buffer) was added and the reaction mixture was incubated at 18ºC overnight with end-over-end rotation (40 rpm). The amount of lipase in solution before and after immobilisation was calculated by measuring absorption at 595 nm using UV-Visible spectrophotometry using a modified version of the Bradford Assay (see Section 2.9.3 for details).[100,429,430]

The entire process, from surface functionalisation, to glutaraldehyde surface modification and enzyme immobilisation is demonstrated in Scheme 2.3.

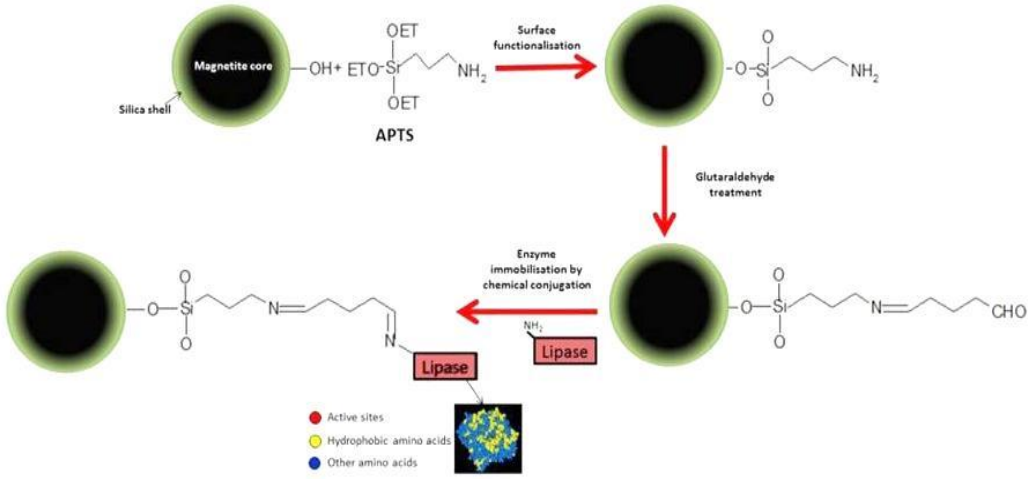

Scheme 2.3: A schematic diagram of surface functionalisation, glutaraldehyde surface modification and enzyme immobilisation on core-shell silica-magnetite nanoparticles (see Appendix II as reference).

2.6.3 Model Catalysis Reaction: Ester Hydrolysis: PNPP[100,431,432]

Hydrolysis of *p*-nitrophenyl palmitate (PNPP) was performed using 500 µg of either free (crude powder) or immobilised lipase (on non-functionalised (physical adsorption) or glutaraldehyde modified surface-functionalised (covalent immobilisation) nanoparticles reacting with 1 mL of ester solution (3.74 µmol/mL). The ester solution was prepared in a 1:1 mixture of isopropanol and reagent A (0.0667 g Gum Arabic + 12 mL of 250 mM Tris-HCl buffer, pH 7.8 + 48 mL of deionised water + 0.267 g of sodium deoxycholate) and the reaction was incubated for 1 hour at 25ºC with end-over-end rotation (40 rpm). After 1 hour, the supernatants were analysed for their absorbance at 410 nm using UV-Visible spectrophotometry (see Section 2.9.5 for details). Lipase-immobilised nanoparticles were then washed 3 times with 1 mL of the 1:1 mixture of isopropanol and reagent A. The washed materials were further used for the hydrolysis of PNPP under identical conditions as above, in order to test the catalytic efficiency and re-usability of lipase-immobilised nanoparticles for further catalytic cycles. The reaction is demonstrated in Section 1.10.

2.6.4 Bio-catalytic Application: Transesterification of Ethyl Butyrate

Initial Method

This reaction was carried out using a modification of the method described by Solanki and Gupta.[301] Ethyl butyrate (60 mM) and *n*-butanol (120 mM) were taken in a 1.5 mL screw-cap centrifuge tube containing 1 ml of hexane followed by the addition of 500 µg free lipase or lipase immobilised nanoparticles containing 500 µg of immobilised lipase. The reaction

mixture was incubated for 24 hours at 37ºC with end-over-end rotation (40 rpm). A 5 µL aliquot of the reaction mixture was withdrawn and analysed by GC and GC-MS (see Section 2.9.6 for details). The remaining reaction supernatant was removed from the lipase immobilised nanoparticles by magnetic separation and the nanoparticles were washed 3 times with 1 mL distilled, deionised water and the reaction was repeated for further cycles under identical conditions as above, in order to test the catalytic efficiency and re-usability of lipase-immobilised nanoparticles. A control experiment was run in which the non-modified nanoparticles (without any lipase) were added. The amount of transesterification product (butyl butyrate) resulting from the reaction was calculated from a calibration curve constructed from the peak areas, obtained using a series of standard butyl butyrate solutions prepared in hexane (see Section 2.9.6). The reaction mechanism is demonstrated in Figure 1.15 in Section 1.10.

Optimised Method

This reaction was carried out using a modification of the method described by Liaquat *et al*[301,303] and was necessary due to poor results obtained using the initial method above. Ethyl butyrate (600 mM) and *n*-butanol (100 mM) were taken in a 1.5 mL screw-cap centrifuge tube containing 1 ml of 10% water/hexane followed by the addition of 500 µg free lipase or lipase immobilised nanoparticles containing 500 µg of immobilised lipase. The reaction mixture was incubated for 24 hours at 37ºC with end-over-end rotation (40 rpm). A 5 µL aliquot of the reaction mixture was withdrawn and analysed by GC and GC-MS (see Section 2.9.6 for details). The remaining reaction supernatant was removed and the lipase-immobilised nanoparticles were washed 3 times with 1 mL distilled, deionised water and the reaction was repeated for further cycles under identical conditions as above, in order to test the catalytic efficiency and re-usability of lipase-immobilised nanoparticles. A control experiment was similarly run in which the non-modified nanoparticles (without any lipase) were added. The amount of transesterification product (butyl butyrate) resulting from the reaction was calculated following the same method described in the initial method.

2.6.5 Bio-catalytic Application: Partial and Selective Hydrolysis of *Cis*-3,5-diacetoxy-1-cyclopentene to (1S,4R)-*cis*-4-acetoxy-2-cyclopenten-1-ol and its Enantiomer

Cis-3,5-diacetoxy-1-cyclopentene (50 µmol) was taken in a 1.5 mL screw-cap centrifuge tube containing 800 µL hexane and 200 µL water (20% water concentration) followed by addition of 500 µg free lipase or lipase immobilised nanoparticles containing 500 µg of immobilised

lipase. The reaction mixture was typically incubated for up to 48 hours at two different temperatures (25ºC and 37ºC) with end-over-end rotation (40 rpm). During the reaction, a 10 µL aliquot of the reaction mixture (water layer) was withdrawn and analysed by GC and GC-MS (see Section 2.9.7 for details) at 1 h, 24 h and 48 h for kinetic experiment. The amount of hydrolysis reaction products (*cis*-3,5-dihydroxycyclopentene, (1S,4R)-*cis*-4-acetoxy-2-cyclopenten-1-ol and its enantiomer) resulting from the reaction were calculated from pre-constructed calibration curves using a series of standard solutions (*cis*-3,5-dihydroxycyclopentene, (1S,4R)-*cis*-4-acetoxy-2-cyclopenten-1-ol and its enantiomer) prepared in water (see Section 2.9.7). The hexane layer was also analysed to calculate initial concentrations of *cis*-3,5-diacetoxy-1-cyclopentene. The reaction is depicted in Scheme 1.10, Section 1.10. The reaction was also repeated using 50% water/hexane (500 µL hexane and 500 µL water) as the solvent system at 25ºC.

2.7 Oligonucleotide Grafting and Hybrid Capture Assay for Bio-sensor and Bio-separation Applications

2.7.1 Conversion of Surface Amine Groups to Aldehyde Groups Using Glutaraldehyde

SSC buffer (20×) was prepared by dissolving sodium chloride (175.3 g) and sodium citrate (88.2 g) in 1 litre distilled, deionised water (final pH 7.4). SSC buffer (1×) was prepared by diluting 50 mL 20×SSC buffer to 1 litre with distilled, deionised water. Glutaraldehyde solutions were prepared immediately prior to their use. Aminosilane-modified silica-magnetite nanoparticles (50 mg) were washed 3 times with 10 mL 1×SSC buffer and the supernatant removed. Subsequently, 4 mL of a 5% w/v glutaraldehyde solution (in 20×SSC buffer) was added and the suspension was incubated for 3 hours at 18ºC with end-over-end rotation (40 rpm). After 3 hours, the nanoparticles were collected by magnetic separation and the supernatant was removed. The nanoparticles were washed 3 times with 5 mL 1×SSC buffer to remove excess glutaraldehyde. The reaction can be seen in Scheme 2.3, above in Section 2.6.2.

2.7.2 Oligonucleotide Grafting on Functionalised Nanoparticle Surface

This method is similar to one previously employed by Bruce *et al.*[80] Immediately following glutaraldehyde surface modification, a 3.3 μM solution (0.5 mL, 1.65 nmol total) of 5′-amine-modified oligonucleotides in 1×SSC coupling buffer solution (corresponding to the oligonucleotides in Table 2.1 or Table 2.2) was added and the mixture was left incubating overnight at 18ºC with end-over-end rotation (40 rpm). The oligonucleotide-modified

nanoparticles were then washed once with 1 mL 1×SSC coupling buffer and placed in 0.8 mL of $NaBH_3CN$ solution [0.1% (w/v) in 1×SSC coupling buffer] for 30 minutes at 18°C with end-over-end rotation (40 rpm). The materials were then washed 3 times with 0.8 mL of 1×SSC coupling buffer and finally re-suspended in 200 µL of the same.

2.7.3 Model Assay: Hybrid Capture of Complementary Oligonucleotide Sequence from Solution (Initial Method)

This method is again similar to one previously employed by Bruce *et al.*[80] Oligonucleotide-grafted particles (1 mg equivalent to 100 µL suspension) were washed twice with 0.5 mL of water and heated to 80°C for 4 minutes. The water was removed and a solution of complementary oligonucleotide sequence containing 200 µL (equivalent to 1.65 nmol total) in 13×SSC coupling buffer / 0.05% BSA at the required concentration (see Table 2.3, Section 2.2) was added and the suspension was incubated with end-over-end rotation (40 rpm) for 30 minutes at 18°C. The supernatant was removed and their absorbance at 260 nm was analysed by UV-Visible spectrophotometry. After the nanoparticles were washed 3 times with 1 mL of 13×SSC coupling buffer, 200 µL of water was added and the nanoparticle suspension was heated to 85°C for 4 minutes to disassociate the annealed complementary/captured sequences. The supernatant was removed and their absorbance at 260 nm was analysed by UV-Visible spectrophotometry (see Section 2.9.4 for details).

2.7.4 Model Assay: Hybrid Capture of Complementary Oligonucleotide Sequence from Solution (Revised Method in Consultation with Q-Bioanalytic GmbH, Germany)

The oligonucleotide sequences which we used for grafting and capture / dehybridisation were specially designed for use in PCR by Q-Bioanalytic GmbH. Oligonucleotide-grafted particles (1 mg equivalent to 100 µL suspension) were washed twice with 0.5 mL of water and heated to 95°C for 10 minutes. Water was removed and a solution of complementary oligonucleotide sequence containing 200 µL (equivalent to 1.65 nmol total) in 13×SSC coupling buffer / 0.05% BSA at the required concentration (see Table 2.3, Section 2.2) was added and the suspension was incubated with end-over-end rotation (40 rpm) for 1 minute at 60°C. The supernatant was removed and their absorbance at 260 nm was analysed by UV-Visible spectrophotometry. After the nanoparticles were washed 3 times with 1 mL of 13×SSC coupling buffer, 200 µL of water was added and the nanoparticle suspension was heated to

95°C for 10 minutes to disassociate the annealed complementary/captured sequences. The supernatant was removed and their absorbance at 260 nm was analysed by UV-Visible spectrophotometry (see Section 2.9.4 for details). The assay can be represented using the following Scheme 2.4.

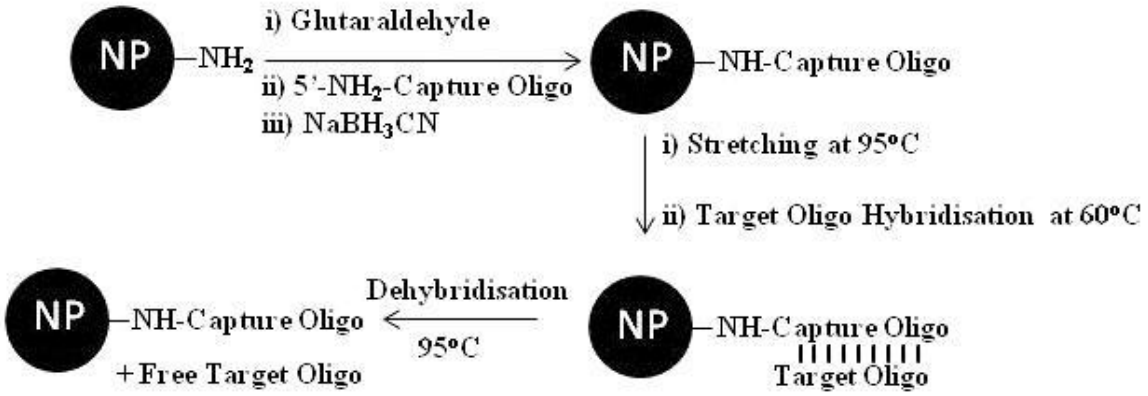

Scheme 2.4: Schematic representation of hybrid capture of target oligonucleotide sequence by an immobilised nucleotide of pre-defined sequence and subsequent dehybridisation of the captured oligonucleotide. The black spheres represent surface-functionalised core-shell silica-magnetite nanoparticles.

2.7.5 Extraction of DNA Protocol (Bio-separation)

1 mL of pre-enrichment culture (in this case either LM, EC, a 1:1 mixture of LM: EC, or water as control) was transferred to a sterile 1.5 mL centrifuge tube. The mixture was centrifuged at 10,000 rpm for 10 minutes and the supernatant was discarded. 400 µL of lysis buffer (100 mM Tris-HCl, 10 mM EDTA, 1 M NaCl, pH 8.0) and 10 µL Proteinase K was pipetted onto the centrifuged bacteria pellet and the solution was mixed well. The mixture was then incubated for 20 minutes at 65ºC on a thermal mixing block. The mixture was then centrifuged again at 10,000 rpm for 5 minutes to remove the matrix and cell debris. The clarified supernatant containing the DNA was transferred to a new sterile 1.5 mL centrifuge tube. 400 µL of binding buffer [20% PEG (M_r 8000) in 4M NaCl] and 25 µL (equivalent to 0.5 mg) of silica-magnetite nanoparticles (QBLSSM, suspension density of 20 mg/mL) were added to the DNA-containing mixture, which was incubated at room temperature for 5 minutes. The nanoparticles were magnetically immobilised and the supernatant was removed and discarded. The nanoparticles were then washed with 400 µL washing buffer (75% ethanol in water). The nanoparticles were magnetically immobilised and the washing buffer was removed and discarded. The centrifuge tube containing the nanoparticles was left open at room temperature to evaporate the ethanol (but not to complete dryness). The nanoparticles

were then re-suspended in 100 μL elution buffer (distilled, deionised water) and incubated for 5 minutes at 65ºC on a thermal mixing block. Finally, the nanoparticles were magnetically immobilised and the supernatant (100 μL, containing eluted DNA) was transferred to a new sterile 1.5 mL centrifuge tube for use in the next step (specific capture of bacterial DNA).

2.7.6 Bio-sensor and Bio-separation Application: Selective detection and determination of LM and EC in food samples

A series of solutions of *Listeria Monocytogenes* (LM) in peptone water; *Escherichia Coli* (EC) in peptone water and a 1:1 mixture of *Listeria Monocytogenes* (LM) and *Escherichia Coli* (EC) in peptone water were prepared. The extraction of DNA from the bacterial samples was carried out using the DNA Extraction Protocol (see Section 2.7.5), which employs the silica-magnetite nanomaterial QBLSSM. The extracted DNA was used for selective detection and determination of either LM or EC from inoculated food samples.

Selective Detection and Determination of Either LM or EC in Food Samples (One-step Assay)

Oligonucleotide-grafted nanoparticles (10 μL equivalent to 100 μg suspension) with specific primer sequences (forward and reverse related to PCR) with C_6 or C_{12} spacers were mixed with each other (C_6-spacer forward primer attached nanomaterials were mixed with C_6-spacer reverse primer attached nanomaterials only and C_{12}-spacer forward primer attached nanomaterials were mixed with C_{12}-spacer reverse primer attached nanomaterials only), providing a total of 200 μg of oligonucleotide-grafted nanoparticles. When amine-functionalised (TTQB) and un-modified silica-magnetite (QBLSSM) nanoparticles were used for comparison, 200 μg of each was also used. The nanoparticles were washed once with 0.5 mL water and 100 μL of extracted bacterial DNA solution obtained from the extraction step was added (see Section 2.7.5).

The mixture containing bacterial DNA and nanoparticles was first incubated for 5 minutes at 95ºC on a thermal mixing block. The mixture was then instantly transferred to a thermal mixing block set at 65ºC for 5 minutes for hybridisation of the complementary sequences in the mixture to the oligonucleotide-grafted nanoparticles, or physical adsorption to other nanoparticles. The nanoparticles were then magnetically immobilised and the supernatant discarded. The nanoparticles were washed twice with 0.5 mL 13×SSC coupling buffer and 100 μL of distilled / deionised water was added to the washed nanoparticles. The suspension

was heated to 95°C for 10 minutes on a thermal mixing block to disassociate the annealed complementary/captured sequences. The nanoparticles were then magnetically immobilised and the supernatant taken for analysis by quantitative real-time PCR (qPCR) (see Section 2.9.8 for details).

Sensitivity of Detection Limits of Either LM or EC in Food Samples (One-step Assay)

A series of diluted solutions of *Listeria Monocytogenes* (LM) or *Escherichia Coli* (EC) in peptone water were prepared and the extraction of DNA from the bacterial samples was carried out using the protocol described earlier.

Oligonucleotide-grafted nanoparticles (10 µL equivalent to 100 µg suspension) with specific primer sequences (forward and reverse, see Table 2.1 and Table 2.2, Section 2.1) were mixed with each other and used for hybrid capture followed by qPCR analysis.

Two Step Hybrid Capture Assay

The reaction protocols for selective detection of LM or EC from a mixture (see Section 0) and determining the sensitivity of detection of LM or EC (see Section 0) were modified slightly by adding the forward and reverse primer-immobilised nanoparticles separately for hybridisation, followed by de-hybridisation and qPCR analysis of complementary sequences separately.

2.8 Chemical and Physical Characterisation Methods

2.8.1 Surface Area Analysis (BET)

Nanoparticles (500 to 1000 mg) were dried overnight in an oven at 80°C. Prior to analysis, bare magnetite and core-shell silica-magnetite nanoparticles were degassed at 100°C for 24 hours. Analysis was performed using a Micromeritics ASAP 2010 (Accelerated Surface Area and Porosimetry System).

2.8.2 Nanoparticle Size Analysis - Transmission Electron Microscopy (TEM)

Images of magnetite nanoparticles were obtained by TEM using a JEOL JEM-2000 EX electron microscope at 200 kV. Images were processed using Gatan Digital Micrograph Software. Prior to analysis nanoparticles suspensions were diluted 50 times in ethanol and approximately 2 µL of diluted suspension was placed on a carbon coated copper grid (400 mesh, Agar Scientific, UK) which was then dried in air for 10 minutes.

2.8.3 Iron Oxide Phase Analysis - X-Ray Diffraction (XRD)

X-ray diffraction (XRD) was used for the confirmation of the identity of magnetite and silica-coated magnetite nanoparticles. Nanoparticles were dried overnight in an oven at 80ºC and then ground to fine powder which was pressed into a clear silicon single crystal low background holder (size: 24.5 mm diameter, 1 mm depth). The holder was then mounted in the spinning auto sampler of a Bruker D2 Phaser desktop X-ray diffractometer and scanned continuously between 5-80º at a scan axis 2θ measuring 3715 steps at 0.9 seconds per step (each step size was 0.02º) with a 5º detector window.

2.8.4 Magnetic Measurements – Vibrating Sample Magnetometry VSM)

The saturation magnetisation and magnetisation curve measurements were carried out using a 7 kOe vibrating sample magnetometer (VSM) at room temperature (298 K). Samples of bare and silica-coated magnetite nanoparticles were crushed into a fine power before being packed into plastic tubes of length ~10 mm and internal diameter ~1.9 mm. This geometry ensures that any demagnetisation effects are kept low.[433]

2.9 Analytical Methods

2.9.1 Silica Coating Homogeneity Analysis

Salmon sperm DNA binding and elution assays were used to confirm silica coating on magnetite nanoparticles and the method[29] was as follows. Salmon sperm DNA solution (50 µL, see Table 2.3, Section 2.2) was mixed with TEN buffer (400 µL, see Table 2.3, Section 2.2) and PEG/NaCl (400 µL, see Table 2.3, Section 2.2) and its absorbance at 260 nm was measured by UV-Visible spectrophotometry using a Jenway 7315 Spectrophotometer (Bibby Scientific Limited, Stone, Staffordshire, UK). The solution was then added to either bare or silica-coated magnetite nanoparticles [2 mg, previously washed in sterile water (3×1 mL)] and the suspension was incubated in a sterile centrifuge tube (1.5 mL capacity) for 5 minutes at room temperature with end-over-end rotation (40 rpm). The nanoparticles were then collected magnetically, the supernatant retained and analysed at 260 nm and the nanoparticles were then washed in 70% aqueous ethanol (1 mL) for 5 minutes to remove any un-bound DNA. Adsorbed DNA was subsequently eluted by incubating the nanoparticles in sterile water (500 µL) for 5 minutes at room temperature with end-over-end rotation (40 rpm). This elution was then repeated one more time and each 500 µL aliquot was assayed independently for its absorbance at 260 nm to estimate its DNA content. The amount of DNA present in both aliquots was added together to calculate total elution of DNA. The DNA concentrations

were determined using a calibration curve constructed from a range of standard DNA solutions prepared in water and 1:1 TEN buffer: PEG/4M NaCl solution.

Figure 2.1 presents two standard curves constructed using a series of dilutions of salmon sperm DNA in a 1:1 TEN:PEG solution (see Table 8, Section 2.2) to assess initial and adsorbed DNA concentrations and then in water, to assess the eluted DNA concentration. Absorbance was measured by UV-Visible spectrophotometry at 260 nm.

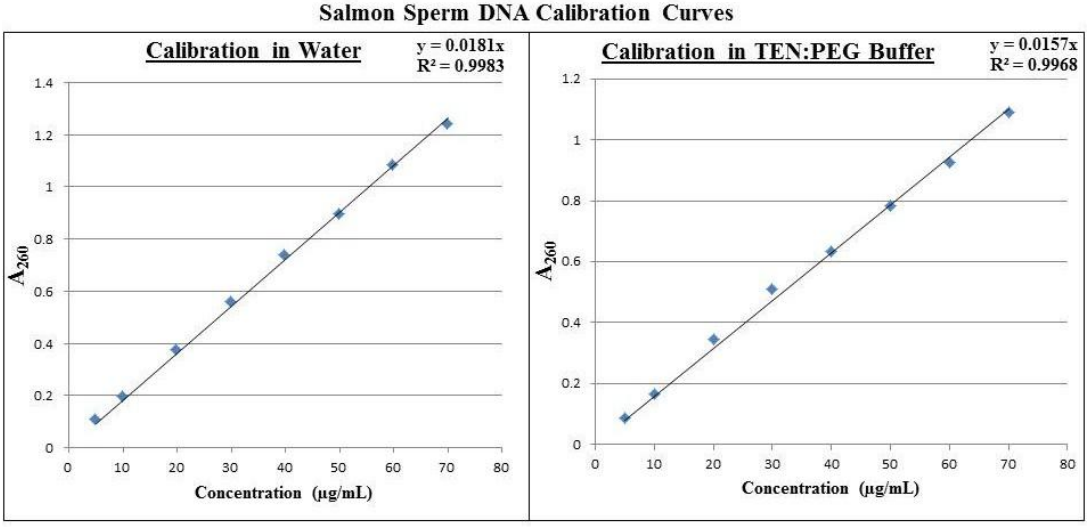

Figure 2.1: Salmon sperm DNA calibration curves constructed in a 1:1 mixture of TEN buffer: 20% PEG in 4M NaCl (top) and water (bottom).

Figure 2.1 shows that linearity is observed over the entire range of 0-70 µg/mL in both cases. New standard curves were produced every six months using fresh samples to maintain reliability and reproducibility.

2.9.2 Surface Amine Density Assay

This assay was used for the detection and quantification of surface amine groups on aminosilane-functionalised nanoparticles. The method used is a modified version of that previously described by Moon *et al*[88,427] and is similar to the method used by Bruce and Sen.[80] Aminosilane-functionalised nanoparticles (5 mg) were placed in a 1.5 mL centrifuge tube and washed 4 times with 1 mL of coupling solution [0.8% (v/v) glacial acetic acid in dry methanol]. Then, 1 mL of 4-NBA (0.7 mg/mL in coupling solution) was added to the nanoparticles and the suspension was allowed to react for 3 h with gentle end-over-end rotation at room temperature. The supernatant was then magnetically removed from the particles and its absorbance was measured at 282 nm by UV-Visible spectrophotometry using a Jenway 7315 Spectrophotometer (Bibby Scientific Limited, Stone, Staffordshire, UK).

After removal of the supernatant and washing 4 times with 1 mL of coupling solution, 1 mL of hydrolysis solution (composition: 75 mL of water, 75 mL of methanol and 0.2 mL of glacial acetic acid) was added to the nanoparticles and the tube was incubated for a further hour with end-over-end rotation (40 rpm) at room temperature. The supernatant was then magnetically removed from the nanoparticles and its absorbance was measured at 282 nm. The amount of 4-NBA in the hydrolysis solution was calculated using a calibration curve previously constructed from a range of standard 4-NBA solutions prepared in hydrolysis solution (see Table 2.3, Section 2.2). Figure 2.2 presents the standard curve constructed using a series of dilutions of 4-NBA in hydrolysis solution.

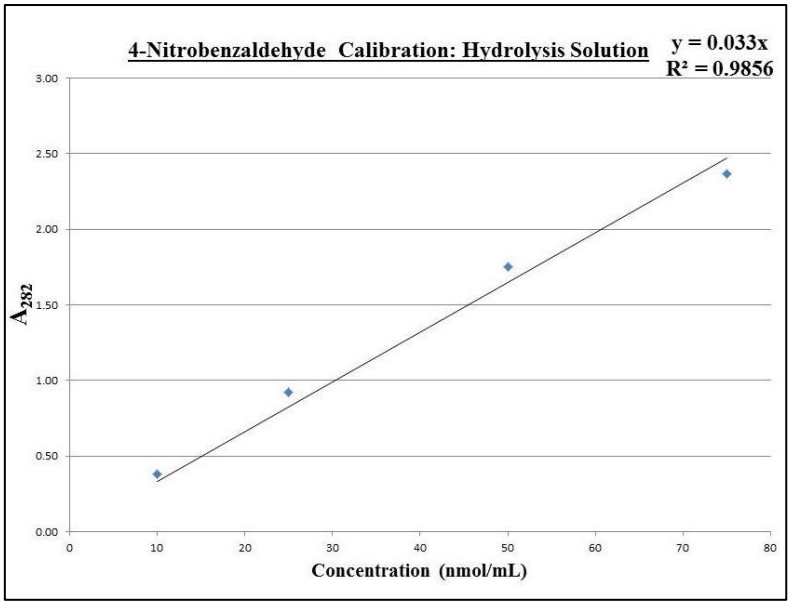

Figure 2.2: Calibration curve for 4-NBA in hydrolysis solution.

Figure 2.2 shows that linearity is observed over the entire range of 0-75 nmol/mL. For further accuracy, samples with $A_{282\ nm} > 1.500$ were diluted for measurement. New standard curves were produced every six months using fresh samples to maintain reliability and reproducibility. This had to be done because surface amine density has been shown to decrease during longer term storage.[428] The assay can be represented by Scheme 2.5.

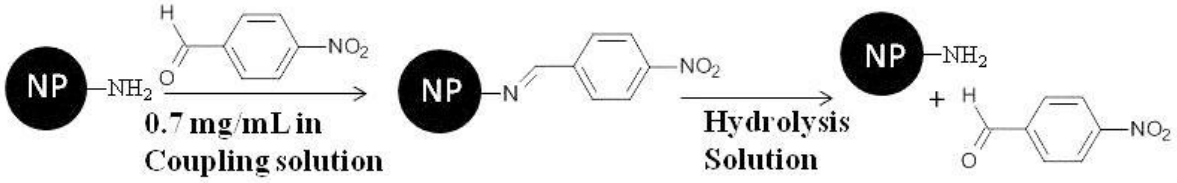

Scheme 2.5: Schematic representation of the 4-NBA colorimetric surface assay.

2.9.3 Bradford Assay for Determination of Adsorbed Lipase on Nanoparticles

This project employed a modified version of the Bradford Assay for quantitative protein determination[429,430] that was used by Sen *et al*[100] in 2010. For lipase immobilised *via* chemical conjugation, following glutaraldehyde surface modification of materials, 4 mL of a 1000 µg/mL solution of free lipase in PBS buffer was added to 50 mg of the glutaraldehyde-modified materials and the mixture was incubated overnight for 20 hours at 25ºC with end-over-end rotation at 40 rpm. For lipase immobilised *via* physical adsorption, 4 mL of a 1000 µg/mL solution of free lipase in PBS buffer was added to 50 mg of silica-magnetite nanoparticles and the mixture was incubated overnight for 20 hours at 25ºC with end-over-end rotation at 40 rpm. Following the 20 hour incubation period, the amount of lipase remaining in the supernatant was calculated using UV-Visible spectrophotometry; by measuring it's absorbance at 595 nm and subtracting the amount remaining in solution from the initial amount of lipase added (4000 µg) using standard curves produced from a set of standard free lipase solutions of known concentration.

Standard curves were constructed using a series of dilutions of lipases in PBS buffer (1 mL) mixed with Bradford Reagent (1.2 mL). Absorbance was measured by UV-Visible spectrophotometry at 595 nm. Figure 2.3 below presents the curves produced for both CRL and PFL. In the case of PFL, the entire standard curve obtained was split into 3 separate graphs as it remained linear in these sections.

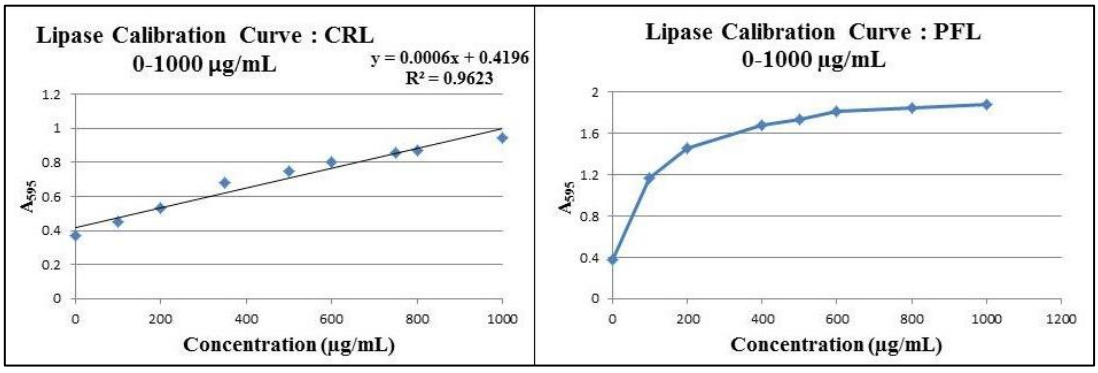

Figure 2.3: Calibration curves for CRL (left) and PFL (right).

Figure 2.3 shows that in the case of CRL, linearity is observed over the entire range of 0-1000 µg/mL, with the line equation y = 0.0006x + 0.4196. In the case of PFL, the curve produced from the entire range is non-linear, but contains 3 distinct regions of linearity, from which concentration could be calculated based on absorbance. The linear range of 0-200 µg/mL for PFL has the line equation y = 0.0054x +0.4565. The linear range from 200-600

μg/mL has the line equation y = 0.0009x + 1.288 and the linear range between 600-1000 μg/mL has the line equation y = 0.0002x + 1.7057. Hence, in order to calculate the amount of lipase present in solution, the correct curve had to be selected depending on the absorbance value produced at 595 nm. New standard curves were produced every six months using fresh samples to maintain reliability and reproducibility. These curves were used to calculate the amount of lipase that had been immobilised on glutaraldehyde-modified nanoparticles (see Section 3.8).

2.9.4 UV-Visible Assay for Determination of Oligonucleotide Concentration

The heterocyclic bases present in nucleic acids are aromatic and absorb light in the UV region. The λ_{max} value for these bases lies between 250-280 nm (values provided with the oligonucleotides by TIB-MOLBIOL, Germany), therefore by measuring the absorbance of a series of aqueous oligonucleotide solutions of known concentration at 260 nm, a set of calibration curves was produced. Absorbance was measured by UV-Visible spectrophotometry at 260 nm. Figure 2.4, Figure 2.5 and Figure 2.6 below present the curves constructed using a series of dilutions of oligonucleotides in water for oligonucleotide sequences specific to both *Listeria Monocytogenes* and *Escherichia Coli*.

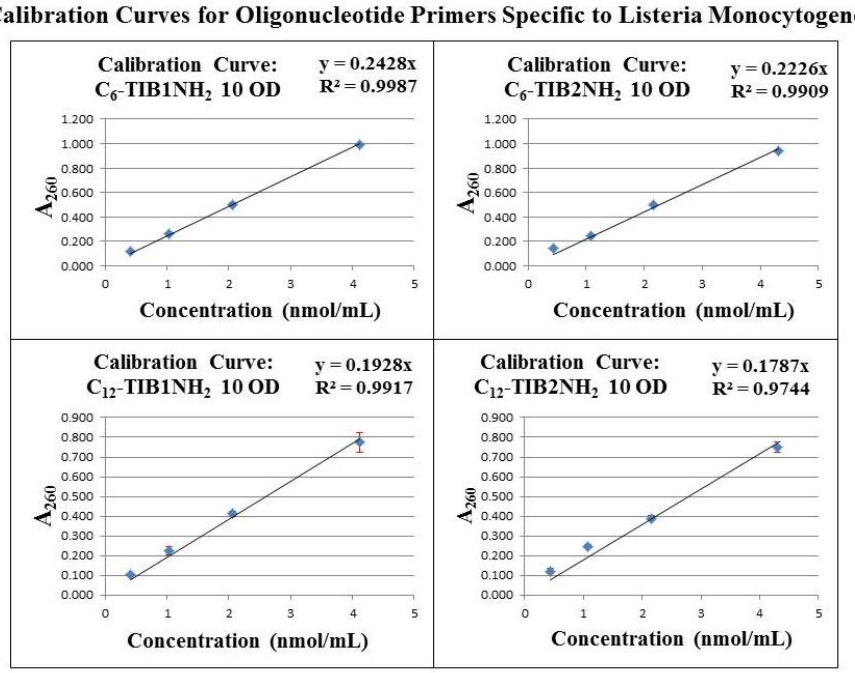

Figure 2.4: Calibration curves for *Listeria Monocytogenes*-specific forward (top-left with C_6-spacer, bottom-left with C_{12}-spacer) and reverse (top-right with C_6-spacer and bottom-right with C_{12}-spacer) oligonucleotides. See Table 2.1, Section 2.1, for the full oligonucleotide sequences. Values are mean ± S.E.M., n = 3.

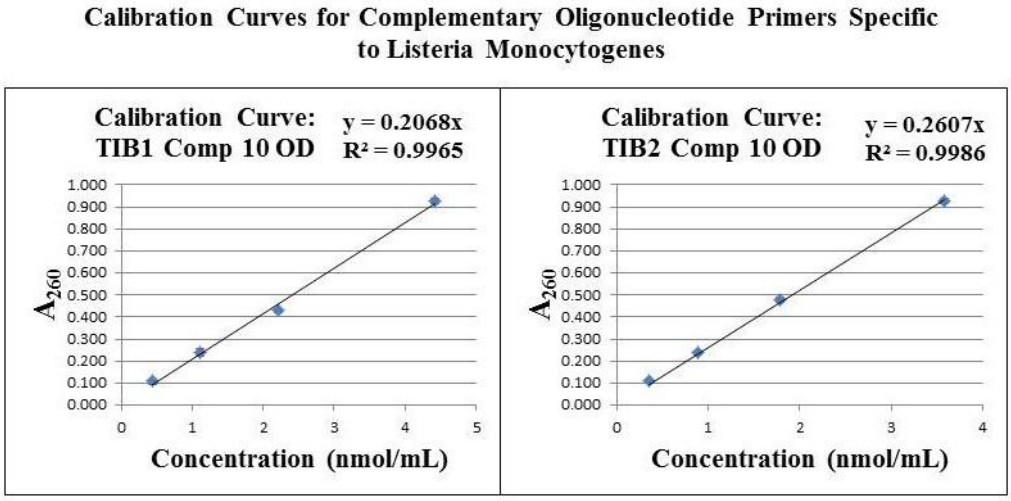

Figure 2.5: Calibration curves for complementary forward (bottom-left) and reverse (bottom-right) oligonucleotides. See Table 2.1, Section 2.1, for the full oligonucleotide sequences. Values are mean ± S.E.M., n = 3.

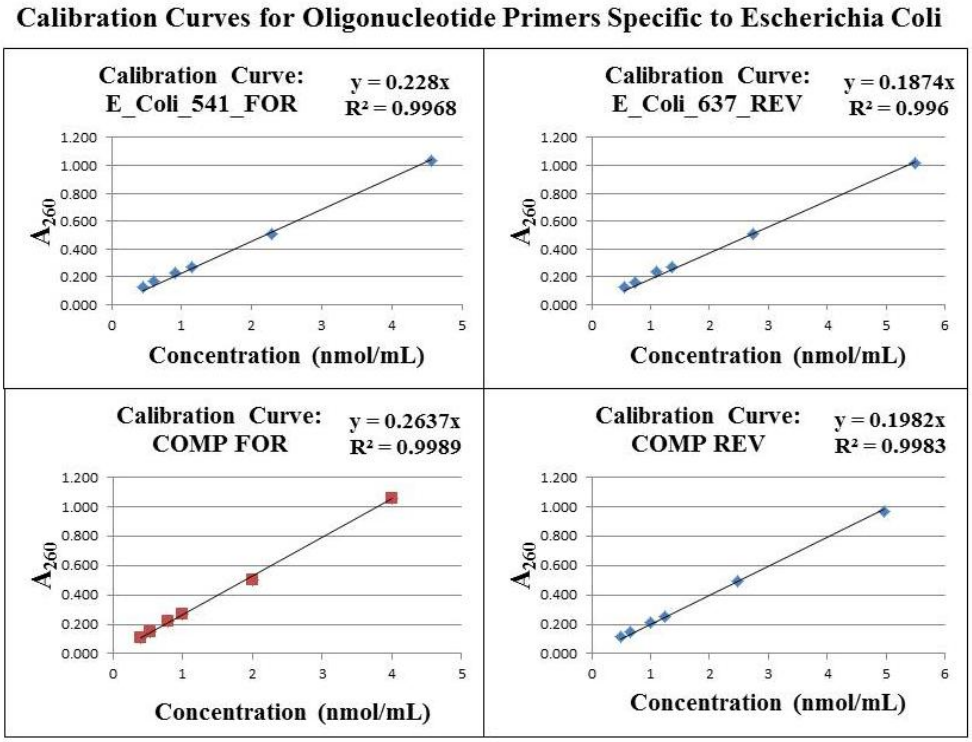

Figure 2.6: Calibration curves for *Escherichia Coli*-specific forward (top-left) and reverse (top-right) oligonucleotides and complementary forward (bottom-left) and reverse (bottom-right) oligonucleotides. See Table 2.2, Section 2.1, for the full oligonucleotide sequences. Values are mean ± S.E.M., n = 3.

Figure 2.4 and Figure 2.5 show that for the oligonucleotides used in the specific *Listeria Monocytogenes* assays, linearity is observed over the entire range of 0 to 5 nmol/mL. Figure

2.6, showing the oligonucleotides used in the specific EC assays, shows that linearity is observed over the entire range of 0 to 5 nmol/mL.

2.9.5 UV-Visible Assay for Determination of *p*-nitrophenol (PNP) Concentration

A model catalysis reaction was used for the characterisation of lipase immobilised nanoparticles as a test for their performance: Hydrolysis of PNPP to produce palmitic acid and PNP (see Section 2.6.3). PNP is an UV-Visible active molecule and its absorbance can be measured at 410 nm. Hence, standard curves were constructed using a series of dilutions of PNP dissolved in a 1:1 mixture of reagent A (see Table 8, Section 2.2) and isopropanol. Absorbance was measured by UV-Visible spectrophotometry at 410 nm. Figure 2.7 presents the curve constructed using a series of dilutions of PNP in a 1:1 mixture of reagent A: isopropanol.

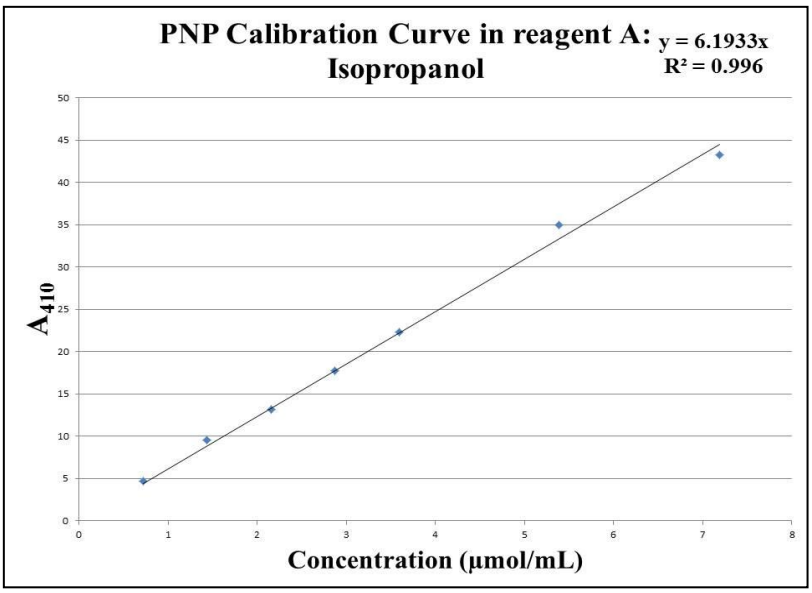

Figure 2.7: Calibration curve for PNP in a 1:1 mixture of reagent A: Isopropanol.

Figure 2.7 shows that linearity is observed over the entire range of 0-7 µmol/mL for the entire range of solutions. As the PNP is UV-active, amounts as low as 1 µmol/mL required dilutions up to 20 times. New standard curves were produced every six months using fresh samples to maintain reliability and reproducibility. The calibration curve was used to calculate the amount of PNP hydrolysed by lipase-immobilised nanoparticles.

2.9.6 Gas Chromatography (GC) and Gas Chromatography-Mass Spectrometry (GC-MS) for the Detection and Quantification of Ethyl Butyrate, *n*-Butanol and Butyl Butyrate in the Transesterification Reaction

The second bio-catalytic application carried out using lipase-immobilised nanoparticles was the transesterification of ethyl butyrate using *n*-butanol. In similar studies, GC and GC-MS have been used to identify and quantify the reaction products.[301,303] Starting materials and products were quantitatively determined using gas-chromatography (GC) on a Varian Chrompack CP-3380 Gas Chromatograph using nitrogen as the carrier gas (California, USA) and chromatograms were interpreted using Varian Star Integrator software version 4.51. The method of analysis involved injecting a 1 µL aliquot of reaction mixture (hexane layer) into the GC using a temperature program starting at 50ºC, increasing to 100ºC at 5ºC per minute. The column was flushed with hexane after every third sample.

Selected reaction products were also analysed (where specified) by gas-chromatography - mass spectrometry (GC-MS) on a Thermoscientific Trace GC ultra (Milan, Italy), with DSQ II Mass Spectrometer (Texas, USA) and a Triplus AS auto-sampler, using helium as the carrier gas. Chromatograms were interpreted using Xcalibur software version 2.0.7. The method of analysis involved injecting a 1 µL aliquot of reaction mixture (the water layer) into the GC using a temperature program starting at 50ºC, increasing to 200ºC at 10ºC per minute. The column was flushed with hexane after every third sample.

The techniques employed a PerkinElmer® Elite-5MS capillary column (length = 30 m, internal diameter = 0.25 mm, film thickness 0.25 µm).

Standard curves were constructed using a series of dilutions of ethyl butyrate, *n*-butanol and butyl butyrate, with hexane chosen as the solvent for the reaction.

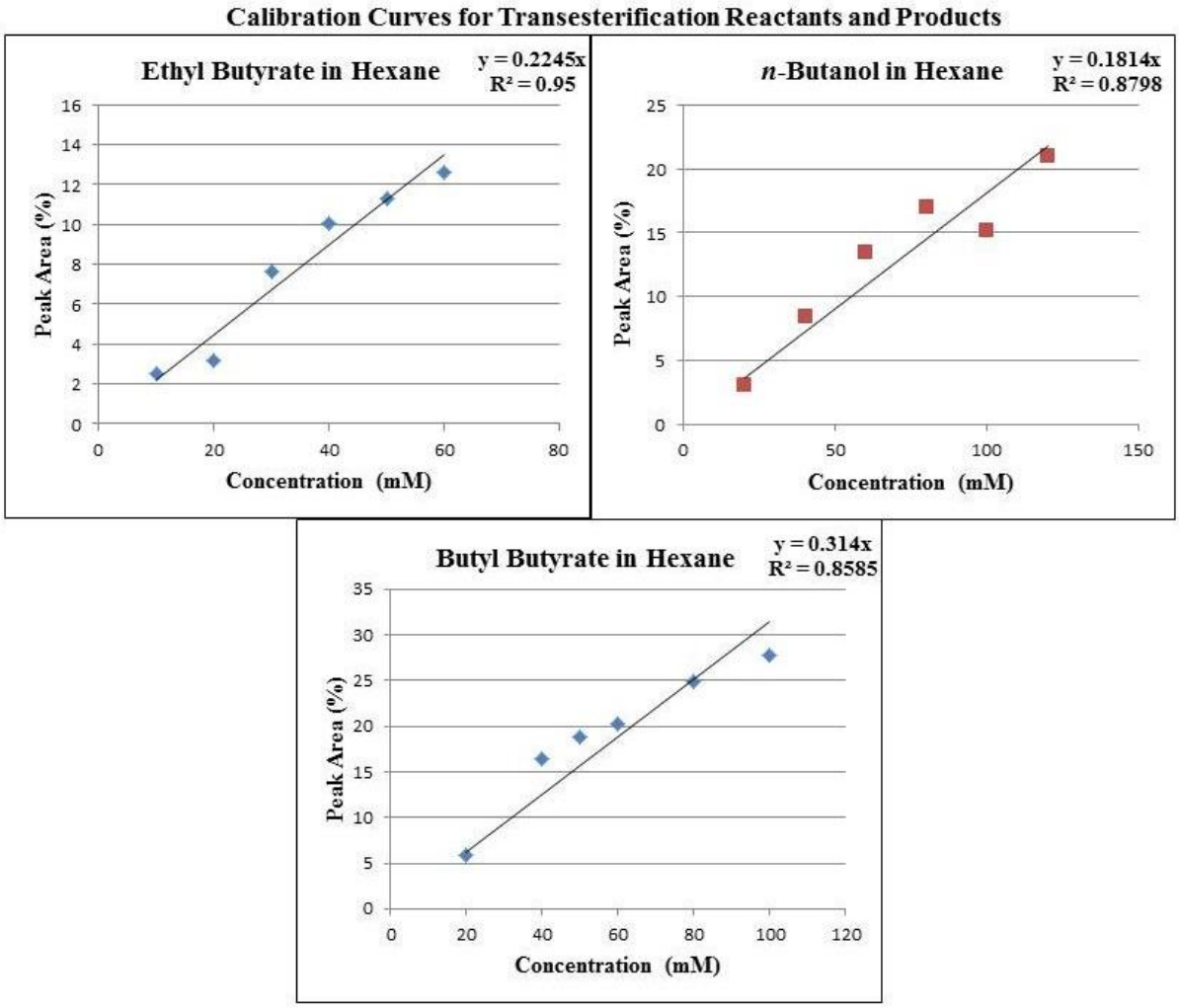

Figure 2.8: Calibration curves for ethyl butyrate (top left), *n*-butanol (top right) and butyl butyrate (bottom) in hexane. Peak area (%) is calculated from GC chromatograms.

Figure 2.8 shows that linearity is observed over the appropriate concentration ranges for each compound involved in the transesterification reaction. All samples were prepared in duplicate; hence the average peak area is presented in the curves.

2.9.7 Gas Chromatography (GC) and Gas Chromatography-Mass Spectrometry (GC-MS) for the Detection of Chiral Products in the Partial and Selective Hydrolysis of *Cis*-3,5-diacetoxy-1-cyclopentene

In similar studies, GC and GC-MS have been used to identify and quantify the reaction products; hence this method was chosen for this reaction too. Following preliminary experiments into lipase activation (using water) in the transesterification of ethyl butyrate (Section 4.3), varying mixtures of water and hexane were chosen as the solvent system for the reaction.

Starting materials and products were quantitatively determined using GC on a Varian Chrompack CP-3380 Gas Chromatograph using nitrogen as the carrier gas (California, USA) and chromatograms were interpreted using Varian Star Integrator software version 4.51. The method of analysis involved injecting a 1 μL aliquot of reaction mixture (the water layer) into the GC using a temperature program starting at 50ºC, increasing to 200ºC at 10ºC per minute.

Selected reaction products were also analysed (where specified) by GC-MS on a Thermoscientific Trace GC ultra (Milan, Italy), with DSQ II Mass Spectrometer (Texas, USA) and a Triplus AS auto-sampler, using helium as the carrier gas. Chromatograms were interpreted using Xcalibur software version 2.0.7.

Both techniques employed a Supelco BETA DEX^{TM} 110 fused silica capillary column (length = 30 m, internal diameter = 0.25 mm, film thickness 0.25 μm), which is specifically produced to separate chiral compounds.[434]

Calibration curves were constructed using a series of dilutions of *cis*-3,5-dihydroxycyclopentene, (1S,4R)-*cis*-4-acetoxy-2-cyclopenten-1-ol and its enantiomer and *cis*-3,5-diacetoxy-1-cyclopentene.

Calibration curves were constructed in water for (1S,4R)-*cis*-4-acetoxy-2-cyclopenten-1-ol and *cis*-3,5-dihydroxycyclopentene, as they are both insoluble in hexane. A calibration curve for *cis*-3,5-diacetoxy-1-cyclopentene was constructed in hexane to calculate the exact amount of starting material at time = 0 minutes and to monitor the conversion. In the case of the compounds calibrated in water, the data were plotted as absolute peak area against concentration, instead of the standard peak area % against concentration. This is because water does not appear on the chromatogram as a solvent, as in the FID, (which ionises all compounds that pass through the hydrogen/air flame), the water is ionised to hydrogen and oxygen, which are the components of the flame; hence, they are not detected. As a result of this, there is no solvent peak to use as a reference point.

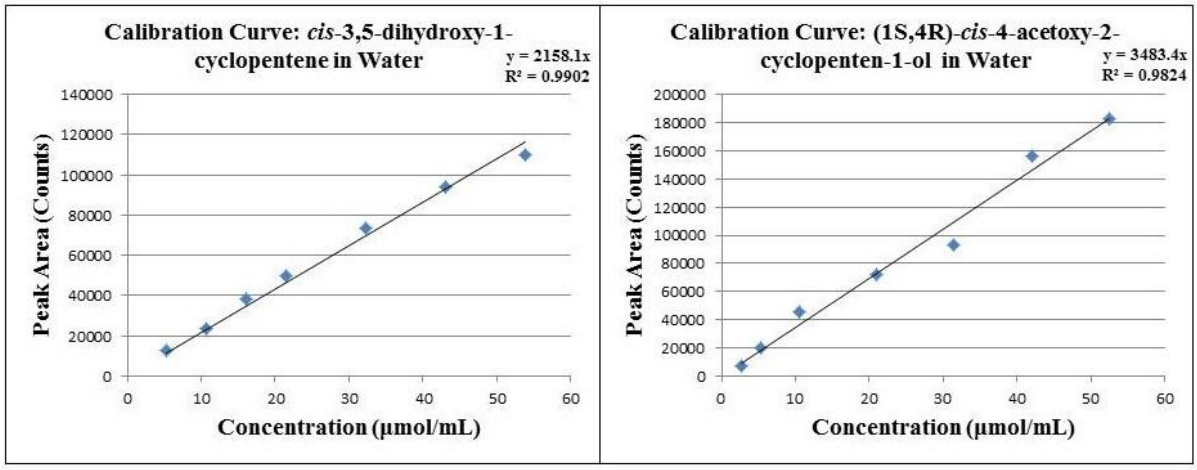

Figure 2.9: Calibration curves for (1S,4R)-*cis*-4-acetoxy-2-cyclopenten-1-ol (left) and *cis*-3,5-dihydroxycyclopentene (right) in water. Peak area (%) is calculated from GC chromatograms.

Figure 2.9 shows that linearity is observed over the appropriate concentration ranges for both compounds. The calibration curve constructed for (1S,4R)-*cis*-4-acetoxy-2-cyclopenten-1-ol was also used for (1R,4S)-*cis*-4-acetoxy-2-cyclopenten-1-ol; peak areas were found to be equal when a 1:1 mixture of both was injected in water.

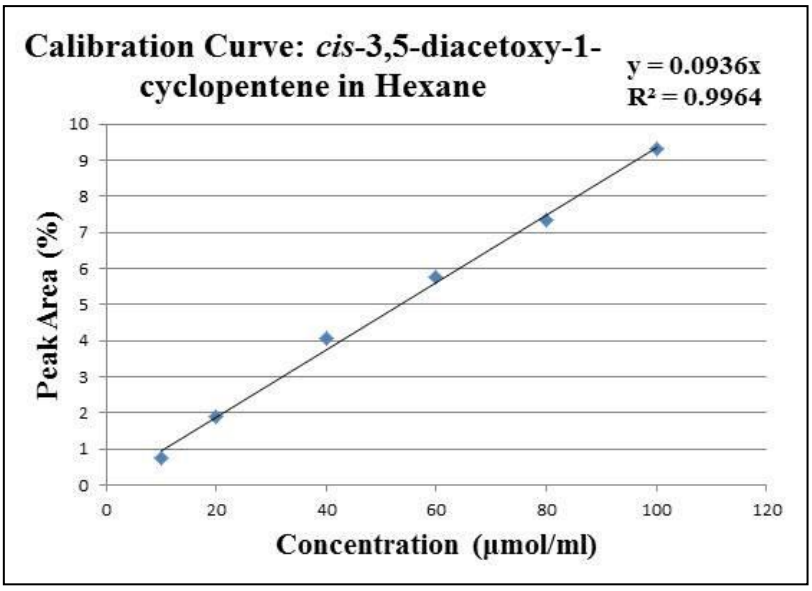

Figure 2.10: Calibration curve for *cis*-3,5-diacetoxy-1-cyclopentene in hexane.

Figure 2.10 shows that linearity is observed over the entire concentration range for *cis*-3,5-diacetoxy-1-cyclopentene. The data is presented as peak area (%) against concentration.

2.9.8 Polymerase Chain Reaction (PCR) Analysis of Selective Isolation, Determination and Enrichment of LM and EC in Food Samples

The detections of LM from food samples and EC from food and wastewater samples were carried out using real-time quantitative PCR (qPCR) using a Roche LightCycler® 480 and all data were interpreted using the Light Cycler® 480 Software version 1.5.0. The temperature program used was as follows: an initial heating phase for 60 seconds at 95ºC, followed by 45 seconds of denaturation for 20 seconds at 95ºC, annealing for 30 seconds at 60ºC and extension for 20 seconds at 72^{o}C. The qPCR premaster mixtures were made up as follows: 2 µL of the extracted DNA sample was added to 15 µL of this mixture for each reaction. Table 2.4 presents a complete list of components of the qPCR premaster mixes used to analyse extracted LM and EC DNA.

Table 2.4: Components of the premaster mixes used for the qPCR analysis of extracted LM and EC DNA.

Component of Mixture (LM-specific)	**Quantity per Reaction (µL)**	**Component of Mixture (EC-specific)**	**Quantity per Reaction (µL)**
Forward primer (See $T1NH_2$ in Table 2.1, Section 2.1) (no spacer or NH_2) 100 pmol/µL	0.075	Forward primer (See EC_541_FOR in Table 2.2, Section 2.1) (no spacer or NH_2) 100 pmol/µL	0.070
Reverse primer (See $T2NH_2$ in Table 2.1, Section 2.1) (no spacer or NH_2) 100 pmol/µL	0.075	Reverse primer (See EC_637_REV in Table 2.2, Section 2.1) (no spacer or NH_2) 100 pmol/µL	0.070
LM-specific fluorescence probe 20 pmol/µL	0.075	EC-specific fluorescence probe 20 pmol/µL	0.070
Internal Amplification Control (IAC) primers (forward and reverse) 100 pmol/µL each	0.04 each	Internal Amplification Control (IAC) primers (forward and reverse) 100 pmol/µL each	0.015 each
IAC fluorescence probe 10 pmol/µL	0.04	IAC fluorescence probe 10 pmol/µL	0.015 0.015
dUTP's	0.12	dUTP's	0.12
Glycerin	0.12	Glycerin	0.14
$MgCl_2$ (25 mM)	0.48	$MgCl_2$ (25 mM)	0.38
pUC19 (Vector-DNA)	0.20	pUC19 (Vector-DNA)	0.20
Uracil-N-glycosylase (UNG) 1U/µL	0.12	Uracil-N-glycosylase (UNG) 1 U/µL	0.12
*Taq*man® Fast Universal PCR Master Mix (2×) (contains dNTP's and *Taq* Polymerase)	7.50	*Taq*man® Fast Universal PCR Master Mix (2×) (contains dNTP's and *Taq* Polymerase)	7.50
Water	6.115	Water	6.285
Total	15.00	**Total**	15.00

CHAPTER 3

CHARACTERISATION OF NANOPARTICLES

3.1 Characterisation and Analytical Methods

The techniques employed in this project have all been commonly used in other studies related to this work and are suitable for the physical and chemical characterisation of magnetic nanoparticles.

Transmission Electron Microscopy (TEM) is widely used to determine both the size and shape of the nanoparticles.[217,283,424,435,436] In this project, it has been used to determine the size and shape of both bare and silica-coated magnetite nanoparticles.

X-Ray Diffraction (XRD) is also widely used to study and confirm the crystalline structure of nanoparticles.[283,424,425,436-438] This project has employed XRD on both bare and silica-coated magnetite nanoparticles.

Vibrating Sample Magnetometry (VSM) is less commonly used, but provides saturation magnetism and magnetisation curve measurements.[425,439,440] This method was used on both bare and silica-coated magnetite nanoparticles in this project.

Brunauer–Emmett–Teller (BET) surface area analysis is a technique used to determine the surface area of a sample using the adsorption and desorption of known amounts of nitrogen gas at low temperatures.[437,438,441] Again, this method was used on both bare and silica-coated magnetite nanoparticles in this project.

UV-Visible spectrophotometry-based assays have been used for calculating the surface amine density,[86,88] DNA binding and elution efficiency of bare- and silica-coated magnetite nanoparticles,[29,78,86] amount of lipase immobilised on surface-functionalised nanoparticles,[429,430] amount of PNP hydrolysed during model catalysis reactions[432] and the amount of oligonucleotides covalently coupled to surface-functionalised nanoparticles and their efficiency in capturing complementary sequences in hybrid capture assay experiments.[80]

Gas Chromatography (GC) and Gas Chromatography-Mass Spectrometry (GC-MS) have both been used to calculate the product conversion in the transesterification and chiral compound hydrolysis reactions.

Table 3.1 provides an outline of the magnetite and silica-coated magnetite materials that have been characterised using each method. The best functionalised materials were then used for further applications, shown in Table 3.2.

Table 3.1: Materials Produced and Characterisation Methods Used.

Name	Details	Characterisation Method					Application Used For	
		TEM	BET	XRD	VSM	DNA Binding and Elution	Bio-catalysis	Bio-sensor
R1MA	Small-scale magnetite (see Section 2.3.1)	√	√	√	√	√	Not used further	Not used further
R2MC	Small-scale magnetite (see Section 2.3.2)	√	√	√	√	√	Not used further	Not used further
QBLSBM	Large-scale magnetite (see Section 2.3.2) used for applications	√	√	√	√	√	√	√
CR2MC	Small-scale amorphous silica-coated magnetite (see Section 2.4.1)	√	√	√	√	√	Not used further	Not used further
QBLSSM	Large-scale amorphous silica-coated magnetite (see Section 2.4.1) used for applications	√	√	√	√	√	√	√

Table 3.2 below provides a list of functionalised silica-magnetite nanoparticles, the characterisation techniques used and how they have been used for further applications.

Table 3.2: Modified and functionalised nanoparticles, characterisation techniques and their uses for further applications

Name	Details	Characterisation Method Used		Application Used For	
		DNA Binding and Elution	UV Colorimetric Assay of Surface Amine Density	Bio-catalysis	Bio-sensor
TTQB	Amine-functionalised QBLSSM using APTS and TPRE method (see Section 2.5.2)	√	√	√	√
TWQB	Amine-functionalised QBLSSM using APTS and water method (see Section 2.5.1)	√	√	√	√
DTQB	Amine-functionalised QBLSSM using APDS and TPRE method (see Section 2.5.2)	√	√	√	N/A
DWQB	Amine-functionalised QBLSSM using APDS and water method (see Section 2.5.1)	√	√	√	N/A
MTQB	Amine-functionalised QBLSSM using APMS and TPRE method (see Section 2.5.2)	√	√	√	N/A
MWQB	Amine-functionalised QBLSSM using APMS and water method (see Section 2.5.1)	√	√	√	N/A

Note: The letters T, D and M represent the aminosilane used (APTS, APDS and APMS respectively). The next letter T or W represents the surface-functionalisation method used: T = TPRE, W = water. QB represents the shortened name of the silica-coated material QBLSSM.

3.2 Nanoparticle Size and Surface Coating Homogenity Analysis

Samples were prepared and images produced using transmission electron microscopy according to methods explained in Section 2.8.2. Images for bare magnetites (R1MA, R2MC and QBLSSM) and amorphous silica-magnetites (CR2MC and QBLSSM) are presented below.

Bare Magnetite Materials

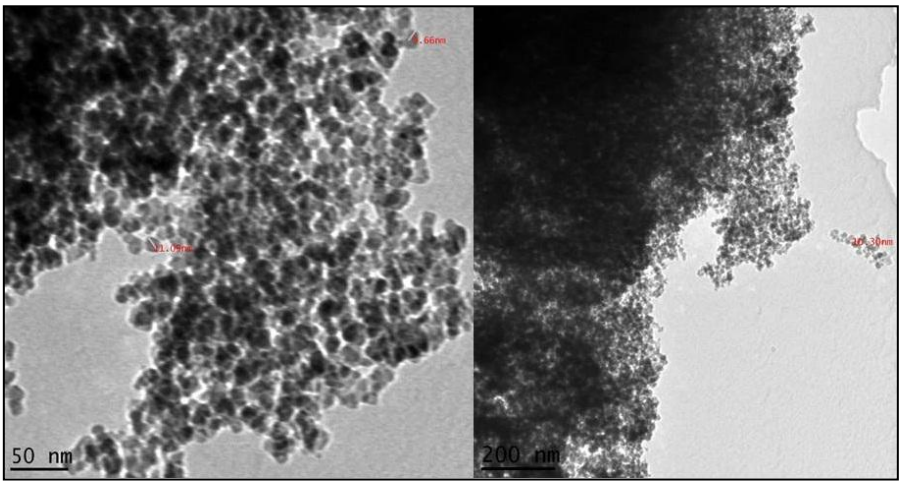

Figure 3.1: TEM images of the bare magnetite material R1MA.

Figure 3.1 shows the bare magnetite R1MA, prepared by the small-scale co-precipitation of ferrous and ferric chloride solutions in alkaline media. The nanoparticles are shown to be spherical and around 10 nm diameter. The size and shape are similar to those reported by Sen *et al* in 2006[424].

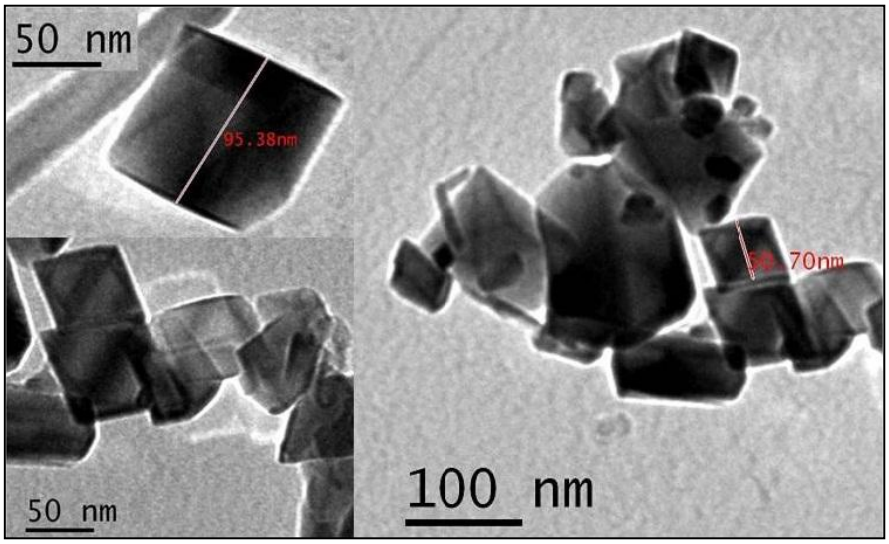

Figure 3.2: TEM images of bare magnetite material R2MC.

Figure 3.2 shows the bare magnetite R2MC, prepared by the small-scale oxidative hydrolysis of ferrous sulphate. The nanoparticles are shown to be rhombic and quite polymorphic, with diameters ranging from 30-200 nm. The size and shape are similar to those reported by Bruce *et al*[29] in 2004 and again, by Sen *et al*[424] in 2006, although some are slightly larger than those reported previously. The needle-like structure seen in the top left image is thought to be goethite; its presence is also confirmed in the XRD pattern, Figure 3.7, Section 3.3.

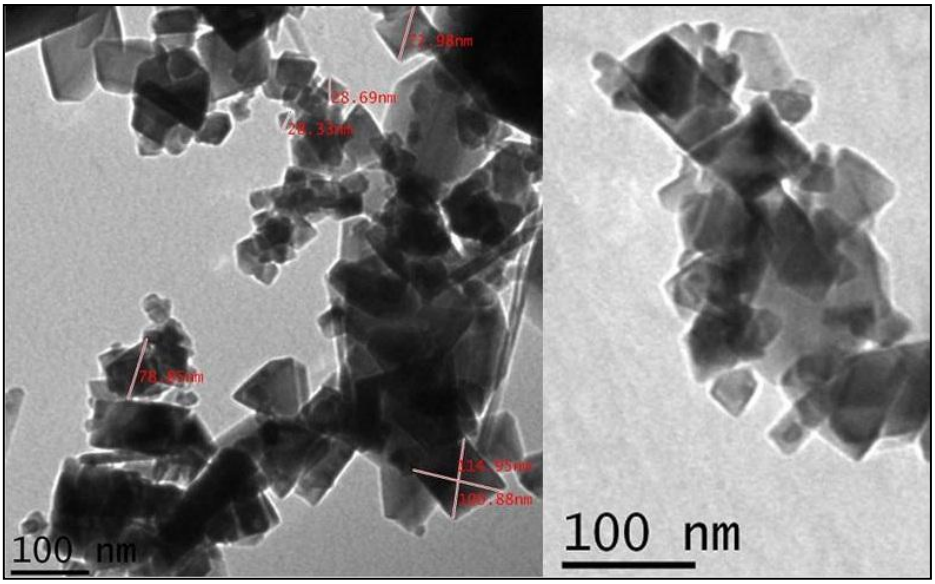

Figure 3.3: TEM images of bare magnetite material QBLSBM.

Figure 3.3 shows the bare magnetite QBLSBM, prepared by the large-scale oxidative hydrolysis of ferrous sulphate. The nanoparticles are shown to be rhombic and polymorphic, with sizes ranging from 25-200 nm. The size and shape are similar to those reported by Bruce *et al*[29] in 2004. The images also confirm that scaling-up the synthesis does not significantly alter the morphology of the nanoparticles.

Amorphous Silica-Coated Magnetite Materials

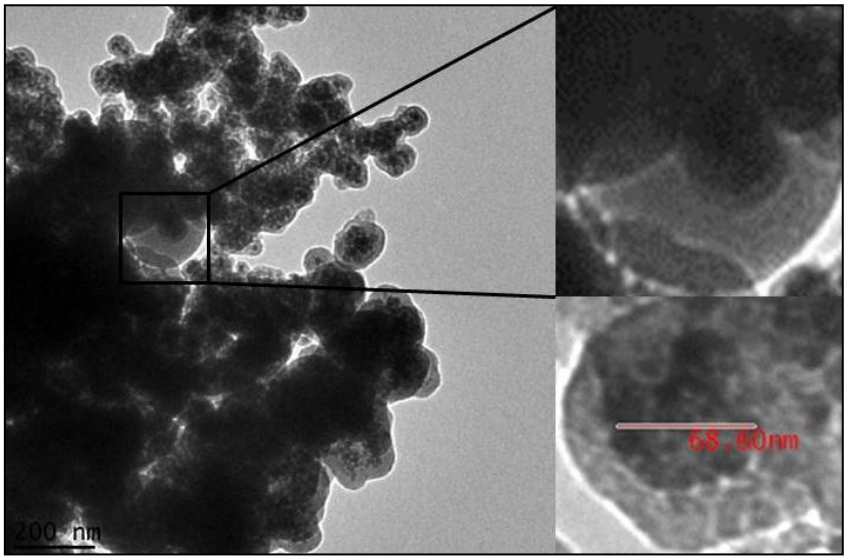

Figure 3.4: TEM images of small-scale amorphous silica-coated magnetite material CR2MC.

Figure 3.4 shows the silica-coated magnetite CR2MC, prepared by coating R2MC *via* silicic acid deposition. The larger image on the left of the figure shows a large area of aggregated rhombic magnetite nanoparticles (darker), coated by a thin layer of silica (lighter). The upper right image shows an enlarged view of the area in the box in the larger image on the left and shows a relatively large (80-100 nm size) rhombic magnetite nanoparticle coated with a thin silica shell, underneath a much larger spherical silica particle. The silica shell can also be seen clearly surrounding a single magnetite nanoparticle (68.5 nm size) in the image in the bottom left of the figure. The nanoparticles are shown to be polymorphic in size, ranging from 30-200 nm, although larger aggregates can be present due to sample preparation techniques involved with TEM. As with R2MC, the size and shape are similar to those reported by Bruce *et al*[29] in 2004 and Sen *et al*[424] in 2006.

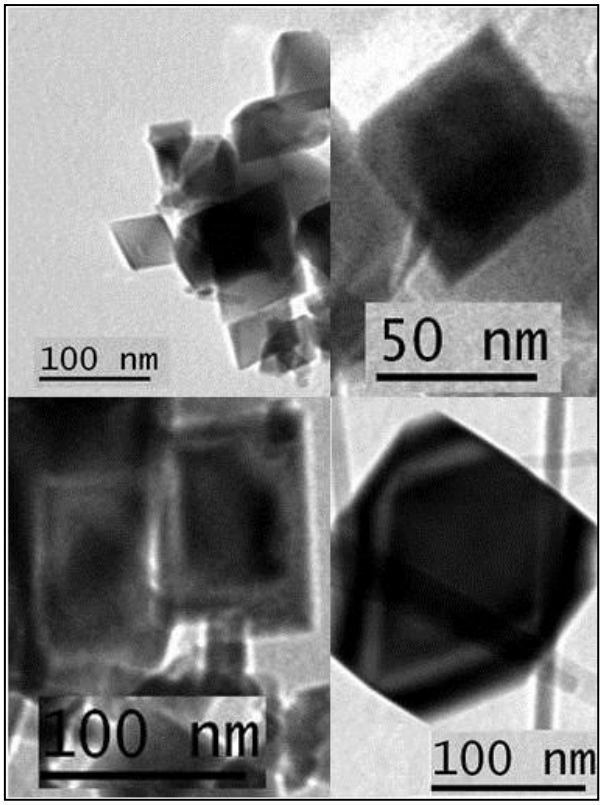

Figure 3.5: TEM images of large-scale amorphous silica-coated magnetite material QBLSSM.

Figure 3.5 shows the silica-coated magnetite QBLSSM, prepared by coating QBLSBM *via* silicic acid deposition. The nanoparticles are shown to be rhombic and polymorphic, with sizes ranging from 25-200 nm, the same as bare QBLSBM, suggesting a thin silica-coating around the nanoparticles. The size and shape are similar to those reported by Bruce *et al*[29] in 2004, who also employed a scaled-up version of producing silica-coated magnetite. The upper left corner of the image shows the rhombic morphology of the nanoparticles has not changed during silica-coating. The other three images show the rhombic magnetite core (dark) surrounded by the thin silica-shell (lighter), which is measured to be around 5-15 nm from the TEM images. The lower right image shows the silica-coated magnetite nanoparticle underneath another nanoparticle.

3.3 Iron Oxide Phase Confirmation

Samples were prepared and X-ray diffraction data were produced according to methods explained in Section 2.8.3.

Bare Magnetite Materials

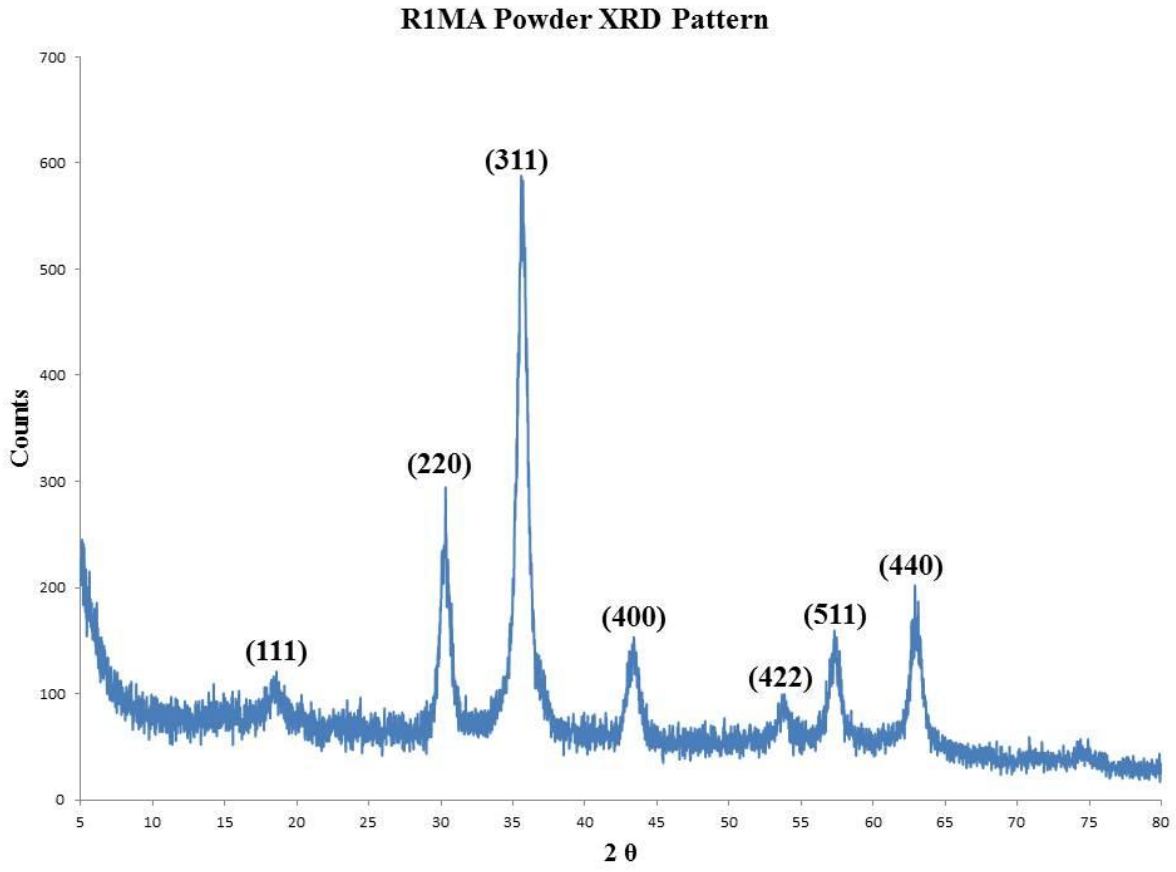

Figure 3.6: Powder XRD Pattern for R1MA. Peaks are labelled with Miller Indices using DIFFRAC.EVA V3.0 Software.

Figure 3.6 shows the XRD pattern for bare magnetite R1MA. The peaks obtained are in accordance with those expected of pure magnetite when compared to standard XRD data for magnetite (JCPDS No. 19-0629, from Yu and Kwak[442] (ESI)) and are also in accordance with those reported in the literature.[54,68,424,443] Many peaks present in hematite can overlap with the ones in magnetite, for example (110) in hematite is present at almost the same 2θ value as the (311) peak in magnetite. Other peaks that could overlap are the broad (018) peak in hematite, present at the same 2θ value as the (511) peak in magnetite and also the (116) peak in hematite at the same 2θ value as the (422) peak in magnetite.[444,445] The red-brown colour of the nanoparticles confirms the presence of an impurity of hematite in the sample.

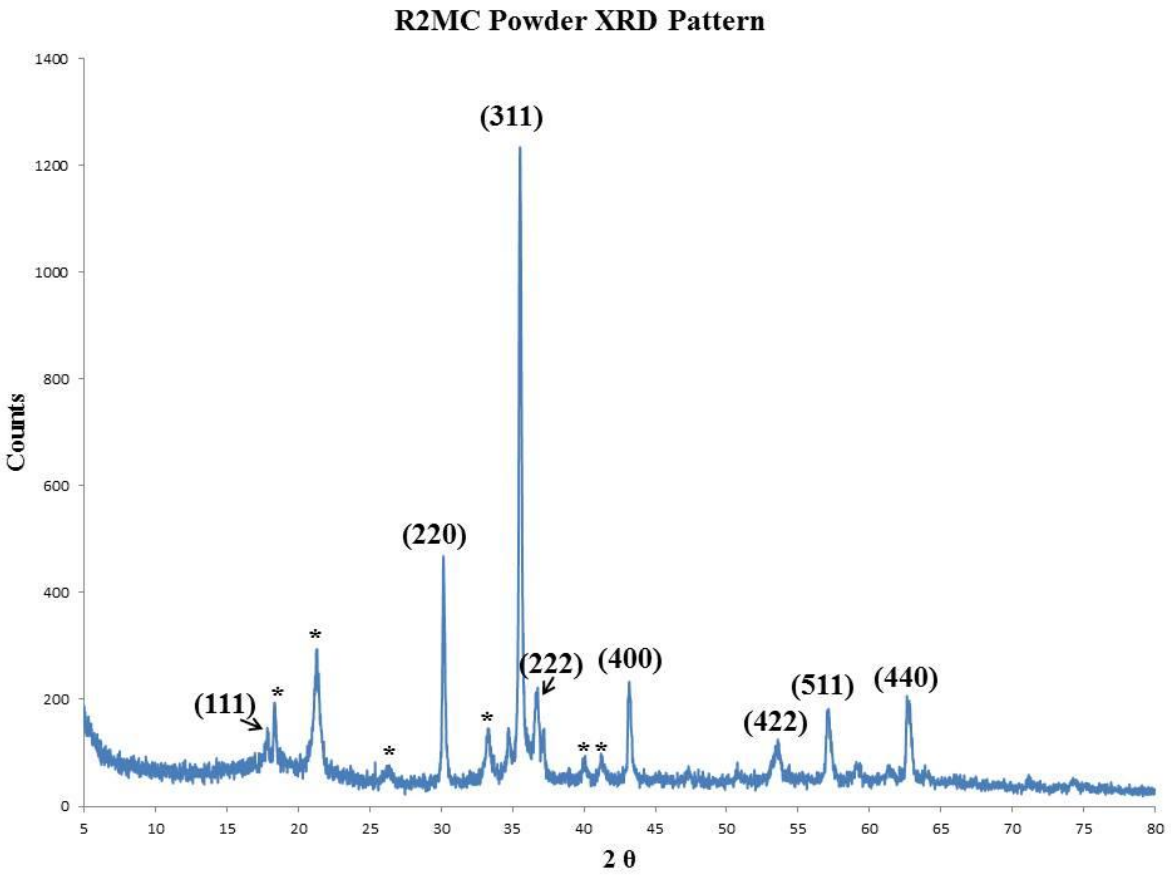

Figure 3.7: Powder XRD Pattern for R2MC. Peaks are labelled with Miller Indices using DIFFRAC.EVA V3.0 Software. Peaks denoted with a * represent peaks corresponding to goethite, FeO(OH).

Figure 3.7 shows the XRD pattern for bare magnetite R2MC. The peaks obtained are in accordance with those expected of pure magnetite when compared to standard XRD data for magnetite (JCPDS No. 19-0629, from Yu and Kwak[442] (ESI)) and are also in accordance with those reported in the literature.[54,68,424,443] However, peaks denoted with a * represent peaks arising from goethite, FeO(OH)[445]. Hence, it can be concluded that R2MC contains an impurity of goethite in magnetite.

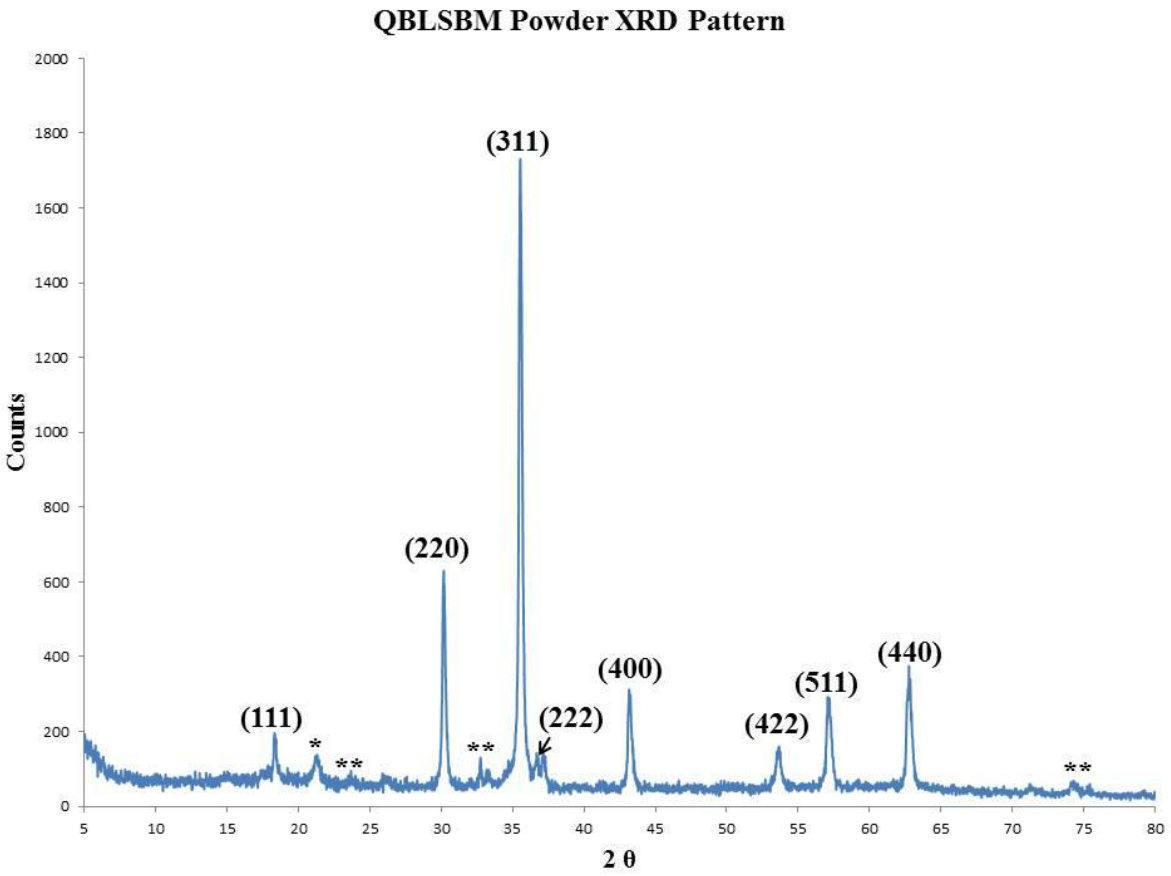

Figure 3.8: Powder XRD Pattern for QBLSBM. Peaks are labelled with Miller Indices using DIFFRAC.EVA V3.0 Software. Peaks denoted with a * represent peaks corresponding to goethite, FeO(OH) and peaks denoted with a ** represent peaks corresponding to maghemite, γ-Fe_2O_3.

Figure 3.8 shows the XRD pattern for bare magnetite QBLSBM. The peaks obtained are in accordance with those expected of pure magnetite when compared to standard XRD data for magnetite (JCPDS No. 19-0629, from Yu and Kwak[442] (ESI)) and are also in accordance with those reported in the literature.[54,68,424,443] However, peaks denoted with a * represent peaks arising from goethite, FeO(OH) and those denoted with a ** represent peaks corresponding to maghemite, γ-Fe_2O_3.[446] Hence, it can be concluded that R2MC contains a mixture of magnetite, goethite and maghemite. However in this case the goethite and magnetite peaks are much smaller than the goethite peaks present in sample R2MC and many goethite and maghemite peaks are missing, indicating that the sample is primarily magnetite with just a small amount of goethite and maghemite impurities.

Due to the amorphous nature of the silica coating on the silica-magnetite nanoparticles CR2MC and QBLSSM, the XRD pattern remains identical to that obtained from the pure

magnetite materials used for coating (R2MC and QBLSBM respectively). Hence, the XRD patterns for these materials are not shown.

3.4 Magnetic Properties of Nanoparticles Analysis

Samples were prepared and magnetic data were obtained using vibrating sample magnetometry according to methods explained in Section 2.8.4.

Bare Magnetite Materials

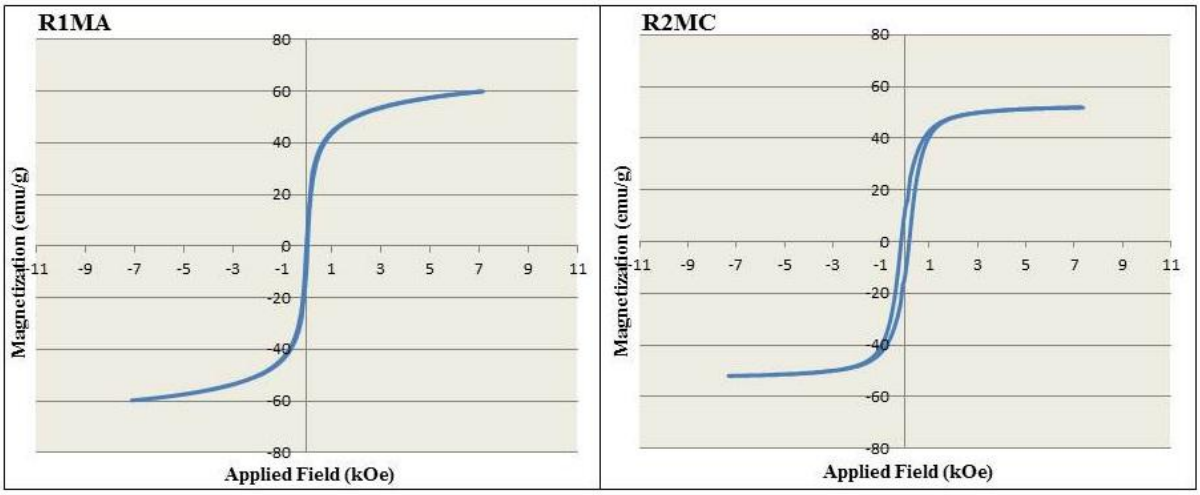

Figure 3.9: Magnetic susceptibility data of small-scale bare magnetite materials R1MA (left) and R2MC (right).

Figure 3.9 shows the magnetisation data for small-scale bare magnetite materials. R1MA, prepared by the small-scale co-precipitation of ferrous and ferric chloride solutions in alkaline media, exhibits close to no hysteresis, with saturation magnetisation (M_S) of 60 emu/g. R2MC, prepared by the small-scale oxidative hydrolysis of ferrous sulphate, exhibits a small amount of hysteresis, with M_S = 52 emu/g. The low M_S of R1MA and R2MC could be explained due to the presence of hematite and goethite in the samples respectively, as seen in the XRD patterns (see Figure 3.6 and Figure 3.7, Section 3.3). Hematite and goethite are both antiferromagnetic[447,448] with M_S values less than 1 emu/g;[449,450] therefore its presence leads to a decrease in saturation magnetisation of the sample, as the typically reported M_S value for bulk magnetite of 92 emu/g.[35,451]

The slight hysteresis present in R2MC may arise from the various sizes of the nanoparticles present in the sample. It is well-known that large magnetic particles are multi-domain structures; each domain containing regions of uniform magnetisation,[35] separated by domain walls. As the size of the particle decreases towards the nanometre range, it becomes

energetically unfavourable to create a domain wall and at this point, the particle becomes a single magnetic domain. This is known as the single-domain limit (or critical diameter, D_C), at which point the particle is uniformly magnetised; all spins aligned in the same direction and the material exhibits superparamagnetic properties. It has been reported that magnetite has a single-domain size of around 128 nm.[35] This can explain the superparamagnetic behaviour exhibited by R1MA, which is around 10 nm in diameter; well below the single-domain limit. However, the critical diameter values can only be strictly applied to spherical particles; particles of different shapes generally have higher coercivity and significantly different D_C values. The nanoparticles present in R2MC are rhombic and between 30-200 nm in size, hence, most of the nanoparticles present fall below the critical diameter and the material exhibits mostly superparamagnetic behaviour. Larger nanoparticles with diameter > D_C are the cause for the slight hysteresis in the magnetisation curve and hence will exhibit ferrimagnetic behaviour instead of superparamagnetic behaviour.

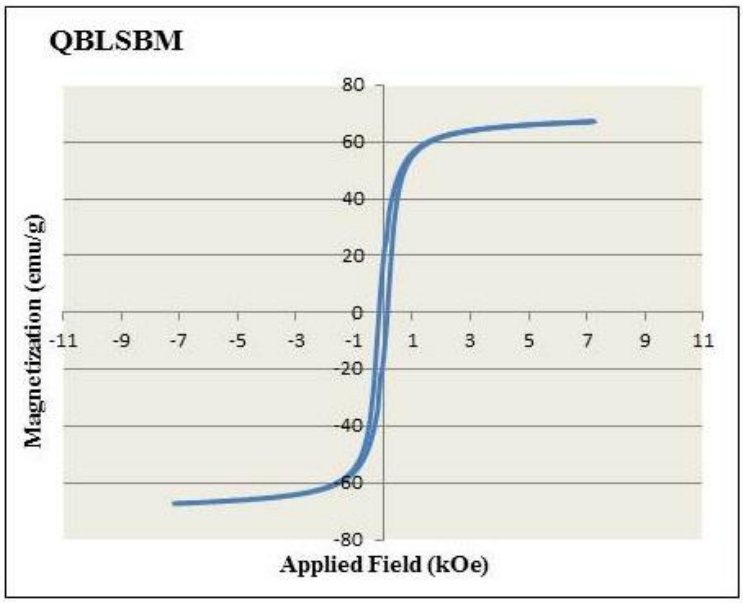

Figure 3.10: Magnetic susceptibility data of large-scale bare magnetite QBLSBM.

Figure 3.10 shows the magnetisation data for large-scale bare magnetite QBLSBM, prepared by the large-scale oxidative hydrolysis of ferrous sulphate. The material exhibits a higher saturation magnetisation than the magnetite materials made on the small-scale, M_S = 67 emu/g. Again, there is slight hysteresis, due to the size distribution of the nanoparticles present in the sample (25-200 nm size). The presence of other iron oxides in the sample (as seen in the XRD pattern, Figure 3.8, Section 3.3) leads to reduced saturation magnetisation due to the lower M_S values (goethite = less than 1 emu/g[449], maghemite is around 74-80

emu/g.[452,453] The presence of iron oxide impurities is possible as magnetic measurements were carried out on QBLSBM that had been synthesised months earlier and stored in water, hence some oxidation of the magnetite is possible.

Amorphous Silica-Coated Magnetite Materials

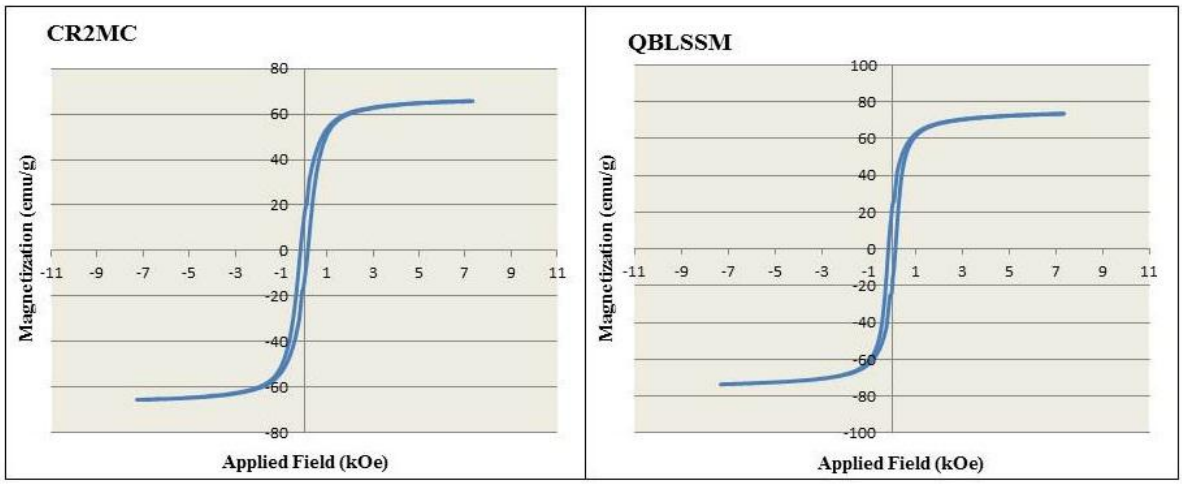

Figure 3.11: Magnetic susceptibility data of small-scale amorphous silica-magnetite CR2MC (left) and large-scale amorphous silica-magnetite QBLSSM (right).

Figure 3.11 shows the magnetisation data for amorphous silica coated magnetite materials (core-shell nanoparticles) made using the small- and large-scale deposition of silicic acid on bare magnetite nanoparticles. Small-scale silica-magnetite CR2MC shows reasonably high saturation magnetisation (66 emu/g), which is unexpectedly higher than the bulk magnetite (R2MC, M_S = 52 emu/g). The same phenomenon is seen in the case of large-scale silica-magnetite, which again has a higher saturation magnetisation (73 emu/g) than bare magnetite, QBLSBM (M_S = 67 emu/g). This could be because silica-coating of the nanoparticles protects the magnetite core against oxidation during the drying step and whilst in solution.

The M_S values for all materials are lower than the typically reported M_S value for bulk magnetite of 92 emu/g[35,451] and are slightly lower than those reported by Bruce *et al*[29] (82 emu/g at 300 K). This can be previously explained partly due to the presence of other iron oxides such as hematite, goethite and maghemite as impurities, which have lower M_S values than magnetite.

3.5 Surface Area Analysis

Samples were prepared and surface area analysis data were obtained *via* nitrogen adsorption techniques using Brunauer-Emmett-Teller surface area measurements according to methods

explained in Section 2.8.1. Due to the amorphous nature of the materials, it is only relevant to present the overall BET surface area values.

Table 3.3: BET surface area data for bare- and silica-coated magnetite nanoparticles used in this project.

Material	Scale	Silica Coating	BET Surface Area (m^2 / g)
R1MA	Small	None	109.30
R2MC	Small	None	27.01
QBLSBM	Large	None	15.73
CR2MC	Small	Amorphous	23.26
QBLSSM	Large	Amorphous	14.66

The bare magnetite R1MA, prepared by the co-precipitation of ferrous and ferric chlorides, has a surface area of 109.30 m^2/g, which is consistent with the value reported by Bruce *et al*: 108.81 m^2/g.[29] The surface area of 27.01 m^2/g obtained for R2MC in this study is slightly higher than that reported in the same study by Bruce *et al*: 21.30 m^2/g. When scaling up the preparation of R2MC, to the synthesis of QBLSBM, surface area decreased to 15.73 m^2/g. This is also in agreement with Bruce *et al*'s results, where scaling-up the synthesis led to the surface area decreasing from 21.30 m^2/g to 14.66 m^2/g. This is possibly due to an increase in aggregation of the nanoparticles as a result of scaling-up the process, arising from a slight decrease in precise control over the synthetic conditions.

Slight decreases are seen in surface area following silica-coating in both the small- and large-scale. Small-scale silica-magnetite CR2MC decreases from 27.01 m^2/g as bare magnetite to 23.26 m^2/g following silica-coating. Large-scale silica-magnetite QBLSSM decreases from 15.73 m^2/g as bare magnetite to 14.66 m^2/g following silica-coating. A small change in surface area is an indication that the materials were un-affected by silica coating and did not aggregate upon silica-coating.

3.6 Surface Amine Density Analysis

An optimised version of Moon's assay[88] (developed for flat surfaces), later used by Del Campo *et al*[217] for nanoparticles, was employed in this study (see Section 2.9.2) in order to assess the surface amine density of aminosilane-surface-functionalised silica-magnetite nanoparticles. The assay involves the coupling of a UV-sensitive molecule (4-NBA) to the amine functionality on the nanoparticle bonds to a single surface amine group, the amount of surface amine groups can be calculated from the amount of 4-NBA present in solution following hydrolysis.

Table 3.4 shows a range of materials used to study DNA binding and elution.

Table 3.4: Surface-functionalised silica-magnetite nanoparticles used in the surface amine density assay.

Material	Description
TTQB	QBLSSM surface-functionalised *via* the TPRE-method using APTS as the aminosilane source (see Section 2.5.2)
TWQB	QBLSSM surface-functionalised *via* the water-method using APTS as the aminosilane source (see Section 2.5.1)
DTQB	QBLSSM surface-functionalised *via* the TPRE-method using APDS as the aminosilane source (see Section 2.5.2)
DWQB	QBLSSM surface-functionalised *via* the water-method using APDS as the aminosilane source (see Section 2.5.1)
MTQB	QBLSSM surface-functionalised *via* the TPRE-method using APMS as the aminosilane source (see Section 2.5.2)
MWQB	QBLSSM surface-functionalised *via* the water-method using APMS as the aminosilane source (see Section 2.5.1)

Note: The letters T, D and M represent the aminosilane used (APTS, APDS and APMS respectively). The next letter T or W represents the surface-functionalisation method used: T = TPRE, W = water. QB represents the shortened name of the silica-coated material QBLSSM.

The 4-NBA assay was carried out (as explained in Section 2.9.2) on all materials made *via* aminosilane surface-functionalisation. Absorbance was measured by UV-Visible spectrophotometry at 282 nm.

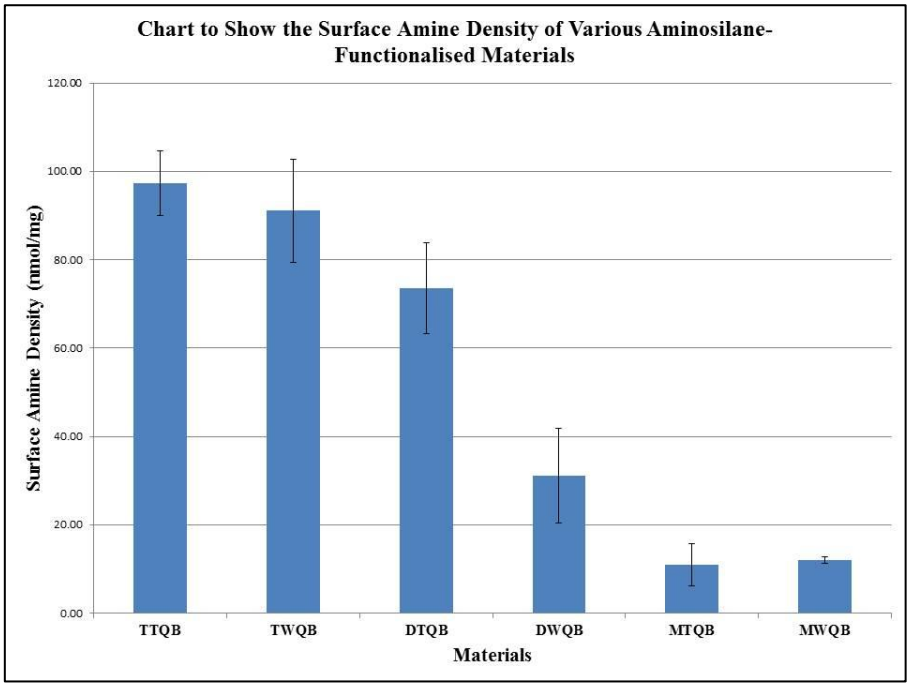

Figure 3.12: Surface amine density of materials made using various aminosilanes (APTS, APDS and APMS) *via* two different methods of surface functionalisation (TPRE and water method). The materials are explained in Table 3.4. Values are mean ± S.E.M., n = 3.

Figure 3.12 shows that materials made using APTS exhibit a much higher surface amine density than both APDS and APMS materials. This may be due to more regular condensation mechanism as the alkoxy groups can also interact with each other, permitting a more dense aminosilicate layer on the surface and thus a higher number of surface amine groups. TPRE materials show a higher surface amine density than water materials in all cases, indicating that the condensation of the aminosilanes onto the surface silanol groups is more controlled using TPRE conditions, whereas self-polymerisation and condensation is harder to control using the water method.

Using the surface area value for the silica-coated magnetite, QBLSSM, which was used to prepare all of the surface-functionalised nanoparticles, it is possible to represent the surface amine density in terms of NH_2-molecules per nm^2, as it is a standard unit reported by others.[86,88,428,454] The surface amine density values are presented as averages of multiple batches of the materials made in the same way each time. As the methods of surface-functionalisation are the same as those reported by De Waterbeemd,[428] the values can be directly compared.

Table 3.5: A comparison between surface amine density values obtained in this study with those obtained by De Waterbeemd.[428]

			Surface Amine Density (NH_2-molecules/ nm^2)	
Material*	**Aminosilane Used**	**Surface Functionalisation Method**	**My Value**	**Literature Value (De Waterbeemd[428])**
TTQB	APTS	TPRE	4.34	~4.1
TWQB	APTS	Water	4.06	1.5
DTQB	APDS	TPRE	3.28	~4.1
DWQB	APDS	Water	1.39	3.4
MTQB	APMS	TPRE	0.49	N/A
MWQB	APMS	Water	0.54	0.2

Note: The letters T, D and M represent the aminosilane used (APTS, APDS and APMS respectively). The next letter T or W represents the surface-functionalisation method used: T = TPRE, W = water. QB represents the shortened name of the silica-coated material QBLSSM. *See Table 3.4 for material details.

As can be seen from Table 3.5, in terms of TPRE-functionalised materials, surface amine density values are similar. The decrease in surface amine density seen from APTS to APDS in my results could be due to more regular ordering leading to a smaller amount of sequestration. As can also be seen, De Waterbeemd did not attempt the TPRE surface functionalisation using APMS; therefore no comparison can be made. In terms of water-functionalised materials, a decreasing trend in surface amine density can be seen from APTS

to APDS to APMS. The low surface amine density given by APMS materials was observed to be similar in both studies. For APTS materials made using both methods and APDS materials made using the TPRE method, surface amine density is similar to that of a monolayer on a flat surface, reported to be 4.0-5.3 NH_2-molecules/nm^2 by Moon *et al*.[88] In both studies, materials made using the TPRE-method exhibit higher surface amine density than those made using the water-method, possibly due to the more regular condensation onto the nanoparticle surface using the more controlled TPRE synthesis – leading to fewer sequestered groups. This is apparent in the significant difference between the surface amine density values of DTQB (3.28 NH_2-molecules per nm^2) and DWQB (1.39 NH_2-molecules per nm^2). Values are similar for materials made using APMS as there is only a single ethoxy group present to make inter-aminosilane condensation possible.

3.7 Silica Coating Homogenity on Magnetite Nanoparticles Analysis

Salmon sperm DNA binding and elution was used to analyse the surface of bare magnetite, silica-magnetite and amine-surface-functionalised silica-magnetite nanoparticles. Both magnetite and silica-magnetite nanoparticles possess surface hydroxyl groups that are partially ionised at physiological pH values in chaotropic (high salt concentration) conditions. At near-neutral or basic pH, the surface of silica is negatively charged due to weakly acidic silanol groups. The point of zero charge (pzc, also known as isoelectric point), is the pH at which the surface density of positive and negative charges are equal.[455] For silica, this value is around pH 2-3,[435,455,456] and for magnetite, it is around pH 6.4-7.3,[456-459] therefore both will carry a negative charge at pH 7-8, although that of silica will be much greater than that of magnetite. Hence, negatively charged Fe-O^- or Si-O^- groups will become shielded by positive counter-ions from the salt solution (Na^+), giving an overall slightly positive surface charge, to which the negative-charge-holding phosphate di-ester groups of the DNA backbone are attracted. Water can be used to break the electrostatic bond formed *via* the "cation bridge", eluting the DNA as the corresponding salt species as the silica surface and DNA backbone electrostatically repel each other. Under the same physiological pH conditions, amine-functionalised nanoparticles are in equilibrium between the NH_2 and NH_3^+ species which can electrostatically attract the negatively-charged phosphate backbone of the DNA.[80,455] In addition, the silica surface that remains un-functionalised by the aminosilane remains negatively charged above pH 7, hence can interact electrostatically with the DNA *via* the "cation bridge".[455]

Table 3.6 below shows which materials were used to study DNA binding and elution.

Table 3.6: Small- and large-scale bare, silica-coated and surface-functionalised silica-magnetite nanoparticles used in the DNA binding and elution study.

Material	Description
QBLSBM	Large-scale rhombic magnetite (see Section 2.3.2)
QBLSSM 2 Coats	Large-scale silica-magnetite coated 2 times with amorphous silica *via* silicic acid deposition (see Section 2.4.2)
QBLSSM 4 Coats (QBLSSM)	Large-scale silica-magnetite coated 4 times with amorphous silica *via* silicic acid deposition (see Section 2.4.2)
R2MC	Small-scale rhombic magnetite (see Section 2.3.2)
R2MC 2 Coats	Small-scale silica-magnetite coated 2 times with amorphous silica *via* silicic acid deposition (see Section 2.4.1)
R2MC 4 Coats	Small-scale silica-magnetite coated 4 times with amorphous silica *via* silicic acid deposition (see Section 2.4.1)
TTQB	QBLSSM surface-functionalised *via* the TPRE-method using APTS as the aminosilane source (see Section 2.5.2)
TWQB	QBLSSM surface-functionalised *via* the water-method using APTS as the aminosilane source (see Section 2.5.1)
DTQB	QBLSSM surface-functionalised *via* the TPRE-method using APDS as the aminosilane source (see Section 2.5.2)
DWQB	QBLSSM surface-functionalised *via* the water-method using APDS as the aminosilane source (see Section 2.5.1)
MTQB	QBLSSM surface-functionalised *via* the TPRE-method using APMS as the aminosilane source (see Section 2.5.2)
MWQB	QBLSSM surface-functionalised *via* the water-method using APMS as the aminosilane source (see Section 2.5.1)

Note: The letters T, D and M represent the aminosilane used (APTS, APDS and APMS respectively). The next letter T or W represents the surface-functionalisation method used: T = TPRE, W = water. QB represents the shortened name of the silica-coated material QBLSSM.

Figure 3.13 and Figure 3.14 below show the DNA binding and elution properties of small- and large-scale bare and amorphous silica-coated (2 and 4 times) magnetite nanoparticles. Figure 3.13 presents the data in terms of µg used, adsorbed and eluted, while Figure 3.14 presents the same data as percentages of the initial amount of DNA used.

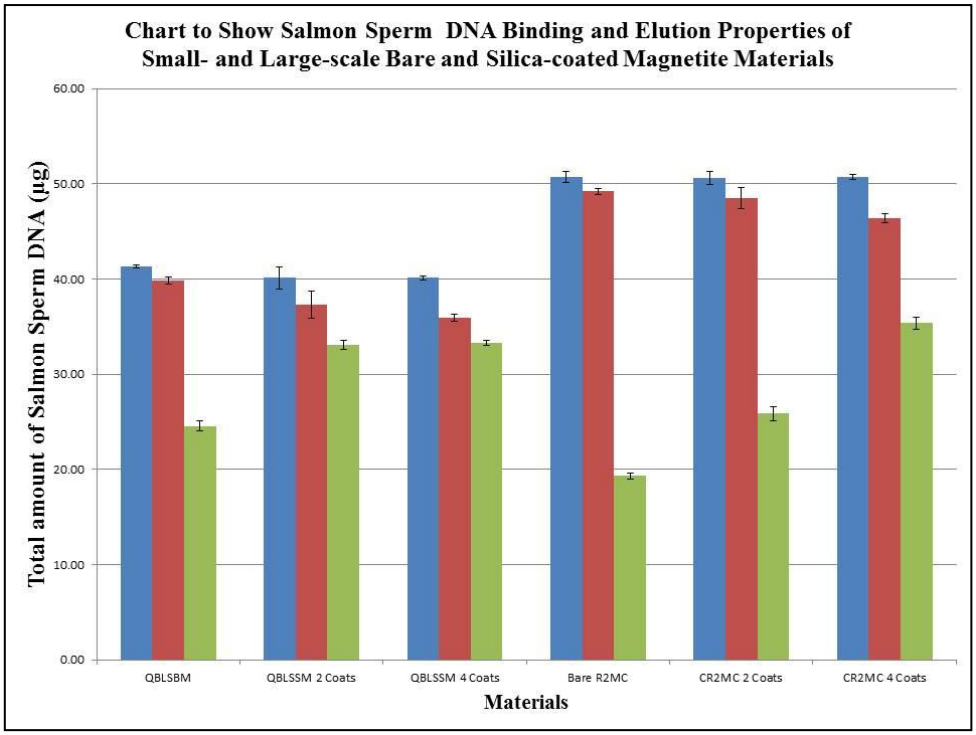

Figure 3.13: The amount of DNA initially used, adsorbed and eluted, in µg. The materials used are explained in Table 3.6 above. The blue bars represent initial amount of DNA used, the red bars represent the amount of DNA adsorbed and the green bars represent the amount of DNA eluted. Values are mean ± S.E.M., n = 3.

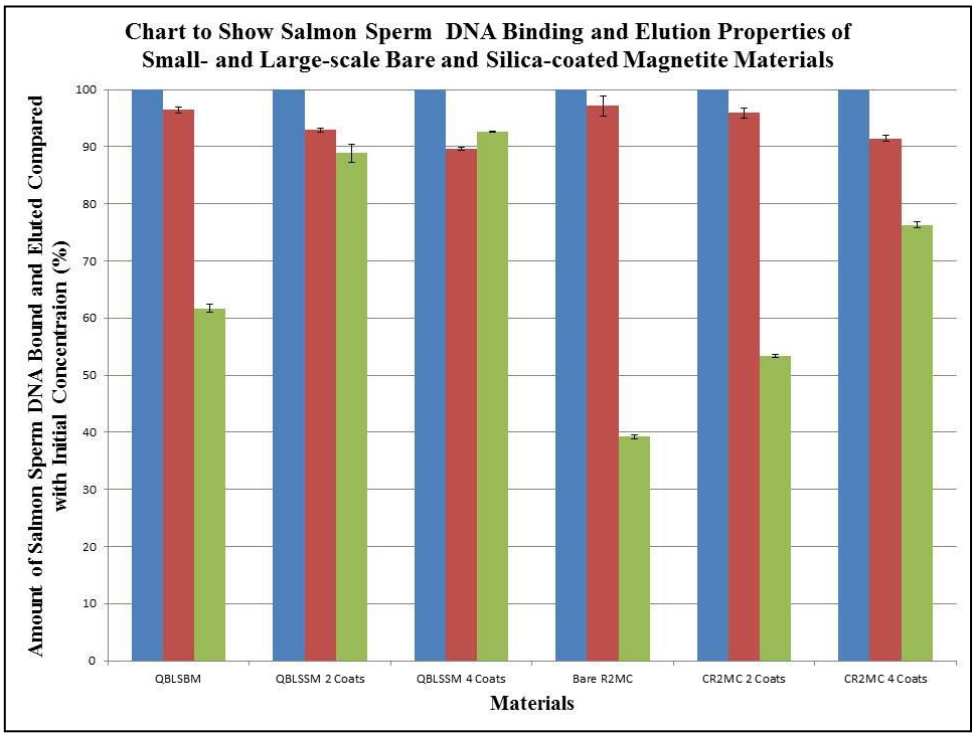

Figure 3.14: The amount of DNA adsorbed and eluted, as percentages of the initial amount of DNA used. The materials used are explained in Table 3.6 above. The blue bars represent initial amount of DNA used, the red bars represent DNA adsorbed and the green bars represent the eluted DNA. Values are mean ± S.E.M., n = 3.

Figure 3.13 and Figure 3.14 indicate that adsorption of DNA is high in the case of all materials (89-97%), indicating that adsorption to these materials occurs *via* a similar mechanism, i.e. the "cation-bridge" under chaotropic conditions. Adsorption is slightly higher in the case of bare magnetite nanoparticles, possibly because the DNA is adsorbed by a different mechanism, as the magnetite surface will not be fully ionised at the neutral pH conditions used. Hence, the "cation-bridge" adsorption mechanism may not be as strong in the case of bare magnetite and the magnetite surface groups may interact with the DNA *via* other mechanisms such as hydrogen bonding, or by direct electrostatic attraction with functional groups present in the DNA. The low elution values of bare magnetite compared to those of silica-coated magnetite again may be explained due to the different adsorption mechanisms, discussed above. As a result, with less "cation-bridge" interactions occurring in the chaotropic conditions, the adsorbed DNA may not be disrupted by altering the ionic strength of the system and more of the DNA will remain adsorbed on the magnetite surface. However, it can clearly be seen that coating with silica drastically changes the elution properties of the material.

In the case of amorphous silica-coated materials, both small-and large scale materials show an increase in elution with further silica-coatings. This follows trends observed by Bruce *et al*,[29] who reported that DNA can be successfully eluted from silica surfaces due to the electrostatic repulsion between ionised silanol groups ($Si\text{-}O^-$) and the negatively-charged phosphate backbone of DNA at low ionic strength, i.e. in water.[80] Hence, it is shown that magnetite coated 4 times produces a more complete core-shell of silica around the magnetite nanoparticle.

Figure 3.15 and Figure 3.16 show the effect that surface-functionalisation using various aminosilanes has on the DNA binding and elution properties of the nanoparticles. Figure 3.15 presents the data in terms of µg used, adsorbed and eluted, while Figure 3.16 presents the same data as percentages of the initial amount of DNA used.

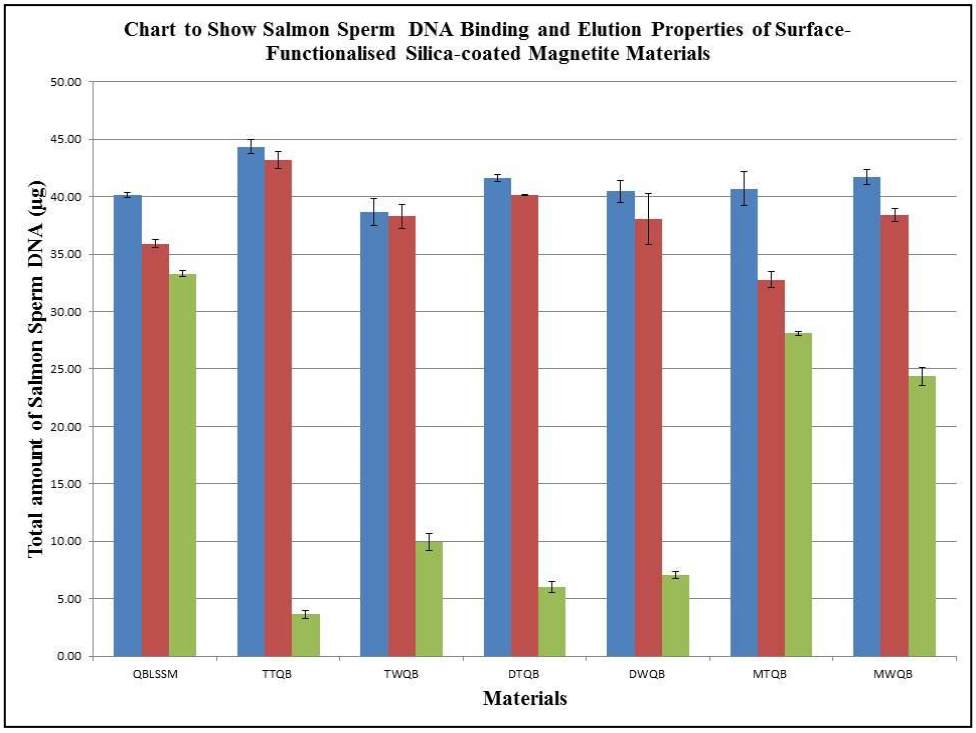

Figure 3.15: The amount of DNA initially used, adsorbed and eluted, in µg. The materials used are explained in Table 3.6 above. The blue bars represent initial amount of DNA used, the red bars represent the amount of DNA adsorbed and the green bars represent the amount of DNA eluted. Values are mean ± S.E.M., n = 3.

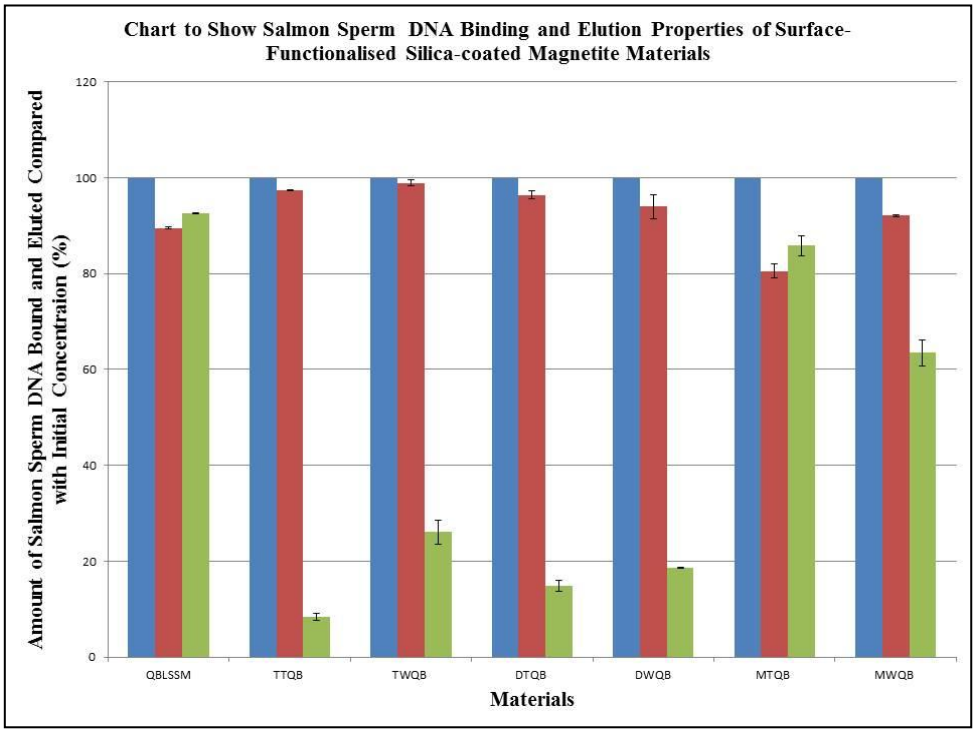

Figure 3.16: The amount of DNA adsorbed and eluted, as percentages of the initial amount of DNA used. The materials used are explained in Table 3.6 above. The blue bars represent initial amount of DNA used, the red bars represent DNA adsorbed and the green bars represent the eluted DNA. Values are mean ± S.E.M., n = 3.

Figure 3.15 and Figure 3.16 show that materials functionalised using APTS and APDS both adsorb more than silica-coated magnetite, but have very low elution values (lower than bare magnetite in both cases). Materials made using APTS and the TPRE-method of surface-functionalisation elute only 8% of adsorbed DNA, while those made using the water-method elute 3 times more DNA at 26%. For APDS materials, there is little difference between the DNA elution values of materials made *via* the TPRE-(15%) or the water-method (18%). However, APMS materials, have slightly lower adsorption than other materials, but have high elution values. The lower adsorption may be due to a lower surface amine density permitting fewer sites for the DNA to interact with. For APMS materials made *via* the TPRE- method, 85% of the DNA adsorbed was then eluted. APMS materials made *via* the water-method have moderately high elution values of 63% compared to APTS and APDS functionalised materials.

High adsorption values of DNA to the amine-surface-functionalised nanoparticles may be due to the fact that the aminosilanes are positively charged at pH 7,[80,455] mediating adsorption *via* electrostatic interactions between positively charged $–NH_3^+$ groups on the surface and the negatively-charged phosphate backbone of DNA.

Due to decreasing steric hindrance on the silica-coated magnetite surface with a decreasing number of alkoxy groups (from APTS to APDS to APMS) (see Figure 1.5, Section 1.6); it was shown that APTS gives the greatest density of surface amine groups (see Section 3.6). Due to the increased surface amine density provided by APTS, materials made using it can adsorb more DNA groups *via* direct electrostatic attraction to the $–NH_3^+$ surface groups. This can explain why elution is the lowest for APTS materials (the electrostatic interaction is unaffected by the change in ionic strength when water is used as an eluent). APDS possesses one methyl group and two alkoxy groups and as a result is slightly less ordered around the silica surface due to the methyl group blocking some of the inter-aminosilane Si-O-Si bonds. In addition to this, oxygen atoms present in the Si (surface)-O-Si (aminosilane) bond will electrostatically repel other similar oxygen atoms around the nanoparticle surface; this means that the aminosilane molecules cannot pack as closely together. Despite adsorption remaining as high as APTS materials, this could be due to there being more space on the silica-surface for the DNA to interact *via* the "cation-bridge" mechanism directly to the silica-surface, hence the slightly higher elution values than APTS. In the same trend, APMS has two methyl groups and just one alkoxy group, eliminating inter-aminosilane Si-O-Si bonds and greatly increasing the amount of space between each group on the surface, as there is no chance to

interact with other aminosilanes. Coupled with lower surface amine density values than APTS and APDS materials, more DNA could interact *via* the "cation-bridge" mechanism directly to the silica-surface, explaining the high adsorption values and the much higher values for elution. The results of the surface amine density assay shown in Section 3.6 help to validate these assumptions.

3.8 Lipase Immobilisation on Amine Functionalised Silica-Magnetite Nanoparticles

For lipase immobilised on surface-functionalised silica-magnetite nanoparticles (see Section 2.6 for method of immobilisation), enzyme loading was calculated using standard curves produced from a set of standard free lipase solutions of known concentration (see Section 2.9.3). Table 3.7 (see the next page) provides a comprehensive list of all lipase-immobilised materials produced for this project and their bio-catalytic applications.

Table 3.7: Immobilised and Physically Adsorbed Lipase Materials and their Use in Bio-catalytic Applications

Name	Details	Bio-catalytic Application Used For		
		Model Catalysis (Hydrolysis of PNPP)	**Transesterification of Ethyl Butyrate**	**Hydrolysis of *cis*-3,5-diacetoxy-1-cyclopentene**
PFLITTQB	PFL immobilised on TTQB (see Section 2.5.2)	√	√	√
PFLITWQB	PFL immobilised on TWQB (see Section 2.5.1)	√	√	N/A
PFLIDTQB	PFL immobilised on DTQB (see Section 2.5.2)	√	√	N/A
PFLIDWQB	PFL immobilised on DWQB (see Section 2.5.1)	√	√	N/A
PFLIMTQB	PFL immobilised on MTQB (see Section 2.5.2)	√	√	N/A
PFLIMWQB	PFL immobilised on MWQB (see Section 2.5.1)	√	√	N/A
CRLITTQB	CRL immobilised on TTQB (see Section 2.5.2)	√	√	N/A
CRLITWQB	CRL immobilised on TWQB (see section 2.5.1)	√	√	√
CRLIDTQB	CRL immobilised on DTQB (see Section 2.5.2)	√	√	N/A
CRLIDWQB	CRL immobilised on DWQB (see Section 2.5.1)	√	√	N/A
CRLIMTQB	CRL immobilised on MTQB (see Section 2.5.2)	√	√	N/A
CRLIMWQB	CRL immobilised on MWQB (see Section 2.5.1)	√	√	N/A
PFLIQBLSSM	PFL physically adsorbed on QBLSSM (see Section 2.6.2)	√	√	N/A
CRLIQBLSSM	CRL physically adsorbed on QBLSSM (see Section 2.6.2)	√	√	N/A

Note: PFLI and CRLI represent materials made using PFL and CRL. The letter T, D and M represent the aminosilane used (APTS, APDS and APMS respectively). The next letter T or W represents the surface-functionalisation method used: T = TPRE, W = water. QB represents the shortened name of the silica-coated material QBLSSM.

Figure 3.17 shows the average enzyme loading data for lipase-immobilised materials made using amorphous silica-coated magnetite nanoparticles functionalised by a variety of aminosilanes; APTS, APDS and APMS.

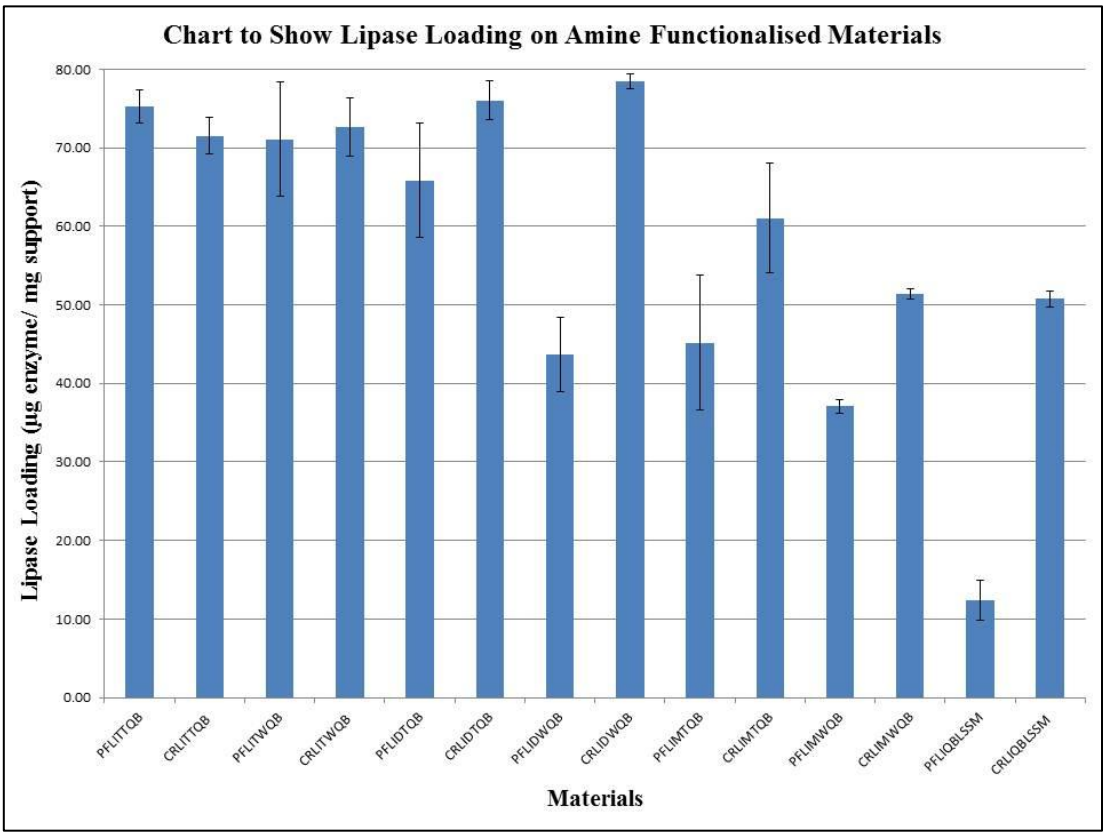

Figure 3.17: Lipase (*Pseudomonas Fluorescens* Lipase: PFL; *Candida Rugosa* Lipase: CRL) loading data for magnetite nanoparticles coated with amorphous silica and functionalised using a variety of aminosilanes by water and TPRE methods. See Table 3.7 for explanations of the names of materials. Values are mean, ± S.E.M., n ≥3 in all cases.

From Figure 3.17, the first comparisons to be made were between the water and TPRE methods of surface functionalisation. It can be seen that among materials functionalised using APTS, there is no significant difference in enzyme loading values between materials made using the water (PFLITWQB, CRLITWQB) or TPRE (PFLITTQB, CRLITTQB) methods. This can be explained by the similar values for surface amine density of the amine-functionalised materials made using APTS: TPRE = 4.34 NH_2-molecules per nm^2 and water = 4.06 NH_2-molecules per nm^2. For materials functionalised using APDS, in the case of PFL immobilisation, the TPRE method produces materials (PFLIDTQB) with around 50% higher enzyme loading values than the water method (PFLIDWQB). For CRL, loading values are slightly higher than those achieved using APTS-functionalised materials, with no clear difference between loading values achieved using the TPRE (CRLIDTQB) or water

(CRLIDWQB) method. It was expected that the loading for APDS materials made *via* the TPRE method would be higher than those made by the water method due to the higher surface amine density (3.28 NH_2-molecules per nm^2 compared to 1.39 NH_2-molecules per nm^2). Finally, for materials functionalised using APMS, in the case of PFL, loading values decrease, following the same trend of TPRE-functionalised materials (PFLIMTQB) having higher loading than water-functionalised materials (PFLIMWQB). For CRL loaded materials functionalised using APMS, loading values decrease significantly compared to APTS- and APDS-functionalised materials: by 15-22% in the case of TPRE-functionalised materials (CRLIMTQB) and 30-35% in the case of water-functionalised materials (CRLIMWQB). Again these lower lipase-loading results for materials functionalised using APMS correlate with a decrease in surface amine density due to a lack of inter-aminosilane cross-linking around the nanoparticle surface. As a result, there are fewer total surface amine groups where the lipase can bind.

For the physical adsorption of lipases, loading values were much lower for PFL than with amine functionalised materials. For CRL, physical adsorption gave similar loading values to those obtained using APMS and the water method, which was the lowest loading value obtained for all CRL materials. The general trend is that physical adsorption gave much lower loading values on average than those immobilised using chemical conjugation.

CHAPTER 4

BIO-CATALYTIC APPLICATIONS OF LIPASE-IMMOBILISED SILICA-MAGNETITE NANOPARTICLES

4.1 Introduction

This section of the thesis will outline three bio-catalytic reactions that have been explored in this project.

1. The first application was a model catalysis reaction; the hydrolysis of *p*-nitrophenyl palmitate (PNPP) to palmitic acid and *p*-nitrophenol (PNP). The hydrolysis of long-chain *p*-nitrophenyl esters has been used widely as a model reaction as it can be followed easily by UV-Visible spectrophotometry; directly following the hydrolysis of PNP by measuring the absorbance at 410 nm.[277,432] The amount of PNP hydrolysed was calculated using calibration curves produced from a set of standard PNP solutions of known concentration (see Figure 2.7, Section 2.9.5).
2. The second application was the transesterification of ethyl butyrate using *n*-butanol to produce butyl butyrate. The reaction is also known as alcoholysis and many studies investigating the effect of varying water concentration, solvent conditions and enzymes to produce flavour esters in this way have been reported.[301,303] The reaction products were monitored using GC and GC-MS and the conversion of ethyl butyrate to butyl butyrate was calculated using calibration curves produced from a set of standard solutions of ethyl butyrate, *n*-butanol and butyl butyrate of known concentration (see Figure 2.8, Section 2.9.6).
3. The final bio-catalytic application was the partial and selective hydrolysis of *cis*-3,5-diacetoxy-1-cyclopentene to produce the chiral optical isomer (1S,4R)-*cis*-4-acetoxy-2-cyclopenten-1-ol and its enantiomer, with *cis*-3,5-dihydroxycyclopentene produced as a by-product. This reaction has not been reported much in the literature, but the chiral products are important pharmaceutical compounds used in the synthesis of prostaglandins and thromboxanes.[289,298] The reaction products were monitored using GC and GC-MS and the conversion to (1S,4R)-*cis*-4-acetoxy-2-cyclopenten-1-ol and its (1R,4S)-enantiomer was calculated using calibration curves produced from a set of standard solutions of *cis*-3,5-diacetoxy-1-cyclopentene, (1S,4R)-*cis*-4-acetoxy-2-cyclopenten-1-ol and *cis*-3,5-dihydroxycyclopentene of known concentration (see Figure 2.9 and Figure 2.10, Section 2.9.7).

All of the bio-catalytic applications have been carried out using lipases (both CRL and PFL), immobilised on surface-functionalised silica-magnetite nanoparticles as efficient, re-usable catalysts, see Section 3.8.

4.2 Bio-catalytic Application: Model Catalysis Reaction - Hydrolysis of PNPP

The reaction was carried out according to the method outlined in Section 2.6.3. The amount of lipase-immobilised nanoparticles (variable amount, in mg) corresponding to 500 µg immobilised lipase was used in each case, except when free lipase was used as catalyst, 500 µg was used directly as catalyst. This type of reaction has been carried out numerous times with both free[277,281,432] and immobilised lipases (mainly commercial supports).[282,460] The reaction has also been carried out using lipase immobilised on surface-functionalised magnetic nanoparticles[100,461,462] (mainly using APTS), however, to the best of my knowledge this reaction has not been carried out in a comparative study using lipase immobilised on APTS, APDS and APMS surface-functionalised nanoparticles. Wang *et al*[463] have investigated the effect of the alkyl chain length of three alkoxy silanes (trimethoxypropyl silane, trimethoxyoctyl silane and trimethoxyoctadecyl silane) on immobilised enzyme activity using CRL. However, the enzyme was immobilised *via* hydrophobic interaction and not *via* chemical cross-linking. This study also compares the activity of lipase-immobilised materials prepared using both the TPRE and water methods of surface functionalisation.

The reaction was carried out using two lipases (PFL and CRL) immobilised on TPRE- and water-method surface-functionalised nanoparticles using three different aminosilanes: APTS, APDS and APMS. Physically adsorbed PFL and CRL on silica-coated magnetite nanoparticles and free lipases were used as comparison for the study.

The main focus of this part of the study is to compare the activity of lipase-immobilised nanoparticles made using various aminosilanes and surface-functionalisation methods. The first materials to be discussed are the PFL materials. The results are shown in Figure 4.1.

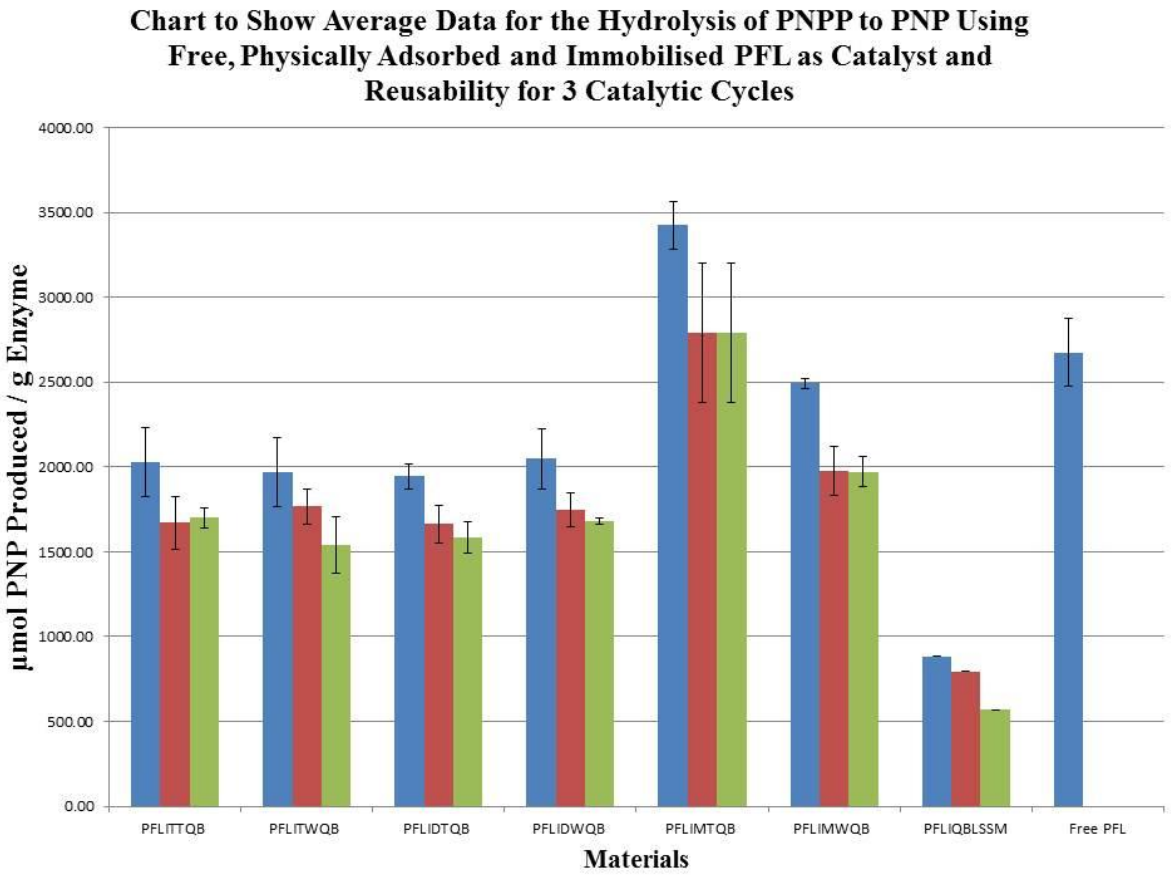

Figure 4.1: The catalytic activity (in µmol PNP produced per gram of enzyme used) of free, physically adsorbed and chemically conjugated PFL on various surface-functionalised silica-magnetite nanoparticles. The re-usability of the materials was also tested and the blue bars represent catalytic activity for the first one hour cycle, the red bars represent activity for the second one hour cycle and the green bars represent activity for the third one hour cycle. See Table 3.7 (Section 4.1) for explanations of the names of materials. Values are mean, ± S.E.M., n ≥3 in all cases.

PFL materials made using APTS show similar activity values, regardless of the surface functionalisation method. PFLITTQB is shown to retain 84% of its initial activity over 3 cycles, whilst PFLITWQB retains 78%. PFL materials made using APDS (and show very similar trends and activity values, with no real difference between materials made using the TPRE (PFLIDTQB) and water (PFLIDWQB) method. However, for PFL materials made using APMS, two interesting trends can be observed. The first is that PFLIMTQB is by far the most effective catalyst for this reaction, producing 3424 µg of PNP per gram of support, which is 1.6-1.75 times more catalytically active than PFL-immobilised on APTS (PFLITTQB and PFLITWQB) or APDS (PFLIDTQB and PFLIDWQB) functionalised nanoparticles and 1.37 times more active than PFLIMWQB. The second is that there is a large, noticeable difference between materials prepared by the TPRE (PFLIMTQB) and water

(PFLIMWQB) method. Both materials retain around 80% of their initial activity over 3 cycles, but PFLIMTQB shows much higher activity over the 3 cycles than PFLIMWQB (37% higher for cycle 1 and 41% higher for both cycles 2 and 3). This could be due to lower enzyme loading values of materials made using APMS for surface functionalisation leading to a decrease in steric hindrance which could be a factor with higher loading values. This may also lead to the active site of PFL being more accessible at low enzyme loading under hydrophobic surfaces (due to the presence of neighbouring methyl groups).

Another interesting observation is that the activity of PFL materials made using APMS decreases by the largest percentage between the 1st and 2nd cycles (activity decreases 19-21% from cycle 1 to cycle 2). This could be due to a decreased steric hindrance around the nanoparticle surface permitting a small amount of physical adsorption directly on the silica-magnetite core-shell, which is then leached into solution in subsequent cycles. This could also explain why activity remains almost equal in cycles 2 and 3, when the physically adsorbed lipase has leached into solution leaving just the chemically conjugated (covalently-linked) PFL. Another possible explanation is that the high loading of PFL on APTS and APDS surface-functionalised nanoparticles leads to the formation of the bi-molecular form of PFL. As immobilisation leads to activation of the lipase and PFL is known to form bi-molecular aggregates[159,234] *via* the hydrophobic regions surrounding its active sites in its open form, high loadings could lead to the simultaneous activation and aggregation of PFL due to the presence of the hydrophilic surfaces on the nanoparticles, leading to a reduction in activity due to competition between the reaction occurring in the active sites and formation of the bi-molecular structure with neighbouring PFL active sites. The catalytic activity of physically adsorbed PFL (PFLIQBLSSM) was shown to be considerably lower than that of chemically conjugated PFL in all cases. This could be caused by the PFL being adsorbed to the nanoparticle surface in a manner that inhibits efficient catalytic activity.

The results of the reaction performed by CRL materials are presented in Figure 4.2.

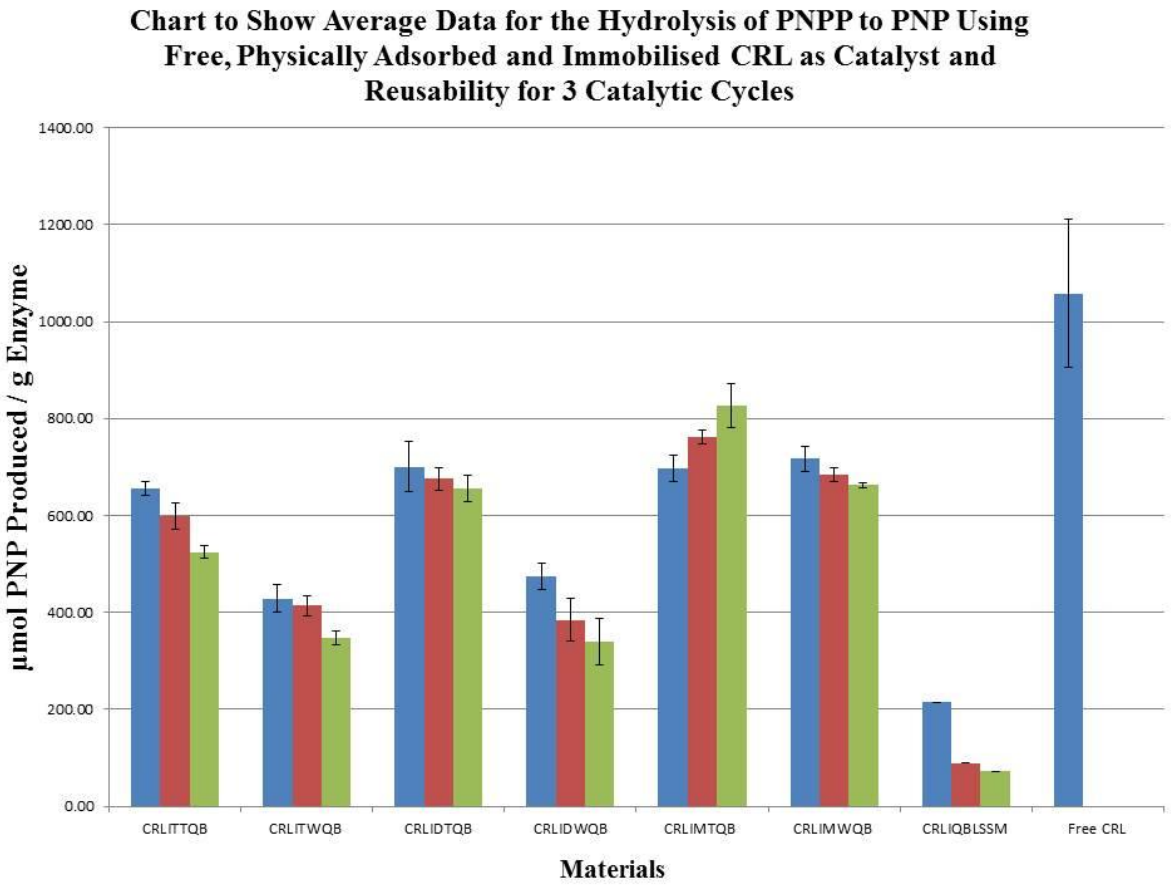

Figure 4.2: The catalytic activity (in µmol PNP produced per gram of enzyme used) of free, physically adsorbed and immobilised CRL on various surface-functionalised silica-magnetite nanoparticles. The re-usability of the materials was also tested and the blue bars represent catalytic activity for the first one hour cycle, the red bars represent activity for the second one hour cycle and the green bars represent activity for the third one hour cycle. See Table 3.7 (Section 4.1) for explanations of the names of materials. Values are mean, ± S.E.M., n ≥3 in all cases.

With regard to CRL materials, APTS surface-functionalised materials made by the TPRE method (CRLITTQB) show markedly higher activity over 3 cycles than those made using the water (CRLITWQB) method. They both retain around 80% of initial activity over 3 cycles, but CRLITTQB shows between 44-53% higher activity per cycle. For materials made using APDS, the same trend can be seen, with CRLIDTQB giving up to 93% higher activity per cycle than CRLIDWQB. An interesting trend is seen in CRL materials made using APMS. CRLIMTQB shows increasing activity over all 3 cycles and higher activity than all other CRL materials. CRLIMWQB also shows increased activity compared to other CRL materials, retaining 92% of its initial activity over 3 cycles. This could again be due to the decreased steric hindrance due to lower enzyme loadings seen in materials prepared using APMS. It is possible that in the case of CRLIMTQB, the lower loading enabled the physical adsorption of some CRL and as it was leached into the solution over the cycles, the

chemically conjugated (covalently linked) CRL became less sterically hindered and more active sites become accessible, similar to PFL.

The final observation that can be made from the results is that all PFL materials (free, physically adsorbed and chemically conjugated) exhibit higher activity than all forms of CRL materials for this reaction. Free lipases (only run for one cycle due to difficulties in isolating the lipase from the reaction mixture) show that PFL is over 2.5 times more active for this reaction than CRL. For physically adsorbed materials, again PFL materials give higher activity than CRL materials. However, in the case of physically adsorbed materials, activity for both materials decreases dramatically for each consecutive cycle. For PFLIQBLSSM, activity during the 3rd cycle drops to 65% that of the 1st while for CRLIQBLSSM, activity drops to just 34% during the 3rd cycle. This is possibly due to the lipase being leached into solution over time during the reaction, as suggested by Sen *et al*.[100]

Brief Conclusions

There are various conclusions which can be drawn from this section of the study. The first is that PFL (free, physically adsorbed or chemically conjugated) is a much more catalytically active lipase than CRL (all forms) for this particular application. The second is that for physically adsorbed lipases (both PFL and CRL), activity decreases by a large margin over a number of cycles, possibly due to the lipase leaching into solution. For PFL-immobilised (chemically conjugated) nanoparticles, activity for APTS and APDS materials is similar, regardless of the surface-functionalisation method used. However, when APMS is used, catalytic activity is increased greatly and a big difference can be seen in materials made using the TPRE and water methods. This increase could be due to decreased steric hindrances leading to more accessible active sites. For CRL-immobilised materials, APTS, APDS and APMS surface-functionalised materials made using the TPRE method give higher activity than the same materials made using the water method. This could be due to a more ordered orientation of the CRL around the nanoparticle surface due to the more ordered amine groups given by the TPRE method.[87,89]

These conclusions can be enhanced by Figure 3.12, Section 3.6, which shows that for APTS and APDS materials in particular, the TPRE method affords a higher surface amine density than the water method. For APMS materials', loading is similar for both methods, but the values are much lower than both APTS and APDS materials. The physically adsorbed enzyme can be leached into solution and will then exhibit behaviour of the free lipase, which

for PFL is higher than APTS and APDS functionalised nanoparticles, but lower than those made using APMS. For CRL, free lipase exhibits higher activity than all materials. Hence, the increased activity of APMS materials in all cases could be due to a combination of covalently immobilised lipase benefiting from less steric hindrance than APTS and APDS materials (hence having more accessible active sites and higher activity) and physically adsorbed lipase being gradually leached into the reaction (exhibiting the increased activity of free lipase). This combination can account for the higher activity values obtained and also the increase in activity over 3 cycles for CRLIMTQB.

4.3 Bio-catalytic Application: Transesterification of Ethyl Butyrate

The amount of lipase-immobilised nanoparticles (variable amount, in mg) corresponding to 500 µg immobilised lipase was used in each case, except when free lipase was used as catalyst, 500 µg was used directly as catalyst. Initially, the reaction was carried out using identical conditions to Solanki and Gupta,[301] who employed surfactant-coated superparamagnetic nanoparticles with immobilised CRL for the transesterification of ethyl butyrate using *n*-butanol and anhydrous hexane. As in the transesterification carried out by Solanki and Gupta, I initially used a 1:2 ratio of ethyl butyrate (60 mM) to *n*-butanol (120 mM), but with the regular 500 µg total lipase, instead of the 1000 µg used in their study. For this initial study, the following materials were used as catalysts: PFLITTQB, CRLITTQB, PFLIQBLSSM, CRLIQBLSSM, free PFL and free CRL. However, results obtained showed almost no butyl butyrate present after 1 hour and 24 hours of reaction time, for any of the catalyst materials. It was observed that there was no miscibility between the nanoparticles (with just a surface water layer) and the hexane layer. The reaction was repeated in THF, with no results either.

It was later during a literature search I found that lipases are only active in water-immiscible solvents, as water miscible solvents extract the water of hydration layer from the enzymes, rendering them inactive, hence this was the reason that no reaction had taken place. I also learned that esterification success is dependent on water concentration in the system and lipase hydration is important, as a minimum amount of water is required to keep it in its' active form.[464] Also, when hydrophobic solvents are used, they can limit enzyme flexibility, so the lipase should be in its active conformation prior to addition of the organic solvent, i.e. the lipase should be dissolved in water prior to hexane addition. Finally, it has been reported[464] that lipase stability can also be improved by covalent attachment of PEG to free

amino-residues on the lipase, giving them amphiphillic properties and allowing their dissolution in organic solvents.[464] By coating the nanoparticles in surfactants, Solanki and Gupta got the transesterification reaction to work without the addition of extra water, hence, I decided to investigate the effects of varying water concentration and PEG in order to allow the lipase to be in its active conformation throughout the reaction and act as an efficient bio-catalyst. The investigation into optimising the water concentration is reported in the following section.

4.3.1 Investigation into Varying Water Concentration

The initial study was to compare the efficiency of the reaction by adding 0.5 and 1% water to the system. In order to reduce wastage of my own materials, free lipases (free PFL and free CRL) and a commercial supported lipase (PFL immobilised on Immobead support) were used for this initial reaction, until the best conditions could be found. Reaction conditions [1:2 ratio of ethyl butyrate (60 mM) to *n*-butanol (120 mM) with the regular 500 µg total lipase at 37ºC] were kept the same as before.

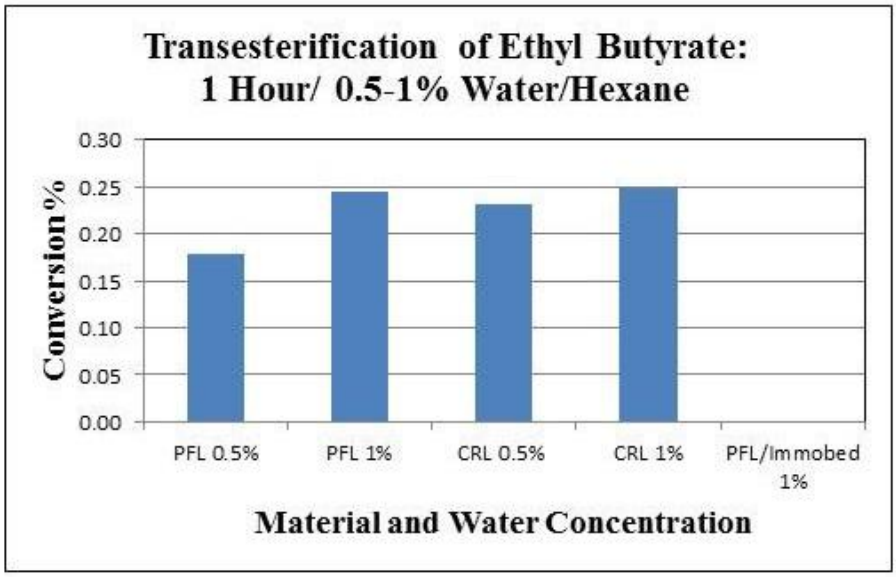

Figure 4.3: Conversion of ethyl butyrate to butyl butyrate after 1 hour using free lipases and commercially available PFL immobilised on Immobead 150 (Product number 90678, Sigma-Aldrich, UK) with 0.5% and 1% water/hexane solvent.

Figure 4.3 above shows that after 1 hour, conversion is extremely low, with around 0.25% being the maximum. It can also be seen that 1% water/hexane gives slightly higher conversion values than 0.5% and hence, reactions in 1% water/hexane were decided to be continued for a further 21 hours. Note that commercially available PFL immobilised on

Immobead 150 did not produce any reaction products (0% conversion) after 1 hour under identical reaction conditions.

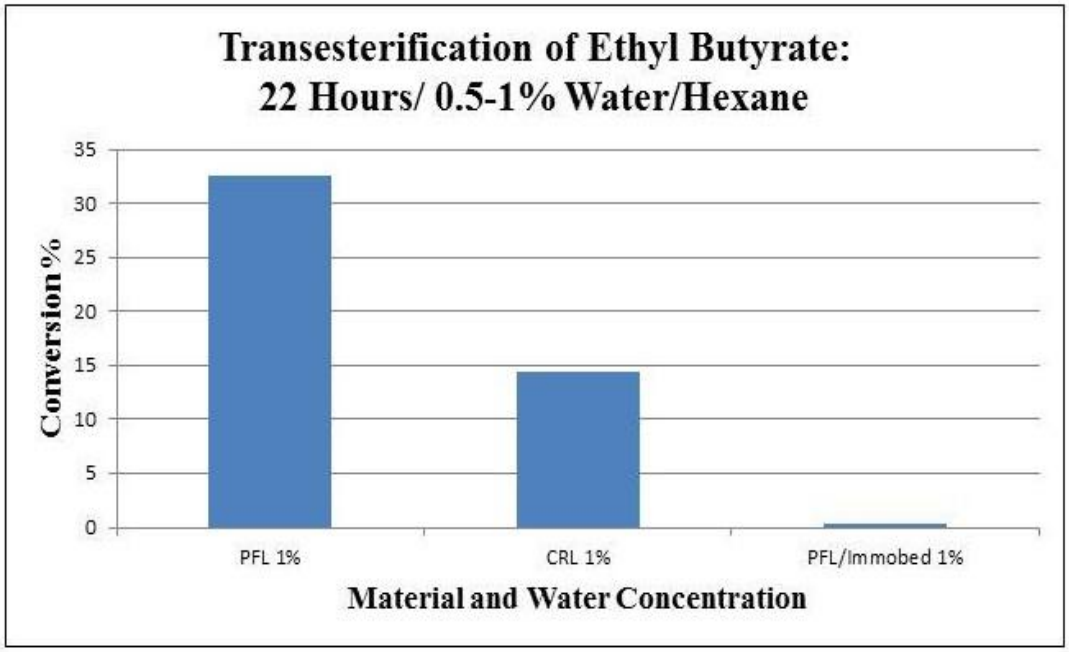

Figure 4.4: Conversion of ethyl butyrate to butyl butyrate after 22 hours using free lipases and commercially available PFL immobilised on Immobead 150 with 1% water/hexane solvent.

Figure 4.4 above shows much higher conversion values for 22 hours reaction time. Free PFL shows product conversion of 32.5%, almost 200 times more than that produced after just 1 hour. Free CRL shows 14.4% conversion, over 50 times the amount of product produced. No reaction took place when the reaction was performed without the presence of lipase catalysts (blank reaction). As the reaction was more successful using a higher water concentration, I decided to perform the reaction using 10% water/hexane as the solvent system. Conditions were kept the same as before (1:2 ratio of ethyl butyrate (60 mM) to *n*-butanol (120 mM), with 500 µg total lipase at 37ºC).

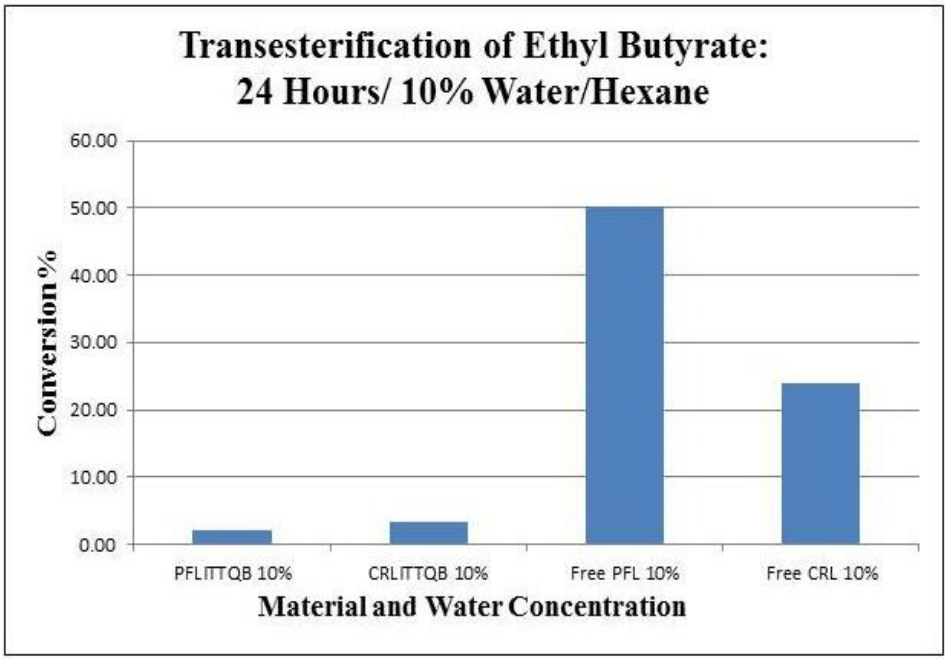

Figure 4.5: Conversion of ethyl butyrate to butyl butyrate after 24 hours using lipase-immobilised materials PFLITTQB and CRLITTQB, as well as free lipases with 10% water/hexane solvent.

Figure 4.5 shows that transesterification of ethyl butyrate increases to 50.2% and 23.8% for free PFL and CRL respectively when water concentration is increased to 10%. Lipase Immobilised materials PFLITTQB (2.2%) and CRLITTQB (3.3%) both showed small conversion figures, but the increase in water concentration definitely provided better conversion results for free lipases. I decided that 10% water/hexane would be used as the best solvent system. As the water content of the system had been decided upon, the next step was to investigate the effect of adding PEG as a stabilising agent for the lipase.

4.3.2 Investigation into Using PEG as Stabilising Agent

The first step in this case was to test the system using a small amount of PEG in the 10% water/hexane system to see if it could improve the conversion. A solution of 1% PEG in water was made, to give a final solvent system of 0.1% PEG in 10% water/hexane. The reaction was first carried out with free lipases to reduce wastage of lipase-immobilised materials. Reaction conditions were kept the same as before (1:2 ratio of ethyl butyrate (60 mM) to *n*-butanol (120 mM), with the regular 500 µg total lipase at 37ºC).

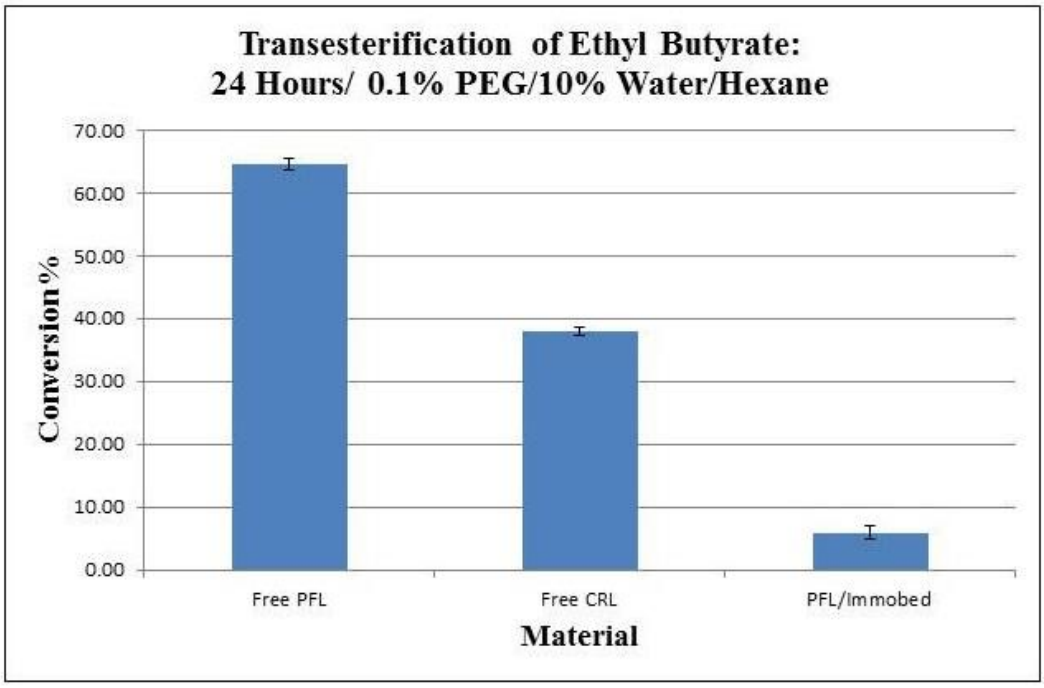

Figure 4.6: Conversion of ethyl butyrate to butyl butyrate after 24 hours using free lipases and commercially available PFL immobilised on Immobead 150 with 0.1% PEG in 10% water/hexane solvent. Values are mean, ± S.E.M., *n* =2.

Figure 4.6 shows conversion for both free PFL (64.6%) and CRL (38.1%) has been improved by the addition of PEG. A reasonable conversion (6%) for PFL immobilised on Immobead 150 was obtained in the presence of PEG. Following the successful results, I decided that this solvent system would be used to test the lipase-immobilised nanoparticles. The reaction was repeated for a further 3 identical catalytic cycles, with the lipase-immobilised nanoparticles washed magnetically with 3×1 mL PBS buffer and re-dispersed in fresh 0.1% PEG in 10% water before addition of a fresh hexane layer and new reactants between cycles. Free lipases and the water layer were centrifuged and re-dispersed, before addition of a fresh hexane layer and new reactants between cycles.

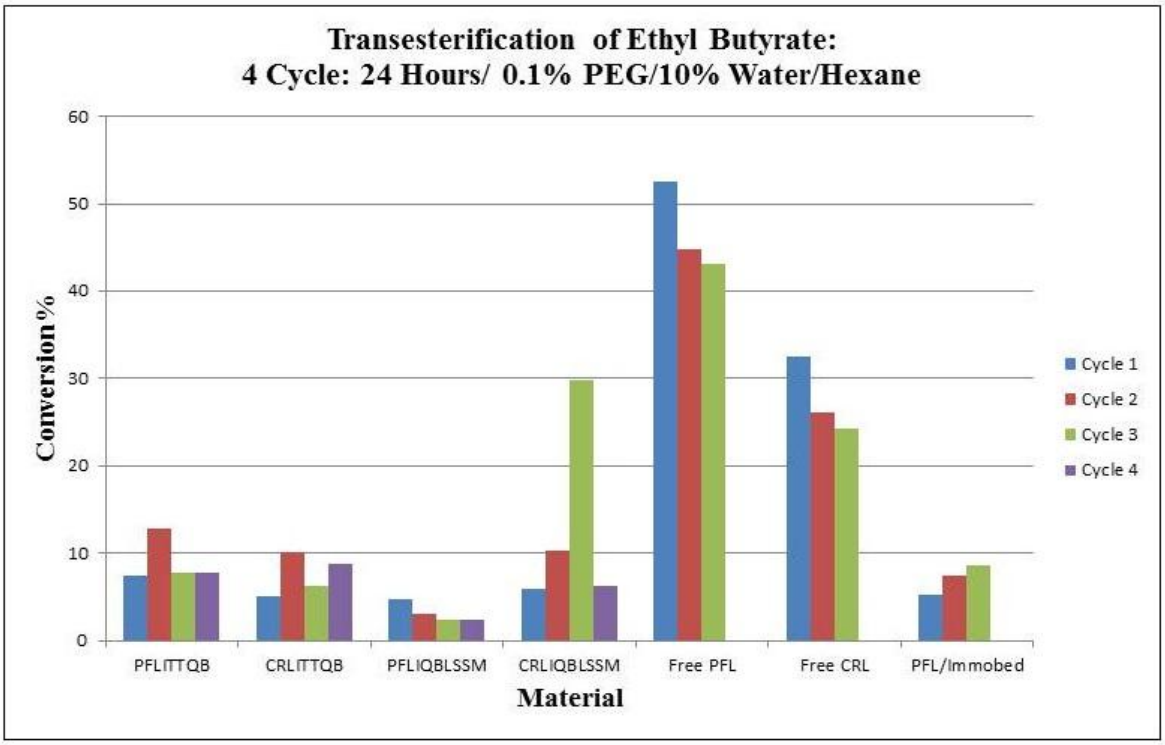

Figure 4.7: Conversion of ethyl butyrate to butyl butyrate over 24 hour reaction (3-4 re-usable cycles) using lipase-immobilised materials PFLITTQB and CRLITTQB, lipase-adsorbed materials PFLIQBLSSM and CRLIQBLSSM, free lipases (PFL and CRL) and commercially available PFL immobilised on Immobead 150 with 0.1% PEG in 10% water/hexane solvent. The blue bars represent cycle 1 conversion values, the red bars represent cycle 2, the green bars represent cycle 3 and the purple bars represent cycle 4. See Table 4.2, Section 4.3.4 for material names.

Figure 4.7 above shows the multi-cycle transesterification reaction using a variety of materials. Firstly, it can be seen that for free lipases, catalytic activity decreases slightly with each cycle, but the overall activity of free lipases is much greater than lipase-immobilised materials. However, free lipases proved difficult to recover and re-disperse because of the loss of some of the water layer between each cycle. Free PFL retains over 82% of its initial catalytic activity in the third cycle of the reaction, dropping from 52.5% conversion to 44.9% in cycle 2 and 43.1% in cycle 3. For free CRL, conversion drops from 32.6% in cycle 1 to 26.1% in cycle 2 and 24.3% in cycle 3, retaining around 74% of its initial activity. The activity of PFL immobilised on Immobead 150 actually increased steadily over 3 cycles.

With regard to lipase-immobilised nanoparticles, conversion is low over all 4 cycles and quite irregular. Both PFLITTQB and CRLITTQB exhibited their highest conversion values of 10-12% in the second cycle, before decreasing for the third cycle. For PFLITTQB, activity was the same in cycles 3 and 4, while for CRLITTQB, activity increased again in cycle 4. As with

the model catalysis reaction, increases in activity could be due to the enzyme leaching into solution after it is washed between cycles. For physically-adsorbed lipase materials, PFLIQBLSSM displayed the lowest activity out of all materials for every cycle and steadily decreased in activity over all 4 cycles (from 4.8% in cycle 1 to 2.3% in cycle 4). CRLIQBLSSM displayed some interesting behaviour, increasing in activity from cycle 1 (6.0%) to cycle 2 (10.3%) and then increasing a large amount to cycle 3 (29.8%). The large conversion exhibited in cycle 3 was higher than free CRL in the same cycle, suggesting leaching of the lipase from the support into the solution during the reaction. The activity decreased to just 6.3% in cycle 4.

Due to the somewhat irregular and unexpected erratic nature of the results obtained using the PEG/water/hexane system, I attempted to find an explanation in the literature, but found no relevant results as the system has not been used (to the best of my knowledge) for this application with these types of catalytic materials. However, I came across an interesting article by Liaquat *et al*[303] who reported the transesterification of ethyl butyrate to butyl butyrate catalysed by rape seedling lipase. They also studied the effect of water concentration and found that transesterification yield was best with water concentrations between 0.5 and 20%, decreasing outside of these limits (although the reaction was carried out a 5 mL scale). It is worth mentioning that increasing the water concentration from 1% to 20% did not have much of an effect on transesterification yield in their study, hence 10% was decided as the maximum concentration for this study. They tested the effect of ethyl butyrate to *n*-butanol ratio, concluding that the optimal system was using a 6:1 ratio of ethyl butyrate (600 mM) to *n*-butanol (100 mM). Hence, the next part of the transesterification reaction investigation has been focussed on the effect of reactant ratio using the best solvent system.

4.3.3 Optimising the Solvent System Using a 6:1 Ratio of Ethyl Butyrate to *n*-Butanol

With the new ratio of starting materials for the reaction, it was important to decide on the correct solvent system to further optimise the reaction for the best results. Therefore, the reaction was performed for 24 hours and a variety of solvent systems using free PFL and free CRL.

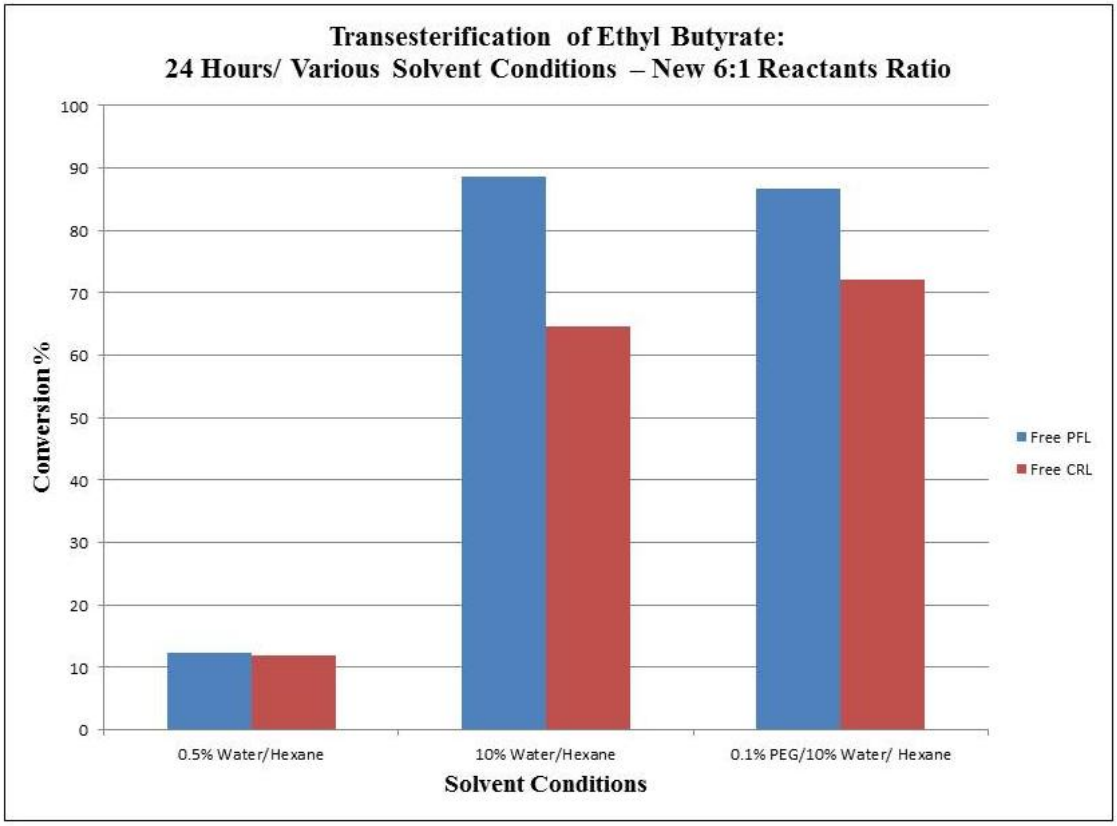

Figure 4.8: Conversion of ethyl butyrate to butyl butyrate after 24 hours using free PFL (blue bars) and free CRL (red bars) and 3 different solvent systems: 0.5% water/hexane, 10% water/hexane and 0.1% PEG in 10% water/hexane. The blue bars represent conversion given by free PFL and the red bars represent free CRL. Reactant ratio (ethyl butyrate to *n*-butanol) of 6:1.

Figure 4.8 shows that 0.5% water/hexane is by far the most ineffective solvent system for the reaction and will not be used any further. It can also be seen that PEG does not have a considerable effect on the conversion of ethyl butyrate to butyl butyrate. It is worth mentioning that the 6:1 ratio of starting materials leads to much higher conversion values for free PFL (around 90%) and free CRL (around 65%), compared with the 1:2 ratio and equal solvent conditions.

Table 4.1: Ethyl butyrate to butyl butyrate conversion values given using different ratios of ethyl butyrate to *n*-butanol. Conditions = 10% water/hexane solvent, 37ºC, 24 hours.

Catalyst Material	**Conversion of Ethyl Butyrate to Butyl Butyrate (%)**	
	1:2 ethyl butyrate : *n*-butanol	**6:1 ethyl butyrate : *n*-butanol**
Free PFL (500 µg)	50.15	88.60
Free CRL (500 µg)	23.84	64.61

4.3.4 Results: Detailed Study on Re-usability and Activity of Lipase-Immobilised Nanoparticles for Transesterification of Ethyl Butyrate Using Optimised 6:1 Ratio of Ethyl Butyrate to *n*-Butanol and Solvent System

The reaction was performed as explained in Section 2.6.4. Ethyl butyrate (600 mM) and *n*-butanol (100 mM) were added to the amount of lipase-immobilised nanoparticles corresponding to 500 µg total lipase. The solvent system used was 10% water/hexane. Materials made using a variety of aminosilanes (APTS, APDS and APMS) for surface functionalisation followed by lipase (PFL and CRL) immobilisation. Table 4.2 shows the materials used for this reaction.

Table 4.2: Materials used for the transesterification of ethyl butyrate.

Name	**Details***	**Name**	**Details***
PFLITTQB	PFL immobilised on TTQB	**CRLITTQB**	CRL immobilised on TTQB
PFLITWQB	PFL immobilised on TWQB	**CRLITWQB**	CRL immobilised on TWQB
PFLIDTQB	PFL immobilised on DTQB	**CRLIDTQB**	CRL immobilised on DTQB
PFLIDWQB	PFL immobilised on DWQB	**CRLIDWQB**	CRL immobilised on DWQB
PFLIMTQB	PFL immobilised on MTQB	**CRLIMTQB**	CRL immobilised on MTQB
PFLIMWQB	PFL immobilised on MWQB	**CRLIMWQB**	CRL immobilised on MWQB

Note: PFLI and CRLI represent materials made using PFL and CRL. The letters T, D and M represent the aminosilane used (APTS, APDS and APMS respectively). The next letter T or W represents the surface-functionalisation method used: T = TPRE, W = water. QB represents the shortened form of the silica-coated material QBLSSM. *See Table 3.7, Section 4.1 for material details.

The reaction was carried out for a total of 24 hours and 3 re-cycles. Lipase-immobilised nanoparticles were washed magnetically with 3×1 mL PBS buffer and re-dispersed in fresh water before addition of fresh hexane and reactants between cycles.

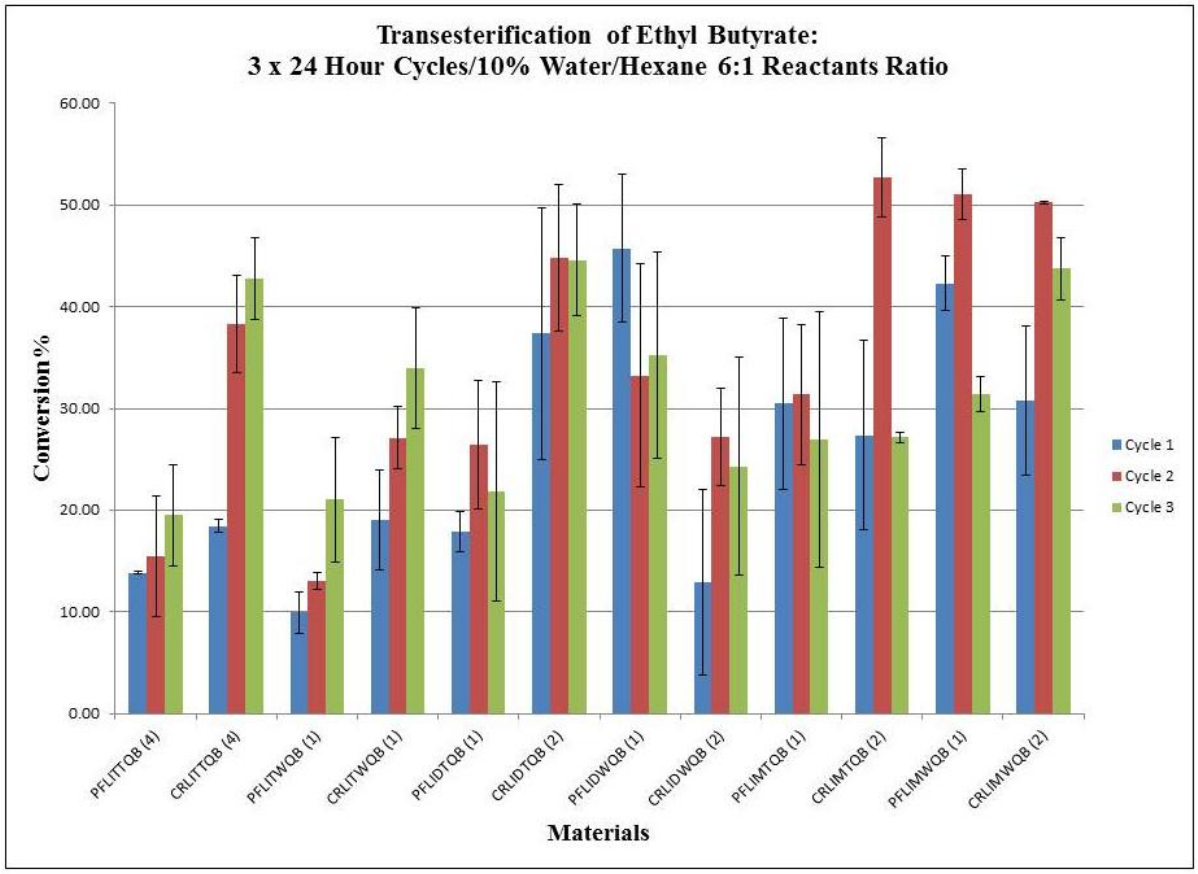

Figure 4.9: Conversion of ethyl butyrate to butyl butyrate over 3×24 hour cycles using lipase-immobilised materials in 10% water/hexane solvent. See Table 4.2 above for details on the materials used. Values are mean, ± S.E.M., n =3 in all cases.

Results and discussion on PFL-immobilised materials: For materials made using APTS as the aminosilane, the trend of increasing activity over all three cycles can be observed for both TPRE- (PFLITTQB: 13.8% cycle 1, 15.4% cycle 2, 19.5% cycle 3) and water- (PFLITWQB: 10.0 % cycle 1, 13.1% cycle 2, 21.0% cycle 3) functionalised materials. For materials made using APDS as the aminosilane, water-functionalised (PFLIDWQB) materials show a markedly higher activity (45.7% cycle 1, 33.2% cycle 2, 35.2% cycle 3) over all three cycles than TPRE-functionalised (PFLIDTQB) materials (17.9% cycle 1, 26.4% cycle 2, 21.8% cycle 3). For materials made using APMS as the aminosilane, again materials made using the water-method (PFLIMWQB) show a much higher activity (42.3% cycle 1, 51.0% cycle 2, 31.4% cycle 3) over all three cycles than those made *via* the TPRE-method (PFLIMTQB: 30. 5% cycle 1, 31.4% cycle 2, 26.9% cycle 3).

For APTS-functionalised materials, those made using TPRE-method perform slightly better than those made using the water method over the first two cycles, with similar conversions for the third. For APDS-functionalised materials, the water-method has a much higher

activity over all 3 cycles and is the most suitable for this application. For APMS-functionalised materials, materials made using the TPRE-method provide more consistent activity over the 3 cycles, but materials made using the water-method show much higher activity over all 3 cycles.

Results and discussion using CRL-immobilised materials: As with PFL, for materials made using APTS as the aminosilane, the trend of increasing activity over all 3 cycles can be observed for both TPRE-(CRLITTQB: 18.4% cycle 1, 38.3% cycle 2, 42.7% cycle 3) and water-functionalised (CRLITWQB: 19.0% cycle 1, 27.1% cycle 2, 34.0% cycle 3) materials. It can be concluded that in the case of CRL materials made using APTS as the aminosilane, that TPRE is the most effective method of surface functionalisation to produce better catalytic materials for the transesterification of ethyl butyrate. For materials made using APDS as the aminosilane, materials made by the TPRE-method (CRLIDTQB) have some of the highest activity out of all of the materials used (37.4% cycle 1, 44.8% cycle 2, 44.6% cycle 3). Materials made by the water-method using APDS (CRLIDWQB) are much less catalytically active (12.9% cycle 1, 27.2% cycle 2, 24.3% cycle 3). Finally, CRL-immobilised materials made using APMS as the aminosilane; water-method (CRLIMWQB) materials produced higher activity for cycles 1 and 3, but for cycle 2, the materials functionalised using the TPRE approach (CRLIMTQB) have the highest activity out of any materials used in any cycle (52.7%).

Brief Conclusions

Preliminary investigations and a thorough literature search led to initial experiments into finding and optimising a suitable solvent system for the reaction. With regard to solvents, initial reactions using hexane and THF gave no successful results, which I later found out was due to enzyme inactivation. Water was introduced to the system and various water concentrations in hexane were tested, with 10% water/hexane (maximum amount of water) providing the best results due to successful interfacial activation of the enzyme permitting exposure of the active site. Next, PEG was investigated as a stabilising agent for the reaction, but conversion of ethyl butyrate to butyl butyrate was not improved significantly, hence, it was left out of the later reactions. The final parameter in my study was the ratio of ethyl butyrate to *n*-butanol. Two systems were used: A 1:2 ratio of ethyl butyrate: *n*-butanol (as used by Solanki and Gupta[301] and a 6:1 ratio of ethyl butyrate: *n*-butanol (as used by Liaquat *et al*[303]). It was clear to see (see Table 4.1) that the 6:1 ratio of ethyl butyrate to *n*-butanol led

to a dramatic increase in conversion values (at least in the case of free lipase) and hence these conditions were used for the detailed investigation into the transesterification using PFL and CRL immobilised materials.

The activity of PFL- and CRL-immobilised materials cannot be compared accurately due to the differing trends observed in the results and their different structures. For PFL materials made using APTS as the aminosilane, those made using the TPRE method perform slightly better over the first two cycles than those made using the water method, while for the third cycle, the conversion values are very similar. For APDS-functionalised materials, those made using the water method give much higher average conversion values for all three cycles, but the values fluctuate a lot between cycles and error is relatively high. For APMS-functionalised materials, again, those made using the water method provide higher conversion values than those made by the TPRE method, but the values fluctuate a lot between cycles and error remains relatively high. Also, every material shows at least one instance of conversion increasing between cycles, possibly due to leaching of the enzyme into solution over the course of the reaction. Interestingly, none of the conversions given by any material were as high as that given by free PFL.

For CRL-immobilised materials, APTS-functionalised materials obtained by the TPRE and water method show similar activity in the first cycle, but in the second and third cycles, those made using the TPRE-method give higher conversions. In the case of APDS-functionalised materials, those made using the TPRE method show drastically higher conversion values (for all cycles) than those made using the water method. Finally, for APMS-functionalised materials, those made using the water method show slightly higher conversions than those made using the TPRE method in the first and third cycles, but both materials show a significant increase in conversion for the second cycle, with the TPRE-functionalised material giving the higher value. Again, every material shows at least one instance of conversion increasing between cycles, possibly due to leaching of the enzyme into solution over the course of the reaction. As was the case with PFL, none of the conversions given by any material were as high as that given by free CRL, but the values were closer than they were with PFL-materials. A possible reason for the fluctuations in catalytic activity between cycles is possibly due to leaching of the enzyme into solution.

4.4 Bio-catalytic Application: Partial and Selective Hydrolysis of *Cis*-3,5-diacetoxy-1-cyclopentene to Synthesise Pharmaceutically Important Chiral Intermediates

The reaction was carried out according to the method outlined in Section 2.6.5. The amount of lipase-immobilised nanoparticles (variable amount, in mg) corresponding to 500 µg immobilised lipase was used in each case, except when free lipase was used as catalyst, 500 µg was used directly as catalyst. Initially, the reaction was carried out using THF as reaction solvent, but yielded no products (data not included). The reaction was put on hold, until work on the transesterification of ethyl butyrate was completed (Section 4.3). It was later decided to employ similar solvent conditions for this reaction, in order to activate the immobilised lipase and the free lipase in solution. The reaction was carried out using three separate conditions: 20% water/hexane solvent system at 25ºC, 20% water/hexane solvent system at 37ºC and 50% water/hexane solvent system at 25ºC. In this way it was possible to manipulate both water concentration and reaction temperature to gain the best results. 20% water in 1 mL of total reaction volume was used as a minimum concentration because small aliquots (1 µL) of the water layer were to be injected into the GC or GC-MS for analysis at various times, hence it was important that enough water should be available to inject for analysis. Due to the slight evaporation of low boiling organic solvent (hexane) during the reaction, it proved difficult to analyse the reaction conversion using the remaining reactants present in the hexane layer. The starting material *cis*-3,5-diacetoxy-1-cyclopentene is mostly soluble in hexane and sparingly soluble in water, whereas the products; (1S,4R)- and (1R,4S)-*cis*-4-acetoxy-2-cyclopenten-1-ol and *cis*-3,5-dihydroxy-1-cyclopentene were only soluble in water. Hence I have calculated conversion percentages based on the concentration of the reaction products in the water layer.

During initial experiments, it was found that when PFL was used as catalyst, a single peak is observed at the retention time (R_T) corresponding to (1S,4R)-*cis*-4-acetoxy-2-cyclopenten-1-ol along with *cis*-3,5-dihydroxy-1-cyclopentene and the reactant *cis*-3,5-diacetoxy-1-cyclopentene. Figure 4.10 presents a scanned GC-MS chromatogram of the reaction products after 48 hours using immobilised PFL as catalyst.

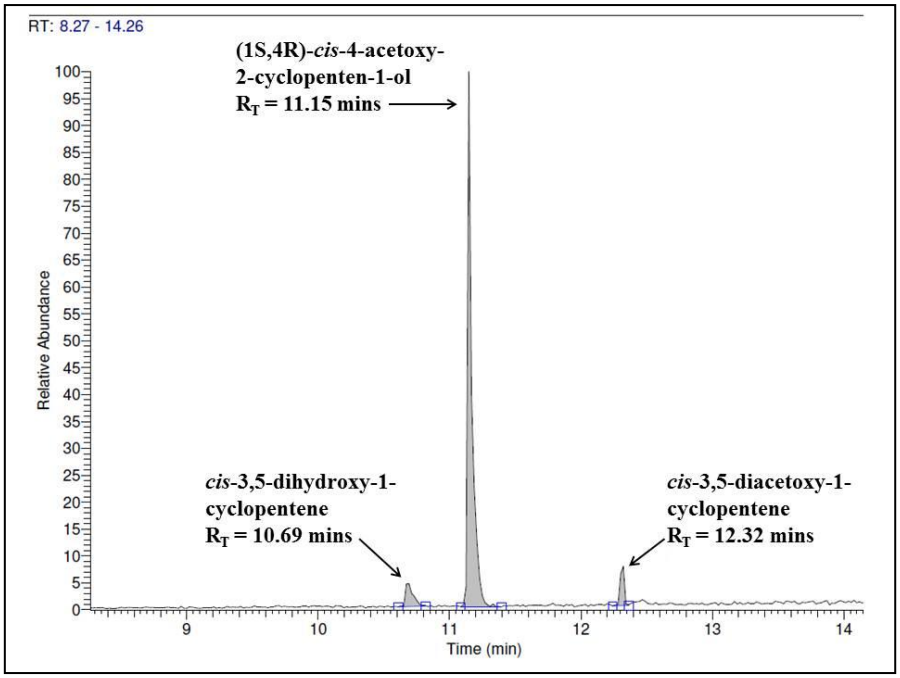

Figure 4.10: Scanned GC chromatogram of the reaction products after 48 hours using PFLITTQB as catalyst. Retention time is indicated by R_T.

However, when CRL was used as catalyst, two peaks were seen at the retention time corresponding to (1S,4R)-*cis*-4-acetoxy-2-cyclopenten-1-ol and (1R,4S)-*cis*-4-acetoxy-2-cyclopenten-1-ol and the reactant *cis*-3,5-diacetoxy-1-cyclopentene, shown in Figure 4.11 below.

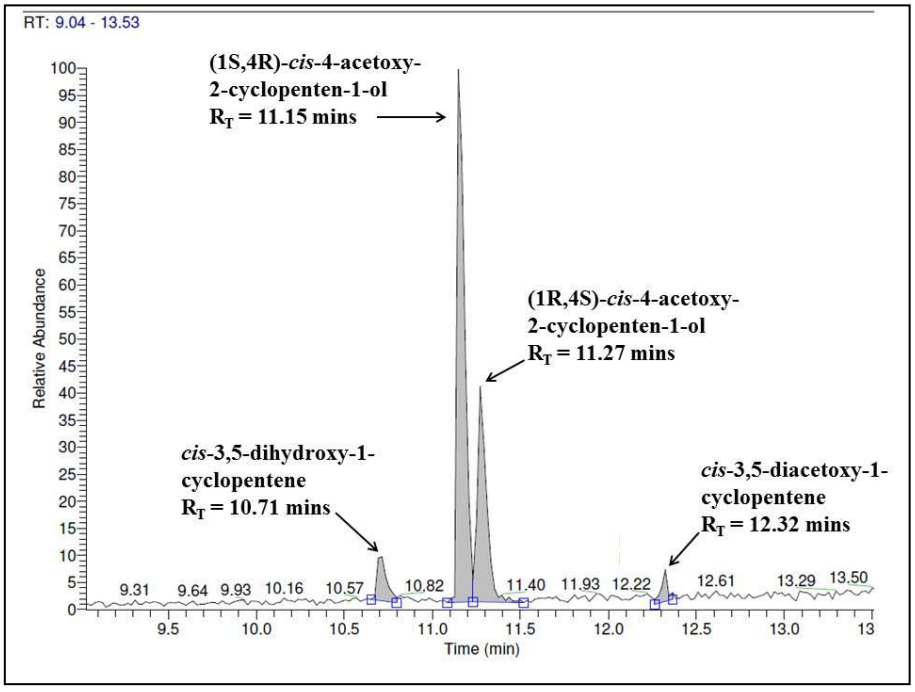

Figure 4.11: Scanned GC chromatogram of the reaction products after 48 hours using immobilised CRL as catalyst. Retention time is indicated by R_T.

Using GC-MS, the compound corresponding to the peak at 11.27 mins was found to have the same mass as (1S,4R)-*cis*-4-acetoxy-2-cyclopenten-1-ol. In order to confirm that the peak was the (1S,4R)-form, a small amount (~5 µmol) of pure (1S,4R)-*cis*-4-acetoxy-2-cyclopenten-1-ol (Sigma-Aldrich cat. No. 446041) was added to the mixture, it was observed that only the area of the peak at 11.15 mins (i.e. (1S,4R)-*cis*-4-acetoxy-2-cyclopenten-1-ol) was seen to increase. Similarly, when a small amount (~5 µmol) of pure (1R,4S)-*cis*-4-acetoxy-2-cyclopenten-1-ol (Sigma-Aldrich cat. No. 00848) was added to the mixture and it was observed that only the area of the peak at 11.27 mins (i.e. (1R,4S)-*cis*-4-acetoxy-2-cyclopenten-1-ol) was seen to increase. Hence, it was concluded from this and the GC-MS data, that the peak at 11.27 mins did correspond to (1R,4S)-*cis*-4-acetoxy-2-cyclopenten-1-ol. In later experiments, PFL materials were seen to produce the (1R,4S)- enantiomer in minute quantities (0-3% conversion). The enantioselective nature of PFL was expected, as *Pseudomonas* lipases are renowned for their enantioselectivity;[161] previously used for the synthesis of chiral intermediates in drug development.[130,465]

Following this discovery, it was now possible to calculate conversion to both the (1S,4R)- and (1R,4S)-forms of the product, as well as the dihydroxy by-product to provide total conversion values. As the enantiomers are of equal molecular weight and functionality, the same calibration curve can be used to calculate concentration for each.

A final point of interest is that acetic acid is formed as a by-product of the reaction following further hydrolysis of the hydrolysed acetoxy groups. With the increasing concentration of acetic acid in the reaction mixture, it is possible that this leads to the acid-catalysed hydrolysis of the newly formed mono-acetoxy products to the dihydroxy by-products. This process coupled with the further lipase-catalysed hydrolysis of the mono-acetoxy product could be an explanation for the increasing amount of undesired dihydroxy by-products present in the reaction mixture with time.

4.4.1 Results: Reaction Using 20% Water/Hexane Solvent System at 25ºC

Figure 4.12 shows the conversion of *cis*-3,5-diacetoxy-1-cyclopentene to the three products, as well as total conversion over 48 hours.

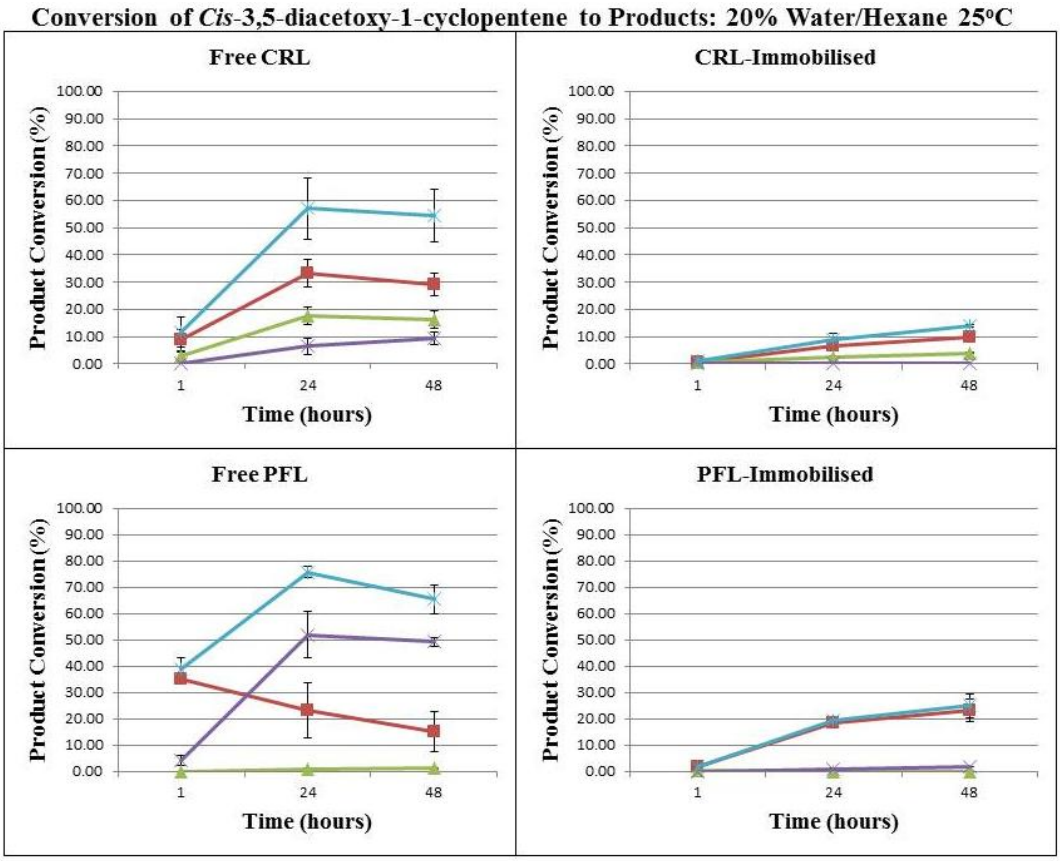

Figure 4.12: Results of the partial and selective hydrolysis of *cis*-3,5-diacetoxy-1-cyclopentene using 20% water/hexane at 25ºC for 48 hours. The red squares represent conversion to (1S,4R)-*cis*-4-acetoxy-2-cyclopenten-1-ol, green triangles represent conversion to (1R,4S)-*cis*-4-acetoxy-2-cyclopenten-1-ol, purple crosses represent conversion to *cis*-3,5-dihydroxy-1-cyclopentene and the blue crosses represent total conversion to products. Values are mean, ± S.E.M., n =2 in all cases.

From Figure 4.12 it can be seen that CRL materials are successful at producing both enantiomers of *cis*-4-acetoxy-2-cyclopenten-1-ol. Over all timeframes, free CRL provides a higher conversion than immobilised CRL. Maximum total conversion is seen at 24 hours (57%) for free CRL, plateauing after this. Immobilised CRL reaches the highest conversion (14%) after 48 hours. The products are obtained in approximately a 2:1 ratio of the (1S,4R)-enantiomer to the (1R,4S)-enantiomer, giving roughly 40% enantiomeric excess (*ee*) of (1S,4R)-*cis*-4-acetoxy-2-cyclopenten-1-ol. As the reaction continues over 24 hours, it can be seen that conversion of the mono-acetoxy products to the dihydroxy by-product occurs in small amounts (17% of total products for free CRL and 2% for immobilised CRL).

From Figure 4.12 it can also be seen that initial conversion (after 1 hour) for free PFL is much higher than immobilised PFL. Free PFL gives 39% total conversion and immobilised PFL gives 2%. For free PFL, maximum conversion to the desired product is seen after 24

hours, with overall conversion decreasing after 48 hours. The high maximum total conversion value (76%) is due to the increased conversion to the dihydroxy by-product, which becomes the most abundant product at 24 hours. The highest conversion to the desired (1S,4R)-enantiomer is highest at 1 hour (35%) and decreases steadily at 24 and 48 hours as a result of its further hydrolysis to the dihydroxy by-product. For immobilised PFL, conversion to the desired products increases steadily up to a maximum of 25% to 48 hours. Immobilised PFL offers the advantage of producing relatively small amounts of the dihydroxy by-product: 7% of total products compared to free PFL, which produces the dihydroxy by-product as 75% of the total products at 48 hours. For both free and immobilised PFL, the (1R,4S)- enantiomer is produced as less than 1% of total products in the reaction.

In terms of comparing CRL and PFL, free CRL offers higher conversion to the desired products and lower conversion to the dihydroxy by-product, at 24 and 48 hours. The highest conversion to the desired products (24 hours, (1R,4S) = 33%, (1S,4R) = 17%), is higher than that given by free PFL at any reaction time. CRL materials (both immobilised and free) produce the (1S,4R)-form in roughly 40% *ee* (around two (1S,4R) molecules to one (1R,4S) molecule). In contrast, PFL materials produce the (1S,4R)- enantiomer in 93-100% enantiomeric excess (*ee*) and free PFL achieves its maximum conversion to the desired products after just 1 hour [(1R,4S) = 35%)]. However, after this, it produces an increasing amount of the undesired dihydroxy by-product. For immobilised lipases, PFL and CRL provide similar initial conversion values after 1 hour, but PFL-immobilised nanoparticles exhibit higher maximum conversion, higher enantioselectivity and both materials give low amounts of the undesired dihydroxy by-product. Larger error bars observed in the case of free lipases could be due to issues such as dissolving the lipase in water prior to the reaction and also re-dispersing the lipases following centrifugation prior to removing aliquots of the water layer for analysis.

As applications for the (1S,4R)-form of the product are numerous,[298,466-468] compared with those of the (1R,4S)-form (only one could be found in the literature search[469]), the (1S,4R)-form is the desired reaction product and the (1R,4S)-form can be considered a by-product, hence enhancing the effectiveness of PFL over CRL for this application. Additionally, the reasonable activities of immobilised lipases coupled with their re-usability and removability from the reaction mixture makes them suitable candidates for catalysing the reaction.

4.4.2 Results: Reaction Using 20% Water/Hexane Solvent System at 37ºC

Figure 4.13 shows the conversion of *cis*-3,5-diacetoxy-1-cyclopentene to the three products, as well as total conversion over 48 hours, at 37ºC.

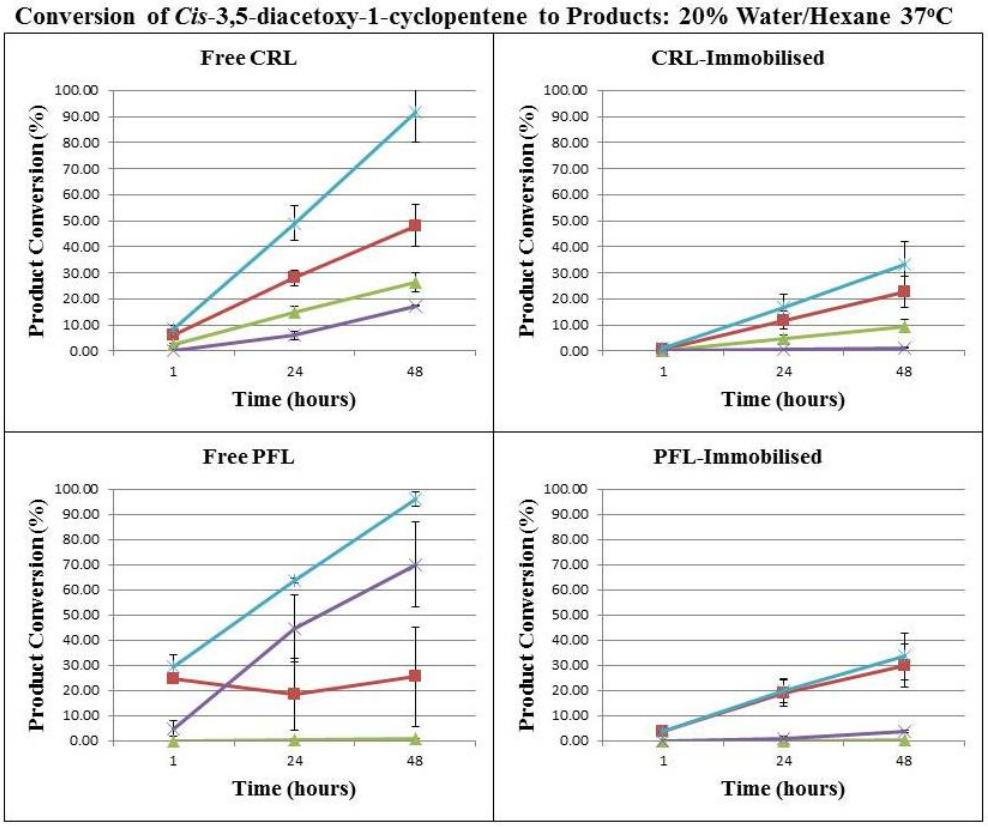

Figure 4.13: Results of the partial and selective hydrolysis of *cis*-3,5-diacetoxy-1-cyclopentene using 20% water/hexane at 37ºC for 48 hours. The red squares represent conversion to (1S,4R)-*cis*-4-acetoxy-2-cyclopenten-1-ol, green triangles represent conversion to (1R,4S)-*cis*-4-acetoxy-2-cyclopenten-1-ol, purple crosses represent conversion to *cis*-3,5-dihydroxy-1-cyclopentene and the blue crosses represent total conversion to products. Values are mean, ± S.E.M., n =2 in all cases.

CRL materials results and discussion: As previously seen in the reaction at 25ºC, CRL materials produce both enantiomers of *cis*-4-acetoxy-2-cyclopenten-1-ol, in roughly a 2:1 ratio of the (1S,4R)-enantiomer to the (1R,4S)-enantiomer, giving around 30-40% (*ee*). Again, over the entire reaction, free CRL provides a higher conversion than immobilised CRL. Maximum conversion is again seen at 48 hours in both cases (92% for free CRL and 33% for immobilised CRL). Compared to the reaction at 25ºC, free CRL exhibits similar activity after 1 hour (8%), as does immobilised CRL (1% in both cases). This is indicative of increased activity of the lipase at higher temperature. In terms of maximum conversion, much higher values are obtained at 37ºC (92% free CRL, 33% immobilised CRL) than 25ºC (57%

free CRL, 14% immobilised CRL). The dihydroxy by-product was formed in similar quantities to those obtained at 25ºC: 19% of the total conversion for free CRL and 4% for immobilised CRL. At 25ºC, the values were 17% and 2% respectively. It has been reported that free CRL has optimum activity at temperatures of 35-40ºC,[470-472] whilst it is somewhat higher for immobilised CRL (around 45-55ºC, depending on the support type and method of immobilisation)[471-473]. This can explain the increase in catalytic activity from 25ºC to 37ºC.

PFL materials results and discussion: Both free and immobilised PFL reached maximum conversion after 48 hours (96% for free PFL, 33% for immobilised PFL). As was the case at 25ºC, free PFL exhibits high initial conversion to the desired products, but also suffers from an increasing amount of undesired dihydroxy by-product over time, which eventually becomes the dominant product in the reaction mixture (73% of total products). The highest conversion to desired products for free PFL was after 1 hour (25% conversion, 84% of total products). Immobilised PFL affords more control over synthesis of the desired product, resulting in 33% total conversion with just 11% of total products being the dihydroxy by-product. Compared to 25ºC, immobilised PFL gives 8% higher total conversion and free PFL gives 22% higher maximum conversion, at 37ºC. Free PFL shows optimum activity in literature of around 30-40ºC,[474,475] increasing to 60-70ºC when immobilised.[240,474] This can again be used to explain the increase in catalytic activity when temperature is increased from 25ºC to 37ºC.

To compare results between CRL and PFL, free CRL and PFL offer similar maximum conversion values (92 and 97% respectively) at 48 hours. Both free and immobilised PFL produce the (1S,4R)- enantiomer in 94-100% *ee*, while both free and immobilised CRL produce the (1S,4R)- enantiomer in 30 and 40 % *ee*, respectively.

The conclusions to this part of the study are very similar to those where the reaction was carried out at 25ºC. PFL materials remain highly enantioselective (94-100% *ee*) and CRL materials produce the (1S,4R)-form 60-70% (roughly 30-40% *ee*). However, in this case (at 37ºC), conversions were much higher and over the entire 48 hour reaction, free PFL proved to be the most effective catalyst, giving an overall conversion of 97%. Free CRL gave 92% conversion after 48 hours and both free lipases gave high amounts of the undesired dihydroxy by-product. This could be due to increasing amounts of acetic acid in the system, as explained in the previous section. Increases in activity were seen in both immobilised lipases

coupled with low amounts of the dihydroxy by-product; immobilised PFL provided the highest conversion values.

It is possible that activity of the immobilised lipases is lower than free lipases because the optimum temperatures for immobilised lipases are slightly higher than those for free lipases (explained earlier in this section).

4.4.3 Results: Reaction Using 50% Water/Hexane Solvent System at 25ºC

Figure 4.14 shows the conversion of *cis*-3,5-diacetoxy-1-cyclopentene to the three products, as well as total conversion over 48 hours, at 25ºC.

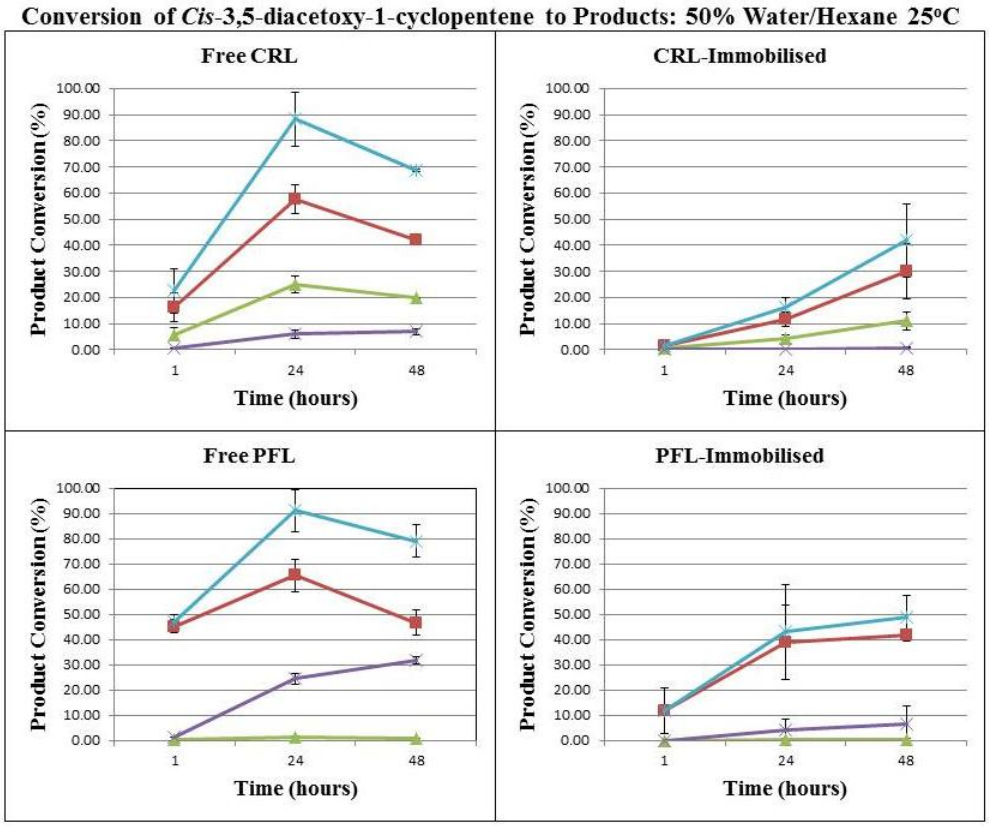

Figure 4.14: Results of the partial and selective hydrolysis of *cis*-3,5-diacetoxy-1-cyclopentene using 50% water/hexane at 25ºC for 48 hours. The red squares represent conversion to (1S,4R)-*cis*-4-acetoxy-2-cyclopenten-1-ol, green triangles represent conversion to (1R,4S)-*cis*-4-acetoxy-2-cyclopenten-1-ol, purple crosses represent conversion to *cis*-3,5-dihydroxy-1-cyclopentene and the blue crosses represent total conversion to products. Values are mean, ± S.E.M., n =2 in all cases.

CRL materials results and discussion: As was the case in the reactions employing 20% water/hexane solvent conditions, CRL materials produce both enantiomers of *cis*-4-acetoxy-2-cyclopenten-1-ol, in roughly a 2:1 ratio of the (1S,4R)-enantiomer to the (1R,4S)-enantiomer, giving roughly 40% *ee*. After 1 hour, total conversion is 22% for free CRL, 2

times higher than using 20% water/hexane at the same temperature. Immobilised CRL is similar to that obtained at 20% water/hexane (1-1.7%). The maximum conversion values are achieved at 24 hours for free CRL (88%), but immobilised CRL reaches its maximum (42%) at 48 hours. Total conversion for free CRL drops to 69% between 24 and 48 hours. In terms of production of the undesired dihydroxy by-product, both free and immobilised CRL produce less than 2% of total products. Maximum conversion for free CRL is much higher than at 20% water/hexane at the same temperature. For immobilised CRL, 50% water/hexane produces the highest maximum conversion (42%), compared to 20% water/hexane at 25ºC (14%) and 37ºC (33%).

PFL materials results and discussion: Free PFL reaches its maximum after 24 hours (91%) and decreases slightly thereafter to 79% after 48 hours. Immobilised PFL has reasonably high initial activity (11% total conversion after 1 hour) and increases to its maximum (48% total conversion) at 48 hours. After 48 hours, free PFL produces the dihydroxy by-product as 40% of the total products, whereas immobilised PFL produces it as 14%. The highest conversion to the desired products [(1S,4R)-*cis*-4-acetoxy-2-cyclopenten-1-ol and (1R,4S)-*cis*-4-acetoxy-2-cyclopenten-1-ol] was 24 hours (66%) for free PFL and 48 hours for immobilised PFL (42%). Hence, it could be beneficial to stop the reaction using free PFL after 24 hours to obtain the maximum amount of desired product with the minimum amount of undesired by-product. Again, PFL materials are more enantioselective in this reaction, producing the (1S,4R)-enantiomer in 97-98% *ee*.

Higher conversions given using 50% water/hexane compared to 20% water/hexane at 25ºC could be due to a higher interfacial area produced between the water and hexane and also due to the lipase being able to dissolve more easily.

4.4.4 Results: Testing the Re-usability of Lipase-Immobilised Nanoparticles Using 20% Water/Hexane Solvent System at 25ºC

CRL- and PFL-immobilised nanoparticles were used to assess their re-usability for the reaction using 20% water/hexane at 25ºC. The reaction was carried out as described in Section 2.6.5; a single aliquot was withdrawn from the water layer after 24 hours for analysis. The lipase-immobilised nanoparticles were then washed with 3×1 mL distilled/deionised water and the reaction was repeated for 4×24 hour cycles.

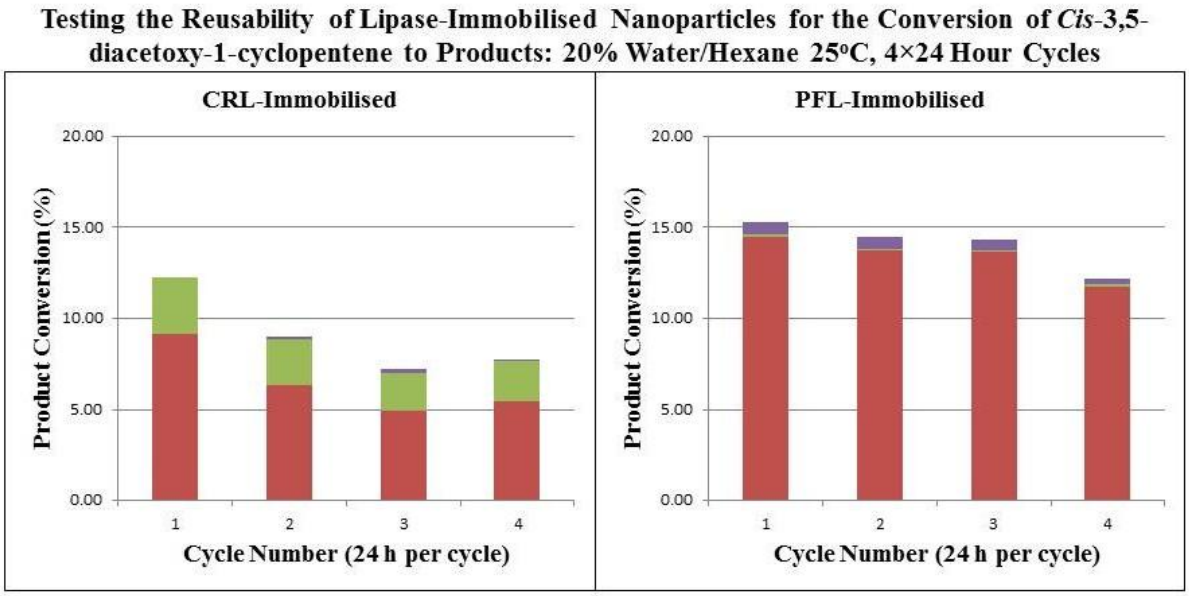

Figure 4.15: Testing the re-usability of lipase-immobilised nanoparticles for the partial and selective hydrolysis of *cis*-3,5-diacetoxy-1-cyclopentene using 20% water/hexane at 25ºC for 4×24 hour cycles. Red bars represent the conversion (1S,4R)-*cis*-4-acetoxy-2-cyclopenten-1-ol, green bars represent conversion to (1R,4S)-*cis*-4-acetoxy-2-cyclopenten-1-ol and purple bars represent conversion to *cis*-3,5-dihydroxy-1-cyclopentene.

Figure 4.15 shows that for both CRL- and PFL-immobilised materials, activity is highest in the first 24 hour cycle. CRL-immobilised materials give 12% conversion of *cis*-3,5-diacetoxy-1-cyclopentene to (1S,4R)- and (1R,4S)- *cis*-4-acetoxy-2-cyclopenten-1-ol in cycle 1, decreasing slightly to 9% in cycle 2, 7% in cycle 3 and 8% in cycle 4. The (1S,4R)-enantiomer is produced in 70-74% *ee*. Small amounts of the dihydroxy by-product are seen in cycles 2, 3 and 4 (less than 0.2%). It is possible that the first cycle exhibits higher total conversion than subsequent cycles as in cycles 2, 3 and 4 some of the active sites may become blocked, or some lipase can be washed away from the nanoparticle surface during either the reaction or washing steps between cycles. In total, CRL-immobilised materials retained 63% of their activity after 4 catalytic cycles of the reaction.

For PFL-immobilised materials, a similar trend is seen in that initial conversion is highest and subsequent cycles show slightly decreasing total conversion values. The (1S,4R)- enantiomer is produced in 98-99% *ee* and the dihydroxy by-product is produced as less than 0.7% of total products. The activity in cycles 1, 2 and 3 is almost equal (15, 14 and 14% respectively), suggesting that PFL-immobilised materials possibly do not suffer from leaching of the lipase into solution during the reaction or washing steps. Cycle 4 sees total conversion decrease to 12%, which is the same as the maximum total conversion achieved by CRL-immobilised

materials in cycle 1. PFL-immobilised materials retained 80% of the their activity after 4 catalytic cycles of the reaction.

Brief Conclusions

In terms of temperature, when 20% water/hexane was used as solvent, 37ºC provided higher conversion values than 25ºC for both free and immobilised lipases, as this is within the optimal activity temperature range for free lipases and closer to the optimal range for immobilised lipases, which is slightly higher on average.

For immobilised lipases, 50% water/hexane proved to be the most successful solvent system, giving highest activity values for both PFL and CRL. For free lipases, 20% water/hexane at 37ºC proved to be the most optimal conditions, as conversion increased to the maximum values obtained in the study at 48 hours for both PFL and CRL.

PFL was shown to be more enantioselective bio-catalyst, producing the desired (1S,4R)-enantiomer of the product in roughly 93-100% *ee*, but suffered from relatively high production of the undesired dihydroxy by-product due to further hydrolysis of the mono-acetoxy product (possibly due to production of acetic acid, leading to acid-catalysed hydrolysis of the mono-acetoxy product). At both temperatures and solvent conditions, CRL was shown to produce both enantiomers in roughly a 2:1 ratio [(1S:4R): (1R,4S)] and produced less of the dihydroxy by-product.

Free lipases provided much higher conversions than immobilised lipases, but immobilised lipases produced much higher ratios of the desired products to by-products; it can be said that immobilised lipases afforded more control over the formation of the desired products. In addition, free PFL reached its maximum conversion to desired products typically after 24 hours (48 hours at 37ºC); predominantly producing the dihydroxy by-product after this. Hence, it can be concluded that immobilised lipases gave reasonable conversion values with excellent control over the desired products, along with re-usability and easy separability from the reaction mixture.

In terms of re-usability, both CRL- and PFL-immobilised materials were shown to retain most of their activity over 4×24 hour cycles at 25ºC using 20% water/hexane as solvent. CRL-immobilised materials retained 63% and PFL-immobilised materials retained 80% of their activity over 4×24 hour cycles. It can be concluded that lipase-immobilised nanoparticles are suitable and re-usable catalysts for this application.

High amounts of the dihydroxy by-product obtained in the reactions can be explained by the reasonably high water concentrations used. The hydrolysis of the diacetoxy starting material to the desired mono-acetoxy product is catalysed by the lipase active site.[476] However, the hydrolysed acetoxy group remains bound to amino acid residues in the active site as an acyl-enzyme intermediate complex (see Scheme 4.1).

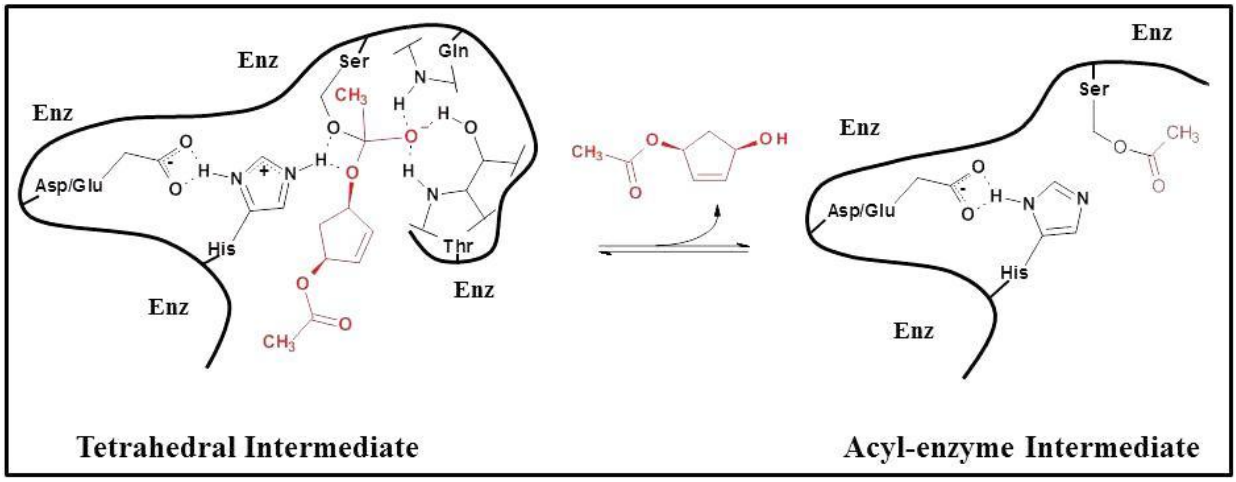

Scheme 4.1: Hydrolysis of *cis*-3,5-diacetoxy-cyclopentene to (1R,4S)-*cis*-4-acetoxy-2-cyclopenten-1-ol (as an example). Enz denotes the enzyme active site. The reactants and products are marked in red. Figure expanded and adapted from reference 476.

The *cis*-3,5-diacetoxy-cyclopentene forms a tetrahedral intermediate complex with the catalytic triad of the lipase active site (Asp/Glu-His-Ser) and the mono-acetoxy product is hydrolysed from the active site. The hydrolysed acetoxy group from the diacetoxy reactant remains bound to the serine residue in the active site as an acyl-enzyme intermediate complex. After the acyl-enzyme intermediate is formed, water hydrolyses the acetoxy group, forming acetic acid in the reaction mixture, which enables the acid-catalysed hydrolysis of the mono-acetoxy product to the dihydroxy by-product.

CHAPTER 5

BIO-SEPARATION AND BIO-SENSOR APPLICATIONS OF OLIGONUCELOTIDE-GRAFTED SILICA-COATED MAGNETITE NANOPARTICLES

5.1 Introduction

The following section will present the bio-separation and bio-sensor applications that have been explored as part of the project. The first section involved the bio-separation application of silica-coated core-shell nanoparticles (QBLSSM). The nanoparticles were used to extract DNA (*via* non-specific physical adsorption) from real food samples and the extraction efficiency was compared with a classical thermal lysis extraction technique. The silica-coated nanoparticles were subsequently employed by Q-Bioanalytic GmbH as part of their commercial DNA Extraction Kit.

The second section focussed on *Listeria Monocytogenes* (LM) and the use of a previously-established model hybrid capture assay.[80,89] The assay employed in this project utilised LM-specific amine-modified oligonucleotides (primers) grafted onto surface-functionalised silica-coated magnetite nanoparticles using glutaraldehyde as a coupling reagent. The oligonucleotide-grafted nanoparticles were used to capture LM-specific complementary oligonucleotides from a buffer solution (bio-separation), which were then dehybridised at high temperature. The capture and dehybridisation of the complementary sequence was followed using UV-Visible spectrophotometry, measuring absorbance at 260 nm (bio-sensing). Following optimisation of the hybrid capture assay to produce the best results, the oligonucleotide-grafted nanoparticles were then used at Q-Bioanalytic, Germany, for the specific detection of LM in real food samples and then finally to explore the sensitivity of detection of LM.

The third section of this application focussed on *Escherichia Coli* (EC) and again the initial use of a hybrid capture assay. EC-specific primers were grafted in the same way as the LM-specific amine-modified primers onto the functionalised nanoparticles. The EC-grafted materials were then used in the previously optimised hybrid capture assay conditions and complementary sequence capture and dehybridisation was monitored using UV-Visible spectrophotometry, measuring absorbance at 260 nm. Again, samples were used at Q-Bioanalytic, Germany for the specific detection of EC in food samples, to explore the sensitivity of detection of EC and were also used in collaboration with Fudan University, China, for the detection of EC in wastewater samples.

Table 5.1 below presents the materials used in this part of the project and the applications they were used for.

Table 5.1: Materials used in bio-separation and bio-sensor applications.

Name	Details	Bacteria Detected	Application			
			DNA Extraction	Hybrid Capture Assay	Specific Detection from a Mixture	Sensitivity of Detection Limits
TTQB-C_6-$T1NH_2$	TTQB with oligonucleotide sequence C_6-$T1NH_2$ covalently attached to the surface*	LM	N/A	√	√	√
TTQB-C_{12}-$T1NH_2$	TTQB with oligonucleotide sequence C_{12}-$T1NH_2$ covalently attached to the surface*	LM	N/A	√	√	√
TTQB-C_6-$T2NH_2$	TTQB with oligonucleotide sequence C_6-$T2NH_2$ covalently attached to the surface*	LM	N/A	√	√	√
TTQB-C_{12}-$T2NH_2$	TTQB with oligonucleotide sequence C_{12}-$T2NH_2$ covalently attached to the surface*	LM	N/A	√	√	√
TTQB-EC_541_FOR	TTQB with oligonucleotide sequence EC_541_FOR covalently attached to the surface**	EC	N/A	√	√	√
TTQB-EC_637_REV	TTQB with oligonucleotide sequence EC_637_REV covalently attached to the surface**	EC	N/A	√	√	√
QBLSSM	Large-scale silica-coated core-shell magnetite nanoparticles	N/A	√	N/A	N/A	N/A

*See Table 2.1, Section 2.1 for LM-specific oligonucleotide sequences.

**See Table 2.2, Section 2.1 for EC-specific oligonucleotide sequences.

5.2 Bio-separation Application: DNA Extraction Using Silica-Coated Core-Shell Nanoparticles

DNA extraction was carried out according to the method in Section 2.7.5. DNA concentration was calculated using a NanoDrop 2000 UV-Visible spectrophotometer (Thermo Scientific, Germany).

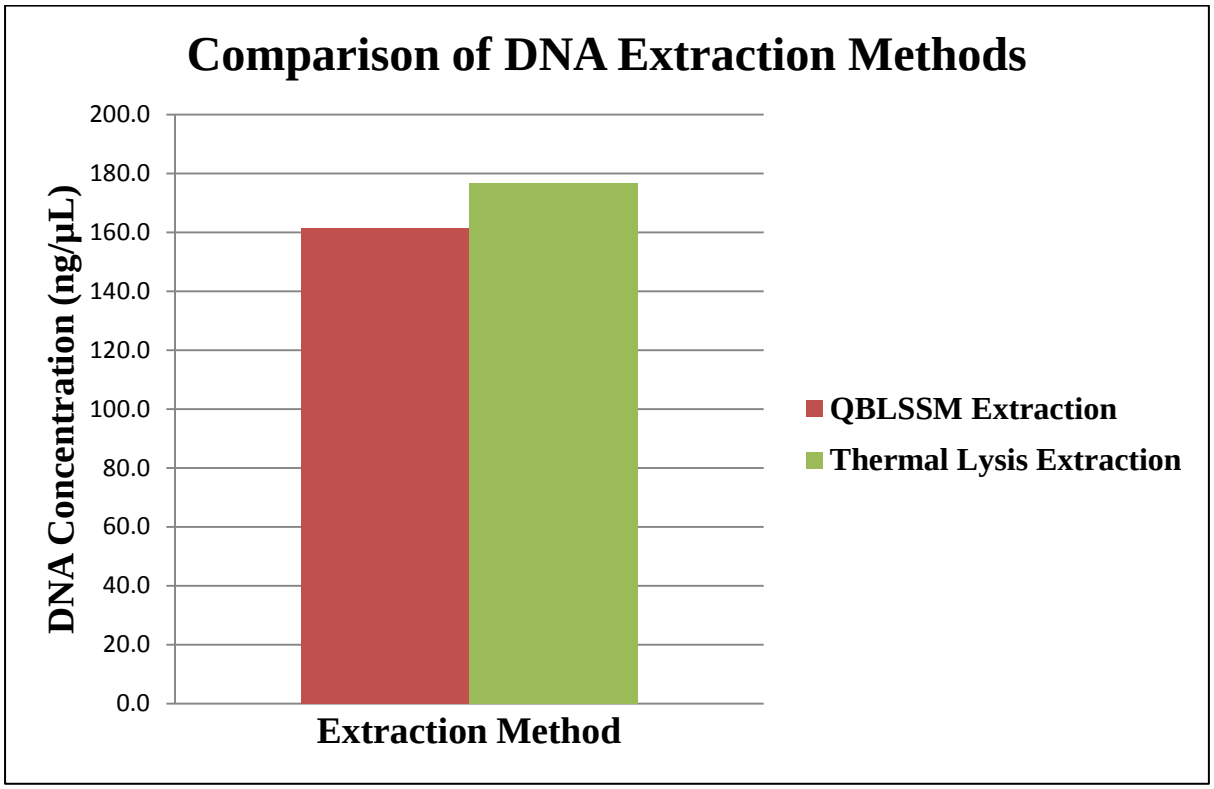

Figure 5.1: Comparison of total DNA extracted from a real food sample using silica-coated core-shell nanoparticles (QBLSSM) and a classical thermal lysis method. Values are mean, ± S.E.M., n = 6 in all cases.

Figure 5.1 shows that silica-coated core-shell nanoparticles (QBLSSM) provide similar values of total DNA extracted compared to the thermal lysis method. As the thermal lysis method uses high temperature to lyse the nucleic acids from the matrix, it can be considered that thermal lysis extracts 100% of total nucleic acids present. Hence, in this experiment, QBLSSM was shown to extract around 91% of total DNA from the matrix. However, nucleic acids extracted using thermal lysis may be contaminated with PCR-inhibiting species. Prior to extraction using the nanoparticles, the sample is enzymatically pre-digested in Proteinase K and lysis buffer to lyse the nucleic acids from the sample. The nanoparticles are then introduced to extract the DNA in the presence of a binding buffer. The bound DNA is purified by washing with aqueous ethanol (70% v/v) and eluted in distilled / deionised water. The purified DNA can then be used directly for qPCR. Small error bars demonstrate the

reliability of the materials for the application. The silica-coated nanoparticles (QBLSSM) were subsequently employed by Q-Bioanalytic GmbH as part of their commercial DNA Extraction Kit.

5.3 Bio-separation and Bio-sensing Applications of Nanoparticles Grafted with *Listeria Monocytogenes*-Specific Primers

5.3.1 Coupling of 5′-amine-modified oligonucleotides to Nanoparticles

5′-amine-modified LM-specific oligonucleotides (primers) (see Table 2.1, Section 2.1) were grafted (or coupled) onto the glutaraldehyde-modified nanoparticle surface according to the method in Section 2.7. Figure 5.2 and Figure 5.3 below present the average coupling data of forward ($T1NH_2$) and reverse ($T2NH_2$) primers (with different spacers: C_6 and C_{12}) on functionalised nanoparticles.

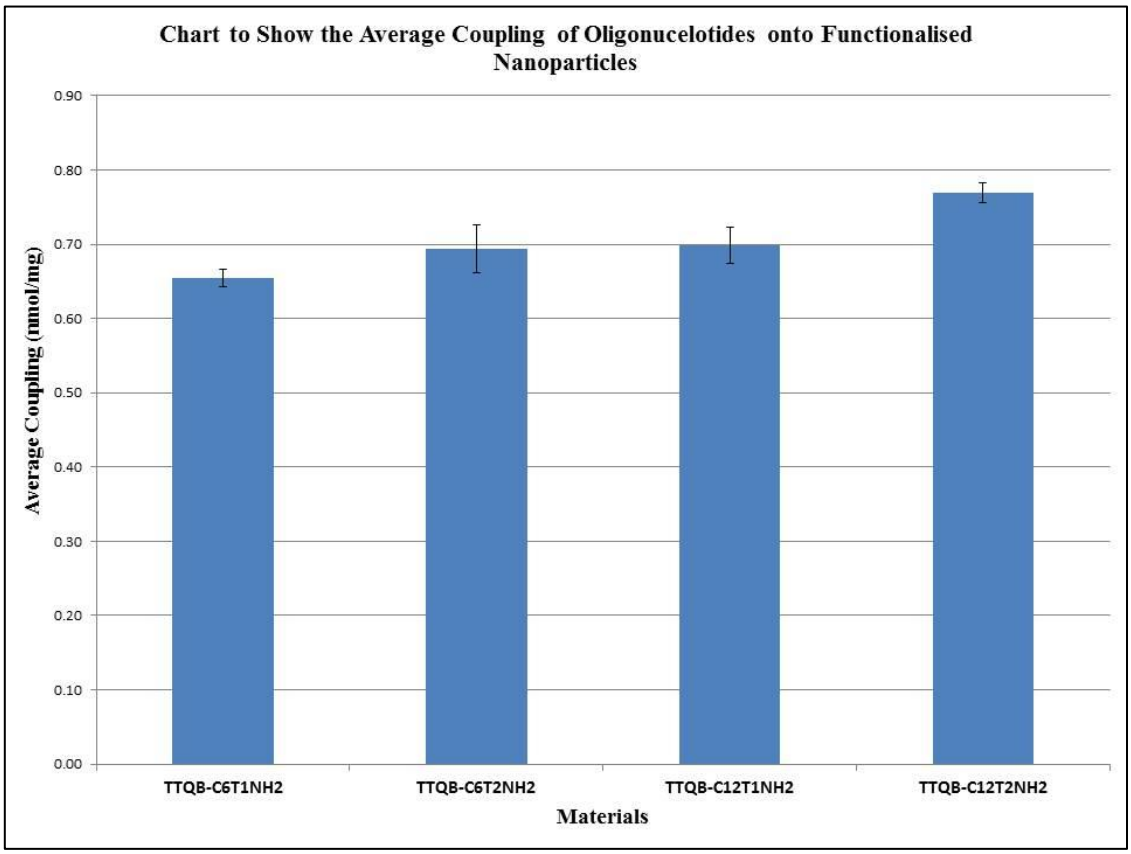

Figure 5.2: Average coupling values of LM-specific oligonucleotides to surface-functionalised nanoparticles, in nmol of oligonucleotide coupled per mg of nanoparticles. Values are mean, ± S.E.M., n ≥6 in all cases.

Figure 5.2 shows that primers functionalised with a C_{12}-spacer have a higher coupling (*via* chemical conjugation between surface –CHO groups with 5′-NH_2 groups of oligonucleotide primers) than those functionalised with the C_6-spacer. However, it can be seen from Figure 5.3 that there is no major difference in the percentage of oligonucleotide coupled. However, coupling efficiency in all cases is high, ranging from 78-85%.

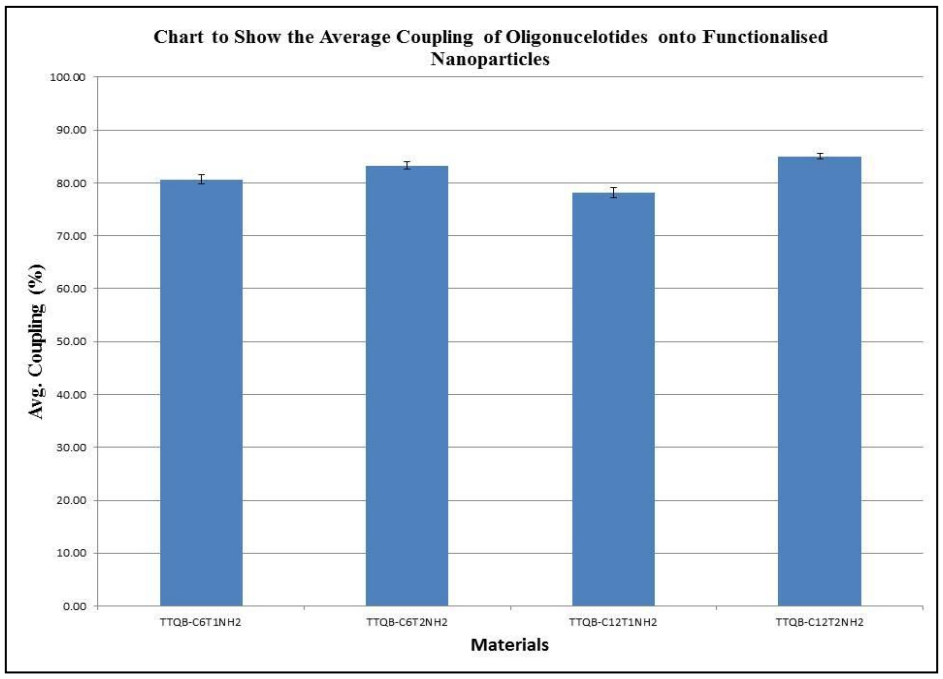

Figure 5.3: Average amount of LM-specific oligonucleotide coupled to surface-functionalised nanoparticles, as a percentage of initial oligonucleotide concentration. Values are mean, ± S.E.M., n ≥6 in all cases.

The initial amount of oligonucleotide used for coupling was supposed to 1.65 nmol, however, fresh solutions were made up prior to each batch and the concentration calculated using UV-Vis spectrophotometry (see Section 2.9.4), hence a small deviation in initial oligonucleotide concentration has been observed. As a result of the high coupling efficiency, this method was used on every batch of new primer-grafted nanoparticles that were made for either hybrid capture testing (model assay) or real-world applications (microbial detection in food at Q-Bioanalytic GmbH, Germany).

5.3.2 Hybrid Capture Assay

The hybrid capture assay was used to capture complementary oligonucleotides from a solution in the same way as PCR. The hybrid capture assay consisted of three key stages that are similar to those used in PCR. The first was the stretching phase (used to denature double-stranded DNA to produce single-stranded DNA in PCR), where the sample was placed at

high temperatures to ensure that the primers were not bound to each other or forming secondary structures (such as primer-dimers or hairpins). The second stage was the capture/hybridisation (known as annealing in PCR), performed at lower temperatures than the stretching/denaturation phase (a few degrees lower than the melting point of the primers), where the grafted-oligonucleotides hybridised to the complementary oligonucleotides in solution. The amount of oligonucleotide captured was determined by measuring the absorbance at 260 nm of the initial solution and the solution after hybridisation. In order to reduce the non-specific binding of both complementary primers and other species in the solution to surface aldehyde groups (which would be a problem in the specific capture of DNA from a mixture), BSA was used as a blocking agent; acting as a competitor by blocking the surface-modified aldehyde groups.[80] The captured complementary sequence (now in duplex form with the grafted oligonucleotide) was then washed with buffer solution to remove the BSA and weakly bound non-specific species. The third and final stage of the hybrid capture assay was the dehybridisation step, performed again at high temperature to denature the double-stranded oligonucleotides formed *via* the hybridisation of the complementary sequence. The amount of oligonucleotide dehybridised was again calculated by measuring the absorbance at 260 nm. The amount of oligonucleotide dehybridised was also used to calculate the hybrid capture efficiency of the material, as the oligonucleotide that was dehybridised was assumed to have been captured specifically. Glutaraldehyde-modified materials without grafted-oligonucleotides were used to calculate the non-specific capture of complementary oligonucleotides.

5.3.3 Initial Conditions

The reaction was carried out according to the method outlined in Section 2.7.3. Figure 5.4 presents the results of the using just TTQB-C_6-T1NH_2. Capture was found to be high at around 55%, but dehybridisation was shown to be low, with only 27% of the hybridised oligonucleotides being dehybridised.

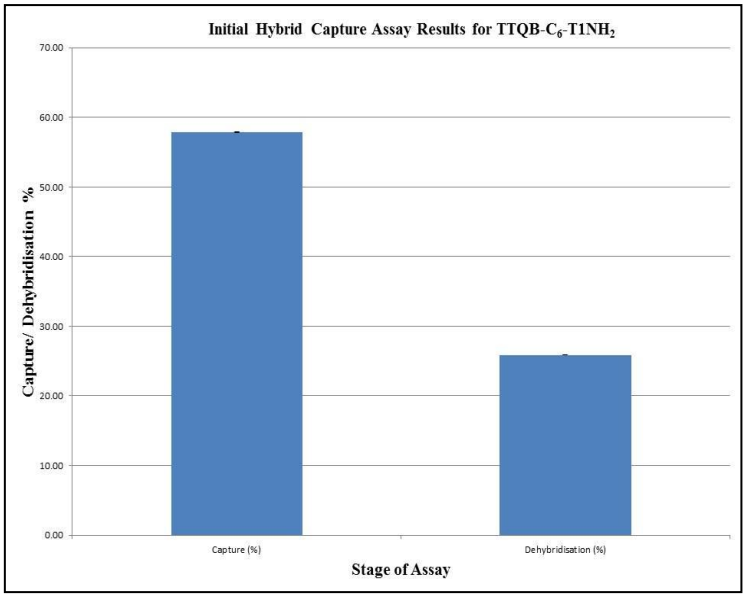

Figure 5.4: Initial hybrid capture assay using just TTQB-C_6-T1NH_2 and identical conditions to Bruce and Sen[80]. Values are mean, ± S.E.M, n =2.

As 1.65 nmol was the maximum amount of 5′-NH_2 oligonucleotides which could have been coupled (conjugated) to the glutaraldehyde-modified nanoparticles in the grafting step, capture (%) has been calculated as a percentage of the total complementary oligonucleotides available for capture in the solution (1.65 nmol).

Due to the low dehybridisation values, I decided to repeat the dehybridisation stage a number of times to determine if more of the hybridised primer and non-specifically physically adsorbed primers could be dehybridised in this way. Figure 5.5 below presents the results of a further 5 consecutive repeats of the dehybridisation step.

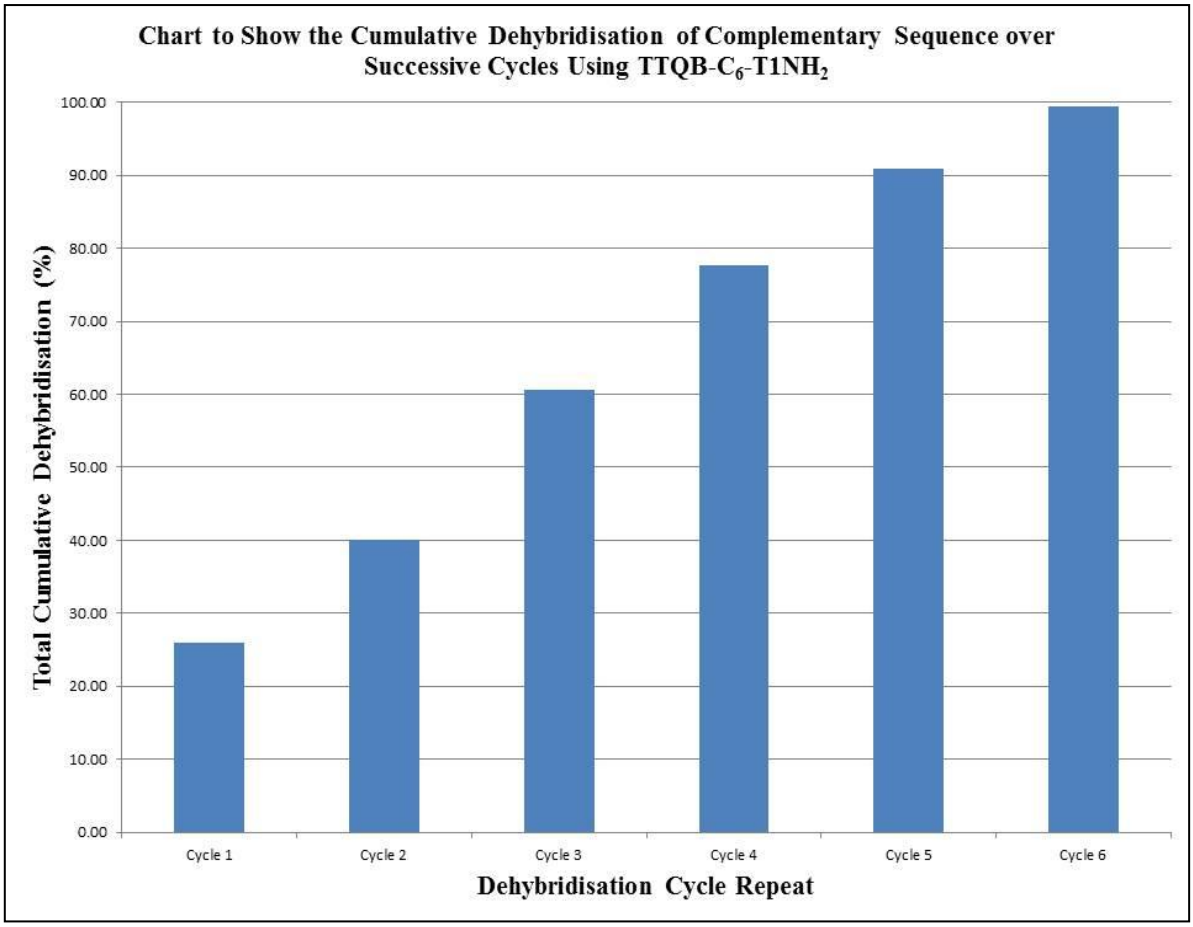

Figure 5.5: Overall dehybridisation of the complementary oligonucleotide sequence captured by TTQB-C_6-T1NH_2 using successive cycles of heating at 85ºC for 4 minutes in water.

From Figure 5.5 it can be seen that it took 6×4 minute dehybridisation cycles at 85ºC to remove almost 100% of the hybridised complementary oligonucleotide. Following on from this, it could therefore be concluded that the assay was not currently optimised for the materials and primers being used in this study. The following conditions have later been adopted based on the suggestion of Q-Bioanalytic GmbH, Germany as a part of PCR analysis: stretching/denaturation at 95ºC for 5 minutes with stirring, capture/hybridisation at 60ºC for 5 minutes with stirring and dehybridisation at 95ºC for 5 minutes with stirring. Due to unavailability of a thermomixer at UCLan to stir the samples whilst maintaining a high temperature, I have decided to increase the stretching and dehybridisation steps to 10 minutes each, including a 10 second vortex step halfway through each phase. The capture/hybridisation at 60ºC has been carried out using a rotator within an incubator (maximum temperature 70ºC).

5.3.4 Optimised Conditions

The hybrid capture assay was carried out from this point forward using the new conditions as described above (see details in Section 2.7.4). The first set of results is the capture of complementary oligonucleotides from solution, representing the second stage of the hybrid capture assay (following initial stretching).

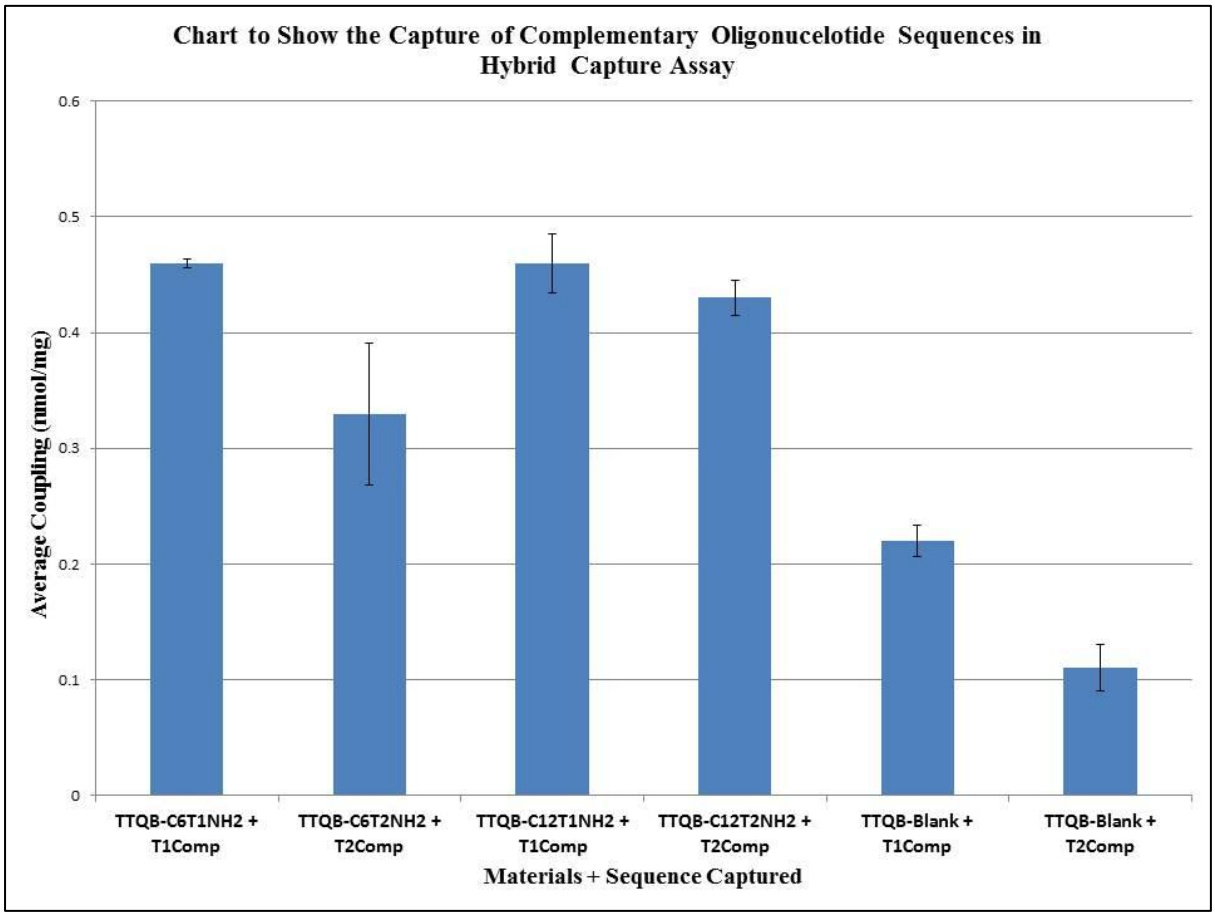

Figure 5.6: Capture of complementary oligonucleotide sequences from solution during the hybrid capture assay, in terms of nmol oligonucleotide captured per mg of LM-specific oligonucleotide-grafted nanoparticles. Values are mean, ± S.E.M, n =3.

Figure 5.6 shows the amount of complementary oligonucleotides captured in nmol mg^{-1} of oligonucleotide-grafted nanoparticles. Materials TTQB-Blank + T1Comp and TTQB-Blank + T2Comp represent the non-specific capture of glutaraldehyde-modified nanoparticles in the assay. As can be seen, there is no significant difference between materials possessing the C_{12}-spacer or the C_6-spacer. The values for all oligonucleotide-grafted nanoparticles are quite close, between 0.43 – 0.46 nmol mg^{-1}, except for the material TTQB-C_6T2NH_2, which has a low capture value of 0.33 nmol mg^{-1}. The non-specific capture of the blank materials is 0.22

nmol mg^{-1} for T1Comp and 0.11 nmol mg^{-1} for T2Comp. Table 5.2 shows the capture as a percentage of the covalently coupled oligonucleotide concentration.

Table 5.2: Capture of complementary oligonucleotides from solution as a percentage of the covalently coupled LM-specific oligonucleotide concentration (see Table 5.1, Section 5.1 for material names).

Oligonucleotide-Grafted Material	Complementary Oligonucleotide Captured	Capture (nmol mg^{-1})	Capture % (in terms of nmol captured per nmol coupled)	Specific Capture (%)
TTQB-C_6T1NH_2	T1Comp	0.46	70.29	52.17
TTQB-C_6T2NH_2	T2Comp	0.33	47.57	33.33
TTQB-C_{12}T1NH_2	T1Comp	0.46	65.90	52.17
TTQB-C_{12}T2NH_2	T2Comp	0.43	55.93	48.84
TTQB-Blank-F	T1Comp	0.22	12.47	0
TTQB-Blank-R	T2Comp	0.11	7.29	0

Note: Specific capture (%) is calculated from the difference between capture (%) using oligonucleotide-grafted materials and capture (%) using glutaraldehyde-modified materials without grafted-oligonucleotides. TTQB-Blank-F is the blank glutaraldehyde-modified material used to capture the forward complementary oligonucleotide and TTQB-Blank-R is the blank glutaraldehyde-modified material used to capture the reverse complementary oligonucleotide.

In terms of percentages, oligonucleotide-grafted nanoparticles were shown to capture between 47% and 70% of complementary oligonucleotides from the solution. The glutaraldehyde-functionalised materials gave non-specific capture values of 12% and 7% for T1Comp and T2Comp respectively. This was calculated as a percentage of total oligonucleotides available for capture in the solution. The reasonably high non-specific capture values may be because the BSA was not used at quite a high enough concentration to block all of the surface aldehyde groups in the blank materials and is something that could be evaluated in future experiments. From these values, it can be deduced that all of the nanoparticles grafted with oligonucleotides captured around 33-52% specifically by the hybridisation mechanism. The spacer group used did not exhibit any effect on the capture efficiency. The final stage of the hybrid capture assay was the dehybridisation step, where the complementary oligonucleotide that was captured in the previous step is removed at high temperature.

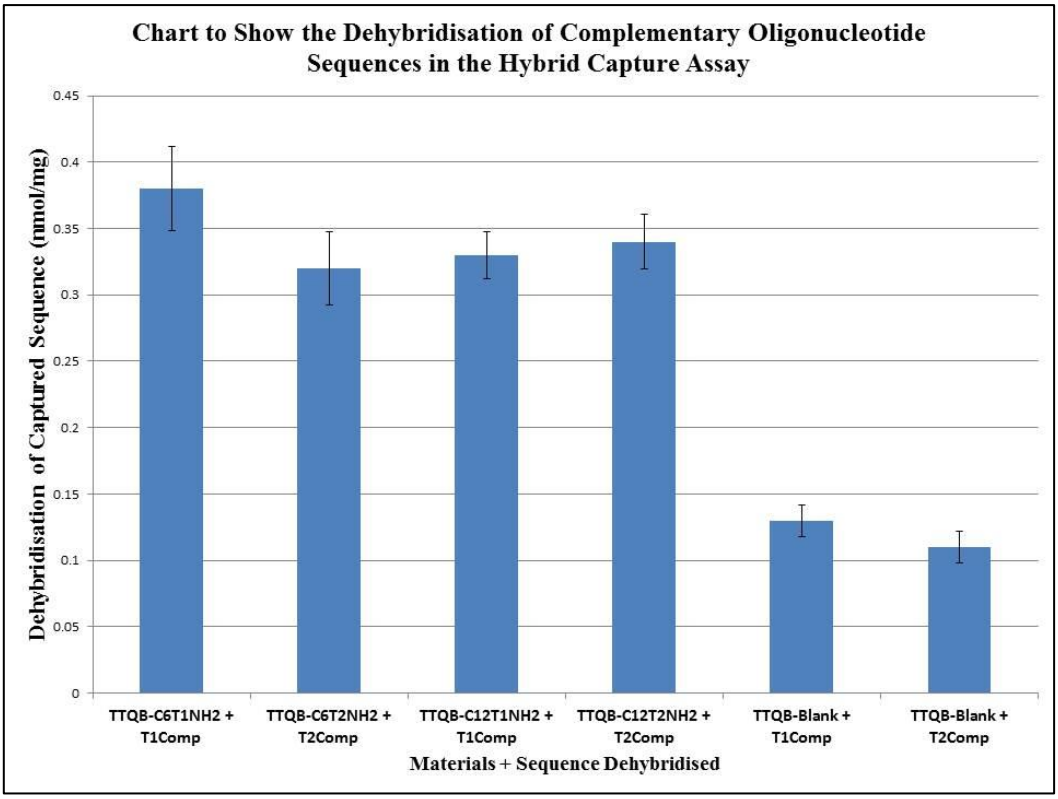

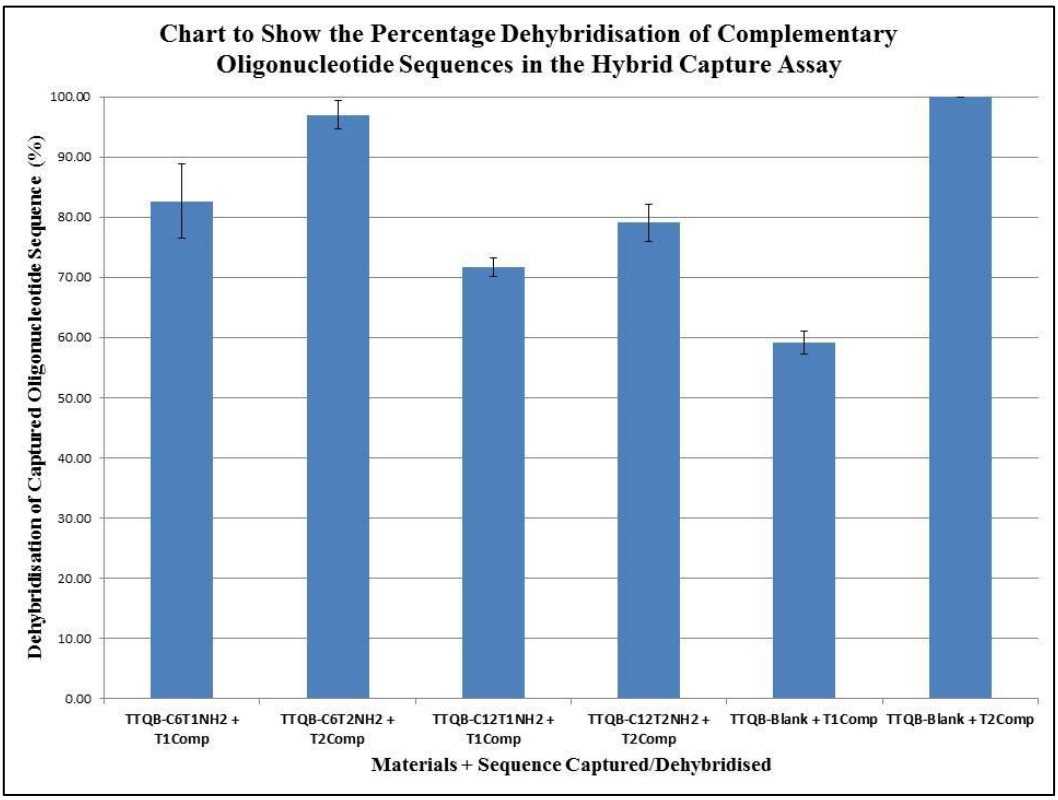

Figure 5.7: Total dehybridisation of captured oligonucleotides (in nmol) per mg of LM-specific oligonucleotide-grafted nanoparticles (top) and the dehybridisation as a percentage of total captured oligonucleotides (bottom). Values are mean, ± S.E.M, n =3.

In terms of total dehybridisation, it can be seen from Figure 5.7 that dehybridisation of both specifically- and non-specifically-captured oligonucleotides is high: oligonucleotide-grafted nanoparticles dehybridised 72-97% of captured oligonucleotides and glutaraldehyde-modified materials without grafted-oligonucleotides dehybridised 59-100% of physically adsorbed (non-specifically captured) oligonucleotides. Oligonucleotide-grafted materials possessing the C_6-spacer show higher dehybridisation of captured oligonucleotides. Figure 5.8 presents a summary of the hybrid capture assay data.

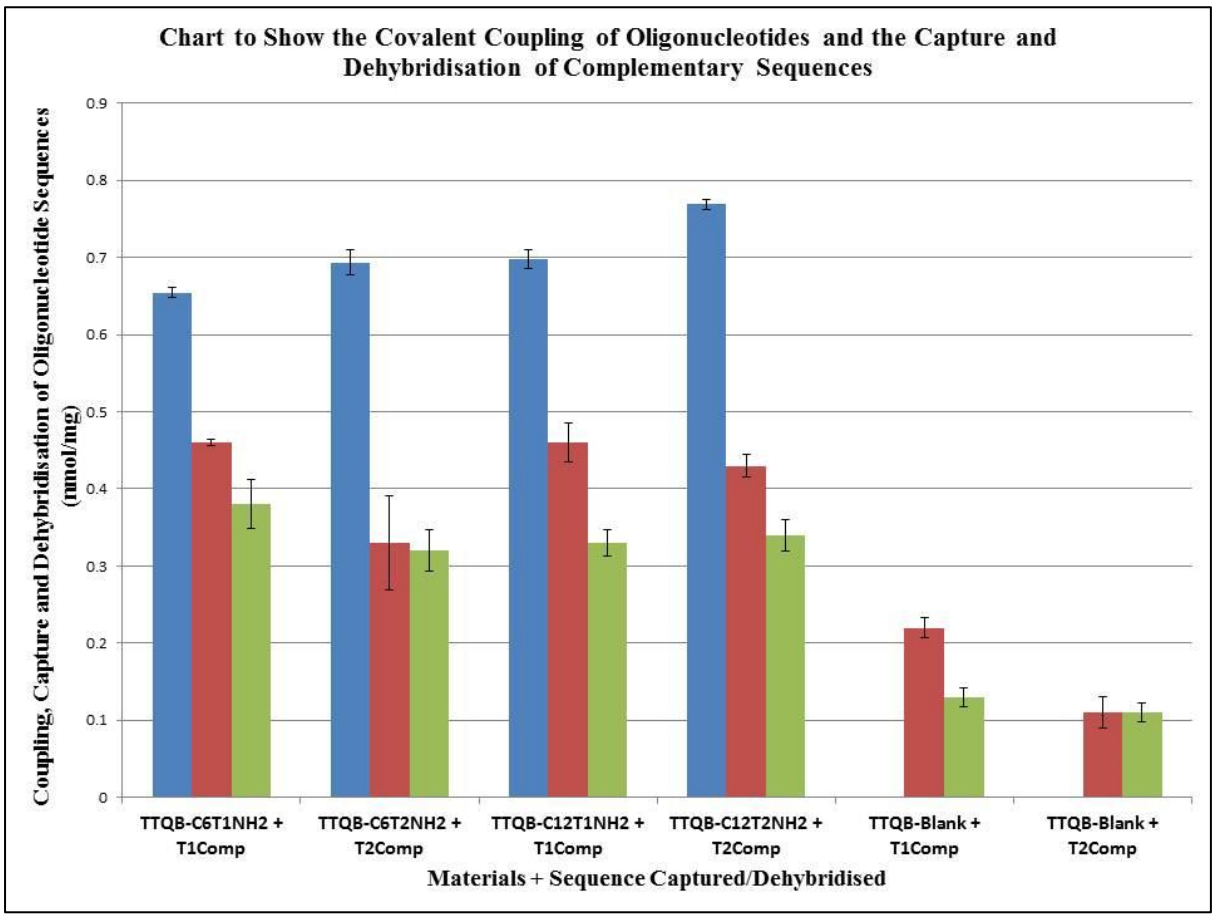

Figure 5.8: Summary of the materials used in the *Listeria Monocytogenes* hybrid capture assay and the complementary oligonucleotides they have captured and dehybridised. The blue bars represent the initial LM-specific oligonucleotide present on the nanoparticles after the glutaraldehyde coupling reaction, the red bars represent the total amount of complementary oligonucleotides captured/physically adsorbed during the hybridisation step and the green bars represent the total amount of captured oligonucleotides dehybridised (specific capture by hybrid capture mechanism). Values are mean, ± S.E.M, n =3.

In conclusion, it can be seen from the above results of the hybrid capture assay that all materials exhibit high coupling values, typically over 80% of the initial oligonucleotide concentration present in the solution during the coupling reaction. Oligonucleotide-grafted nanoparticles exhibit both specific and non-specific capture of complementary

oligonucleotide sequences from solution. Dehybridisation is shown to be high for both specifically captured (72-97%) and non-specifically adsorbed (59-100%) oligonucleotides.

5.4 Bio-separation and Bio-sensing Applications of Nanoparticles Grafted with *Escherichia Coli* -Specific Primers

5.4.1 Coupling of 5′-amine-modified oligonucleotides to Nanoparticles

5′-Amine-modified EC-specific oligonucleotides (primers) (see Table 2.2, Section 2.1) were grafted (or coupled) onto the glutaraldehyde-modified nanoparticle surface according to the method in Section 2.7.2. Figure 5.9 below presents the average coupling data of forward (EC_541_FOR) and reverse (EC_637_REV) primers with C_6-spacers on functionalised nanoparticles.

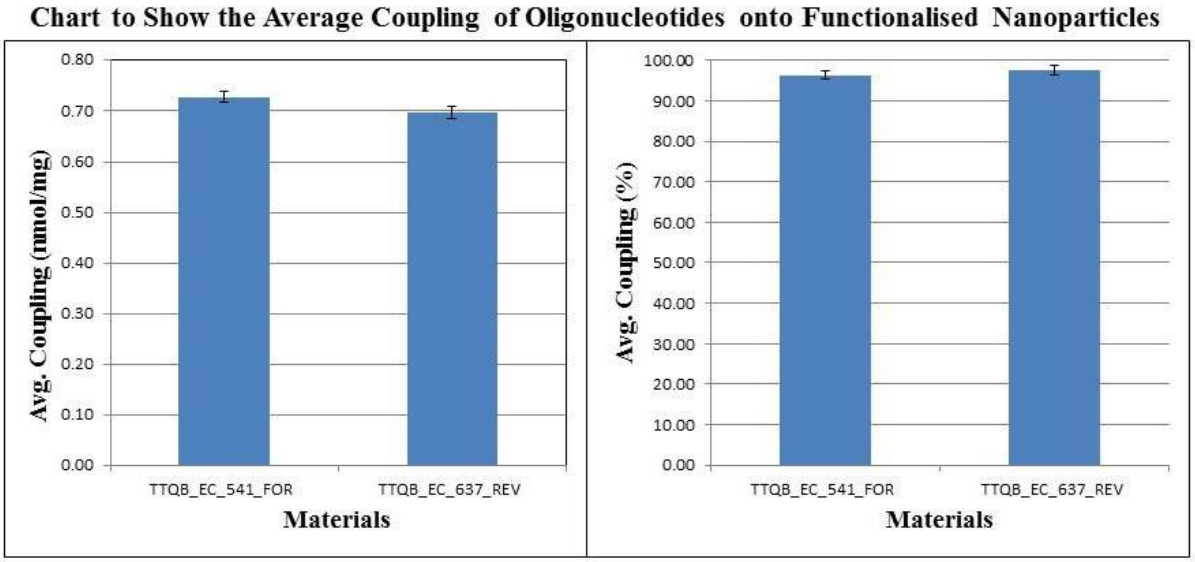

Figure 5.9: Average coupling values of EC-specific oligonucleotides to surface-functionalised nanoparticles, in nmol of oligonucleotide coupled per mg of nanoparticles (left) and the average amount of oligonucleotide coupled to surface-functionalised nanoparticles, as a percentage of initial oligonucleotide concentration (right). Values are mean, ± S.E.M., n=3 in all cases.

Figure 5.9 shows that coupling is very high for both forward (EC_541_FOR) and reverse (EC_637_REV) primers, over 96% and 97% respectively. Hence, it can be concluded that glutaraldehyde-modified surface-functionalised materials are very efficient for the grafting of these particular EC-specific primers. Due to the high coupling efficiency, these materials were then used for the hybrid capture assay, using the same optimised conditions from the LM hybrid capture assay in Section 2.7.4.

5.4.2 Hybrid Capture Assay

The conditions for the hybrid capture assay were kept the same as those used for the LM-specific hybrid capture assay.

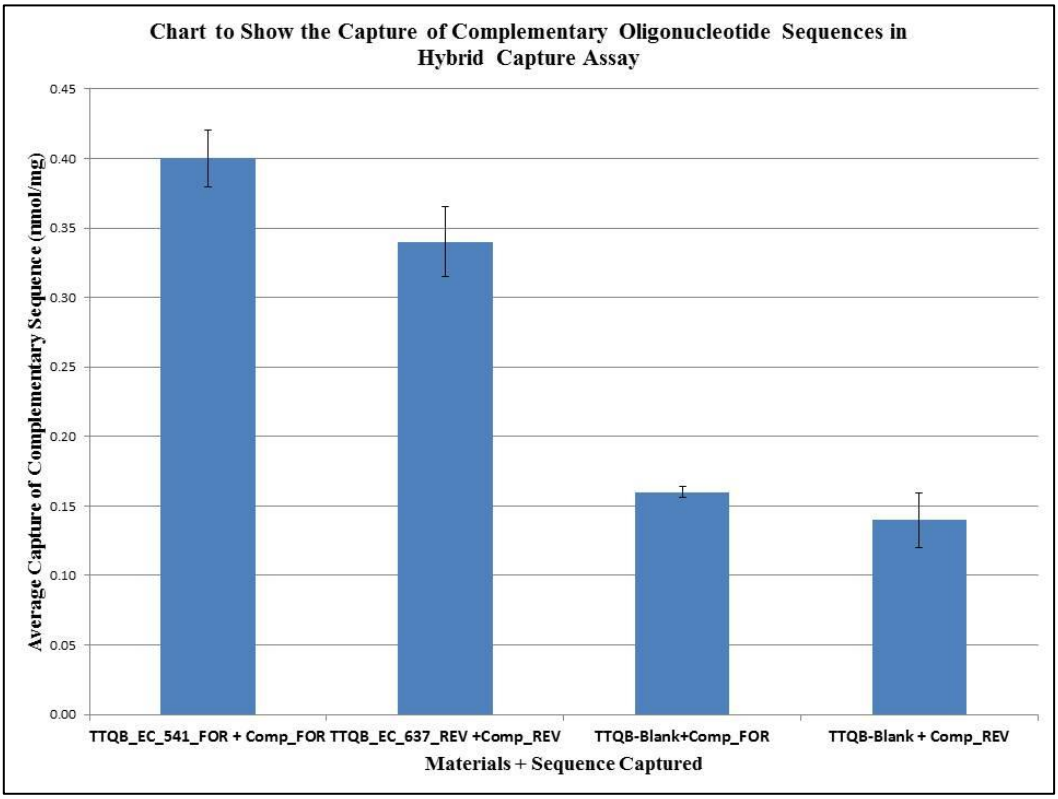

Figure 5.10: Capture of complementary EC-specific oligonucleotide sequences from solution during the hybrid capture assay, in terms of nmol oligonucleotide captured per mg of oligonucleotide-grafted nanoparticles. Values are mean, ± S.E.M, n =3.

Figure 5.10 shows the amount of complementary oligonucleotides captured in nmol mg^{-1} of oligonucleotide-grafted nanoparticles. Materials TTQB-Blank + Comp_FOR and TTQB-Blank + Comp_Rev represent the non-specific capture of glutaraldehyde-modified nanoparticles in the assay. It can be seen that oligonucleotide-grafted nanoparticles capture much more (0.40 nmol mg^{-1} for forward primer immobilised nanoparticles and 0.34 nmol mg^{-1} for reverse primer immobilised nanoparticles) than the glutaraldehyde-modified materials (0.16 nmol mg^{-1} for non-specific capture of the forward complementary sequence and 0.14 nmol mg^{-1} for non-specific capture of the reverse complementary sequence), confirming the specific capture of the complementary oligonucleotides from the solution. Table 5.3 below shows the capture as a percentage of the covalently coupled oligonucleotide concentration.

Table 5.3: Capture of complementary oligonucleotides from solution as a percentage of the covalently coupled EC-specific oligonucleotide concentration (see Table 5.1, Section 5.1 for material names).

Oligonucleotide-Grafted Material	Complementary Oligonucleotide Captured	Capture (nmol mg^{-1})	Capture % (in terms of nmol captured per nmol coupled)	Specific Capture (%)
TTQB_EC_541_FOR	Comp FOR	0.40	54.95	60.00
TTQB_EC_637_REV	Comp Rev	0.34	48.80	58.82
TTQB-Blank-F	Comp FOR	0.16	10.60	0
TTQB-Blank-R	Comp Rev	0.14	8.94	0

Note: Specific capture (%) is calculated from the difference between capture (%) using oligonucleotide-grafted materials and capture (%) using glutaraldehyde-modified materials without grafted-oligonucleotides. TTQB-Blank-F is the blank glutaraldehyde-modified material used to capture the forward complementary oligonucleotide and TTQB-Blank-R is the blank glutaraldehyde-modified material used to capture the reverse complementary oligonucleotide.

For the immobilised forward primer (TTQB_EC_541_FOR), 60% of the capture is specific. For the immobilised reverse primer (TTQB_EC_637_REV), around 59% of the capture is specific. As with LM-specific materials, capture is reasonably high, 55% and 49% for forward and reverse oligonucleotide-grafted nanoparticles respectively.

The final stage of the hybrid capture assay was the dehybridisation step, where the complementary oligonucleotide that was captured in the previous step is removed at high temperature. Figure 5.11 presents total dehybridisation of captured EC-specific oligonucleotides in nmol mg^{-1} oligonucleotide-grafted nanoparticles.

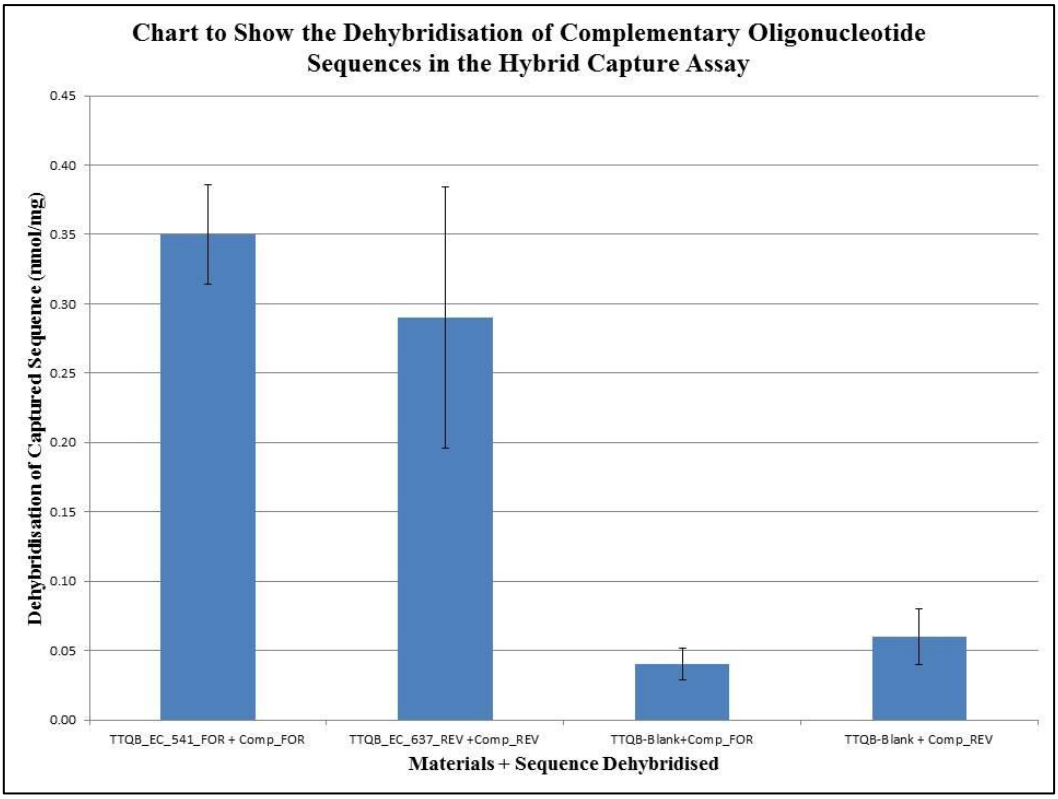

Figure 5.11: Total dehybridisation of captured EC-specific oligonucleotides (in nmol) per mg oligonucleotide-grafted nanoparticles. Values are mean, ± S.E.M, n =3.

Figure 5.12 presents total dehybridisation of captured EC-specific oligonucleotides in nmol mg^{-1} oligonucleotide-grafted nanoparticles as a percentage of total captured oligonucleotides.

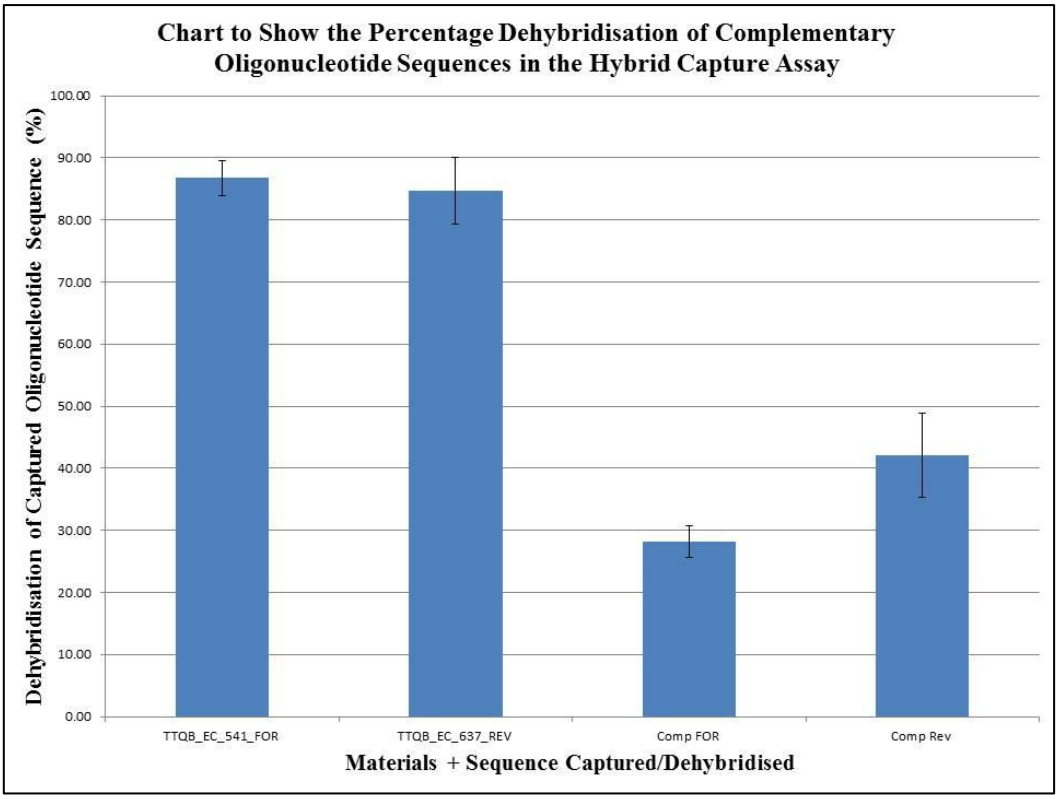

Figure 5.12: Total dehybridisation of captured EC-specific oligonucleotides as a percentage of total captured oligonucleotides. Values are mean, ± S.E.M, n =3.

Figure 5.12 shows that dehybridisation of specifically captured sequences is highly efficient; 87% for forward oligonucleotide-grafted nanoparticles and 86% for reverse oligonucleotide-grafted nanoparticles. In comparison, only around 28-42% of non-specifically adsorbed oligonucleotides are dehybridised, making this assay efficient at specific hybrid capture and dehybridisation. Figure 5.13 presents a summary of the EC hybrid capture data.

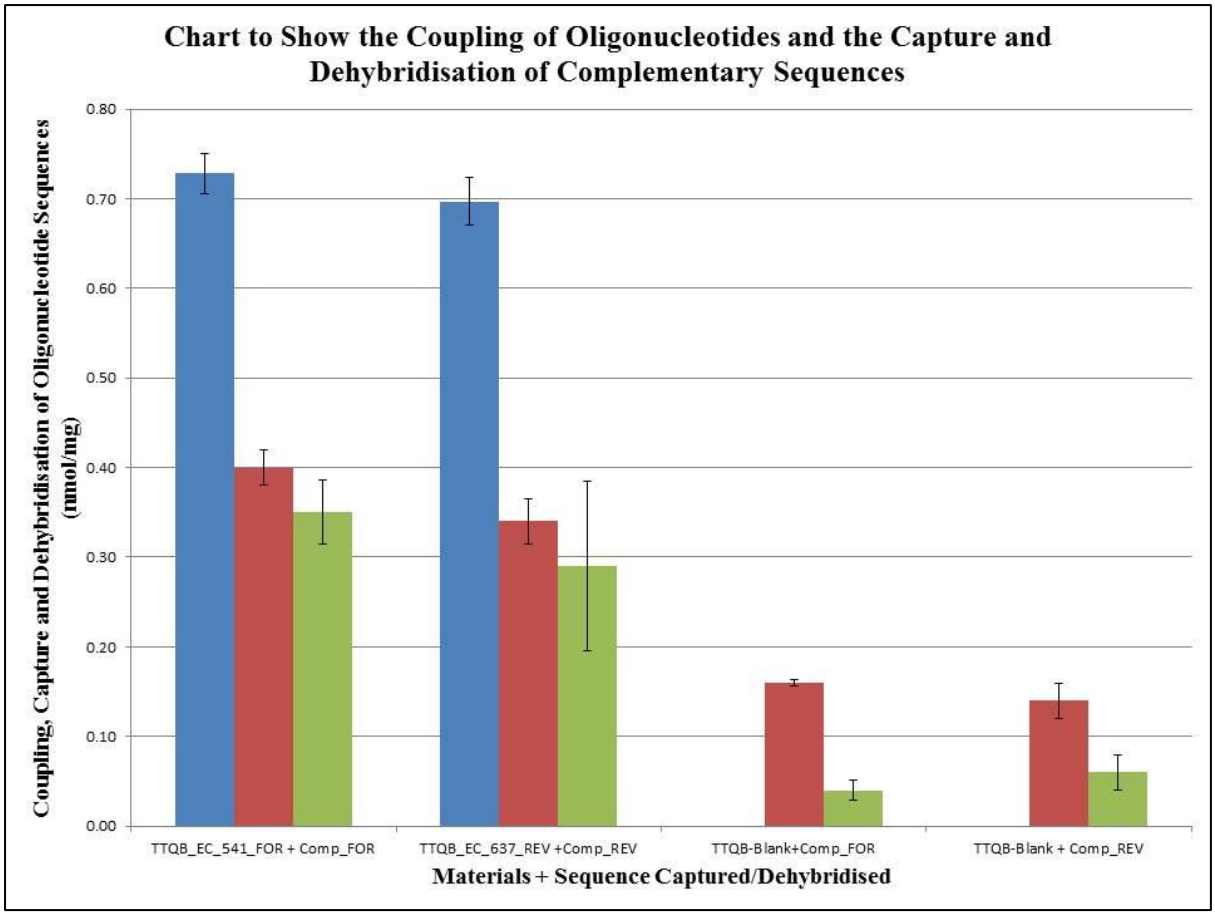

Figure 5.13: Summary of the materials used in the *Escherichia Coli* hybrid capture assay and the complementary oligonucleotides they have captured and dehybridised. The blue bars represent the initial EC-specific oligonucleotide present on the nanoparticles after the glutaraldehyde coupling reaction, the red bars represent the total amount of complementary oligonucleotides captured during the hybridisation step and the green bars represent the total amount of captured oligonucleotides dehybridised (specific capture by hybrid capture mechanism). Values are mean, ± S.E.M, n =3.

In conclusion, it can be seen from results of the hybrid capture assay that all materials exhibit very high coupling values, typically over 96% of the initial oligonucleotide concentration. Oligonucleotide-grafted nanoparticles exhibit both specific and non-specific capture of complementary oligonucleotide sequences from solution, but the majority (over 59% in all cases) is specific. Dehybridisation of specifically captured oligonucleotides is especially high (85-88%) compared to non-specifically adsorbed oligonucleotides (28-42%), suggesting that those adsorbed non-specifically may be bound to the surface functional groups and that the interaction is not fully disrupted by dehybridisation in water at 95ºC.

5.5 Bio-sensor Application: Selective Determination of *Listeria Monocytogenes* (LM) from a mixture of LM and EC in collaboration with Q-Bioanalytic GmbH, Germany

Initially the reaction has been carried out using LM-specific oligonucleotide-grafted nanoparticles (using C_6 or C_{12} spacers), aminosilane-functionalised nanoparticles (TTQB) and silica-coated core-shell nanoparticles (QBLSSM) for the specific capture of LM from a 1:1 mixture of LM and EC, as described in Section 2.7.6. In the amplification curve, there is a horizontal line (corresponding to a certain fluorescence value, not shown) called the crossing threshold, that when passed, confirms the presence of amplified DNA within the sample. The point at which the amplification plot crosses the crossing threshold is called the crossing point (C_p) and is presented as a cycle number (see Figure 5.14). A lower C_p value signifies a higher amount of amplified DNA in the sample. Due to the nature of the PCR amplification process, each cycle produces approximately double the amount of previously amplified DNA, therefore a sample with $C_p = 23$ will contain 32 times (2^5) more DNA than a sample with $C_p = 28$.

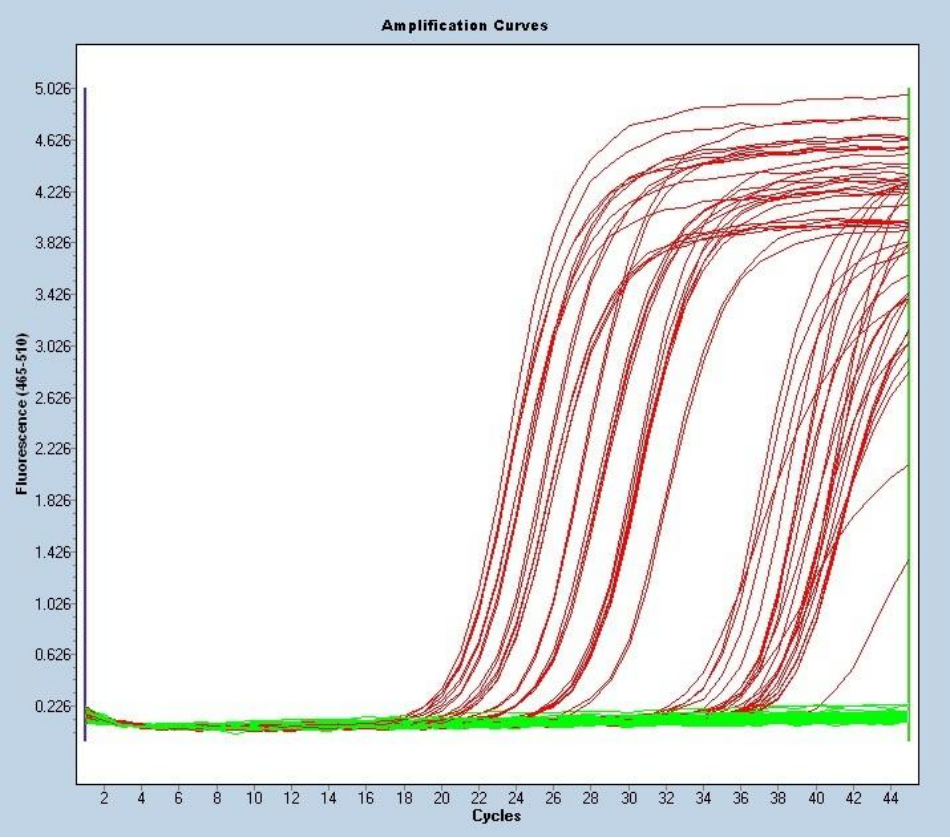

Figure 5.14: qPCR amplification curves for selective capture of LM from a mixture of LM and EC (first testing of materials).

Figure 5.14 presents the qPCR amplification curve for LM-specific materials, aminosilane-functionalised nanoparticles (TTQB) and silica-coated core-shell nanoparticles (QBLSSM). The green lines represent the background experiments ran using only water. Table 5.4 shows the C_p values for the materials used in the reaction. Experiments performed using water as the target mixture are omitted as fluorescence does not exceed the crossing threshold in all cases, except where contamination has taken place.

Table 5.4: C_p values for LM-specific oligonucleotide-grafted nanoparticles for specific detection of LM from a 1:1 mixture of LM and EC.

Sample Details	**Target Mixture**	**C_p Value**	**Positive/Negative Result (P/N)**
TTQB-C_6T1NH_2 + TTQB-C_6T2NH_2	LM only	28.69	P
		28.60	P
		34.52	P
		33.95	P
TTQB-C_6T1NH_2 + TTQB-C_6T2NH_2	1:1 mixture LM/EC	24.92	P
		24.87	P
		22.64	P
		22.71	P
TTQB-C_{12}T1NH_2 + TTQB-C_{12}T2NH_2	LM only	26.66	P
		26.83	P
		26.87	P
		26.96	P
TTQB-C_{12}T1NH_2 + TTQB-C_{12}T2NH_2	1:1 mixture LM/EC	25.10	P
		25.10	P
		26.92	P
		27.00	P

Table 5.4 shows that LM-specific oligonucleotide-grafted nanoparticles are successful at capturing LM from a solution containing LM only and also from a solution containing LM and EC.

The reaction was also performed using a two-step hybrid capture assay (see Section 0) where the forward-specific oligonucleotide-grafted nanoparticles were used first for hybridisation and the reaction mixture was subsequently added to reverse-specific oligonucleotide-grafted nanoparticles. The captured complementary sequences were then dehybridised separately and amplified separately for qPCR.

For the capture of LM from the 1:1 mixture of LM and EC, no capture was observed at all using LM-specific materials. For the capture of EC from the mixture using EC-specific

materials, only the material grafted with the reverse-specific oligonucleotide exhibited positive results (C_p = 39.80).

5.6 Bio-sensor Application: Determining the Sensitivity of Detection of LM from a Dilution Series using LM-specific oligonucleotide-grafted nanoparticles in collaboration with Q-Bioanalytic GmbH, Germany

The hybrid capture reaction was performed using real food samples inoculated with either LM or EC as described in Section 2.7.6. For LM-specific oligonucleotide-grafted nanoparticles, capture was shown to be successful for detecting LM in an undiluted mixture (see Table 5.4). The reaction was performed with new batches of oligonucleotide-grafted nanoparticles using a 2-step hybrid capture assay (see Section 2.7.6).

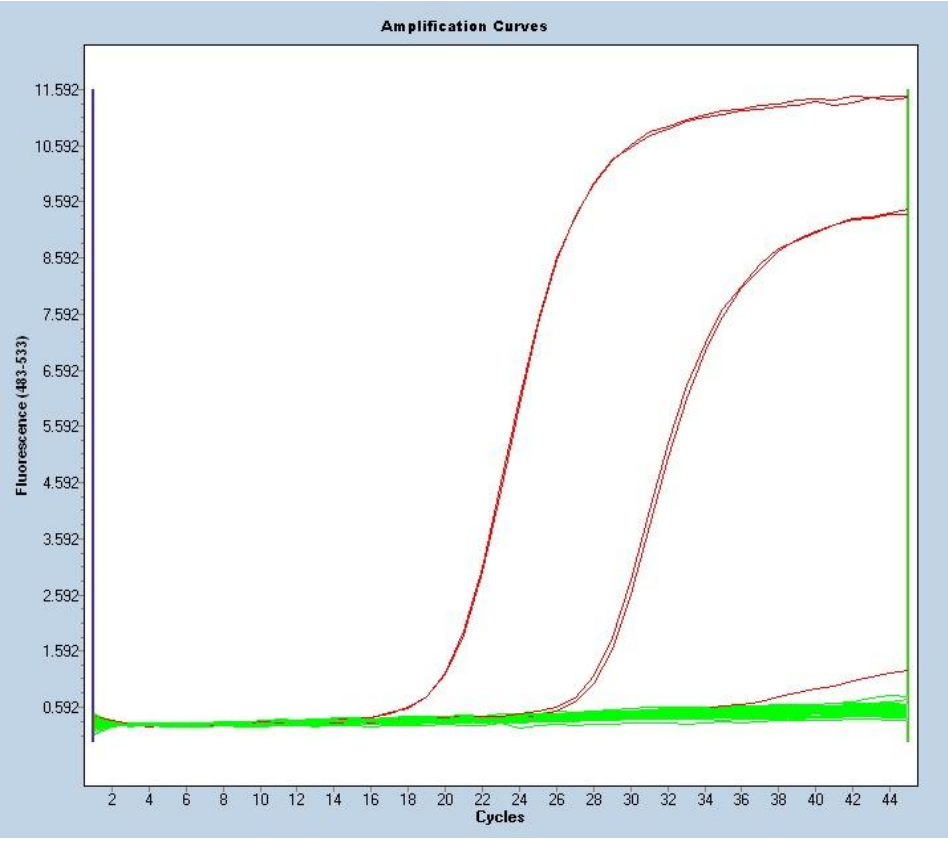

Figure 5.15: qPCR amplification curves for determining the sensitivity of detection for capture of LM from a dilution series of LM in peptone water using the two-step hybrid capture mechanism.

Figure 5.15 shows that for the two-step hybrid capture assay using LM-specific nanoparticles, no detection was observed within the dilution series. The only positive results obtained were for blank glutaraldehyde-modified TTQB nanoparticles, which detected LM at standard

concentration (without dilution), giving C_P values of 27.70 and 27.41. The curves appearing with C_P values of around 19 correspond to positive control samples of LM.

5.7 Bio-sensor Application: Determining the Sensitivity of Detection of EC from a Dilution Series using EC-specific oligonucleotide-grafted nanoparticles in collaboration with Q-Bioanalytic GmbH, Germany

The hybrid capture reaction was performed using real food samples inoculated with either LM or EC as described in Section 2.7.6. The reaction was performed with new batches of oligonucleotide-grafted nanoparticles using a 2-step hybrid capture assay (see Section 2.7.6).

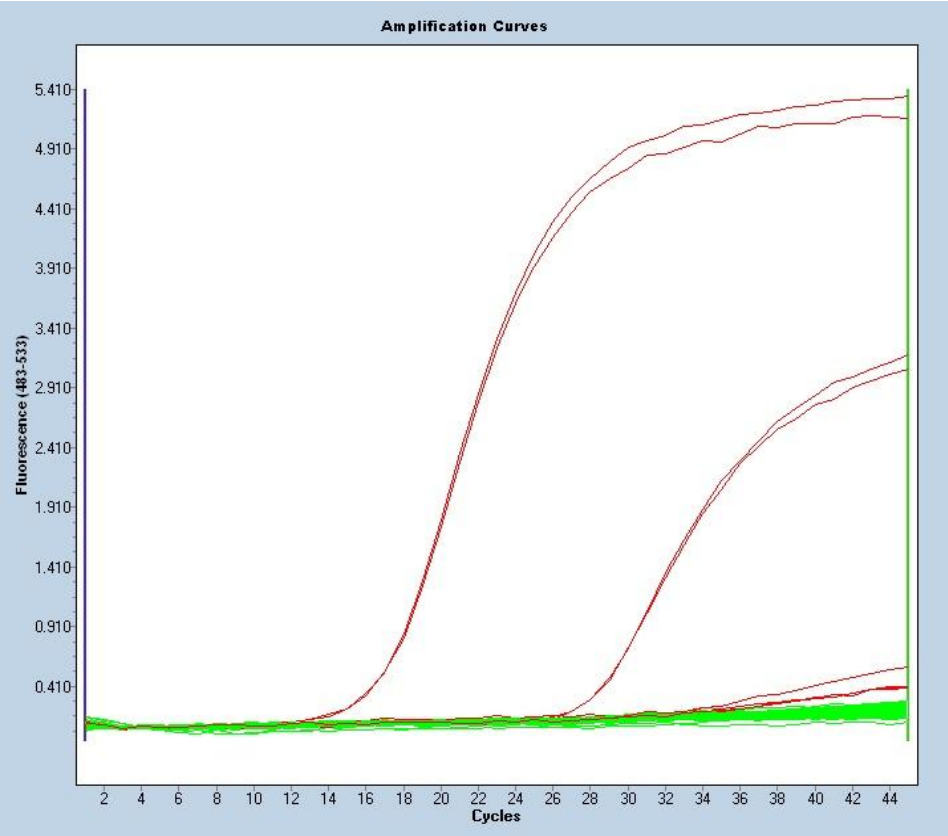

Figure 5.16: qPCR amplification curves for determining the sensitivity of detection for capture of EC from a dilution series of EC in peptone water using the two-step hybrid capture mechanism.

Error! Reference source not found. shows that for EC-specific nanoparticles positive esults were obtained for nanoparticles grafted with the forward oligonucleotide (EC_541_FOR) at standard concentration (without dilution), C_P = 38.78 and 35.13. The curves appearing with C_P values of around 15 correspond to positive control samples of EC.

CHAPTER 6

CONCLUSIONS AND FUTURE WORK

The work presented in this thesis has been carried out in order to explore the various applications of functionalised magnetic nanoparticles with bio-molecules on the surface. The materials were then used to investigate their applications in two main areas: Bio-catalysis and bio-separation/bio-sensing.

6.1 Synthesis and Characterisation of Magnetite and Silica-Magnetite nanoparticles

Magnetite nanoparticles were produced using two popular synthetic methods: the chemical co-precipitation of ferrous and ferric chloride solutions in alkaline media and the oxidative hydrolysis of ferrous sulphate. Magnetite nanoparticles made *via* the co-precipitation method were found to be spherical, around 10nm in diameter, with reasonably high saturation magnetisation (M_S) and high surface area. However, they were dark red-brown possibly due to the presence of hematite and had seemingly slow response to a bar magnet and hence were not used for further applications. Nanoparticles made *via* the oxidative hydrolysis method were jet-black in colour with rhombic (25-200 nm size) morphology. The synthesis method was scaled up successfully to produce the materials in a larger amount with no significant change in the size, shape or magnetic response. Surface areas for the nanoparticles made on the small-scale were around two times greater than that observed for large-scale materials, perhaps due to the aggregation of the nanoparticles during storage.

Following the production of silica-coated core-shell nanoparticles, TEM images show an amorphous silica-coating surrounding both individual nanoparticles and small aggregates of nanoparticles. Magnetic measurements show an interesting trend; silica-coated nanoparticles have higher saturation magnetisation than bare magnetite nanoparticles. BET surface area results show that the surface area of silica-coated nanoparticles is slightly lower than those obtained from bare magnetite. The homogeneity of the silica core-shell coating was proven using a salmon sperm DNA binding and elution assay. Binding was shown to be high in all materials (bare magnetite and silica-coated magnetite) whereas elution behaviour was different depending on the number of silica coating steps or bare magnetite. Elution was shown to increase with an increase in silica-coatings hence proving the homogeneity of the silica shell on core-magnetite due to the presence of a “cation-bridge” bonding system between the surface silanol groups, sodium cations present in the salt buffer and the negatively charged phosphate groups on the DNA backbone.

6.2 Surface Functionalisation of Silica-Coated Magnetite Nanoparticles

Following silica-coating, the nanoparticles were functionalised using a variety of aminosilanes (APTS, APDS and APMS) and two different functionalisation methods – a classical method in water and a recently-developed TPRE method using toluene and a non-ionic surfactant.

Materials made using TPRE methods gave higher surface amine density values than those made using the classical water method, when the same aminosilane was used. Also, surface amine density was highest using APTS and decreased when APDS and APMS were used. This is possibly due to APTS molecules forming a more ordered monolayer around the silica-coated surface, with less steric hindrances than the other aminosilanes (due to the presence of 'capped' methyl groups in APDS and APMS). The surface amine density values given by APTS- and APDS-functionalised materials are comparable to the values obtained for that of a monolayer on a flat surface, reported by Moon *et al*.[88]

Glutaraldehyde was used as a cross-linking reagent to attach the surface amine groups of the aminosilane-functionalised nanoparticles covalently to the amine groups on the bio-molecule surface – lipases for bio-catalysis and amine functionalised oligonucleotides for bio-sensing.

6.3 Bio-catalytic Applications of Lipase-Immobilised Nanoparticles

Enzyme Loading

Two lipases – CRL and PFL – were immobilised onto various glutaraldehyde-modified surface-functionalised nanoparticles for use as bio-catalysts; on average, PFL materials showed slightly lower loading values than CRL materials. APTS and APDS-functionalised materials exhibited higher loadings (65-80 μg/mg) than those made using APMS (35-60 μg/mg) for both CRL and PFL. One of the reasons for this is possibly that APTS and APDS materials have higher surface amine density values than APMS materials on average and have more possible binding sites. Physical adsorption of both lipases onto silica-coated non-functionalised nanoparticles was also performed, giving lower loading values when compared to immobilisation *via* chemical conjugation. In addition, physically adsorbed lipases could also leach into solution during a reaction, whereas immobilised lipases remained attached to the nanoparticle surface.

Model Catalysis Reaction: Hydrolysis of PNPP to PNP and Palmitic Acid

The hydrolysis of *p*-nitrophenyl palmitate (PNPP) to *p*-nitrophenol (PNP) and the corresponding acid is a widely used reaction to determine the hydrolytic activity of lipases and lipase-immobilised materials.

For PFL-immobilised materials, those made using APTS and APDS showed no significant differences in activity over three catalytic cycles, regardless of whether the TPRE or water method was used for surface functionalisation. When APMS was used for surface functionalisation, catalytic activity increased greatly and was higher than when free PFL was used. There was also a significant difference in activity of materials made using the TPRE and water methods; activity of the TPRE materials being much higher. Free PFL gave higher activity than PFL-immobilised materials made using APTS and APDS for surface functionalisation, but was lower than those made using APMS.

For CRL-immobilised materials, APTS, APDS and APMS surface-functionalised materials made using the TPRE method give higher activity than the same materials made using the water method. Free CRL was seen to have higher activity than all CRL-immobilised materials. Materials made using APMS were seen to exhibit the highest catalytic activity values again, despite having the lowest loading values.

For both lipases, the increased activity of APMS functionalised materials over the others is possibly due to lower surface amine density leading to decreased steric hindrance around the nanoparticle surface and therefore more accessible active sites.

In the case of physically adsorbed lipases, activity was seen to be much lower, initially, than that of immobilised-lipases and activity decreased greatly with subsequent cycles, due to the lipase leaching from the nanoparticle surface into the reaction mixture. For free lipases, PFL was notably more catalytically active than CRL, producing around 2.5 times more PNP than CRL.

Transesterification of Ethyl Butyrate and *n*-Butanol to Butyl Butyrate

The first step of this application involved testing various reaction conditions to optimise the reaction. For PFL-immobilised materials, those made using the water method of surface functionalisation gave higher conversion values than those made using the TPRE method, except when APTS was used as the aminosilane, in which case the conversion values were similar regardless of the method used. This trend is opposite to that observed in the model

catalysis reaction, where PFL materials made using the TPRE and water methods had similar catalytic activity. This suggests that the PFL reacts differently to the different reaction conditions and performs differently for hydrolysis and transesterification reactions. For CRL-immobilised materials, those made using the TPRE method performed slightly better on average than those made using the water method. Materials made using APMS as the aminosilane source provided the highest conversion values overall. These trends for CRL materials were similar to those observed in the hydrolysis of PNPP reaction, suggesting that CRL performs in a similar way for both reactions. Both free lipases gave higher conversion values than all of the corresponding lipase-immobilised materials, with free PFL giving the highest overall conversion at around 90% and free CRL at around 65% conversion.

Partial and Selective Hydrolysis of *Cis*-3,5-diacetoxy-1-cyclopentene to Synthesise Pharmaceutically Important Chiral Intermediates

A variety of temperatures and solvent conditions were investigated for this reaction in order to produce the best results. PFL- and CRL-immobilised nanoparticles made using APTS as the aminosilane source and the TPRE method were used for the reaction due to their high enzyme loading and reproducibility of results in other applications. Free lipases were also used for comparison.

For free lipases, the highest total conversion values were given at 37ºC using 20% water/hexane as the solvent. For immobilised lipases, the highest conversions were obtained at 25ºC using 50% water/hexane as the solvent. This could be because 50% water/hexane permits a larger interfacial area for the reaction to take place. When free lipases are used in 50% water/hexane, maximum conversion to desired products is reached after 24 hours. After this, conversion to the desired products is seen to decrease and production of the dihydroxy by-product increases significantly. At 25°C and 37°C using 20% water/hexane and free PFL, the dihydroxy becomes the dominant product at 24 hours, suggesting that the desired mono-acetoxy products are hydrolysed further.

In all cases, immobilised enzymes reach maximum conversion values at 48 hours and conversion to the dihydroxy by-product is always very low (under 5% of total products). It can be concluded that the re-usability and separability advantages offered by lipase-immobilised nanoparticles coupled with low amounts of by-products formed makes them suitable catalysts for this reaction.

6.4 Bio-sensor Applications of Oligonucleotide-Grafted Nanoparticles

Oligonucleotide Grafting

Amine-functionalised oligonucleotide sequences specific to either LM or EC were conjugated onto glutaraldehyde-modified nanoparticles. LM-specific forward and reverse oligonucleotides modified with C_6 or C_{12} spacers were used; conjugation was high in all cases (78-85%) and no significant differences were seen, regardless of the spacer group. For EC-specific primers (with only C_6 spacer group), conjugation for the forward and reverse primers was extremely high at 96-97%.

Hybrid Capture Assay: Capture of Complementary Oligonucleotide Sequences Using LM-Specific Oligonucleotide-Grafted Nanoparticles

Initial conditions led to reasonable capture values of 58%, but only 27% of those captured oligonucleotides were dehybridised. The assay conditions were then optimised based on actual qPCR conditions used by Q-Bioanalytic GmbH and the results were improved.

Using the optimised conditions, capture was observed to be relatively high as a percentage of nmol complementary sequence captured per nmol of sequence grafted for materials containing both C_6 and C_{12} spacers (48-70% capture). Non-specific capture using glutaraldehyde modified nanoparticles was found to be low (7 to 12%) for the complementary forward and reverse sequences. Of the oligonucleotides captured using oligonucleotide-grafted nanoparticles, 33-52% were deemed to be *via* specific hybridisation.

There was no significant difference in dehybridisation values for oligonucleotide-grafted materials possessing the C_6-spacer and the C_{12}-spacer group (72-97%). Dehybridisation of non-specifically adsorbed sequences using glutaraldehyde modified nanoparticles was also high at 59-100%. Optimising the conditions to suit the oligonucleotides used in the assay led to a significant increase in capture and dehybridisation efficiency and it can be concluded that the oligonucleotide-grafted nanoparticles are efficient for the specific capture and dehybridisation of complementary oligonucleotides from a buffer solution.

Hybrid Capture Assay: Capture of Complementary Oligonucleotide Sequences Using EC-Specific Oligonucleotide-Grafted Nanoparticles

Again, capture using the new, optimised conditions was observed to be relatively high as a percentage of nmol complementary sequence captured per nmol of sequence grafted (coupled *via* glutaraldehyde modification): 55% and 49% for forward and reverse oligonucleotide-

grafted nanoparticles respectively. Capture was observed to be low (9-11%) for the materials without attached primers (only glutaraldehyde modified nanoparticles). Of the total capture, 59-60% was determined to be *via* specific hybridisation between the grafted and complementary oligonucleotides.

In terms of dehybridisation, oligonucleotide-grafted nanoparticles dehybridised 85-88% of captured complementary sequences, whereas glutaraldehyde-functionalised nanoparticles without the primers (only glutaraldehyde modified nanoparticles) dehybridised only 28-42% of physically captured sequences. It can be concluded that the oligonucleotide-grafted nanoparticles are efficient for the specific hybrid capture from a buffer solution.

In terms of hybrid capture efficiency for both LM and EC specific primer functionalised nanoparticles, a better negative control would be to test the capture of non-specific oligonucleotide sequences from solution, rather than using glutaraldehyde-functionalised nanoparticles. The glutaraldehyde functional groups on the nanoparticles' surface may promote capture of the non-specific nucleotide sequences, giving a less accurate indicator of non-specific capture from the solution.

6.5 DNA Extraction Using Silica-Coated Core-Shell Nanoparticles

Silica-coated core-shell nanoparticles (QBLSSM) were shown to exhibit similar efficiency for extraction of DNA from a food matrix when compared to total DNA extracted using a classical thermal lysis method. However, DNA extracted using the nanoparticles can be purified by washing and then eluted for direct use in qPCR, whereas DNA extracted from the thermal lysis method can contain many PCR-inhibiting species. The silica-coated nanoparticles (QBLSSM) were subsequently employed by Q-Bioanalytic GmbH as part of their commercial DNA Extraction Kit.

6.6 Selective Determination of *Listeria Monocytogenes* or *Escherichia Coli* from a Mixture of Both

Using a one-step hybrid capture mechanism (see Section 2.7.3) involving LM-specific forward and reverse oligonucleotide-grafted nanoparticles, the nanoparticles (containing both C_6 and C_{12} spacers) were shown to be successful for the detection of LM from mixtures containing a 1:1 mixture of LM and EC.

Later, in testing a two-step hybrid capture mechanism in which forward and reverse oligonucleotide-grafted nanoparticles were employed separately for capture and dehybridisation, only the material grafted with the EC-specific reverse-oligonucleotide was successful for detection of EC.

6.7 Determining the Sensitivity of Detection of *Listeria Monocytogenes* from a Dilution Series

Using a one-step hybrid capture mechanism (see Section 2.7.6), LM-specific forward and reverse oligonucleotide-grafted nanoparticles were successful at detecting LM in undiluted samples. The capture and detection was unsuccessful using the two-step hybrid capture mechanism.

6.8 Determining the Sensitivity of Detection of *Escherichia Coli* from a Dilution Series

Using only a two-step hybrid capture mechanism ((see Section 2.7.6), EC-specific forward oligonucleotide-grafted nanoparticles were successful at detecting EC in undiluted samples. EC-specific reverse oligonucleotide-grafted nanoparticles were unsuccessful at detecting EC in the samples.

6.9 Future Work

This work has presented the synthesis and characterisation of rhombic magnetite and silica-coated magnetite nanoparticles, on the small and large scale, and their subsequent uses for immobilising bio-molecules for further applications. In future, it would be worth comparing a range of morphologies with a narrow size distribution.

In terms of bio-catalytic applications such as (i) the transesterification of ethyl butyrate and (ii) the partial and selective hydrolysis of *cis*-3,5-diacetoxy-1-cyclopentene, it would be interesting to scale-up the reaction to investigate a wider range of water concentrations; to avoid issues dissolving the free lipase in minute quantities of water. This is more of an issue in the partial and selective hydrolysis of *cis*-3,5-diacetoxy-1-cyclopentene as the products are formed in the water layer, from which aliquots are withdrawn for analysis. In this reaction, as the by-products become the predominant product in some cases, it would be interesting to carry out a full kinetic study to pinpoint the exact moment when the production of desired products is highest compared to undesired products. Due to the formation of acetic acid in the

reaction leading to hydrolysis of the desired reaction products, addition of small amounts of base to the reaction to neutralise the acid could lead to higher ratios of desired products to undesired by-products.

For bio-sensor applications, optimising the protocols for the specific capture of bacteria from real food samples is a priority. A two-step protocol could be employed, where nanoparticles grafted with the forward-specific oligonucleotide could be used for capture first, followed by those grafted with the reverse-specific oligonucleotide. The dehybridisation of captured complementary sequences could be carried out separately and the two could be mixed before amplification by PCR. This would overcome problems associated with non-specific capture of sequences from the mixture. Incorporating BSA into the buffer system during the specific capture of bacteria from real food samples would also help to block the non-specific nucleic acids from binding to the un-grafted glutaraldehyde groups on the surface of the nanoparticles. Also, assessing the capture of non-specific oligonucleotides using oligonucleotide-grafted nanoparticles would be a better negative control experiment as the glutaraldehyde-functionalised nanoparticles possess different surface properties to oligonucleotide-grafted nanoparticles and may facilitate the non-specific capture. Due to some successful results, with some assay optimisation, the nanoparticles could be grafted with oligonucleotides specific to other strains of pathogenic bacteria and also allergens in food.

List of Figures

List of Schemes

List of Tables

Appendix I (Project Output)

Manuscripts Under Submission:

1) Enzyme Immobilised Magnetic Nanoparticles for Bio-catalysis
   Ben Hodgson**,** Boris Oberheitmann, and Tapas Sen
   2nd International Conference on Materials and Applications for. Sensors and Transducers. May 24-28, *2012*, *Budapest*, Hungary http://www.*icmast*.net
   See Appendix II for attached manuscript as supplementary information

2) Enzyme immobilised magnetic nanoparticles with controlled hydrophobicity as efficient bio-catalysts
   Ben Hodgson**,** Boris Oberheitmann, and Tapas Sen
   Chem. Cat. Chem. (2013 under preparation)

3) Single stranded oligonucleotides attached superparamagnetic iron oxide nanoparticles for the detection of *Escherichia Coli* and *Listeria Monocytogenes* from food matrices
   Ben Hodgson**,** Boris Oberheitmann, Jens-Oliver Axe and Tapas Sen
   Langmuir (2013 under preparation)

Appendix II (Full Paper from Appendix I)

Enzyme Immobilised Magnetic Nanoparticles for Bio-catalysis

Ben Hodgson[1,a], Boris Oberheitmann[2,b] and Tapas Sen[1,3,c]

[1]Centre for Materials Science, Chemistry Section, School of Forensic and Investigative Sciences, University of Central Lancashire, Preston, PR1 2HE, United Kingdom

[2]Q-Bioanalytic GmbH, Fischkai 1, D-27572, Bremerhaven, Germany

[3]Surface Patterning Group, Institute of Nanotechnology and Bio-engineering, University of Central Lancashire, Preston, PR1 2HE, United Kingdom

[a]bhodgson1@uclan.ac.uk, [b]Oberheitmann@q-bioanalytic.com, [c]tsen@uclan.ac.uk

Keywords: Superparamagnetic iron oxide nanoparticles (SPIONs), Surface modification, Lipase enzymes, Bio-catalysis, Magnetic separation.

Abstract. Superparamagnetic iron oxide nanoparticles (SPIONs) have been fabricated and modified with silica shell followed by functionalization with aminosilanes. The non-functionalised core-shell and amino-functionalized SPIONs were used for the immobilisation of lipase enzymes (*Candida Rugosa Lipase:CRL* and *Pseudomonas Fluorescens Lipase:PFL*). The materials have been used for the hydrolysis of *p*-nitrophenyl palmitate (PNPP) to palmitic acid and *p*-nitrophenol (PNP) under the heterogeneous condition. PFL immobilised SPIONs were observed to be highly reactive compared to CRL immobilised SPIONs. Similarly chemically conjugated lipases *via* glutaraldehyde modification to the amino-functionalised SPIONs were reactive and stable up to 3 recycles compared to physically adsorbed lipase immobilised SPIONs.

Introduction

Enzymes are widely used in the chemical industry for homogeneous catalysis as a result of their high chemo-, regio- and enantioselectivity [1]. Since mid-to-late 1990's, bio-catalysis using enzymes has been extensively used in the pharmaceutical industry due to increased demand for new, more potent drugs and medicines [2]. It is also important to mention that enzymes typically require mild reaction conditions and produce much less waste and harmful by-products than other catalysts, making them an even more attractive option for chemical synthesis. However, the use of free enzymes presents a problem such as they can't be recycled or reused once introduced into the reaction system. Also, enzymes are fairly expensive so being able to reuse them is cost effective and would make the system more commercially viable. Another problem is that most organic compounds that are of commercial interest are often insoluble/partially soluble in water. A way around this is to use organic solvents, which leads to high substrate solubility, higher reaction rates and increased ease of recovery of the enzyme from the system. However, a disadvantage of using lipases in organic solvents is that catalytic activity can decrease dramatically compared to aqueous systems [3], due to diffusional limitations, enzyme destabilisation and changes in protein flexibility [4,5].

A solution to these problems is to immobilise the enzymes onto a solid support, which would create a heterogeneous system where the supported enzyme can be introduced into the reaction mixture. The enzyme immobilised solid supports can be recovered by simple filtration and reused for further reactions. It is also well documented that enzyme activity increases when immobilised on solid supports matrix [4] especially when interfacially adsorbed on hydrophobic supports [6]. This occurs because the hydrophobicity of the support surface promotes interfacial activation of the lipase. The strong adsorption on the hydrophobic surfaces produces conformational changes that favour the more-stable "open" form of the enzyme i.e. catalytically active centres are more exposed, leading to greater catalytic activity.

Immobilisation of enzymes on magnetisable solid supports has added advantage as they can be separated by applying an external magnetic field. Dyal *et al* [7] first reported the immobilisation of candida rugosa lipase (CRL) on magnetic (maghemite) nanoparticles for the hydrolysis of *p*-

nitrophenyl palmitate. Sen *et al* [8] have later reported a novel materials "hierarchically ordered porous magnetic nanocomposites" for the same reaction under heterogeneous medium. Netto *et al* [9] have reported superparamagnetic silica-coated nanoparticles for immobilisation of *Candida Antarctica* lipase (CAL) for enantioselective transesterification reactions. In the context of our manuscript, both *Candida Rugosa lipase* (CRL) and *Pseudomonas Fluorescence lipase* (PFL) were employed under homogeneous condition for the enantiomeric synthesis of citronellyl butyrate, a flavouring agent i.e. a fruity and floral aroma [10].

Herein we report the immobilisation of CRL and PFL on the silica coated superparamagnetic iron oxide nanoparticles (SPIONs) by (i) physical adsorption and (ii) chemical conjugation *via* surface functionalisation using aminosilanes for the hydrolysis of *p*-nitrophenyl palmitate (PNPP) to *p*-nitrophenol and palmitic acid under heterogeneous condition and efficient reusability by simple magnetic separation.

Materials and methods

All chemicals were purchased from Sigma-Aldrich and used without further purification. Superparamagnetic iron oxide nanoparticles (SPIONs) were synthesised by earlier published protocol [11]. In an actual process ferrous sulphate (23.60 g), potassium nitrate (5.39 g) and potassium hydroxide (12.60 g) were mixed and dissolved in 220 mL deionised water. The mixture was stirred for 4 hours under nitrogen atmosphere at 90°C. The black materials obtained were washed with deionised water by magnetic separation using a bench top flat magnet until the pH 7. The core SPIONs were coated with a thin layer of amorphous silica by reported protocol [11] using silicic acid at alkaline pH.

The silica coated magnetite nanoparticles were used for the immobilisation of CRL and PFL by two different methods:

Physical adsorption: Silica-coated SPIONs (50 mg) and 4 mL of a 1 mg/mL solution of either CRL or PFL in PBS buffer were mixed in 25 mL falcon tubes and the reactions were allowed to proceed for 20 hours at 25°C (temperature programmed incubator) with gentle end-over-end rotation.

Chemical conjugation: Silica coated magnetite nanoparticles were functionalized using aminopropyl triethoxy silane (APTS) in water at 50°C for 24hrs following the reported protocol [12]. The surface amine density was determined by standard colorimetric assay [13] before treatment with glutaraldehyde for the conversion of surface amine to aldehyde (see Fig.1). The glutaraldehyde modified SPIONs (50 mg) were used for immobilisation of lipase enzymes following the same protocol described earlier in the physically adsorption route.

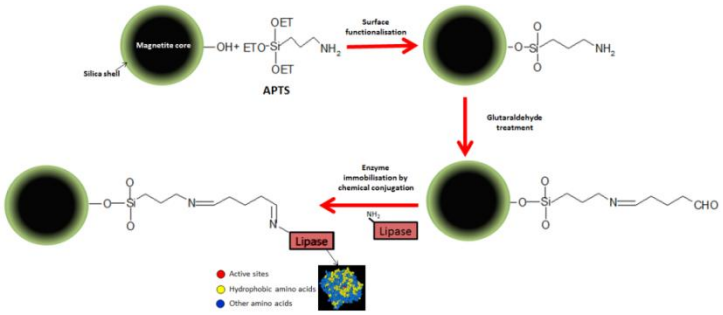

Fig.1 Reaction scheme for the immobilisation of enzymes onto SPIONs by chemical conjugation route

Analysis of enzymes immobilisation on the surface of SPIONs: 1 mL of the supernatant from each reactions were removed (using magnetic separator) and recorded the absorbance at λ_{595nm} (A_{595}) by UV-Vis spectrophotometer. The amounts of CRL and PFL immobilised on SPIONs were determined by calculating the concentrations using a pre-established standard curves (data not shown). The lipase-immobilised nanoparticles were then washed with PBS buffer (4×5mL) and finally resuspended in PBS buffer for use as bio-catalysts.

Bio-catalysis: The required amount of enzyme immobilised SPIONs containing 500 µg lipases were used for each reaction. A 3.74 µmol/mL (1 mL total volume) solution of *para*-nitro phenyl palmitate (PNPP) in a 1:1 mixture of reagent A (0.0667 g Gum Arabic, 0.267 g sodium deoxycholate, 12 mL of 250 mM Tris-HCl buffer at pH 7.8 + 48mL deionised water) and isopropanol was added to the lipase-immobilised nanoparticles. The reactions were allowed to proceed with gentle end-over-end rotation at 25°C for 1 hour. After 1 hour, the absorbance at λ_{410nm} (A_{410}) was recorded by UV-Vis

spectrophotometer to calculate the concentration of *para*-nitrophenol (PNP) in solution using a pre-established standard curve (data not shown). The lipase-immobilised nanoparticles were then washed in PBS buffer (4×1mL) and the reactions were repeated for 3 cycles in total to assess catalytic efficiency and reusability over time. Fig.2 presents the reaction scheme with magnetic separation of reaction products.

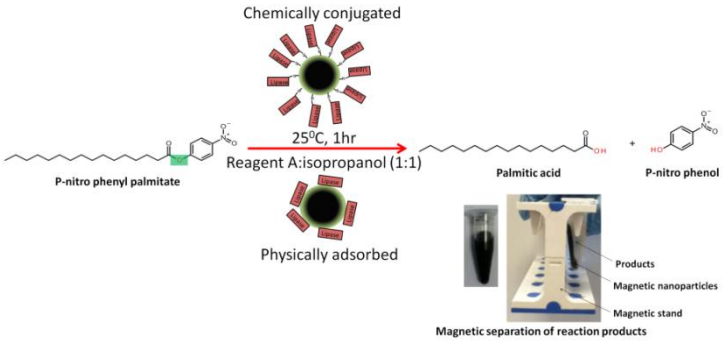

Fig.2 Bio-catalysis of p-nitro phenyl palmitate to p-nitro phenol and palmitic acid using enzyme immobilised SPIONs and magnetic separation

Results and Discussion

The silica coated SPIONs were rhombic in morphology of sizes around 30 to 150nm from Transmission Electron Microscope (data not shown). The materials were observed to be superparamagnetic in nature with saturation magnetization of ~80 Emu/G (see Fig.3). Fig.4 presents the amount of lipase immobilised by physical adsorption and chemically conjugated routes. Chemically conjugated route produced highest lipase immobilisation for both CRL and PFL compared to physically adsorbed route. PFL immobilisation was lowest (~4µg/mg of solid) in value when physically adsorbed on SPIONs. The highest values of PFL immobilisation was ~70µg/mg of solid when chemically conjugated route was used. Similarly the value of CRL immobilisation was~65µg/mg of solid when the chemically conjugated route was used.

When the materials were used for bio-catalysis, the chemically conjugated PFL immobilised SPIONs exhibited the highest catalytic activity (see C1 to C3 in Fig.5) compared to other materials including the free enzymes. It is noteworthy to mention that free PFL also exhibited a high catalytic activity however we could not reuse for cycles 2 and 3 due to the difficulty involved in separation from the reaction mixture. In was clearly observed that PFL immobilised SPIONs exhibited nearly 6 folds increase in catalytic activity (see C1 in Fig.5) compared to CRL immobilised SPIONs (see A1 in Fig.5). Free CRL exhibited 3 folds higher catalytic activity (see D1 in Fig.5) compared to chemically conjugated (see A1 in Fig.5) or physically adsorbed (see B1 in Fig.5) CRL immobilised SPIONs. Both PFL and CRL immobilised SPIONs by physically adsorbed route showed a gradual reduction in catalytic activity during reusable cycles (1 to 3) however, the catalytic activity nearly unchanged (in case of CRL) or increased in values (in case of PFL) when chemically conjugated route was used for the immobilisation. The loss of catalytic activity for physically adsorbed lipases could be due to the leaching of enzymes from the surface of SPIONs to the reaction mixture. However, enzymes immobilised by chemically conjugated route produced a stable catalyst for the hydrolysis of PNPP with efficient reusability. The increase in catalytic activity in the case of chemically conjugated PFL immobilised SPIONs could be due to the exposure of active sites of the enzymes with different cycles.

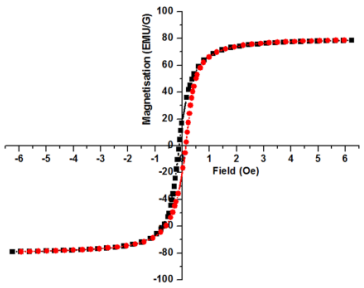

Fig.3 Magnetic data of silica coated SPIONs

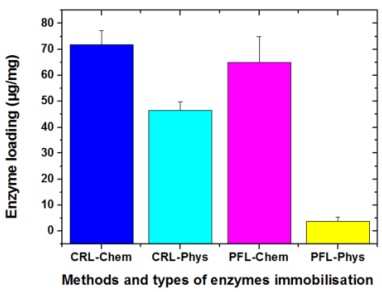

Fig.4 Immobilisation of CRL and PFL on SPIONs by chemical conjugation and physical adsorption

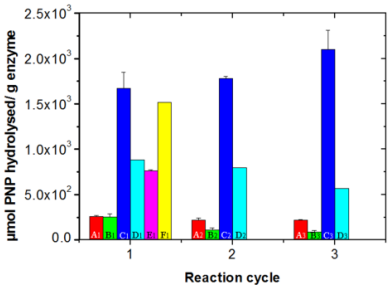

Fig.5 Bio-catalysis of PNPP using enzyme immobilised magnetic nanoparticles: chemically conjugated CRL on SPIONs (A); physically adsorbed CRL on SPIONs (B); chemically conjugated PFL on SPIONs (C); physically adsorbed PFL on SPIONs (D); free CRL (E); free PFL (F1).

Summary

Both PFL and CRL enzymes were successfully immobilised on the surface of superparamagnetic iron oxide nanoparticles (SPIONs). Chemical conjugation route produced novel enzyme immobilised magnetic nanoparticles which exhibited a high catalytic activity with an efficient reusability. We have also identified that PFL is the best enzyme for hydrolysis of PNPP.

Acknowledgement

Authors thank to Dr Tim Mercer for helping BH during the magnetic measurement study. BH would like to thank Q-Bioanalytic GmbH, Germany for a partial funding to his PhD study and the Centre for Materials Science, School of Forensic and Investigative Science for an additional funding.

References

[1] S. M. Roberts: J. Chem. Soc. Perkin Trans. Vol. 1 (2000), p.611
[2] R. S. Rogers: Chem. Eng. News. Vol. 77 (1999), p. 87.
[3] H. Kitaguchi, P. A. Fitzpatrick, J. E. Huber, A. M. Klibanov: J. Am. Chem. Soc. Vol.111 (1989), p.3094.
[4] Y. Z. Chen, C. B. Ching, R. Xu: Process Biochem. Vol. 44 (2009), p.1245.
[5] R. Fernandez-Lafuente, P. Armisn, P. Sabuquillo, G. Fernadez-Lorente, M. Guisin: Chem. Phys. Lipids. Vol. 93 (1998), p.185.
[6] G. Fenandez-Lorente, J. M. Palomo, M. Fuentes, C. Mateo, J. M. Guisin, R. Fernandez-Lafuente: Biotechol. Bioeng. Vol. 82 (2003), p.232.
[7] A. Dyal, K. Loos, M. Noto, S. W. Chang, C. Spagnoli, R. A. Gross: J. Am. Chem. Soc. Vol. 125 (2003), p.1684.
[8] T. Sen, I. J. Bruce, T. Mercer: Chem. Commun. Vol. 46 (2010), p.6807.
[9] C. G. C. M. Netto, L. H. Andrade, H. E. Toma: Tet. Lett. Vol. 20 (2009), p. 2299.
[10] Cargill Aroma Chemicals 2009 information on http://www.cargill.com/food/wcm/groups/public/@cseg/@food/@all/documents/document/na3024026.pdf
[11] I. J. Bruce, J. Taylor, M. Todd, M. J. Davies, E. Borioni, T. Sen: J. Magn. Magn. Mater.Vol. 284 (2004), p.145.
[12] I. J. Bruce, T. Sen: Langmuir Vol. 21 (2005), p.7029.
[13] J. H. Moon, J. W. Shin, S. Y. Kim, J. W. Park: Langmuir Vol.12 (1996), p.4621.

Reference List

1. Poole Jr., C. P.; Owens, F. J. Introduction to Nanotechnology. In *Introduction to Nanotechnology*, John Wiley & Sons, Inc: Hoboken, New Jersey, 2003; pp 1-7.

2. Tian, Y.; Pesika, N.; Zeng, H.; Rosenberg, K.; Zhao, B.; McGuiggan, P.; Autumn, K.; Israelachvili, J. Adhesion and Friction in Gecko Toe Attachment and Detachment. *Proc Natl Acad Sci USA* **2006,** *103* (51), 19320-19325.

3. Huang, J.; Wang, X.; Wang, Z. L. Controlled Replication of Butterfly Wings for Achieving Tunable Photonic Properties. *Nano Letters* **2006,** *6* (10), 2325-2331.

4. Buehler, M. J. Molecular Nanomechanics of Nascent Bone: Fibrillar Toughening by Mineralization. *Nanotechnology* **2007,** *18* (29), 1-9.

5. Poole Jr., C. P.; Owens, F. J. Introduction to Physics of the solid State. In *Introduction to Nanotechnology*, John Wiley & Sons, Inc: Hoboken, New Jersey, 2003; pp 8-34.

6. Capek, I. Preparation of Metal Nanoparticles in Water-in-Oil (w/o) Microemulsions. *Advances in Colloid and Interface Science* **2004,** *110*, 49-74.

7. Kreuter, J. Nanoparticles - A Historical Perspective. *International Journal of Pharmaceuticals* **2007,** *331*, 1-10.

8. Birrenbach, G.; Spesier, P. P. Polymerized Micelles and their Use as Adjuvants in Immunology. *J. Pharm. Sci.* **1976,** *65*, 1763-1766.

9. Kramer, P. A. Albumin Microspheres As Vehicles for Achieving Specificity in Drug Delivery. *J. Pharm. Sci.* **1974,** 1646-1647.

10. Kreuter, J. Nanoparticles and Nanocapsules - New Dosage Forms in Nanometer Size Range. *Pharm. Acta Helv.* **1978,** *53*, 33-39.

11. Kreuter, J. Evaluation of Nanoparticles as Drug Delivery Systems. *Habilitationsschrift, ETH Zurich, Nr. 5417* **1981**.

12. Kreuter, J. Evaluation of nanoparticles as drug delivery systems I: Preparation methods. *Pharm. Acta Helv.* **1983,** *58*, 196-209.

13. Marty, J. J.; Oppenheim, R. C. Colloidal Systems for Drug Delivery. *Aust. J. Pharm. Sci.* **1977,** *6*, 65-76.

14. Bertling, W. M.; Gareis, M.; Paspaleeva, V.; Zimmer, A.; Kreuter, J.; Nurnberg, E.; Harrer, P. Use of Liposomes, Viral Capsids, and Nanoparticles as DNA Carriers. *Biotech. Appl. Biochem.* **1991,** *13*, 390-405.

15. Sugibayashi, K.; Morimoto, Y.; Nadai, T.; Kato, Y.; Hasegawa, A.; Arita, T. Drug-carrier property of albumin microspheres in chemotherapy.II. Preparation and tissue distribution in mice of microsphere-entrapped 5-fluorouracil. *Chem. Pharm. Bull.* **1979,** *27*, 204-209.

16. Widder, K. J.; Morris, R. M.; Poore, G. A.; Howard, D. P.; Senyei, A. E. Selective targeting of magnetic albumin microspheres containing low-dose doxorubicin:Total remission in Yoshida Sarcoma-bearing rats. *Eur. J. Cancer* **1983,** *19*, 135-139.

17. Widder, K. J.; Marino, P. A.; Morris, R. M.; Howard, D. P.; Poore, G. A.; Senyei, A. E. Selective targeting of magnetic albumin microspheres to the Yoshida Sarcoma: Ultrastructural evaluation of microsphere disposition. *Eur. J. Cancer* **1983,** *19*, 141-147.

18. Brasseur, F.; Couvreur, P.; Kante, B.; Deckers-Passau, L.; Roland, M.; Deckers, C.; Speiser, P. P. *Actinomycin D adsorbed on polymethylcyanoacrylate nanoparticles: Increased efficiency against an experimental tumor;* 16 ed.; 1980.pp. 1441-1445.

19. Guiot, P.; Couvreur, P. *Polymeric Nanoparticles and Microspheres;* CRC Press: Boca Raton, 1986.pp. 27-93.

20. Kattan, J.; Droz, J. P.; Couvreur, P.; Marino, J.-P.; Boutan-Laroze, A.; rougier, P.; Brault, P.; Vranckx, H.; Grognet, J.-M.; Morge, X.; Sancho-Garnier, H. Phase I clinical trial and pharmacokinetic evaluation of doxorubicin carried by polyisohexylcyanoacrylate nanoparticles. *Invest. New Drugs* **1992,** *10*, 191-199.

21. Lobenberg, R.; Kreuter, J. Macrophage targeting of azidothymidine: A promising strategy for AIDS therapy. *AIDS Res. Hum. Retroviruses* **1996,** *12*, 1709-1715.

22. Lobenberg, R.; Araujo, L.; von Briesen, H.; Rodgers, E.; Kreuter, J. Body distribution of azidothymidine bound to hexyl-cyanoacrylate nanoparticles after i.v. injection to rats. *J. Control. Rel.* **1998,** *50*, 21-30.

23. Pankhurst, Q. A.; Connolly, J.; Jones, S. K.; Dobson, J. Applications of magnetic nanoparticles in biomedicine. *J. Phys. D: Appl. Phys.* **2003,** *36*, 167-181.

24. Albrecht, M. A.; Evans, C. W.; Raston, C. L. Green Chemistry and the Health Implications of Nanoparticles. *Green Chem.* **2006,** *8*, 417-432.

25. Thorek, D. L. J.; Chen, A. K.; Czupryna, J.; Tsourkas, A. Superparamagnetic Iron Oxide Nanoparticle Probes for Molecular Imaging. *Annals of Biomedical Engineering* **2006,** *34* (1), 23-38.

26. Dzyaloshinsky, I. A Thermodynamic Theory of "Weak" Ferromagnetism of Antiferromagnetics. *Journal of Physics and Chemistry of Solids* **1958,** *4* (4), 241-255.

27. Kodama, R. H. Magnetic Nanoparticles. *Journal of Magnetism and Magnetic Materials* **1999,** *200*, 359-372.

28. Robinson, P. J.; Dunnill, P.; Lilly, M. D. The properties of magnetic supports in relation to immobilized enzyme reactors. *Biotechnol. Bioeng.* **1973,** *15* (3), 603-606.

29. Bruce, I. J.; Taylor, J.; Todd, M.; Davies, M. J.; Borioni, E.; Sangregorio, C.; Sen, T. Synthesis, characterisation and application of silica-magnetite nanocomposites. *Journal of Magnetism and Magnetic Materials* **2004,** *284*, 145-160.

30. Thapa, D.; Palkar, V. R.; Kurup, M. B.; Malik, S. K. Properties of magnetite nanoparticles synthesized through a novel chemical route. *Materials Letters* **2004,** *58* (21), 2692-2694.

31. Roonasi, P. Adsorption and surface reaction properties of synthesized magnetite nano-particles. PhD Lulea University of Technology, 2007.

32. Fleet, M. E. The structure of magnetite. *Acta Crystallographica Section B: Structural Crystallography and Crystal Chemistry* **1981,** *37* (4), 917-920.

33. Sorescu, M. Phase transformations induced in magnetite by high energy ball milling. *Journal of materials science letters* **1998,** *17* (13), 1059-1061.

34. Sugimoto, T.; Matijevic, E. Formation of Uniform Spherical Magnetite Particles by Crystallization from Ferrous Hydroxide Gels. *Journal of Colloid and Interface Science* **1980,** *74* (1), 227-243.

35. Lu, A.-H.; Salabas, E. L.; Schuth, F. Magnetic Nanoparticles: Synthesis, Protection, Functionalization, and Application. *Angewandte Chemie International Edition* **2007,** *46*, 1222-1244.

36. Philipse, A. P.; van Bruggen, M. P. B.; Pathmamanoharan, C. Magnetic Silica Dispersions: Preparation and Stability of Surface-Modified Silica Particles with a Magnetic Core. *Langmuir* **1994,** *10*, 92-99.

37. Massart, R. Preparation iof Aqueous Magnetic Liquids in Alkaline and Acidic Media. *IEEE Transactions on Magnetics* **1981,** *17* (2), 1247-1248.

38. Kang, Y. S.; Risbud, S.; Rabolt, J. F.; Stroeve, P. Synthesis and Characterization of Nanometer-Size Fe_3O_4 and γ-Fe_2O_3 Particles. *Chem. Mater.* **1996,** *8*, 2209.

39. Lee, J.; Isobe, T.; Senna, M. Magnetic properties of ultrafine magnetite particles and their slurries prepared *via in-situ* precipitation. *Colloid Surface A* **1996,** *109*, 121-127.

40. Willis, A. L.; Turro, N. J.; O'Brien, S. Spectroscopic Characterization of the Surface of Iron Oxide Nanocrystals. *Chem. Mater.* **2005,** *17*, 5970-5975.

41. Grzeta, B.; Ristic, M.; Nowik, I.; Music, S. Formation of nanocrystalline magnetite by thermal decomposition of iron choline citrate. *Journal of Alloys and Compounds* **2002,** *334*, 304-312.

42. Narasimhan, B. R. V.; Prabhakar, S.; Manohar, P.; Gnanam, F. D. Synthesis of gamma ferric oxide by direct thermal decomposition of iron carboxylate salts. *Materials Letters* **2002,** *52* (4-5), 295-300.

43. Yu, W. W.; Falkner, J. C.; Yavuz, C. T.; Colvin, V. L. Synthesis of monodisperse iron oxide nanocrystals by thermal decomposition of iron carboxylate salts. *Chem. Commun.* **2004,** *20*, 2306-2307.

44. Mahmoudi, M.; Sant, S.; Wang, B.; Laurent, S.; Sen, T. Superparamagnetic iron oxide nanoparticles (SPIONs): Development, surface modification and applications in chemotherapy. *Advanced Drug Delivery Reviews* **2010,** *63* (1-2), 24-46.

45. Inouye, K.; Endo, R.; Otsuka, Y.; Miyashiro, K.; Kaneko, K.; Ishikawa, T. Oxygenation of Ferrous-Ions in Reversed Micelle and Reversed Micro-Emulsion. *The Journal of Physical Chemistry* **1982,** *86* (8), 1465-1469.

46. Muller, B. W.; Muller, R. H. Particle-size distributions and particle-size alterations in microemulsions. *Journal of Pharmaceutical Sciences* **1984,** *73* (7), 919-922.

47. Sun, S.; Zeng, H. Size-Controlled Synthesis of Magnetite Nanoparticles. *J. Am. Chem. Soc.* **2002,** *124*, 8204-8205.

48. Wang, X.; Peng, Q.; Li, Y. A General Strategy for Nanocrystal Synthesis. *Nature* **2005,** *437*, 121-124.

49. Khollam, Y. B.; Dhage, S. R.; Potdar, H. S.; Deshpande, S. B.; Bakare, P. P.; Kulkarni, S. D.; Date, S. K. Microwave hydrothermal preparation of submicron-sized spherical magnetite (Fe_3O_4) powders. *Materials Letters* **2002,** *56* (4), 571-577.

50. Vijayakumar, R.; Koltypin, Y.; Felner, I.; Gedanken, A. Sonochemical Synthesis and Characterization of Pure Nanometer-Sized Fe_3O_4 Particles. *Mater. Sci. Eng.* **2000,** *286*, 101.

51. Amemiya, Y.; Arakaki, A.; Staniland, S. S.; Tanaka, T.; Matsunaga, T. Controlled formation of magnetite crystal by partial oxidation of ferrous hydroxide in the presence of recombinant magnetotactic bacterial protein Mms6. *Biomaterials* **2007,** *28* (35), 5381-5389.

52. Coker, V. S.; Telling, N. D.; van der Laan, G.; Pattrick, R. A. D.; Pearce, C. I.; Arenholz, E.; Tuna, F.; Winpenny, R. E. P.; Lloyd, J. R. Harnessing the extracellular bacterial production of nanoscale cobalt ferrite with exploitable magnetic properties. *ACS Nano* **2009,** *3* (7), 1922-1928.

53. Bharde, A.; Rautaray, D.; Bansal, V.; Ahmad, A.; Sarkar, I.; Yusuf, S. M.; Sanyal, M.; Sastry, M. Extracellular biosynthesis of magnetite using fungi. *Small* **2006,** *2* (1), 135-141.

54. Itoh, H.; Sugimoto, T. Systematic control of size, shape, structure, and magnetic properties of uniform magnetite and maghemite particles. *Journal of Colloid and Interface Science* **2003,** *265* (2), 283-295.

55. Pascal, C.; Pascal, J. L.; Favier, F.; Moubtassim, M. L. E.; Payen, C. Electrochemical synthesis for the control of γ-Fe_2O_3 nanoparticle size.Morphology,microstructure, and magnetic behavior. *Chem. Mater.* **1999,** *11* (1), 141-147.

56. Stark, W. J.; Pratsinis, S. E. Aerosol Flame Reactors for Manufacture of Nanoparticles. *Powder Technology* **2002,** *126* (2), 103-108.

57. Salavati-Niasari, M.; Javidi, J.; Dadkhah, M. Ball Milling Synthesis of Silica Nanoparticle form Rice Husk Ash for Drug Delivery Application. *Comb Chem High Throughput Screen* **2012,** *Epub Ahead of Print*.

58. Kim, J. H.; Sohn, Y.; Kim, I.; Han, B.; Shin, W. G. Electron Beam Assisted Gas Phase Synthesis of SiO_2 Nanoparticles in an Ambient Condition. *Aerosol and Air Quality Research* **2012,** *12*, 1467-1471.

59. Kobayashi, Y.; Horie, M.; Konno, M.; Rodriguez-Gonzalez, B.; Liz-Marzan, L. M. Preparation and properties of silica-coated cobalt nanoparticles. *J. Phys. Chem. B.* **2003,** *107*, 7420-7425.

60. Lu, A.-H.; Li, W.; Matoussevich, N.; Spliethoff, B.; Bonneman, H.; Schuth, F. Highly stable carbon-protected cobalt nanoparticles and graphite shells. *Chem. Commun.* **2005,** *98* (1), 98-100.

61. Sobal, N. S.; Hilgendorff, M.; Moehwald, H.; Giersig, M.; Spasova, M.; Radetic, T.; Farle, M. Synthesis and Structure of Colloidal Bimetallic Nanocrystals: The Non-Alloying System Ag/Co. *Nano Letters* **2002,** *2*, 621-624.

62. Liu, Q.; Xu, Z.; Finch, A. J.; Egerton, R. A novel two-step silica-coating process for engineering magnetic nanocomposites. *Chem. Mater.* **1998,** *10*, 3936-3940.

63. Liu, X.; Guan, Y.; Ma, Z.; Liu, H. Surface modification and characterization of magnetic polymer nanospheres prepared by microemulsion polymerization. *Langmuir* **2004,** *20*, 10278-10282.

64. Hong, R.; Fischer, N. O.; Emrick, T.; Rotello, V. M. Surface PEGylation and Ligand Exchange Chemistry of FePt Nanoparticles for Biological Applications. *Chem. Mater.* **2005,** *17*, 4617-4621.

65. Stober, W.; Fink, A.; Bohn, E. Controlled growth of monodisperse silica spheres in the micron size range . *Journal of Colloid and Interface Science* **1968,** *26* (1), 62-69.

66. Rother, D.; Sen, T.; East, D.; Bruce, I. J. Silicon, silica and its surface patterning/activation with alkoxy- and amino-silanes for nanomedical applications. *Nanomedicine* **2011,** *6*, 281-300.

67. van Ewijk, G. A.; Vroege, G. J.; Philipse, A. P. Convenient Preparation Methods for Magnetic Colloids. *Journal of Magnetism and Magnetic Materials* **1999,** *201*, 31-33.

68. Deng, Y. H.; Wang, C.-C.; Hu, J.-H.; Yang, W.-L.; Fu, S.-K. Investigation of formation of silica-coated magnetite nanoparticles *via* sol-gel approach. *Colloids and Surfaces A: Phtsiochem. Eng. Aspects* **2005,** *262*, 87-93.

69. Slowing, I. I.; Vivero-Escoto, J. L.; Wu, C.-W.; Lin, V. S. Y. Mesoporous silica nanoparticles as controlled release drug delivery and gene transfection carriers. *Advanced Drug Delivery Reviews* **2008,** *60*, 1278-1288.

70. Gupta, A. K.; Wells, S. Surface-modified superparamagnetic nanoparticles for drug delivery: preparation, characterization, and cytotoxicity studies. *IEEE Transactions on Nanobioscience* **2004,** *3* (1), 66-73.

71. Wu, P.; Zhu, J.; Xu, Z. Template-Assisted Synthesis of Mesoporous Magnetic Nanocomposite Particles. *Advanced Functional Materials* **2004,** *14* (4), 345-351.

72. Zhao, W.; Gu, J.; Zhang, L.; Chen, H.; Shi, J. Fabrication of Uniform Magnetic Nanocomposite Spheres with a Magnetic Core/Mesoporous Silica Shell Structure. *J. Am. Chem. Soc.* **2005,** *127*, 8916-8917.

73. Sen, T.; Sebastianelli, A.; Bruce, I. J. Mesoporous Silica−Magnetite Nanocomposite: Fabrication and Applications in Magnetic Bioseparations. *J. Am. Chem. Soc.* **2006,** *128* (22), 7130-7131.

74. Deng, Y.; Deng, C.; Qi, D.; Liu, C.; Liu, J.; Zhang, X.; Zhao, D. Synthesis of Core/Shell Colloidal Magnetic Zeolite Microspheres for the Immobilization of Trypsin. *Advanced Materials* **2009,** *21* (13), 1377-1382.

75. Vogelstein, B.; Gillespie, D. Preparative and Analytical Purification of DNA from Agarose. *Proc. Natl. Acad. Sci. USA* **1979,** *76* (2), 615-619.

76. Taylor, J. I.; Hurst, C. D.; Davies, M. J.; Sachsinger, N.; Bruce, I. J. Application of magnetite and silica-magnetite composites to the isolation of genomic DNA. *Journal of Chromatography A* **2000,** *890* (1), 159-166.

77. Goloub, T. P.; Koopal, L. K.; Bijsterbosch, B. H.; Sidorova, M. P. Adsorption of Cationic Surfactants on Silica. Surface Charge Effects. *Langmuir* **1996,** *12* (13), 3188-3194.

78. Melzak, K. A.; Sherwood, C. S.; Turner, R. F. B.; Haynes, C. A. Driving Forces for DNA Adsorption to Silica in Perchlorate Solutions. *Journal of Colloid and Interface Science* **1996,** *181* (2), 635-644.

79. Deng, Y.; Qi, D.; Deng, C.; Zhang, X.; Zhao, D. Superparamagnetic High-Magnetization Microspheres with an Fe_3O_4@SiO_2 Core and Perpendicularly Aligned Mesoporous SiO_2 Shell for Removal of Microcystins. *J. Am. Chem. Soc.* **2007,** *130* (1), 28-29.

80. Bruce, I. J.; Sen, T. Surface Modification of Magnetic Nanoparticles with Alkoxysilanes and Their Application in Magnetic Bioseparations. *Langmuir* **2005,** *21*, 7029-7035.

81. Huang, C.; Hu, B. Silica-coated magnetic nanoparticles modified with γ-mercaptopropyltrimethoxysilane for fast and selective solid phase extraction of trace amounts of Cd, Cu, Hg, and Pb in environmental and biological samples prior to their determination by inductively coupled plasma mass spectrometry. *Spectrochimica Acta Part B: Atomic Spectroscopy* **2008,** *63* (3), 437-444.

82. Antochshuk, V.; Jaroniec, M. 1-Allyl-3-propylthiourea modified mesoporous silica for mercury removal. *Chem. Commun.* **2002,** (3), 258-259.

83. Hultberg, B.; Andersson, A.; Isaksson, A. Alterations of tiol metabolism in human cell lines induced by low amounts of copper, mercury or cadmium ions. *Toxicology* **1998,** *126* (3), 203-212.

84. Zhao, J.; Li, Y.; Guo, H.; Gao, L. Relative surface density and stability of the amines on the biochip. *Chinese Journal of Analytical Chemistry* **2006,** *34* (9), 1235-1238.

85. Metwalli, E.; Haines, D.; Becker, O.; Conzone, S.; Pantano, C. G. Surface characterizations of mono-, di-, and tri-aminosilane treated glass substrates. *Journal of Colloid and Interface Science* **2006,** *298* (2), 825-831.

86. De Waterbeemd, M. V.; Sen, T.; Biagini, S.; Bruce, I. J. Surface functionalisation of magnetic nanoparticles: Quantification of surface to bulk amine density. *Micro & Nano Letters, IET* **2010,** *5* (5), 282-285.

87. Sen, T.; Bruce, I. J. Surface engineering of nanoparticles in suspension for particle based bio-sensing. *Sci. Rep.* **2012,** *2*.

88. Moon, J. H.; Shin, J. W.; Kim, S. Y.; Park, J. W. Formation of Uniform Aminosilane Thin Layers: An Imine Formation To Measure Relative Surface Density of the Amine Group. *Langmuir* **1996,** *12* (20), 4621-4624.

89. Sen, T.; Bruce, I. J. A generalized approach for the surface engineering of nanoparticles in suspension for highly efficient hybrid capture of bio-molecules. In *Nanotechnology 2010: Advanced Materials, CNTs, Particles, Films and Composites*, CRC press, Taylor & Francis group.: 2010; pp 596-599.

90. Nakajima, N.; Ikada, Y. Mechanism of Amide Formation by Carbodiimide for Bioconjugation in Aqueous Media. *Bioconjugate Chem.* **1995,** *6* (1), 123-130.

91. Hermanson, G. T. Zero-Length Crosslinkers. In *Bioconjugate Techniques*, 3 ed.; Hermanson, G. T., Ed.; Academic Press, Elsevier: London, UK, 2013; pp 259-274.

92. Ducker, R. E.; Montague, M. T.; Leggetta, G. J. A Comparative investigation for methods for protein immobilization on self-assembled monolayers using glutaraldehyde, carbodiimide and anhydride reagents. *Biointerphases* **2008,** *3* (3), 59-65.

93. Jones, M. M.; Williams, J. M. J. Dynamic kinetic resolution in the hydrolysis of an alpha-bromo ester. *Chem. Commun.* **1998,** *22*, 2519-2520.

94. Kim, J.; Lee, J.; Na, H.–B.; Kim, B.-C.; Youn, J.–K.; Kwak, J.–H.; Moon, K.; Lee, E.; Kim, J.; Park, J.; Dohnalkova, A.; Park, H.–G.; Gu, M.–B.; Chang, H.–N.; Grate, J.–W.; Hyeon, T. A Magnetically Separable, Highly Stable Enzyme System Based on Nanocomposites of Enzymes and Magnetic Nanoparticles Shipped in Hierarchically Ordered, Mesocellular, Mesoporous Silica. *Small* **2005,** *1* (12), 1203-1207.

95. López-Gallego, F.; Betancor, L.; Mateo, C.; Hidalgo, A.; Alonso-Morales, N.; Dellamora-Ortiz, G.; Guisán; J.M.; Fernández-Lafuente, R. Enzyme stabilization by glutaraldehyde crosslinking of adsorbed proteins on aminated supports. *Journal of Biotechnology* **2005,** *119* (1), 70-75.

96. Fernández-Lafuente, R.; Rosell, C. M.; Rodriguez, V.; Guisán, J. M. Strategies for enzyme stabilization by intramolecular crosslinking with bifunctional reagents. *Enzyme and Microbial Technology* **1995,** *17* (6), 517-523.

97. Kennedy, J. F.; Kalogerakis, B.; Cabral, J. M. S. Surface immobilization and entrapping of enzymes on glutaraldehyde crosslinked gelatin particles. *Enzyme and Microbial Technology* **1984,** *6* (3), 127-131.

98. Zhou, Q. Z. K.; Dong Chen, X. Immobilization of β-galactosidase on graphite surface by glutaraldehyde. *Journal of Food Engineering* **2001,** *48* (1), 69-74.

99. Sen, T. Novel Nanocomposites: Hierarchically Ordered Porous Silica for the Immobilisation of Enzyme as Bio-catalyst. In *NSTI-Nanotech 2010*, CRC Press, Taylor & Francis Group: 2010; pp 784-787.

100. Sen, T.; Bruce, I. J.; Mercer, T. Fabrication of novel hierarchically ordered porous magnetic nanocomposites for bio-catalysis. *Chem. Commun.* **2010,** *46* (36), 6807-6809.

101. Alvaro, G.; Blanco, R. M.; Fernandez-Lafuente, R.; Guisán, J. M. Immobilization-Stabilization of Penicillin G Acylase from *Escherichia Coli*. *Appl. biochem. Biotechnol.* **1990,** *26*, 210-214.

102. Pedroche, J.; Yust, M. M.; Giron-Calle, J.; Vioque, J.; Alaiz, M.; Mateo, C.; et al. Stabilization–immobilization of carboxypeptidase a to aldehyde-agarose gels. A practical example in the hydrolysis of casein. *Enzyme and Microbial Technology* **2002,** *31*, 711-718.

103. Fernández-Lafuente, R.; Cowan, D. A.; Wood, A. N. P. Hyperstabilization of a Thermophilic Esterase by Multipoint Covalent Attachment. *Enzyme and Microbial Technology* **1995,** *17*, 366-372.

104. Mateo, C.; Palomo, J. M.; Fuentes, M.; Betancor, L.; Grazu, V.; López-Gallego, F.; Pessela, B. C. C.; Hidalgo, A.; Hidalgo, A.; Hernández-Lorente, G.; Fernández-Lafuente, R.; Guisán, J. M. Glyoxyl agarose: A fully inert and hydrophilic support for immobilization and high stabilization of proteins. *Enzyme and Microbial Technology* **2006,** *39* (2), 274-280.

105. Silverman, R. B. Enzymes As Catalysts. In *The Organic Chemistry of Enzyme-Catalyzed Reactions*, Revised ed.; Academic Press: 2002; pp 1-38.

106. Schramm, V. L. Enzymatic Transition States and Transition State Analog Design. *Annu. Rev. Biochem.* **1998,** *67*, 693-720.

107. Hunter, T. Protein Kinases and Phosphatases: The Yin and Yang of Protein Phosphorylation and Signaling. *Cell* **1995,** *80* (2), 225-236.

108. Berg, J. S.; Powell, B. C.; Cheney, R. E. A millenial Myosin Consensus. *Mol Biol Cell* **2001,** *12* (4), 780-794.

109. Chiu, T. K.; Davies, D. R. Structure and Function of HIV-1 Integrase. *Curr Top Med Chem* **2004,** *4* (9), 965-977.

110. von Itzstein, M. The War Against Influenza: Discovery and Development of Sialidase Inhibitors. *Nature Reviews Drug Discovery* **2007,** *6*, 967-974.

111. Ellis, R. J. The Most Abundant Protein in the World. *Trends in Biochemical Sciences* **1979,** *4* (11), 241-244.

112. Rogers, R. S. Companies Turn To Biocatalysis. *Chemical & Engineering News* **1999,** *77* (29), 87-91.

113. Roberts, S. M. Preparative biotransformations. *J. Chem. Soc. , Perkin Trans. 1* **2000,** (5), 611-633.

114. Cipiciani, A.; Cittadini, M.; Fringuelli, F. Improving the enantioselectivity of *Candida rugosa* lipase in the kinetic resolution of racemic methyl 2-(2,4-dichlorophenoxy)propionate. *Tetrahedron* **1998,** *54* (27), 7883-7890.

115. Katayama, S.; Ae, N.; Nagata, R. Enzymatic resolution of 2-substituted tetrahydroquinolines. Convenient approaches to tricyclic quinoxalinediones as potent NMDA-glycine antagonists. *Tetrahedron: Asymmetry* **1998,** *9* (24), 4295-4299.

116. Chillemi, R.; Russo, D.; Sciuto, S. Chemoenzymatic Synthesis of Lysophosphatidylnucleosides. *The Journal of Organic Chemistry* **1998,** *63* (10), 3224-3229.

117. Ferraboschi, P.; Rezaelahi, S.; Verza, E.; Santaniello, E. Lipase-catalyzed resolution of stereogenic centers in steroid side chains by transesterification in organic solvents: the case of a 26-hydroxycholesterol. *Tetrahedron: Asymmetry* **1998,** *9* (13), 2193-2196.

118. Yoshida, N.; Kamikubo, T.; Ogasawara, K. Lipase-mediated kinetic resolution of a synthetic equivalent of 2-hydroxymethylcyclopentadien-5-ol. *Tetrahedron: Asymmetry* **1998,** *9* (18), 3325-3329.

119. Aitken, J.; Grogan, G.; Chow, Y.; Turner, J.; Flitsch, L. Biohydroxylations of Cbz-protected alkyl substituted piperidines by *Beauveria bassiana* ATCC 7159. *J. Chem. Soc. , Perkin Trans. 1* **1998,** (20), 3365-3370.

120. Fritz-Langhals, E.; Kunath, B. Synthesis of aromatic aldehydes by laccase-mediator assisted oxidation. *Tetrahedron Letters* **1998,** *39* (33), 5955-5956.

121. Pchelka, K.; Gelo-Pujic, M.; Guibe-Jampel, E. Chemoenzymatic autocatalytic Baeyer-Villiger oxidation. *J. Chem. Soc. , Perkin Trans. 1* **1998,** (17), 2625-2628.

122. Han, S.; Lin, G.; Li, Z. Synthesis of (R)-cyanohydrins by crude (R)-oxynitrilase-catalyzed reactions in micro-aqueous medium. *Tetrahedron: Asymmetry* **1998,** *9* (11), 1835-1838.

123. Sheflyan, G. Y.; Howe, D. L.; Wilson, T. L.; Woodard, R. W. Enzymatic Synthesis of 3-Deoxy-d-manno-octulosonate 8-Phosphate, 3-Deoxy-d-altro-octulosonate 8-Phosphate, 3,5-Dideoxy-d-gluco(manno)-octulosonate 8-Phosphate by 3-Deoxy-d-arabino-heptulosonate 7-Phosphate Synthase. *J. Am. Chem. Soc.* **1998,** *120* (43), 11027-11032.

124. Bisht, K. S.; Deng, F.; Gross, R. A.; Kaplan, D. L.; Swift, G. Ethyl Glucoside as a Multifunctional Initiator for Enzyme-Catalyzed Regioselective Lactone Ring-Opening Polymerization. *J. Am. Chem. Soc.* **1998,** *120* (7), 1363-1367.

125. Yuan, D. Q.; Dong, S. D.; Breslow, R. Cyclodextrin-based class I aldolase enzyme mimics to catalyze crossed aldol condensations. *Tetrahedron Letters* **1998,** *39* (42), 7673-7676.

126. Jaeger, K. E.; Ransac, S.; Dijkstra, B. W.; Colson, C.; van Heuvel, M.; Misset, O. Bacterial lipases. *FEMS Microbiology Reviews* **1994,** *15* (1), 29-63.

127. Gilbert, E. J. *Pseudomonas* lipases: Biochemical properties and molecular cloning. *Enzyme and Microbial Technology* **1993,** *15* (8), 634-645.

128. Turcu, M. C. Lipase-Catalyzed Approaches Towards Secondary Alcohols: Intermediates For Enantiopure Drugs. University of Turku, Finland, 2010.

129. Heck, A. M.; Yanovski, J. A.; Calis, K. A. Orlistat, a New Lipase Inhibitor for the Management of Obesity. *Pharmacotherapy: The Journal of Human Pharmacology and Drug Therapy* **2000,** *20* (3), 270-279.

130. Gupta, R.; Gupta, N.; Rathi, P. Bacterial Lipases: An Overview of Production, Purification and Biochemical Properties. *Applied Microbiology and Biotechnology* **2004,** *64* (6), 763-781.

131. Ollis, D. L.; Cheah, E.; Cygler, M.; Dijkstra, B.; Frolow, F.; Franken, S. M.; Harel, M.; Remington, S. J.; Silman, I.; Schrag, J.; Sussman, J. L.; Verschueren, K. H. G.; Goldman, A. The α/β Hydrolase Fold. *Protein Engineering* **1992,** *5* (3), 197-211.

132. Jaeger , K. E.; Dijkstra, B. W.; Reetz, M. T. Bacterial Biocatalysts: Molecular Biology, Three-Dimensional Structures and Biotechnological Applications of Lipases. *Annu. Rev. Microbiol.* **1999,** *53*, 315-351.

133. Pascale, D.; Cusano, A.; Autore, F.; Parrilli, E.; Prisco, G.; Marino, G.; Tutino, M. L. The cold-active Lip1 lipase from the Antarctic bacterium *Pseudoalteromonas haloplanktis* TAC125 is a member of a new bacterial lipolytic enzyme family. *Extremophiles* **2008,** *12* (3), 311-323.

134. Akoh, C. C.; Lee, G. C.; Liaw, Y. C.; Huang, T. H.; Shaw, J. F. GDSL family of serine esterases/lipases. *Progress in Lipid Research* **2004,** *43* (6), 534-552.

135. Nardini, M.; Dijkstra, B. W. α/β Hydrolase fold enzymes: the family keeps growing. *Curr Opin Struct Biol.* **1999,** *9* (6), 732-737.

136. Yahya, A. R. M.; Anderson, W. A.; Moo-Young, M. Ester synthesis in lipase-catalyzed reactions. *Enzyme and Microbial Technology* **1998,** *23* (7–8), 438-450.

137. Hanefield, U.; Gardossi, L.; Magner, E. Understanding enzyme immobilisation. *Chemical Society Reviews* **2009,** *38*, 453-468.

138. Reis, P.; Holmberg, K.; Watzke, H.; Leser, M. E.; Miller, R. Lipases at Interfaces: A Review. *Advances in Colloid and Interface Science* **2009,** *147-148*, 237-250.

139. Schmid, R. D.; Verger, R. Lipases: Interfacial Enzymes with Attractive Applications. *Angewandte Chemie International Edition* **1998,** *37* (12), 1608-1633.

140. Hasan, F.; Shah, A. A.; Hameed, A. Industrial applications of microbial lipases. *Enzyme and Microbial Technology* **2006,** *39* (2), 235-251.

141. Demain, A. L. Overproduction of microbial metabolites and enzymes due to alteration of regulation. In *Advances in Biochemical Engineering, Volume 1*, 1 ed.; Springer Berlin Heidelberg: 1971; pp 113-142.

142. Arpigny, J. L.; Jaeger, K. E. Bacterial lipolytic enzymes: classification and properties. *Biochem. J.* **1999,** *343* (1), 177-183.

143. Murty, V. R.; Bhat, J.; Muniswaran, P. K. A. Hydrolysis of Oils by Using Immobilized Lipase Enzyme: A Review. *Biotechnol. Bioprocess. Eng.* **2002,** *7*, 57-66.

144. Gandhi, N. Applications of lipase. *J Amer Oil Chem Soc* **1997,** *74* (6), 621-634.

145. Sharma, R.; Chisti, Y.; Banerjee, U. C. Production, Purification, Characterization, and Applications of Lipases. *Biotechnology Advances* **2001,** *19*, 627-662.

146. Berglund, P. Controlling lipase enantioselectivity for organic synthesis. *Biomolecular Engineering* **2001,** *18* (1), 13-22.

147. Lalonde, J. J.; Govardhan, C.; Khalaf, N.; Martinez, A. G.; Visuri, K.; Margolin, A. L. Cross-Linked Crystals of *Candida rugosa* Lipase: Highly Efficient Catalysts for the Resolution of Chiral Esters. *J. Am. Chem. Soc.* **1995,** *117* (26), 6845-6852.

148. Margolin, A. L. Novel crystalline catalysts. *Trends in Biotechnology* **1996,** *14* (7), 223-230.

149. Kim, M. G.; Lee, E. G.; Chung, B. H. Improved enantioselectivity of *Candida rugosa* lipase towards ketoprofen ethyl ester by a simple two-step treatment. *Process Biochemistry* **2000,** *35* (9), 977-982.

150. Colton, I. J.; Ahmed, S. N.; Kazlauskas, R. J. A 2-Propanol Treatment Increases the Enantioselectivity of *Candida rugosa* Lipase toward Esters of Chiral Carboxylic Acids. *The Journal of Organic Chemistry* **1995,** *60* (1), 212-217.

151. Okahata, Y.; Mori, T. Lipid-coated enzymes as efficient catalysts in organic media. *Trends in Biotechnology* **1997,** *15* (2), 50-54.

152. Giorno, L.; Drioli, E. Biocatalytic membrane reactors: applications and perspectives. *Trends in Biotechnology* **2000,** *18* (8), 339-349.

153. Lotti, M.; Tramontano, A.; Longhi, S.; Fusetti, F.; Brocca, S.; Pizzi, E.; Alberghina, L. Variability within the *Candida rugosa* Upases family. *Protein Engineering* **1994,** *7* (4), 531-535.

154. Benjamin, S.; Pandey, A. *Candida rugosa* lipases: Molecular biology and versatility in biotechnology. *Yeast* **1998,** *14* (12), 1069-1087.

155. Grochulski, P.; Li, Y.; Schrag, J. D.; Bouthillier, F.; Smith, P.; Harrison, D.; Rubin, B.; Cygler, M. Insights into interfacial activation from an open structure of *Candida rugosa* lipase. *Journal of Biological Chemistry* **1993,** *268* (17), 12843-12847.

156. Monecke, P.; Friedemann, R.; Naumann, S.; Csuk, R. Molecular Modelling Studies on the Catalytic Mechanism of *Candida rugosa* Lipase. *J Mol Model* **1998,** *4* (12), 395-404.

157. Zhang, A.; Gao, R.; Diao, N.; Xie, G.; Gao, G.; Cao, S. Cloning, expression and characterization of an organic solvent tolerant lipase from *Pseudomonas fluorescens* JCM5963. *Journal of Molecular Catalysis B: Enzymatic* **2009,** *56* (2–3), 78-84.

158. Salis, A.; Bhattacharyya, M. S.; Monduzzi, M.; Solinas, V. Role of the support surface on the loading and the activity of *Pseudomonas fluorescens* lipase used for biodiesel synthesis. *Journal of Molecular Catalysis B: Enzymatic* **2009,** *57* (1–4), 262-269.

159. Fernández-Lorente, G.; Palomo, J. M.; Fuentes, M.; Mateo, C.; Guisán, J. M.; Fernández-Lafuente, R. Self-assembly of *Pseudomonas fluorescens* lipase into bimolecular aggregates dramatically affects functional properties. *Biotechnology and Bioengineering* **2003,** *82* (2), 232-237.

160. Schrag, J. D.; Li, Y.; Cygler, M.; Lang, D.; Burgdorf, T.; Hecht, H. J.; Schmid, R.; Schomburg, D.; Rydel, T. J.; Oliver, J. D.; Strickland, L. C.; Dunaway, C. M.; Larson, S. B.; Day, J.; McPherson, A. The open conformation of a *Pseudomonas* lipase. *Structure* **1997,** *5* (2), 187-202.

161. Reetz, M. T.; Jaeger, K. E. Overexpression, immobilization and biotechnological application of *Pseudomonas* lipases. *Chemistry and Physics of Lipids* **1998,** *93* (1–2), 3-14.

162. Cadirci, B. H.; Yasa, I. An organic solvents tolerant and thermotolerant lipase from *Pseudomonas fluorescens* P21. *Journal of Molecular Catalysis B: Enzymatic* **2010,** *64* (3–4), 155-161.

163. Burini, J. F.; Gugi, B.; Merieau, A.; Guespin-Michel, J. F. Lipase and acidic phosphatase from the psychrotrophic bacterium *Pseudomonas fluorescens*: Two enzymes whose synthesis is regulated by the growth temperature. *FEMS Microbiology Letters* **1994,** *122* (1–2), 13-18.

164. Kojima, Y.; Yokoe, M.; Mase, T. Purification and Characterization of an Alkaline Lipase from *Pseudomonas fluorescens* AK102. *Bioscience, Biotechnology, and Biochemistry* **1994,** *58* (9), 1564-1568.

165. Kojima, Y.; Shimizu, S. Purification and characterization of the lipase from *Pseudomonas fluorescens* HU380. *Journal of Bioscience and Bioengineering* **2003,** *96* (3), 219-226.

166. Kim, K. R.; Kwon, D. Y.; Yoon, S. H.; Kim, W. Y.; Kim, K. H. Purification, refolding, and characterization of recombinant *Pseudomonas fluorescens* lipase. *Protein Expression and Purification* **2005,** *39* (1), 124-129.

167. Sugiura, M.; Oikawa, T. Physicochemical properties of a lipase from *Pseudomonas fluorescens*. *Biochim Biophys Acta* **1977,** *489* (2), 262-268.

168. Hoshino, T.; Yamana, T.; Shimizu, S. Selective Hydrolyis of Fish Oil by Lipase to Concentrate *n-3* Polyunsaturated Fatty Acids. *Agric. Biol. Chem.* **1989,** *54* (6), 1459-1467.

169. Hedström, G.; Backlund, M.; Slotte, J. P. Enantioselective synthesis of ibuprofen esters in AOT/isooctane microemulsions by *Candida cylindracea* lipase. *Biotechnol. Bioeng.* **1993,** *42* (5), 618-624.

170. Garcia, H. S.; Malcata, F. X.; Hill, J.; Amundson, C. H. Use of *Candida rugosa* lipase immobilized in a spiral wound membrane reactor for the hydrolysis of milkfat. *Enzyme and Microbial Technology* **1992,** *14* (7), 535-545.

171. Guit, R. P. M.; Kloosterman, M.; Meindersma, G. W.; Mayer, M.; Meijer, E. M. Lipase kinetics: Hydrolysis of triacetin by lipase from *Candida cylindracea* in a hollow-fiber membrane reactor. *Biotechnol. Bioeng.* **1991,** *38* (7), 727-732.

172. Seino, H.; Uchibori, T.; Nishitani, T.; Inamasu, S. Enzymatic synthesis of carbohydrate esters of fatty acid (I) esterification of sucrose, glucose, fructose and sorbitol. *J Am Oil Chem Soc* **1984,** *61* (11), 1761-1765.

173. Ikeda, I.; Tanaka, J.; Suzuki, K. Synthesis of acrylic esters by lipase. *Tetrahedron Letters* **1991,** *32* (47), 6865-6866.

174. Tsai, S. W.; Wu, G. H.; Chiang, C. L. Kinetics of enzymatic hydrolysis of olive oil in biphasic organic-aqueous systems. *Biotechnol. Bioeng.* **1991,** *38* (7), 761-766.

175. Sonnet, P.; Baillargeon, M. Methyl-branched octanoic acids as substrates for lipase-catalyzed reactions. *Lipids* **1991,** *26* (4), 295-300.

176. Uemura, A.; Nozaki, K.; Yamashita, J. i.; Yasumoto, M. Regioselective deprotection of 3',5'-O-acylated pyrimidine nucleosides by lipase and esterase. *Tetrahedron Letters* **1989,** *30* (29), 3819-3820.

177. WELSH, F. W.; WILLIAMS, R. E.; DAWSON, K. H. Lipase Mediated Synthesis of Low Molecular Weight Flavor Esters. *Journal of Food Science* **1990,** *55* (6), 1679-1682.

178. Yamane, T.; Kojima, Y.; Ichiryu, T.; Nagata, M.; Shimizu, S. Intramolecular esterification by lipase powder in microaqueous benzene: Effect of moisture content. *Biotechnol. Bioeng.* **1989,** *34* (6), 838-843.

179. Uemura, A.; Nozaki, K.; Yamashita, J. i.; Yasumoto, M. Lipase-catalyzed regioselective acylation of sugar moieties of nucleosides. *Tetrahedron Letters* **1989,** *30* (29), 3817-3818.

180. Xier, Z. F.; Sakai, K. Preparation of a chiral building block based on 1,3-syn-diol using *Pseudomonas fluorescens* lipase and its application to the synthesis of a hunger modulator. *Chem. Pharm. Bull.* **1989,** *37*, 1650-1652.

181. Nguyen, B. V.; Hedenström, E. *Candida rugosa* lipase as an enantioselective catalyst in the esterification of methyl branched carboxylic acids: resolution of rac-3,7-dimethyl-6-octenoic acid (citronellic acid). *Tetrahedron: Asymmetry* **1999,** *10* (9), 1821-1826.

182. SalgIn, U.; SalgIn, S.; Serpil, T. The enantioselective hydrolysis of racemic naproxen methyl ester in supercritical CO_2 using *Candida rugosa* lipase. *The Journal of Supercritical Fluids* **2007,** *43* (2), 310-316.

183. Lohith, K.; Divakar, S. *Candida rugosa* lipase catalysed preparation of L-prolyl, L-phenylalanyl, L-tryptophanyl and L-histidyl esters of carbohydrates. *Biochemical Engineering Journal* **2007,** *34* (1), 28-43.

184. Persichetti, R. A.; Lalonde, J. J.; Govardhan, C. P.; Khalaf, N. K.; Margolin, A. L. *Candida rugosa* lipase: Enantioselectivity enhancements in organic solvents. *Tetrahedron Letters* **1996,** *37* (36), 6507-6510.

185. Hedenström, E.; Edlund, H.; Lund, S. Stereoselective esterification of 2,6-dimethyl-1,7-heptanedioic acid, catalysed by *Candida rugosa* lipase. *Journal of Molecular Catalysis B: Enzymatic* **2003,** *23* (1), 53-59.

186. Knezovic, S.; Sunjic, V.; Lévai, A. Enantioselective hydrolysis of some 3-(2-nitrophenoxy) butanoates catalyzed by *Pseudomonas fluorescens* and *Pseudomonas sp.* lipase. *Tetrahedron: Asymmetry* **1993,** *4* (3), 313-320.

187. Kato, K.; Gong, Y.; Saito, T.; Yokogawa, Y. Enzymatic resolution of 2,2,2-trifluoro-1-arylethylamine derivatives by *Pseudomonas fluorescens* lipase in organic solvents. *Journal of Molecular Catalysis B: Enzymatic* **2004,** *30* (2), 61-68.

188. Brem, J.; Tosa, M. I.; Paizs, C.; Munceanu, A.; Matkovic-Calogovic, D.; Irimie, F. D. Lipase-catalyzed kinetic resolution of racemic 1-(10-alkyl-10H-phenothiazin-3-yl)ethanols and their butanoates. *Tetrahedron: Asymmetry* **2010,** *21* (16), 1993-1998.

189. Lin, G.; Midha, K. K.; Hawes, E. M. Synthesis of the piperidinone metabolites of piperidine type phenothiazine antipsychotic drugs *via* ruthenium tetroxide oxidation. *Journal of Heterocyclic Chemistry* **1991,** *28* (2), 215-219.

190. Kato, K.; Katayama, M.; Fujii, S.; Kimoto, H. Effective preparation of optically active 4,4,4-trifluoro-3-(indole-3-)butyric acid, a novel plant growth regulator, using lipase from *Pseudomonas fluorescens*. *Journal of Fermentation and Bioengineering* **1996,** *82* (4), 355-360.

191. Chakraborty, K.; Paul Raj, R. Selective enrichment of *n–3* polyunsaturated fatty acids with C18–20 acyl chain length from sardine oil using *Pseudomonas fluorescens* MTCC 2421 lipase. *Food Chemistry* **2009,** *114* (1), 142-150.

192. Hiratake, J.; Inagaki, M.; Nishioka, T.; Oda, J. Irreversible and highly enantioselective acylation of 2-halo-1-arylethanols in organic solvents catalyzed by a lipase from *Pseudomonas fluorescens*. *The Journal of Organic Chemistry* **1988,** *53* (26), 6130-6133.

193. Kalo, P.; Huotari, H.; Antila, M. *Pseudomonas fluorescens* Lipase-catalysed Interesterification of Butter Fat. *Fett/Lipid* **1989,** *91* (7), 276-281.

194. Grisenti, P.; Ferraboschi, P.; Manzocchi, A.; Santaniello, E. Enantioselective transesterification of 2-methyl-1,3-propanediol derivatives catalyzed by *Pseudomonas fluorescens* lipase in an organic solvent. *Tetrahedron* **1992,** *48* (18), 3827-3834.

195. Dahlan, I.; Harun, A.; Najafpour, G. D. Free *Candida rugosa* Lipase-Catalyzed Synthesis of Citronelly Butyrate in *n*-Hexane By Direct Esterification: Effect of Reaction Parameters. *Jurnal Teknologi* **2009,** *50,* 29-40.

196. Xiong, J.; Huang, Y. J.; Zhang, H. Lipase-catalyzed transesterification synthesis of citronellyl acetate in a solvent-free system and its reaction kinetics. *Eur Food Res Technol* **2012,** *235* (5), 907-914.

197. Ma, F.; Hanna, M. A. Biodiels Production: A Review. *Bioresource Technology* **1999,** *70*, 1-15.

198. Fukuda, H.; Kondo, A.; Noda, H. Biodiesel fuel production by transesterification of oils. *Journal of Bioscience and Bioengineering* **2001,** *92* (5), 405-416.

199. Molinari, F.; Solange Cavenago, K.; Romano, A.; Romano, D.; Gandolfi, R. Enantioselective hydrolysis of (RS)-isopropylideneglycerol acetate with *Kluyveromyces marxianus*. *Tetrahedron: Asymmetry* **2004,** *15* (12), 1945-1947.

200. Sauvageot, N.; Gouffi, K.; Laplace, J. M.; Auffray, Y. Glycerol metabolism in *Lactobacillus collinoides*: production of 3-hydroxypropionaldehyde, a precursor of acrolein. *Int. J. Food Microbiol.* **2000,** *55* (1-3), 167-170.

201. Kaieda, M.; Samukawa, T.; Kondo, A.; Fukuda, H. Effect of Methanol and water contents on production of biodiesel fuel from plant oil catalyzed by various lipases in a solvent-free system. *Journal of Bioscience and Bioengineering* **2001,** *91* (1), 12-15.

202. Al-Zuhair, S. Production of biodiesel: possibilities and challenges. *Biofuels, Bioprod. Bioref.* **2007,** *1* (1), 57-66.

203. Fjerbaek, L.; Christensen, K. V.; Norddahl, B. A Review of the Current State of Biodiesel Production Using Enzymatic Transesterification. *Biotechnol. Bioeng.* **2008,** *102* (5), 1298-1315.

204. Chen, Y. Z.; Ching, C. B.; Xu, R. Lipase immobilization on modified zirconia nanoparticles: Studies on the effects of modifiers. *Process Biochemistry* **2009,** *44* (11), 1245-1251.

205. Clark, S. D. Characteristics of nearly dry enzymes in organic solvents: implications for biocatalysis in the absence of water. *Phil. Trans. R. Soc. Lond. B* **2004,** (359), 1299-1307.

206. Kitaguchi, H.; Fitzpatrick, P. A.; Huber, J. E.; Klibanov, A. M. Enzymic resolution of racemic amines: crucial role of the solvent. *J. Am. Chem. Soc.* **1989,** *111* (8), 3094-3095.

207. Dodson, G.; Verma, C. Protein flexibility: its role in structure and mechanism revealed by molecular simulations. *Cellular and Molecular Life Sciences* **2006,** *63* (2), 207-219.

208. Klibanov, A. M. Why are enzymes less active in organic solvents than in water? *Trends in Biotechnology* **1997,** *15* (3), 97-101.

209. Mateo, C.; Palomo, J. M.; Fernandez-Lorente, G.; Guisan, J. M.; Fernandez-Lafuente, R. Improvement of enzyme activity, stability and selectivity via immobilization techniques. *Enzyme and Microbial Technology* **2007,** *40* (6), 1451-1463.

210. Hidalgo, A.; Betancor, L.; Lopez-Gallego, F.; Moreno, R.; Berenguer, J.; Fernández-Lafuente, R.; Guisan, J. M. Design of an immobilized preparation of catalase from *Thermus thermophilus* to be used in a wide range of conditions.: Structural stabilization of a multimeric enzyme. *Enzyme and Microbial Technology* **2003,** *33* (2-3), 278-285.

211. Palomo, J. M.; Munoz, G.; Fernández-Lorente, G.; Mateo, C.; Fernandez-Lafuente, R.; Guisan, J. M. Interfacial adsorption of lipases on very hydrophobic support (octadecyl-Sepabeads): immobilization, hyperactivation and stabilization of the open form of lipases. *Journal of Molecular Catalysis B: Enzymatic* **2002,** *19-20*, 279-286.

212. Tardioli, P. W.; Fernandez-Lafuente, R.; Guisan, J. M.; uisan, J. M.; ordano, R. L. C. Design of New Immobilized-Stabilized Carboxypeptidase A Derivative for Production of Aromatic Free Hydrolysates of Proteins. *Biotechnol Progress* **2003,** *19* (2), 565-574.

213. Tardioli, P. W.; Pedroche, J.; Giordano, R. L. C.; Fernandez-Lafuente, R.; Guisan, J. M. Hydrolysis of Proteins by Immobilized-Stabilized Alcalase-Glyoxyl Agarose. *Biotechnol Progress* **2003,** *19* (2), 352-360.

214. Lie, E.; Molin, G. Hydrolysis and esterification with immobilized lipase on hydrophobic and hydrophilic zeolites. *Journal of Chemical Technology and Biotechnology* **1991,** *50* (4), 549-553.

215. Serralha, F. N.; Lopes, J. M.; Lemos, F.; Prazeres, D. M. F.; Aires-Barros, M. R.; Cabral, J. M. S.; Ramoa Ribeiro, F. Zeolites as supports for an enzymatic alcoholysis reaction. *Journal of Molecular Catalysis B: Enzymatic* **1998,** *4* (5-6), 303-311.

216. Xing, G. W.; Li, X. W.; Tian, G. L.; Ye, Y. H. Enzymatic Peptide Synthesis in Organic Solvent with Different Zeolites as Immobilization Matrixes. *Tetrahedron* **2000,** *56* (22), 3517-3522.

217. del Campo, A.; Sen, T.; Lellouche, J. P.; Bruce, I. J. Multifunctional magnetite and silica-magnetite nanoparticles: Synthesis, surface activation and applications in life sciences. *Journal of Magnetism and Magnetic Materials* **2005,** *293* (1), 33-40.

218. Karakus, E.; PekyardImcI, S. Immobilization of apricot pectinesterase (*Prunus armeniaca L.*) on porous glass beads and its characterization. *Journal of Molecular Catalysis B: Enzymatic* **2009,** *56* (1), 13-19.

219. Katsuragi, T.; Sakai, T.; Tonomura, K. Implantable enzyme capsules for cancer chemotherapy from bakers' yeast cytosine deaminase immobilized on epoxy-acrylic resin and urethane prepolymer. *Appl. biochem. Biotechnol.* **1987,** *16*, 61-69.

220. Hernandez, K.; Fernandez-Lafuente, R. Lipase B from *Candida antarctica* immobilized on octadecyl Sepabeads: A very stable biocatalyst in the presence of hydrogen peroxide. *Process Biochemistry* **2011,** *46* (4), 873-878.

221. Pessela, B. C. C.; Mateo, C.; Fuentes, M.; Vian, A.; Garcia, J. L.; Carrascosa, A. V.; Guisan, J. M.; Fernandez-Lafuente, R. The immobilization of a thermophilic β-galactosidase on Sepabeads supports decreases product inhibition: Complete hydrolysis of lactose in dairy products. *Enzyme and Microbial Technology* **2003,** *33* (2-3), 199-205.

222. Dyal, A.; Loos, K.; Noto, M.; Chang, S. W.; Spagnoli, C.; Shafi, K. V. P. M.; Ulman, A.; Cowman, M.; Gross, R. A. Activity of *Candida rugosa* Lipase Immobilized on γ-Fe_2O_3 Magnetic Nanoparticles. *J. Am. Chem. Soc.* **2003,** *125* (7), 1684-1685.

223. Palomo, J. M.; Fernández-Lorente, G.; Mateo, C.; Fuentes, M.; Fernández-Lafuente, R.; Guisan, J. M. Modulation of the enantioselectivity of *Candida antarctica B* lipase via conformational engineering. Kinetic resolution of (±)-α-hydroxy-phenylacetic acid derivatives. *Tetrahedron: Asymmetry* **2002,** *13* (12), 1337-1345.

224. Soylak, M.; Tuzen, M. Sorbent extraction of rubeanic acid-metal chelates on a new adsorbent: Sepabeads SP70. *Journal of Hazardous Materials* **2006,** *138* (1), 195-200.

225. Bommarius, A. S.; Karau, A. Deactivation of Formate Dehydrogenase (FDH) in Solution and at Gas-Liquid Interfaces. *Biotechnol Progress* **2005,** *21* (6), 1663-1672.

226. Cao, L. Immobilised enzymes: science or art? *Current Opinion in Chemical Biology* **2005,** *9* (2), 217-226.

227. Sheldon, R. A. Enzyme Immobilization: The Quest for Optimum Performance. *Adv. Synth. Catal.* **2007,** *349* (8-9), 1289-1307.

228. Lalonde, J.; Margolin, A. *Immobilization of Enzymes;* Wiley-VCH Verlag GmbH: 2002.pp. 163-184.

229. Brady, D.; Jordaan, J. Advances in enzyme immobilisation. *Biotechnology Letters* **2009,** *31* (11), 1639-1650.

230. St.Clair, N. L.; Navia, M. A. Cross-linked enzyme crystals as robust biocatalysts. *J. Am. Chem. Soc.* **1992,** *114* (18), 7314-7316.

231. Sheldon, R. A. Cross-linked enzyme aggregates (CLEAs): stable and recyclable biocatalysts. *Biochem. Soc. Trans.* **2007,** *35*, 1583-1587.

232. Sheldon, R. A.; Schoevaart, R.; Van Langen, L. M. Cross-linked enzyme aggregates (CLEAs): A novel and versatile method for enzyme immobilization (a review). *Biocatalysis and Biotransformation* **2005,** *23* (3-4), 141-147.

233. Brem, J.; Turcu, M. C.; Paizs, C.; Lundell, K.; Tosa, M.-L.; Irimie, F. D.; Kanerva, L. T. Immobilization to improve the properties of *Pseudomonas fluorescens* lipase for the kinetic resolution of 3-aryl-3-hydroxy esters. *Process Biochemistry* **2012,** *47* (1), 119-126.

234. de Lima, L. N.; Aragon, C. C.; Mateo, C.; Palomo, J. M.; Giordano, R. L. C.; Tardioli, P. W.; Guisan, J. M.; Fernandez-Lorente, G. Immobilization and stabilization of a bimolecular aggregate of the lipase from *Pseudomonas fluorescens* by multipoint covalent attachment. *Process Biochemistry* **2013,** *48* (1), 118-123.

235. Bolivar, J. M.; Wilson, L.; Ferrarotti, S. A.; Fernandez-Lafuente, R.; Guisan, J. M.; Mateo, C. Stabilization of a Formate Dehydrogenase by Covalent Immobilization on Highly Activated Glyoxyl-Agarose Supports. *Biomacromolecules* **2006,** *7* (3), 669-673.

236. Klibanov, A. M. Enzyme stabilization by immobilization. *Analytical Biochemistry* **1979,** *93*, 1-25.

237. Bolivar, J. M.; López-Gallego, F.; Godoy, C.; Rodrigues, D. S.; Rodrigues, R. C.; Batalla, P.; Rocha-Martin, J.; Mateo, C.; Giordano, R. L. C.; Guisan, J. M. The presence of thiolated compounds allows the immobilization of enzymes on glyoxyl agarose at mild pH values: New strategies of stabilization by multipoint covalent attachment. *Enzyme and Microbial Technology* **2009,** *45* (6-7), 477-483.

238. Nagayama, K.; Yamasaki, N.; Imai, M. Fatty acid esterification catalyzed by *Candida rugosa* lipase in lecithin microemulsion-based organogels. *Biochemical Engineering Journal* **2002,** *12* (3), 231-236.

239. Shao, P.; Meng, X.; He, J.; Sun, P. Analysis of immobilized *Candida rugosa* lipase catalyzed preparation of biodiesel from rapeseed soapstock. *Food and Bioproducts Processing* **2008,** *86* (4), 283-289.

240. Iso, M.; Chen, B.; Eguchi, M.; Kudo, T.; Shrestha, S. Production of biodiesel fuel from triglycerides and alcohol using immobilized lipase. *Journal of Molecular Catalysis B: Enzymatic* **2001,** *16* (1), 53-58.

241. Soumanou, M. M.; Bornscheuer, U. T. Improvement in lipase-catalyzed synthesis of fatty acid methyl esters from sunflower oil. *Enzyme and Microbial Technology* **2003,** *33* (1), 97-103.

242. Huang, L.; Cheng, Z. M. Immobilization of lipase on chemically modified bimodal ceramic foams for olive oil hydrolysis. *Chemical Engineering Journal* **2008,** *144* (1), 103-109.

243. Yu, D.; Wang, Z.; Zhao, L.; Cheng, Y.; Cao, S. Resolution of 2-octanol by SBA-15 immobilized *Pseudomonas* sp. lipase. *Journal of Molecular Catalysis B: Enzymatic* **2007,** *48* (3-4), 64-69.

244. Polytrans.Alcohols: 2-Octanol. http://www.polytrans.be/p_alcohols_octanol.htm . 2011. 5-5-2011.

245. Han, Y.; Lee, S. S.; Ying, J. Y. Pressure-Driven Enzyme Entrapment in Siliceous Mesocellular Foam. *Chemistry of Materials* **2006,** *18* (3), 643-649.

246. Fadnavis, N.; Bhaskar, V.; Kantam, M. L.; Choudary, B. M. Highly Efficient Tight Fit Immobilization of α-Chymotrypsin in Mesoporous MCM-41: A Novel Approach Using Precursor Immobilization and Activation. *Biotechnol Progress* **2003,** *19* (2), 346-351.

247. Overmeyer, A.; Schrader-Lippelt, S.; Kasche, V.; Brunner, G. Lipase-catalysed kinetic resolution of racemates at temperatures from 40°C to 160°C in supercritical CO_2. *Biotechnology Letters* **1999,** *21* (1), 65-69.

248. Rebelo, L. P.; Netto, C. G. C. M.; Toma, H. E.; Andrade, L. H. Enzymatic kinetic resolution of (RS)-1-(Phenyl)ethanols by *Burkholderia cepacia* lipase immobilized on magnetic nanoparticles. *Journal of the Brazilian Chemical Society* **2010,** *21*, 1537-1542.

249. Andrade, L. H.; Rebelo, L. P.; Netto, C. G. C. M.; Toma, H. E. Kinetic resolution of a drug precursor by *Burkholderia cepacia* lipase immobilized by different methodologies on superparamagnetic nanoparticles. *Journal of Molecular Catalysis B: Enzymatic* **2010,** *66* (1–2), 55-62.

250. Fu, Y.; Huang, T.; Chen, B.; Shen, J.; Duan, X.; Zhang, J.; Li, W. Enantioselective resolution of chiral drugs using BSA functionalized magnetic nanoparticles. *Separation and Purification Technology* **2013,** *107* (0), 11-18.

251. Ziegler, T.; Jurisch, C. Chemoenzymatic synthesis of enantiomerically enriched aminoalkenols and glycosides thereof. *Tetrahedron: Asymmetry* **2000,** *11* (16), 3403-3418.

252. Yang, G.; Wu, J.; Xu, G.; Yang, L. Enantioselective resolution of 2-(1-hydroxy-3-butenyl)-5-methylfuran by immobilized lipase. *Appl Microbiol Biotechnol* **2009,** *81* (5), 847-853.

253. Das, S.; Berke-Schlessel, D.; Ji, H. F.; McDonough, J.; Wei, Y. Enzymatic hydrolysis of biomass with recyclable use of cellobiase enzyme immobilized in sol-gel routed mesoporous silica. *Journal of Molecular Catalysis B: Enzymatic* **2011,** *70* (1-2), 49-54.

254. Ahn, K. W.; Ye, S. H.; Chun, W. H.; Rah, H.; Kim, S. G. Yield and component distribution of biodiesel by methanolysis of soybean oil with lipase-immobilized mesoporous silica. *Microporous and Mesoporous Materials* **2011,** *142* (1), 37-44.

255. Lomako, O. V.; Menyailova, I. I.; Nakhapetyan, L. A.; Nikitin, Y.; Kiselev, A. V. Immobilization of glucoamylase on porous silicas. *Enzyme and Microbial Technology* **1982,** *4* (2), 89-92.

256. Cabral, J. M. S.; Cardoso, J. P.; Novais, J. M.; Kennedy, J. F. A simple kinetic model for the hydrolysis of α-glucans using glucoamylase immobilized on titanium (IV) activated porous silica. *Enzyme and Microbial Technology* **1984,** *6* (8), 365-370.

257. Ding, H.; Wen, L.; Chen, J. Porous silica nano-tube as host for enzyme immobilization. *China Particuology* **2004,** *2* (6), 270-273.

258. He, F.; Zhuo, R. X.; Liu, L. J.; Jin, D. B.; Feng, J.; Wang, X. L. Immobilized lipase on porous silica beads: preparation and application for enzymatic ring-opening polymerization of cyclic phosphate. *Reactive and Functional Polymers* **2001,** *47* (2), 153-158.

259. Dandavate, V.; Keharia, H.; Madamwar, D. Ethyl isovalerate synthesis using *Candida rugosa* lipase immobilized on silica nanoparticles prepared in nonionic reverse micelles. *Process Biochemistry* **2009,** *44* (3), 349-352.

260. Hartmann, M.; Jung, D. Biocatalysis with enzymes immobilized on mesoporous hosts: the status quo and future trends. *J. Mater. Chem.* **2010,** *20*, 844-857.

261. Chiang, C. L.; Sung, C. S.; Chen, C. Y. Application of silica-magnetite nanocomposites to the isolation of ultrapure plasmid DNA from bacterial cells. *Journal of Magnetism and Magnetic Materials* **2006,** *305* (2), 483-490.

262. Sebastianelli, A.; Sen, T.; Bruce, I. J. Extraction of DNA from soil using nanoparticles by magnetic bioseparation. *Letters in Applied Microbiology* **2008,** *46* (4), 488-491.

263. Son, S. J.; Reichel, J.; He, B.; Schuchman, M.; Bai, X.; Lee, S. B. Magnetic-field-assisted bioseparation and drug delivary by magnetic silica/magnetite composite nanotubes. *Abstracts of Papers of the American Chemical Society* **2005,** *230*, 152.

264. Zhao, X.; Shi, Y.; Wang, T.; Cai, Y.; Jiang, G. Preparation of silica-magnetite nanoparticle mixed hemimicelle sorbents for extraction of several typical phenolic compounds from environmental water samples. *Journal of Chromatography A* **2008,** *1188* (2), 140-147.

265. Sen, T.; Bruce, I. J. Mesoporous silica-magnetite nanocomposites: Fabrication, characterisation and applications in biosciences. *Microporous and Mesoporous Materials* **2009,** *120* (3), 246-251.

266. Souza, K.; Ardisson, J.; Sousa, E. Study of mesoporous silica/magnetite systems in drug controlled release. *Journal of Materials Science: Materials in Medicine* **2009,** *20* (2), 507-512.

267. Yang, P.; Quan, Z.; Hou, Z.; Li, C.; Kang, X.; Cheng, Z.; Lin, J. A magnetic, luminescent and mesoporous core-shell structured composite material as drug carrier. *Biomaterials* **2009,** *30* (27), 4786-4795.

268. Martín-Saavedra, F. M.; Ruíz-Hernández, E.; Boré, A.; Arcos, D.; Vallet-Regí, M.; Vilaboa, N. Magnetic mesoporous silica spheres for hyperthermia therapy. *Acta Biomaterialia* **2010,** *6* (12), 4522-4531.

269. Qu, L.; Tie, S. Mesoporous silica-coated superparamagnetic magnetite functionalized with CuO and its application as a desulfurizer. *Microporous and Mesoporous Materials* **2009,** *117* (1-2), 402-405.

270. Kim, J.; Kim, H.-S.; Lee, N.; Kim, T.; Kim, H.; Yu, T.; Song, I.-C.; Moon, W.–K.; Hyeon, T. Multifunctional Uniform Nanoparticles Composed of a Magnetite Nanocrystal Core and a Mesoporous Silica Shell for Magnetic Resonance and Fluorescence Imaging and for Drug Delivery. *Angewandte Chemie International Edition* **2008,** *47* (44), 8438-8441.

271. Shubayev, V. I.; Pisanic II, T. R.; Jin, S. Magnetic nanoparticles for theragnostics. *Advanced Drug Delivery Reviews* **2009,** *61* (6), 467-477.

272. Naqvi, S.; Samim, M.; Abdin, M.; Ahmed, F. J.; Maitra, A.; Prashant, C.; Dinda, A. K. Concentration-dependent toxicity of iron oxide nanoparticles mediated by increased oxidative stress. *Int J Nanomedicine* **2010,** *5*, 983-989.

273. Park, E. J.; Kim, H.; Kim, Y.; Yi, J.; Choi, K.; Park, K. Inflammatory responses may be induced by a single intratracheal instillation of iron nanoparticles in mice. *Toxicology* **2010,** *275* (1), 65-71.

274. Ramesh, V.; Ravichandran, P.; Copeland, C. L.; Gopikrishnan, R.; Biradar, S.; Goornavar, V.; Ramesh, G. T.; Hall, J. C. Magnetite induces oxidative stress and apoptosis in lung epithelial cells. *Molecular and cellular biochemistry* **2012,** *363* (1-2), 225-234.

275. Sun, C.; Lee, J. S. H.; Zhang, M. Magnetic nanoparticles in MR imaging and drug delivery. *Advanced Drug Delivery Reviews* **2008,** *60* (11), 1252-1265.

276. Singh, R. K.; Kim, T. H.; Patel, K. D.; Knowles, J. C.; Kim, H. W. Biocompatible magnetite nanoparticles with varying silica-coating layer for use in biomedicine: Physicochemical and magnetic properties, and cellular compatibility. *J. Biomed. Mater. Res.* **2012,** *100A* (7), 1734-1742.

277. Teng, Y.; Xu, Y. A modified *para*-nitrophenyl palmitate assay for lipase synthetic activity determination in organic solvent. *Analytical Biochemistry* **2007,** *363* (2), 297-299.

278. Abdullah, A. A. B. A. H. The Biopetrol Synthesis from Palmitic Acid - Heterogenous Catalytic Cracking with Zeolite Catalyst. PhD Universiti Malaysia Panang, 2010.

279. Baldessarini, R. J.; Campbell, A.; Webb, N. L.; Swindell, C. S.; Flood, J. G.; Shashoua, V. E.; Kula, N. S.; Hemamalini, S.; Bradley, M. O. Fatty Acid Derivatives of Clozapine: Prolonged Antidopaminergic Activity of Docosahexaenoylclozapine in the Rat. *Neuropsychopharmacology* **2001,** *24* (1), 55-65.

280. Kalam, M. A.; Masjuki, H. H. Biodiesel from palmoil−an analysis of its properties and potential. *Biomass and Bioenergy* **2002,** *23* (6), 471-479.

281. Lima, V. M. G.; Krieger, N.; Mitchell, D. A.; Baratti, J. C.; Filippis, I. d.; Fontana, J. D. Evaluation of the potential for use in biocatalysis of a lipase from a wild strain of Bacillus megaterium. *Journal of Molecular Catalysis B: Enzymatic* **2004,** *31* (1−3), 53-61.

282. Costa, L.; Brissos, V.; Lemos, F.; Ribeiro, F.; Cabral, J. Comparing the effect of immobilization methods on the activity of lipase biocatalysts in ester hydrolysis. *Bioprocess and Biosystems Engineering* **2008,** *31* (4), 323-327.

283. Santra, S.; Tapec, R.; Theodoropoulou, N.; Dobson, J.; Hebard, A.; Tan, W. Synthesis and Characterization of Silica-Coated Iron Oxide Nanoparticles in Microemulsion: The Effect of Nonionic Surfactants. *Langmuir* **2001,** *17* (10), 2900-2906.

284. Lu, Y.; Yin, Y.; Mayers, B. T.; Xia, Y. Modifying the Surface Properties of Superparamagnetic Iron Oxide Nanoparticles through A Sol−Gel Approach. *Nano Letters* **2002,** *2* (3), 183-186.

285. Yusdy; Patel, S. R.; Yap, M. G. S.; Wang, D. I. C. Immobilization of L-lactate dehydrogenase on magnetic nanoclusters for chiral synthesis of pharmaceutical compounds. *Biochemical Engineering Journal* **2009,** *48* (1), 13-21.

286. Netto, C. G. C. M.; Andrade, L. H.; Toma, H. E. Enantioselective transesterification catalysis by *Candida antarctica* lipase immobilized on superparamagnetic nanoparticles. *Tetrahedron: Asymmetry* **2009,** *20* (19), 2299-2304.

287. Theil, F.; Schick, H.; Weichert, D.; Tannenberger, K.; Klappach, G. Enzymes in Organic Synthesis. Part 6. Enzyme-catalyzed Synthesis of (1S,4R)-(–)-4-Hydroxycyclopent-2-enyl Acetate and its (+)-Antipode - an Improved Procedure Using Lipase from *Mucor sp*. *J. Prakt. Chem.* **1991,** *333* (3), 497-499.

288. Theil, F.; Schick, H.; Lapitskaya, M. A.; Pivnitsky, K. K. Enzymes in organic synthesis, 4. Investigation of the pancreatin-catalyzed acylation of cis-cyclopent-2-ene-1,4-diol with various trichloroethyl and vinyl Alkanoates. *Liebigs Ann. Chem.* **1991,** *1991* (3), 195-200.

289. Ghorpade, S. R.; Kharul, R. K.; Joshi, R. R.; Kalkote, U. R.; Ravindranathan, T. Desymmetrization of *meso*-cyclopenten-*cis*-1,4-diol to 4-(R)-hydroxycyclopent-2-en-1-(S)-acetate by irreversible transesterification using Chirazyme. *Tetrahedron. Asymm.* **1999,** *10*, 891.

290. Borcherding, D. R.; Edwards III, C. K.; Esser, R. E.; Cole, D. L. Carbocyclic nucleoside analogs useful as immunosuppressants. US5470857 A, 1997.

291. Beare-Rogers, J.; Dieffenbacher, A.; Holm, J. V. Lexicon of Lipid Nutrition. *Pure Appl. Chem.* **2001,** *73* (4), 685-744.

292. Roy Baker, R. The eicosanoids: A historical overview. *Clinical Biochemistry* **1990,** *23* (5), 455-458.

293. Nicolaou, A. Eicosanoids in skin inflammation. *Prostaglandins, Leukotrienes and Essential Fatty Acids* **2013,** *88* (1), 131-138.

294. Kendall, A. C.; Nicolaou, A. Bioactive lipid mediators in skin inflammation and immunity. *Progress in Lipid Research* **2013,** *52* (1), 141-164.

295. Harizi, H.; Corcuff, J. B.; Gualde, N. Arachidonic-acid-derived eicosanoids: roles in biology and immunopathology. *Trends in Molecular Medicine* **2008,** *14* (10), 461-469.

296. Harre, M.; Raddatz, P.; Walenta, R.; Winterfeldt, E. 4-Oxo-2-cyclopentenyl Acetate: A Synthetic Intermediate. *Angew. Chem. Int. Ed. Engl.* **1982,** *21* (7), 480-492.

297. Noyori, R.; Suzuki, M. Prostaglandin Syntheses by Three-Component Coupling. *Angew. Chem. Int. Ed.* **1984,** *23*, 847.

298. Danishefsky, S. J.; Cabal, M. P.; Choe, K. Novel stereospecific silyl group transfer reactions: Practical routes to the prostaglandins. *J. Am. Chem. Soc.* **1989,** *111*, 3456-3457.

299. Padma-Nathan, H.; Hellstrom, W. J. G.; Kaiser, F. E.; Labasky, R. F.; Lue, T. F.; Nolten, W. E.; Norwood, P. C.; Peterson, C. A.; Shabsigh, R.; Tam, P. Y.; Place, V. A.; Gesundheit, N.; Cowley, C.; Nemo, K. J.; Spivack, A. P.; Stephens, D. E.; Todd, L. K. Treatment of Men with Erectile Dysfunction with Transurethral Alprostadil. *N Engl J Med* **1997,** *336* (1), 1-7.

300. Cawello, W.; Leonhardt, A.; Schweer, H.; Seyberth, H. W.; Bonn, R.; Lomeli, A. L. Dose proportional pharmacokinetics of alprostadil (prostaglandin E1) in healthy volunteers following intravenous infusion. *British journal of clinical pharmacology* **1995,** *40* (3), 273-276.

301. Solanki, K.; Gupta, M. N. Simultaneous purification and immobilization of *Candida rugosa* lipase on superparamagnetic Fe_3O_4 nanoparticles for catalyzing transesterification reactions. *New J. Chem.* **2011,** *35*, 2551-2556.

302. Paiva, A. L.; van Rossum, D.; Malcata, F. X. Kinetics of Lipase-mediated Synthesis of Butyl Butyrate in *n*-hexane. *Biocatal Biotransformation* **2002,** *20* (1), 43-51.

303. Liaquat, M.; Khan, S.; Aslam, S.; Khan, A.; Khan, H.; Khan, S. M.; Ali, S.; Wahad, S.; Bhatti, H. N. Rape Seedling Lipase Catalyzed Synthesis of Flavor Esters Through Transesterification in Hexane. *J. Chem. Soc. Pak.* **2012,** *34* (1), 144-150.

304. Sen, T.; Tiddy, G. J. T.; Casci, J. L.; Anderson, M. W. Meso-cellular silica foams, macro-cellular silica foams and mesoporous solids: a study of emulsion-mediated synthesis. *Microporous and Mesoporous Materials* **2005,** *78* (2-3), 255-263.

305. Keller, K.; Friedmann, T.; Boxman, A. The bioseparation needs for tomorrow. *Trends in Biotechnology* **2001,** *19* (11), 438-441.

306. Ghosh, R. Separation of human albumin and IgG by a membrane-based integrated bioseparation technique involving simultaneous precipitation, microfiltration and membrane adsorption. *Journal of Membrane Science* **2004,** *237* (1–2), 109-117.

307. Sii, D.; Sadana, A. Bioseparation using affinity techniques. *Journal of Biotechnology* **1991,** *19* (1), 83-98.

308. Leung, W. W.-F. 6 - Commercial Applications of Centrifugation in Biotechnology. In *Centrifugal Separations in Biotechnology*, Academic Press: Oxford, 2007; pp 109-128.

309. Bilir Ormanci, F. S.; Erol, I.; Ayaz, N. D.; Iseri, O.; Sariguzel, D. Immunomagnetic separation and PCR detection of *Listeria monocytogenes* in turkey meat and antibiotic resistance of the isolates. British Poultry Science 49[5], 560-565. 2008.

310. Cudjoe, K. S.; Hagtvedt, T.; Dainty, R. Immunomagnetic separation of *Salmonella* from foods and their detection using immunomagnetic particle (IMP)-ELISA. *International Journal of Food Microbiology* **1995,** *27* (1), 11-25.

311. Soltanieh, M.; Sahebdelfar, S. Interaction effects in multicomponent separation by reverse osmosis. *Journal of Membrane Science* **2001,** *183* (1), 15-27.

312. Käppler, T. E.; Hickstein, B.; Peuker, U. A.; Posten, C. Characterization of magnetic ion-exchange composites for protein separation from biosuspensions. *Journal of Bioscience and Bioengineering* **2008,** *105* (6), 579-585.

313. Fiedler, E.; Fiedler, M.; Proetzel, G.; Scheuermann, T.; Fiedler, U.; Rudolph, R. Affilin Molecules: Novel Ligands for Bioseparation. *Food and Bioproducts Processing* **2006,** *84* (1), 3-8.

314. Singh, P. C.; Singh, R. K. Choosing an appropriate bioseparation technique. *Trends in Food Science & Technology* **1996,** *7* (2), 49-58.

315. Gu, H.; Xu, K.; Xu, C.; Xu, B. Biofunctional magnetic nanoparticles for protein separation and pathogen detection. *Chem. Commun.* **2006,** *0* (9), 941-949.

316. Bucak, S.; Jones, D. A.; Laibinis, P. E.; Hatton, T. A. Protein Separations Using Colloidal Magnetic Nanoparticles. *Biotechnol Progress* **2003,** *19* (2), 477-484.

317. Saiyed, Z.; Telang, S.; Ramchand, C. Application of magnetic techniques in the field of drug discovery and biomedicine. *Biomagn Res Technol* **2003,** *1* (1), 2.

318. Jing, Y.; Moore, L. R.; Williams, P. S.; Chalmers, J. J.; Farag, S. S.; Bolwell, B.; Zborowski, M. Blood progenitor cell separation from clinical leukapheresis product by magnetic nanoparticle binding and magnetophoresis. *Biotechnol. Bioeng.* **2007,** *96* (6), 1139-1154.

319. Matsunaga, T.; Kawasaki, M.; Yu, X.; Tsujimura, N.; Nakamura, N. Chemiluminescence Enzyme Immunoassay Using Bacterial Magnetic Particles. *Analytical chemistry* **1996,** *68* (20), 3551-3554.

320. Nakamura, N.; Burgess, J. G.; Yagiuda, K.; Kudo, S.; Sakaguchi, T.; Matsunaga, T. Detection and removal of *Escherichia coli* using fluorescein isothiocyanate conjugated monoclonal antibody immobilized on bacterial magnetic particles. *Analytical chemistry* **1993,** *65* (15), 2036-2039.

321. Pour Yazdankhah, S.; Hellemann, A. L.; Rønningen, K.; Olsen, E. Rapid and sensitive detection of *Staphylococcus* species in milk by ELISA based on monodisperse magnetic particles. *Veterinary Microbiology* **1998,** *62* (1), 17-26.

322. Xu, Y.; Wang, E. Electrochemical biosensors based on magnetic micro/nano particles. *Electrochimica Acta* **2012,** *84* (0), 62-73.

323. Fan, X.; White, I. M.; Shopova, S. I.; Zhu, H.; Suter, J. D.; Sun, Y. Sensitive optical biosensors for unlabeled targets: A review. *Analytica Chimica Acta* **2008,** *620* (1–2), 8-26.

324. Bruls, D. M.; Evers, T. H.; Kahlman, J. A. H.; Van Lankvelt, P. J. W.; Ovsyanko, M.; Pelssers, E. G. M.; Schleipen, J. J. H. B.; De Theije, F. K.; Verschuren, C. A.; Van Der Wijk, T. Rapid integrated biosensor for multiplexed immunoassays based on actuated magnetic nanoparticles. *Lab Chip* **2009,** *9* (24), 3504-3510.

325. Haes, A. J.; Chang, L.; Klein, W. L.; Van Duyne, R. P. Detection of a Biomarker for Alzheimer's Disease from Synthetic and Clinical Samples Using a Nanoscale Optical Biosensor. *J. Am. Chem. Soc.* **2005,** *127* (7), 2264-2271.

326. Tang, L.; Casas, J.; Venkataramasubramani, M. Magnetic Nanoparticle Mediated Enhancement of Localized Surface Plasmon Resonance for Ultrasensitive Bioanalytical Assay in Human Blood Plasma. *Analytical chemistry* **2012,** *85* (3), 1431-1439.

327. Wang, L.; Sun, Y.; Wang, J.; Wang, J.; Yu, A.; Zhang, H.; Song, D. Preparation of surface plasmon resonance biosensor based on magnetic core/shell Fe_3O_4/SiO_2 and $Fe_3O_4/Ag/SiO_2$ nanoparticles. *Colloids and Surfaces B: Biointerfaces* **2011,** *84* (2), 484-490.

328. Ravindranath, S. P.; Mauer, L. J.; Deb-Roy, C.; Irudayaraj, J. Biofunctionalized Magnetic Nanoparticle Integrated Mid-Infrared Pathogen Sensor for Food Matrixes. *Analytical chemistry* **2009,** *81* (8), 2840-2846.

329. Dubus, S.; Gravel, J. F.; Le Drogoff, B.; Nobert, P.; Veres, T.; Boudreau, D. PCR-Free DNA Detection Using a Magnetic Bead-Supported Polymeric Transducer and Microelectromagnetic Traps. *Analytical chemistry* **2006,** *78* (13), 4457-4464.

330. Wang, Y.; Dostalek, J.; Knoll, W. Magnetic nanoparticle-enhanced SPR biosensor. *Procedia Engineering* **2010,** *5* (0), 1017-1020.

331. Sun, Y.; Bai, Y.; Song, D.; Li, X.; Wang, L.; Zhang, H. Design and performances of immunoassay based on SPR biosensor with magnetic microbeads. *Biosensors and Bioelectronics* **2007,** *23* (4), 473-478.

332. Smith, J. E.; Sapsford, K. E.; Tan, W.; Ligler, F. S. Optimization of antibody-conjugated magnetic nanoparticles for target preconcentration and immunoassays. *Analytical Biochemistry* **2011,** *410* (1), 124-132.

333. Centi, S.; Laschi, S.; Mascini, M. Improvement of analytical performances of a disposable electrochemical immunosensor by using magnetic beads. *Talanta* **2007,** *73* (2), 394-399.

334. Liao, M. H.; Guo, J. C.; Chen, W. C. A disposable amperometric ethanol biosensor based on screen-printed carbon electrodes mediated with ferricyanide-magnetic nanoparticle mixture. *Journal of Magnetism and Magnetic Materials* **2006,** *304* (1), e421-e423.

335. Lu, B. W.; Chen, W. C. A disposable glucose biosensor based on drop-coating of screen-printed carbon electrodes with magnetic nanoparticles. *Journal of Magnetism and Magnetic Materials* **2006,** *304* (1), e400-e402.

336. Zhang, Y.; Zeng, G. M.; Tang, L.; Huang, D. L.; Jiang, X. Y.; Chen, Y. N. A hydroquinone biosensor using modified core–shell magnetic nanoparticles supported on carbon paste electrode. *Biosensors and Bioelectronics* **2007,** *22* (9–10), 2121-2126.

337. Liu, Z.; Liu, Y.; Yang, H.; Yang, Y.; Shen, G.; Yu, R. A phenol biosensor based on immobilizing tyrosinase to modified core-shell magnetic nanoparticles supported at a carbon paste electrode. *Analytica Chimica Acta* **2005,** *533* (1), 3-9.

338. Chauhan, N.; Narang, J.; Meena; Pundir, C. S. An amperometric glutathione biosensor based on chitosan–iron coated gold nanoparticles modified Pt electrode. *International Journal of Biological Macromolecules* **2012,** *51* (5), 879-886.

339. Chandra, S.; Arora, K.; Bahadur, D. Impedimetric biosensor based on magnetic nanoparticles for electrochemical detection of dopamine. *Materials Science and Engineering: B* **2012,** *177* (17), 1531-1537.

340. Uyttendaele, M.; De Troy, P.; Debevere, J. Incidence of *Salmonella*, *Campylobacter jejuni*, *Campylobacter coli*, and *Listeria monocytogenes* in poultry carcasses and different types of poultry products for sale on the Belgian retail market. *Journal of Food Protection* **1999,** *62* (7), 735-740.

341. Yang, H.; Qu, L.; Wimbrow, A. N.; Jiang, X.; Sun, Y. Rapid detection of *Listeria monocytogenes* by nanoparticle-based immunomagnetic separation and real-time PCR. *International Journal of Food Microbiology* **2007,** *118* (2), 132-138.

342. Walker, K. R. Rapid Detection of *Listeria monocytogenes* in Salad by Polymerase Chain Reaction. Auburn University, Alabama, 2005.

343. Sutherland, P. S.; Porrit, R. J. *Listeria monocytogenes*. In *Food-borne Microorganisms of Public Health Significance*, Hocking, A. D., Ed.; Food Microbiology Group: Syndney, Australia, 1997; pp 333-378.

344. Amagliani, G.; Omiccioli, E.; del Campo, A.; Bruce, I. J.; Brandi, G.; Magnani, M. Development of a magnetic capture hybridization-PCR assay for *Listeria monocytogenes* direct detection in milk samples. *Journal of Applied Microbiology* **2006,** *100* (2), 375-383.

345. Furchtgott, L.; Wingreen, N. S.; Huang, K. C. Mechanisms for maintaining cell shape in rod-shaped Gram-negative bacteria. *Molecular Microbiology* **2011,** *81* (2), 340-353.

346. Antaoa, E. M.; Laturnusa, C.; Diehla, I.; Gloddea, S.; Homeier, T.; Bohnke, U.; Steinruck, H.; Philipp, H. C.; Wieler, L. H. Avian pathogenic, uropathogenic, and newborn meningitis-causing *Escherichia coli*: how closely related are they? *International Journal of Medical Microbiology* **2007,** *297*, 163-176.

347. Todar, K. Pathogenic E. coli. Todar's Online Textbook of Bacteriology , 1-4. 2012. 14-6-2013.
Ref Type: Online Source

348. Nataro, J. P.; Kaper, J. B. Diarrheagenic *escherichia coli*. *Clinical microbiology reviews* **1998,** *11* (1), 142-201.

349. Muniesa, M.; Hammerl, J. A.; Hertwig, S.; Appel, B.; Brüssow, H. Shiga toxin-producing *Escherichia coli* O104: H4: a new challenge for microbiology. *Appl. Environ. Microbiol.* **2012,** *78* (12), 4065-4073.

350. Robins−Browne, R. M.; Hartland, E. L. *Escherichia coli* as a cause of diarrhea. *Journal of gastroenterology and hepatology* **2002,** *17* (4), 467-475.

351. Varshney, M.; Yang, L.; Su, X.-L.; Li, Y. Magnetic Nanoparticle-Antibody Conjugates for the Separation of *Escherichia coli* O157:H7 in Ground Beef. *Journal of Food Protection* **2005,** *68*, 1804-1811.

352. Mora, A.; Herrera, A.; López, C.; Dahbi, G.; Mamani, R.; Pita, J. M.; Alonso, M. P.; Llovo, J.; Bernárdez, M. I.; Blanco, J. E.; Blanco, M.; Blanco, J. Characteristics of the Shiga-toxin-producing enteroaggregative *Escherichia coli* O104:H4 German outbreak strain and of STEC strains isolated in Spain. *Int Microbiol* **2011,** *14* (3), 121-141.

353. Vogt, R. L.; Dippold, L. *Escherichia coli* O157: H7 outbreak associated with consumption of ground beef, June-July 2002. *Public Health Reports* **2005,** *120* (2), 174.

354. Donnelly, C. W. Detection and Isolation of *Listeria monocytogenes* from Food Samples: Implications of Sublethal Injury. Journal of AOAC International 85[2], 495-500. 2002.

355. Noble, R. T.; Weisberg, S. B. A review of technologies for rapid detection of bacteria in recreational waters. *J. Water Health* **2005,** *3* (4), 381-392.

356. Scheu, P.; Gasch, A.; Berghof, K. Rapid detection of *Listeria monocytogenes* by PCR-ELISA. *Letters in Applied Microbiology* **1999,** *29* (6), 416-420.

357. Norton, D. M. Polymerase Chain Reaction-Based Methods for Detection of *Listeria monocytogenes*: Toward Real-Time Screening for Food and Environmental Samples. Journal of AOAC International 85[2], 505-515. 2002.
Ref Type: Abstract

358. O'Grady, J.; Sedano-Balbás, S.; Maher, M.; Smith, T.; Barry, T. Rapid real-time PCR detection of *Listeria monocytogenes* in enriched food samples based on the ssrA gene, a novel diagnostic target. *Food Microbiology* **2008,** *25* (1), 75.

359. Bej, A. K.; Steffan, R. J.; DiCesare, J.; Haff, L.; Atlas, R. M. Detection of coliform bacteria in water by polymerase chain reaction and gene probes. *Appl. Environ. Microbiol.* **1990,** *56* (2), 307-314.

360. Iqbal, S.; Robinson, J.; Deere, D.; Saunders, J. R.; Edwards, C.; Porter, J. Efficiency of the polymerase chain reaction amplification of the uid gene for detection of *Escherichia coli* in contaminated water. *Letters in Applied Microbiology* **1997,** *24* (6), 498-502.

361. Gannon, V. P.; Rashed, M.; King, R. K.; Thomas, E. J. Detection and characterization of the eae gene of Shiga-like toxin-producing *Escherichia coli* using polymerase chain reaction. *Journal of clinical microbiology* **1993,** *31* (5), 1268-1274.

362. Fluit, A. C.; Torensma, R.; Visser, M. J.; Aarsman, C. J.; Poppelier, M. J.; Keller, B. H.; Klapwijk, P.; Verhoef, J. Detection of *Listeria monocytogenes* in cheese with the magnetic immuno-polymerase chain reaction assay. *Appl. Environ. Microbiol.* **1993,** *59* (5), 1289-1293.

363. Hudson, J. A.; Lake, R. J.; Savill, M. G.; Scholes, P.; McCormick, R. E. Rapid detection of *Listeria monocytogenes* in ham samples using immunomagnetic separation followed by polymerase chain reaction. *Journal of Applied Microbiology* **2001,** *90* (4), 614-621.

364. Skjerve, E.; Rørvik, L. M.; Olsvik, O. Detection of *Listeria monocytogenes* in foods by immunomagnetic separation. *Appl. Environ. Microbiol.* **1990,** *56* (11), 3478-3481.

365. Bickley, J.; Short, J. K.; McDowell, D. G.; Parkes, H. C. Polymerase chain reaction (PCR) detection of *Listeria monocytogenes* in diluted milk and reversal of PCR inhibition caused by calcium ions. *Letters in Applied Microbiology* **1996,** *22* (2), 153-158.

366. Choi, W. S.; Hong, C. H. Rapid enumeration of *Listeria monocytogenes* in milk using competitive PCR. *International Journal of Food Microbiology* **2003,** *84* (1), 79-85.

367. Nogva, H. K.; Rudi, K.; Naterstad, K.; Holck, A.; Lillehaug, D. Application of 5'-nuclease PCR for quantitative detection of *Listeria monocytogenes* in pure cultures, water, skim milk, and unpasteurized whole milk. *Appl. Environ. Microbiol.* **2000,** *66* (10), 4266-4271.

368. Wernars, K.; Heuvelman, C. J.; Chakraborty, T.; Notermans, S. H. W. Use of the polymerase chain reaction for direct detection of *Listeria monocytogenes* in soft cheese. *Journal of Applied Bacteriology* **1991,** *70* (2), 121-126.

369. Safarik, I.; Safarikova, M. Magnetic nano- and microparticles in biotechnology. *Chem. Pap.* **2009,** *63* (5), 497-505.

370. Wright, D. J.; Chapman, P. A.; Siddons, C. A. Immunomagnetic separation as a sensitive method for isolating *Escherichia coli* O157 from food samples. *Epidemiol Infect* **1994,** *113* (1), 31-39.

371. Pappert, G.; Rieger, M.; Niessner, R.; Seidel, M. Immunomagnetic nanoparticle-based sandwich chemiluminescence-ELISA for the enrichment and quantification of *E.coli*. *Microchimica Acta* **2010,** *168* (1), 1-8.

372. Yu, H.; Bruno, J. G. Immunomagnetic-electrochemiluminescent detection of *Escherichia coli* O157 and *Salmonella typhimurium* in foods and environmental water samples. *Appl. Environ. Microbiol.* **1996,** *62* (2), 587-592.

373. Bennett, A. R.; MacPhee, S.; Betts, R. P. The isolation and detection of *Escherichia coli* O157 by use of immunomagnetic separation and immunoassay procedures. *Letters in Applied Microbiology* **1996,** *22* (3), 237-243.

374. Seo, K. H.; Brackett, R. E.; Frank, J. F.; Hilliard, S. Immunomagnetic Separation and Flow Cytometry for Rapid Detection of *Escherichia coli* O157:H7. *Journal of Food Protection* **1998,** *61* (7), 812-816.

375. Radke, S. M.; Alocilja, E. C. A high density microelectrode array biosensor for detection of *E. coli* O157:H7. *Biosensors and Bioelectronics* **2005,** *20* (8), 1662-1667.

376. Liu, Y.; Li, Y. Detection of *Escherichia coli* O157:H7 using immunomagnetic separation and absorbance measurement. *Journal of Microbiological Methods* **2002,** *51* (3), 369-377.

377. Boyaci, I. H.; Aguilar, Z.; Hossain, M.; Halsall, H. B.; Seliskar, C.; Heineman, W. Amperometric determination of live *Escherichia coli* using antibody-coated paramagnetic beads. *Anal Bioanal Chem* **2005,** *382* (5), 1234-1241.

378. Yang, Y.; Xu, F.; Xu, H.; Aguilar, Z. P.; Niu, R.; Yuan, Y.; Sun, J.; You, X.; Lai, W.; Xiong, Y.; Wan, C.; Wei, H. Magnetic nano-beads based separation combined with propidium monoazide treatment and multiplex PCR assay for simultaneous detection of viable *Salmonella Typhimurium*,

Escherichia coli O157:H7 and *Listeria monocytogenes* in food products. *Food Microbiology* **2013,** (0).

379. Favrin, S. J.; Jassim, S. A.; Griffiths, M. W. Application of a novel immunomagnetic separation–bacteriophage assay for the detection of *Salmonella enteritidis* and *Escherichia coli* O157:H7 in food. *International Journal of Food Microbiology* **2003,** *85* (1–2), 63-71.

380. Dye, M. The enrichment of *Rhizobium* from a model system using immunomagnetic separation. *Journal of Microbiological Methods* **1994,** *19* (3), 235-245.

381. de Len, L.; Siverio, F.; Rodriguez, A. Detection of *Clavibacter michiganensis* subsp. *michiganensis* in tomato seeds using immunomagnetic separation. *Journal of Microbiological Methods* **2006,** *67* (1), 141-149.

382. Yang, W.; Gu, A. Z.; Zeng, S. y.; Li, D.; He, M.; Shi, H. c. Development of a combined immunomagnetic separation and quantitative reverse transcription-PCR assay for sensitive detection of infectious rotavirus in water samples. *Journal of Microbiological Methods* **2011,** *84* (3), 447-453.

383. Chakraborty, R.; Hazen, T. C.; Joyner, D. C.; Kusel, K.; Singer, M. E.; Sitte, J.; Torok, T. Use of immunomagnetic separation for the detection of *Desulfovibrio vulgaris* from environmental samples. *Journal of Microbiological Methods* **2011,** *86* (2), 204-209.

384. Heermann, K. H.; Hagos, Y.; Thomssen, R. Liquid-phase hybridization and capture of hepatitis B virus DNA with magnetic beads and fluorescence detection of PCR product. *Journal of virological methods* **1994,** *50* (1), 43-57.

385. Millar, D. S.; Withey, S. J.; Tizard, M. L. V.; Ford, J. G.; Hermontaylor, J. Solid-Phase Hybridization Capture of Low-Abundance Target DNA Sequences: Application to the Polymerase Chain Reaction Detection of *Mycobacterium paratuberculosis* and *Mycobacterium avium* subsp. *silvaticum*. *Analytical Biochemistry* **1995,** *226* (2), 325-330.

386. Mangiapan, G.; Vokurka, M.; Schouls, L.; Cadranel, J.; Lecossier, D.; Van Embden, J.; Hance, A. J. Sequence capture-PCR improves detection of mycobacterial DNA in clinical specimens. *Journal of clinical microbiology* **1996,** *34* (5), 1209-1215.

387. Regan, P. M.; Margolin, A. B. Development of a nucleic acid capture probe with reverse transcriptase-polymerase chain reaction to detect poliovirus in groundwater. *Journal of virological methods* **1997,** *64* (1), 65-72.

388. Miyachi, H.; Masukawa, A.; Ohshima, T.; Hirose, T.; Impraim, C.; Ando, Y. Automated specific capture of hepatitis C virus RNA with probes and paramagnetic particle separation. *Journal of clinical microbiology* **2000,** *38* (1), 18-21.

389. Tanaka, M.; Fujiyama, S.; Tanaka, M.; Itoh, K.; Matsushita, K.; Matsushita, K.; Matsuyama, K.; Kakuda, H.; Tomita, K. Clinical Usefulness of a New Hepatitis C Virus RNA Extraction Method Using Specific Capture Probe and Magnetic Particle in Hemodialysis Patients. *Therapeutic Apheresis and Dialysis* **2004,** *8* (4), 328-334.

390. Maibach, R. C.; Dutly, F.; Altwegg, M. Detection of *Tropheryma whipplei* DNA in feces by PCR using a target capture method. *Journal of clinical microbiology* **2002,** *40* (7), 2466-2471.

391. Zhu, X.; Zhou, X.; Xing, D. Nano-magnetic primer based electrochemiluminescence-polymerase chain reaction (NMPE-PCR) assay. *Biosensors and Bioelectronics* **2012,** *31* (1), 463-468.

392. Amagliani, G.; Omiccioli, E.; Brandi, G.; Bruce, I. J.; Magnani, M. A multiplex magnetic capture hybridisation and multiplex Real-Time PCR protocol for pathogen detection in seafood. *Food Microbiology* **2010,** *27* (5), 580-585.

393. Paripurana, P.; Pinsaeng, S.; Polpanich, D.; Tangboriboonrat, P.; Jangpatarapongsa, K. Primer-immobilized Magnetic Nanoparticle for Bacterial DNA separation. IACSIT Press: Singapore, 2012; pp 152-155.

394. Chen, S. H.; Wu, V. C. H.; Chuang, Y. C.; Lin, C. S. Using oligonucleotide-functionalized Au nanoparticles to rapidly detect foodborne pathogens on a piezoelectric biosensor. *Journal of Microbiological Methods* **2008,** *73* (1), 7-17.

395. Redondo-Marugan, J.; Petit-Dominguez, M. D.; Casero, E.; Vázquez, L.; García, T.; Parra-Alfambra, A. M.; Lorenzo, E. Sol–gel derived gold nanoparticles biosensing platform for *Escherichia coli* detection. *Sensors and Actuators B: Chemical* **2013,** *182* (0), 307-314.

396. Mariotti, E.; Minunni, M.; Mascini, M. Surface plasmon resonance biosensor for genetically modified organisms detection. *Analytica Chimica Acta* **2002,** *453* (2), 165-172.

397. Galluzzi, L.; Bertozzini, E.; del Campo, A.; Penna, A.; Bruce, I. J.; Magnani, M. Capture probe conjugated to paramagnetic nanoparticles for

purification of *Alexandrium* species (Dinophyceae) DNA from environmental samples. *Journal of Applied Microbiology* **2006,** *101* (1), 36-43.

398. Zhan, F.; Zhou, X.; Xing, D. Rapid and sensitive electrochemiluminescence detection of rotavirus by magnetic primer based reverse transcription-polymerase chain reaction. *Analytica Chimica Acta* **2013,** *761* (0), 71-77.

399. Bartlett, J. M. S.; Stirling, D. A Short History of the Polymerase Chain Reaction. *PCR Protocols* **2003,** *226*, 3-6.

400. Coen, D. M. The Polymerase Chain Reaction. In *Current Protocols in Molecular Biology*, John Wiley & Sons, Inc.: 2001.

401. Yang, S.; Rothman, R. E. PCR-based diagnostics for infectious diseases: uses, limitations, and future applications in acute-care settings. *The Lancet Infectious Diseases* **2004,** *4* (6), 337-348.

402. Dieffenbach, C. W.; Lowe, T. M. J.; Dveksler, G. S. General Concepts for PCR Primer Design. In *PCR Primer: A Laboratory Manual*, Dieffenbach, C. W., Dveksler, G. S., Eds.; Cold Spring Harbor Laboratory Press: New York, 1995; pp 133-155.

403. Singh, V. K.; Govindarajan, R.; Naik, S.; Kumar, A. The Effect of Hairpin Structure on PCR Amplification Efficiency. *Molecular Biology Today* **2000,** *1* (3), 67-69.

404. Abd-Elsalam, K. A. Bioinformatic tools for PCR primer design. *African Journal of Biotechnology* **2003,** *2* (5), 91-95.

405. Tuffaha, M. S. A. Molecular Diagnosis of Tumors. In *Phenotypic and Genotypic Diagnosis of Malignancies*, Wiley-VCH Verlag GmbH & Co. KGaA: 2008; pp 81-250.

406. Tuffaha, M. *Phenotypic and Genotypic Diagnosis of Malignancies: An Immunohistochemical and Molecular Approach;* Wiley-VCH: 2008.

407. Yang, W.; Lee, J. Y.; Nowotny, M. Making and Breaking Nucleic Acids: Two-Mg^{2+}-Ion Catalysis and Substrate Specificity. *Molecular Cell* **2006,** *22* (1), 5-13.

408. Holland, P. M.; Abramson, R. D.; Watson, R.; Gelfand, D. H. Detection of specific polymerase chain reaction product by utilizing the 5' -* 3' exonuclease activity of Thermus aquaticus DNA polymerase. *Proc. Natl. Acad. Sci. USA* **1991,** *88*, 7276-7280.

409. Tindall, K. R.; Kunkel, T. A. Fidelity of DNA synthesis by the *Thermus aquaticus* DNA polymerase. *Biochemistry* **1988,** *27* (16), 6008-6013.

410. Zhou, Y.; Zhang, X.; Ebright, R. H. Random mutagenesis of gene-sized DNA molecules by use of PCR with *Taq* DNA polymerase. *Nucleic Acids Research* **1991,** *19* (21), 6052.

411. Saiki, R. K.; Gelfand, D. H.; Stoffel, S.; Scharf, S. T.; Higuchi, R.; Horn, G. T.; Mullis, K. B.; Ehrlich, H. A. Primer-directed enzymatic amplification of DNA. *Science* **1988,** *239*, 487-491.

412. Ronaghi, M.; Karamohamed, S.; Pettersson, B.; Uhlén, M.; Nyrén, P. Real-time DNA sequencing using detection of pyrophosphate release. *Analytical Biochemistry* **1996,** *242* (1), 84-89.

413. Steitz, T. A. DNA polymerases: structural diversity and common mechanisms. *Journal of Biological Chemistry* **1999,** *274* (25), 17395-17398.

414. Yang, L.; Arora, K.; Beard, W. A.; Wilson, S. H.; Schlick, T. Critical role of magnesium ions in DNA polymerase β's closing and active site assembly. *J. Am. Chem. Soc.* **2004,** *126* (27), 8441-8453.

415. Berg, J. M.; Tymoczko, J. L.; Stryer, L. DNA Polymerases Require a Template and a Primer. In *Biochemistry*, 5th ed.; W H Freeman: New York, 2002.

416. Eom, S. H.; Wang, J.; Steitz, T. A. Structure of *Taq* polymerase with DNA at the polymerase active site. *Nature* **1996,** *382* (6588), 278-281.

417. Nellemann, L. J.; Frederiksen, J.; Morling, N. PCR typing of DNA fragments of the two short tandem repeat (STR) systems upstream of the human myelin basic protein (MBP) gene in Danes and Greenland Eskimos. *Forensic Science International* **1996,** *78* (2), 139-156.

418. Taylor, C. Y.; Guillén, I. A.; Nazabal, M.; Fernández, J. R.; Silva, J. A. Electrophoretic techniques applied to the detection and analysis of the human microsatellite DG10s478. *Journal of biomolecular techniques: JBT* **2007,** *18* (5), 298.

419. Van Pelt-Verkuil, E. Analysis of PCR Amplification Products. In *Principles and Technical Aspects of PCR Amplification*, Springer Netherlands: 2008; pp 141-182.

420. Heid, C. A.; Stevens, J.; Livak, K. J.; Williams, P. M. Real time quantitative PCR. *Genome Res* **1996,** *6* (10), 986-994.

421. Dorak, M. T. *Real-time PCR;* Taylor & Francis: New York, NY., 2006.pp. 2-12.

422. Holst-Jensen, A.; Berdal, K. G.; Thorstensen, T.; Tengs, T.; Bøydler, C. Equal Performance of *Taq*Man, MGB, Molecular Beacon, and SYBR Green-Based Detection Assays in Detection and Quantification of Roundup Ready Soybean. *J. Agric. Food Chem.* **2006,** *54* (26), 9658-9663.

423. Spahn, C.; Minteer, S. D. Enzyme Immobilization in Biotechnology. *Recent Patents on Engineering* **2008,** *2*, 195-200.

424. Sen, T.; Magdassi, S.; Nizri, G.; Bruce, I. J. Dispersion of magnetic nanoparticles in suspension. *Micro & Nano Letters* **2006,** *1* (1), 39-42.

425. Petcharoen, K.; Sirivat, A. Synthesis and characterization of magnetite nanoparticles via the chemical co-precipitation method. *Materials Science and Engineering: B* **2012,** *177* (5), 421-427.

426. Wijnen, P. W.; Beelen, T. P.; van Santen, R. A. Silica Gels from Aqueous Silicate Solutions. *The Colloid Chemistry of Silica* **1994,** 517-531.

427. Moon, J. H.; Kim, J. H.; Kim, K.-J.; Kang, T.-H.; Kim, B.; Kim, C.-H.; Hahn, J. H.; Park, J. W. Absolute Surface Density of the Amine Group of the Aminosilylated Thin Layers: Ultraviolet-Visible Spectroscopy, Second Harmonic Generation, and Synchrotron-Radiation Photoelectron Spectroscopy Study. *Langmuir* **1997,** *13*, 4305-4310.

428. De Waterbeemd, M. V. Silane Condensation to Nanoparticles in Suspension. PhD The University of Kent, 2009.

429. Kruger, N. J. The Bradford Method for Protein Quantitation. In *The Protein Protocols Handbook*, 2 ed.; Walker, J. M., Ed.; Humana Press: Totowa, NJ, 2002; pp 15-21.

430. Bradford, M. M. A rapid and sensitive method for the quantitation of microgram quantities of protein utilizing the principle of protein-dye binding. *Analytical Biochemistry* **1976,** *72* (1), 248-254.

431. Brady, D.; Jordaan, J.; Simpson, C.; Chetty, A.; Arumugam, C.; Moolman, F. Spherezymes: A novel structured self-immobilisation enzyme technology. *BMC Biotechnol* **2008,** *8* (1), 1-11.

432. Gupta, N.; Rathi, P.; Gupta, R. Simplified *para*-nitrophenyl palmitate assay for lipases and esterases. *Analytical Biochemistry* **2002,** *311* (1), 98-99.

433. Jiles, D. *Introduction to Magnetism and Magnetic Materials;* 1 ed.; Chapman and Hall Publishers: 1991.

434. Sigma-Aldrich . Supelco DEX Chiral Columns. http://www.sigmaaldrich.com . 2013. 10-9-2013.

435. Liang, S.; Wang, Y.; Zhang, C.; Liu, X. Synthesis of amino-modified magnetite nanoparticles coated with Hepama-1 and radiolabeled with ^{188}Re for bio-magnetically targeted radiotherapy. *Journal of Radioanalytical and Nuclear Chemistry* **2006,** *269* (1), 3-7.

436. Yi, D. K.; Selvan, S. T.; Lee, S. S.; Papaefthymiou, G. C.; Kundaliya, D.; Ying, J. Y. Silica-coated nanocomposites of magnetic nanoparticles and quantum dots. *J. Am. Chem. Soc.* **2005,** *127* (14), 4990-4991.

437. Setyawan, H.; Fajaroh, F.; Widiyastuti, W.; Winardi, S.; Lenggoro, I. W.; Mufti, N. One-step synthesis of silica-coated magnetite nanoparticles by electrooxidation of iron in sodium silicate solution. *Journal of Nanoparticle Research* **2012,** *14* (4), 1-9.

438. Mürbe, J.; Rechtenbach, A.; Tõpfer, J. Synthesis and physical characterization of magnetite nanoparticles for biomedical applications. *Materials Chemistry and Physics* **2008,** *110* (2), 426-433.

439. Liu, Z. L.; Wang, H. B.; Lu, Q. H.; Du, G. H.; Peng, L.; Du, Y. Q.; Zhang, S. M.; Yao, K. L. Synthesis and characterization of ultrafine well-dispersed magnetic nanoparticles. *Journal of Magnetism and Magnetic Materials* **2004,** *283* (2–3), 258-262.

440. Ditsch, A.; Laibinis, P. E.; Wang, D. I.; Hatton, T. A. Controlled clustering and enhanced stability of polymer-coated magnetic nanoparticles. *Langmuir* **2005,** *21* (13), 6006-6018.

441. Zhao, W.; Gu, J.; Zhang, L.; Chen, H.; Shi, J. Fabrication of Uniform Magnetic Nanocomposite Spheres with a Magnetic Core/Mesoporous Silica Shell Structure. *J. Am. Chem. Soc.* **2005,** *127* (25), 8916-8917.

442. Yu, B. Y.; Kwak, S. Y. Assembly of magnetite nanocrystals into spherical mesoporous aggregates with a 3-D wormhole-like pore structure. *Journal of Materials Chemistry* **2010,** *20* (38), 8320-8328.

443. Ma, M.; Zhang, Y.; Yu, W.; Shen, H. y.; Zhang, H. q.; Gu, N. Preparation and characterization of magnetite nanoparticles coated by amino silane. *Colloids and Surfaces A: Physicochemical and Engineering Aspects* **2003,** *212* (2–3), 219-226.

444. Chernyshova, I. V.; Hochella Jr, M. F.; Madden, A. S. Size-dependent structural transformations of hematite nanoparticles. 1. Phase transition. *Physical Chemistry Chemical Physics* **2007,** *9* (14), 1736-1750.

445. Mahadevan, S.; Gnanaprakash, G.; Philip, J.; Rao, B. P. C.; Jayakumar, T. X-ray diffraction-based characterization of magnetite nanoparticles in presence of goethite and correlation with magnetic properties. *Physica E: Low-dimensional Systems and Nanostructures* **2007,** *39* (1), 20-25.

446. Thünemann, A. F.; Schütt, D.; Kaufner, L.; Pison, U.; Möhwald, H. Maghemite Nanoparticles Protectively Coated with Poly (ethylene imine) and Poly (ethylene oxide)-block-poly (glutamic acid). *Langmuir* **2006,** *22* (5), 2351-2357.

447. Llavona, A.; Prados, A.; Velasco, V.; Crespo, P.; Sanchez, M. C.; Perez, L. Electrochemical synthesis and magnetic properties of goethite single crystal nanowires. *CrystEngComm* **2013,** *15* (24), 4905-4909.

448. Lin, S. T. Magnetic Properties of Hematite Single Crystals. I. Magnetization Isotherms, Antiferromagnetic Susceptibility, and Weak Ferromagnetism of a Natural Crystal. *Physical Review* **1959,** *116* (6), 1447.

449. Martin-Hernandez, F.; Garcìa-Hernández, M. M. Magnetic properties and anisotropy constant of goethite single crystals at saturating high fields. *Geophysical Journal International* **2010,** *181* (2), 756-761.

450. Kletetschka, G.; Wasilewski, P. J.; Taylor, P. T. Hematite vs. magnetite as the signature for planetary magnetic anomalies? *Physics of the Earth and Planetary Interiors* **2000,** *119* (3), 259-267.

451. Guardia, P.; Batlle-Brugal, B.; Roca, A. G.; Iglesias, O.; Morales, M. P.; Serna, C. J.; Labarta, A.; Batlle, X. Surfactant effects in magnetite nanoparticles of controlled size. *Journal of Magnetism and Magnetic Materials* **2007,** *316* (2), e756-e759.

452. Goss, C. J. Saturation magnetisation, coercivity and lattice parameter changes in the system Fe_3O_4-γ–Fe_2O_3, and their relationship to structure. *Phys Chem Minerals* **1988,** *16* (2), 164-171.

453. Kanazawa, T.; Liu, X.; Morisako, A. Structure and magnetic properties of γ-Fe_2O_3-multi walled carbon nanotubes nanocomposites prepared by sol-gel method. IOP Publishing: 2011; p 012071.

454. Ek, S.; Iiskola, E. I.; Niinistö, L. Gas-phase deposition of aminopropylalkoxysilanes on porous silica. *Langmuir* **2003,** *19* (8), 3461-3471.

455. Carré, A.; Lacarrière, V.; Birch, W. Molecular interactions between DNA and an aminated glass substrate. *Journal of Colloid and Interface Science* **2003,** *260* (1), 49-55.

456. Sun, Y.; Duan, L.; Guo, Z.; DuanMu, Y.; Ma, M.; Xu, L.; Zhang, Y.; Gu, N. An improved way to prepare superparamagnetic magnetite-silica core-shell nanoparticles for possible biological application. *Journal of Magnetism and Magnetic Materials* **2005,** *285* (1), 65-70.

457. Tewari, P. H.; McLean, A. W. Temperature dependence of point of zero charge of alumina and magnetite. *Journal of Colloid and Interface Science* **1972,** *40* (2), 267-272.

458. Marmier, N.; Delisée, A.; Fromage, F. Surface Complexation Modeling of Yb(III), Ni(II), and Cs(I) Sorption on Magnetite. *Journal of Colloid and Interface Science* **1999,** *211* (1), 54-60.

459. Yean, S.; Cong, L.; Yavuz, C. T.; Mayo, J. T.; Yu, W. W.; Kan, A. T.; Colvin, V. L.; Tomson, M. B. Effect of magnetite particle size on adsorption and desorption of arsenite and arsenate. *Journal of Materials Research* **2005,** *20* (12), 3255-3264.

460. Krakowiak, A.; Trzcinska, M.; Sieliwanowicz, B.; Sawicka-Zukowska, R.; Jedrychowska, B.; Ajzenberg, V. Properties of immobilised and free lipase from *Rhizopus cohnii*. *Polish journal of food and nutrition sciences* **2003,** *12* (3), 39-44.

461. Ranjbakhsh, E.; Bordbar, A. K.; Abbasi, M.; Khosropour, A. R.; Shams, E. Enhancement of stability and catalytic activity of immobilized lipase on silica-coated modified magnetite nanoparticles. *Chemical Engineering Journal* **2012,** *179* (0), 272-276.

462. Kalantari, M.; Kazemeini, M.; Arpanaei, A. Evaluation of Biodiesel Production Using Lipase Immobilized on Magnetic Silica Nanocomposite Particles of Various Structures. *Biochemical Engineering Journal* (0).

463. Wang, J.; Meng, G.; Tao, K.; Feng, M.; Zhao, X.; Li, Z.; Xu, H.; Xia, D.; Lu, J. R. Immobilization of Lipases on Alkyl Silane Modified Magnetic Nanoparticles: Effect of Alkyl Chain Length on Enzyme Activity. *PLoS ONE* **2012,** *7* (8), e43478.

464. Kuo, T. M.; Gardner, H. W. Lipases: Structures, function and properties. In *Lipid Biotechnology*, Taylot & Francis Inc: New York, 2002; pp 417-418.

465. Xie, Z. F.; Suemune, H.; Sakai, K. Synthesis of chiral building blocks using Pseudomonas Fluorescens lipase catalyzed asymmetric hydrolysis of Meso diacetates. *Tetrahedron: Asymmetry* **1993,** *4* (5), 973-980.

466. Henegar, K. E. Process for preparing enantiomerically enriched (1S,4R) 1-acetoxy-4-hydroxycyclopent-2-ene . EP1587937 A1, 2005.

467. Deardorff, D. R.; Linde, R. G.; Martin, A. M.; Shulman, M. J. Enantioselective preparation of functionalized cyclopentanoids *via* a common chiral (pi-allyl) palladium complex. *The Journal of Organic Chemistry* **1989,** *54* (11), 2759-2762.

468. Kitade, Y.; Kojima, H.; Zulfiqur, F.; Kim, H. S.; Wataya, Y. Synthesis of 2-fluoronoraristeromycin and its inhibitory activity against *Plasmodium falciparum S*-Adenosyl-L-homocysteine hydrolase. *Bioorganic & Medicinal Chemistry Letters* **2003,** *13* (22), 3963-3965.

469. Gurjar, M. K.; Nageswar Reddy, C.; Kalkote, U. R.; Chorghade, M. S. Studies toward the total synthesis of carba analogue of motif C of M. Tb cell wall Ag complex. *Heterocycles* **2009,** *77* (2), 909-925.

470. Santos, J. C.; Nunes, G. F.; Moreira, A. B.; Perez, V. H.; de Castro, H. F. Characterization of Candida rugosa Lipase Immobilized on Poly (*N*–methylolacrylamide) and Its Application in Butyl Butyrate Synthesis. *Chemical Engineering & Technology* **2007,** *30* (9), 1255-1261.

471. Soares, C. M.; De Castro, H.; Moraes, F. F.; Zanin, G. Characterization and utilization of Candida rugosa lipase immobilized on controlled pore silica. *Appl Biochem Biotechnol* **1999,** *79* (1-3), 745-757.

472. Ozmen, E. Y.; Sezgin, M.; Yilmaz, M. Synthesis and characterization of cyclodextrin-based polymers as a support for immobilization of *Candida rugosa* lipase. *Journal of Molecular Catalysis B: Enzymatic* **2009,** *57* (1–4), 109-114.

473. Pereira, E. B.; de Castro, H. F.; De Moraes, F. F.; Zanin, G. M. Kinetic studies of lipase from Candida rugosa. *Applied Biochemistry and Biotechnology* **2001,** *91* (1-9), 739-752.

474. Boscolo, B.; Trotta, F.; Ghibaudi, E. High catalytic performances of Pseudomonas fluorescens lipase adsorbed on a new type of cyclodextrin-based nanosponges. *Journal of Molecular Catalysis B: Enzymatic* **2010,** *62* (2), 155-161.

475. Salis, A.; Pinna, M.; Monduzzi, M.; Solinas, V. Comparison among immobilised lipases on macroporous polypropylene toward biodiesel synthesis. *Journal of Molecular Catalysis B: Enzymatic* **2008,** *54* (1–2), 19-26.

476. Raza, S.; Fransson, L.; Hult, K. Enantioselectivity in Candida antarctica lipase B: a molecular dynamics study. *Protein Science* **2001,** *10* (2), 329-338.